DOE/MC/11089--3107

DE92 041343

Pressurized Fluidized-Bed Hydroretorting of Eastern Oil Shales

Topical Report, Sulfur Control

By
M.J. Roberts
J. Abbasian
C. Akin
F.S. Lau
A. Maka
M.C. Mensinger
D. Gidaspow
R. Gupta
D.T. Wasan
R.M. Pfister
E.J. Krieger

May 1992

Work Performed Under Contract No.: DE-AC21-87MC11089

For
U.S. Department of Energy
Office of Fossil Energy
Morgantown Energy Technology Center
Morgantown, West Virginia

By
Institute of Gas Technology
Chicago, Illinois

DISCLAIMER

DOE/MC/11089-3107

Pressurized Fluidized-Bed Hydroretorting of Eastern Oil Shales

Topical Report, Sulfur Control

By
M.J. Roberts
J. Abbasian
C. Akin
F.S. Lau
A. Maka
M.C. Mensinger
D. Gidaspow
R. Gupta
D.T. Wasan
R.M. Pfister
E.J. Krieger

Work Performed Under Contract No.: DE-AC21-87MC11089

For
U.S. Department of Energy
Office of Fossil Energy
Morgantown Energy Technology Center
P.O. Box 880
Morgantown, West Virginia 26507-0880

By
Institute of Gas Technology
IIT Center, 3424 S. State Street
Chicago, Illinois 60616

May 1992

EXECUTIVE SUMMARY

The removal of sulfur from oil shale prior to or during hydroretorting could significantly improve the overall efficiency of recovering oil from shale. Oil produced by retorting Eastern shales typically contains 1 to 2 weight percent sulfur. The sulfur must be removed by hydrotreating. Furthermore, the conversion of sulfur in shale to hydrogen sulfide (H_2S) during hydroretorting increases hydrogen consumption. Therefore, there are significant economic and environmental incentives for controlling the distribution of sulfur during shale processing.

This topical report on "Sulfur Control" presents the results of work conducted by the Institute of Gas Technology (IGT), the Illinois Institute of Technology (IIT), and the Ohio State University (OSU) to develop three novel approaches for desulfurization that have shown good potential with coal and could be cost-effective for oil shales. These are 1) In-Bed Sulfur Capture using different sorbents (IGT), 2) Electrostatic Desulfurization (IIT), and 3) Microbial Desulfurization and Denitrification (OSU and IGT).

The work was conducted as part of the overall program on "Pressurized Fluidized-Bed Hydroretorting of Eastern Oil Shales," sponsored by the Laramie Project Office of the U.S. Department of Energy/Morgantown Energy Technology Center (DOE/METC) under Contract No. DE-AC21-87MC11089. The primary objective of the program was to perform the research necessary to develop the pressurized fluidized-bed hydroretorting (PFH) process for producing oil from Eastern oil shales. The program also incorporated research on technologies that have the potential to improve the economics and/or environmental acceptability of recovering oil shales using the PFH process.

The objective of the task on In-Bed Sulfur Capture was to determine the effectiveness of different sorbents (that is, limestone, calcined limestone, dolomite, and siderite) for capturing sulfur (as H_2S) in the reactor during hydroretorting. Tests were conducted in the batch PFH unit at temperatures ranging from 900° to 1050°F (482° to 565°C) and pressures of 400 and 600 psig (2.8 and 4.2 MPa). The ratio of sorbent-to-feed sulfur was tested in the range of 0.5 to 1.5 mol/mol. Because only about one-half of the feed sulfur in the shale is converted, the "effective" sorbent-to-feed sulfur ratio investigated was 1.0 to 3.0 mol/mol. The effect of product gas recycling was also determined.

Overall, calcined limestone was found to be very effective at capturing H_2S. Sulfur capture efficiency is defined as the percent of the available H_2S (generated at the reactor conditions utilized) that is captured by the sorbent. Maximum sulfur capture efficiencies obtained for tests using the Alabama, Indiana, Kentucky, Michigan, Ohio, and Tennessee shales were 59.1%, 98%, 40.3%, 78.4%, 100%, and 57.6%, respectively. The original batch of calcined limestone sorbent used may have been inadvertently hydrated during preparation, which significantly affected its sulfur capture ability for specific tests with the Indiana, Michigan, and Ohio shales.

Batch PFH tests were performed with Indiana shale and siderite in-bed sulfur capture sorbents. Raw siderite did not prove to be as effective a sorbent as calcined siderite. Tests conducted with calcined siderite at 1050°F and 600 psig (565°C and 4.2 MPa) with residence times of 5 and

30 minutes produced sulfur capture efficiencies of 95.5% and 100%, respectively. One drawback to the use of raw siderite is that raw siderite, as mined, usually contains pyrite, which when calcined generates H_2S.

The objective of the task on Electrostatic Desulfurization was to determine the operating conditions necessary to achieve a high degree of sulfur removal and kerogen recovery in IIT's electrostatic separator. By examining scanning electron microscope photographs, IIT researchers determined that shale must be ground to a particle size of 10 to 15 μm to liberate the majority of pyritic sulfur. In parametric studies using their experimental apparatus, IIT investigated the effects of different methods of charging the shale particles (tribocharging), gas velocities, particle sizes and loadings, and surface moisture on pyrite reduction and kerogen recovery. During a typical test, the applied electric field across the electrostatic separator electrodes was 2000 volt/cm.

The results showed that at a gas velocity of 15 m/s, an applied voltage of 2000 v/cm, and a solids loading of 0.1 lb shale/lb air, the pyritic sulfur content of the treated shale could be reduced by about 53%. At the same time, the kerogen content of the shale increased from 12.4% to 33.5%. IIT also conducted modeling studies of the electroseparation process.

The objectives of the task on Microbial Desulfurization and Denitrification were to 1) isolate microbial cultures and evaluate their ability to desulfurize and denitrify shale, 2) conduct laboratory-scale batch and continuous tests to improve and enhance microbial removal of these components, and 3) determine the effects of processing parameters, such as shale slurry concentration, solids settling characteristics, agitation rate, and pH on the process.

OSU isolated 16 different cultures from shale and 1 from coal to be tested for the ability to desulfurize and/or denitrify shale. They tested a mixed culture that was capable of metabolizing pyridine (a model nitrogen compound). They also chemically pretreated (5 M nitric acid or 5 M sodium hydroxide) a sample of beneficiated shale and removed more than 50% of the sulfur. OSU was able to remove an additional 9.5% of the sulfur remaining after chemical pretreatment using a mixed culture.

IGT conducted shake flask experiments with the OSU cultures and several others that had been isolated previously by IGT researchers with slurries of fine-ground beneficiated shale. The results of these experiments showed that as much as 78% of the pyritic sulfur in the shale could be transformed to microbial organic sulfur within 30 days, and 83% could be transformed within 63 days of incubation. There was no apparent metabolism of organic sulfur by these particular microorganisms. However, the nitrogen-metabolizing organism transformed 50% of the nitrogen into microbial protein within 7 days of incubation. This reduction in shale nitrogen using microbial means is significant; improved nitrogen reductions could be achieved with additional acclimation of the organisms.

TABLE OF CONTENTS

	Page
INTRODUCTION	1
Electrostatic Desulfurization	1
Microbial Desulfurization and Denitrification	1
In-Bed Desulfurization	2
TASK 3. TESTING OF PROCESS IMPROVEMENT CONCEPTS	3
Subtask 3.1. In-Bed Sulfur Capture Tests	3
Discussion	3
TGA Tests With Ca-Based Sorbents	5
Subtask 3.1.1. Lab-Scale Batch Tests	9
Experimental Equipment	14
Batch PFH Tests With Calcined Limestone and Indiana Shale	14
Batch PFH Tests With Calcined Limestone and Other Shales	20
TGA Tests With Calcined Limestone Used in PFH Tests	21
TGA Siderite Tests	24
Batch PFH Siderite Tests	25
Subtask 3.1.2. Lab-Scale Continuous Tests	29
Experimental Equipment	29
Results and Discussion	29
Subtask 3.1.3. Bench-Scale Tests	31
Discussion	31
Subtask 3.2. Dry Electrostatic Desulfurization of Eastern Oil Shales	32
Preface	32
Summary	32
Program Objectives	34
Introduction	34
Literature Review	39
Introduction	39
Sulfur Distribution in Coal	40
Coal Beneficiation Methods	40
Dry Beneficiation Methods	45
Mechanical Methods	45

TABLE OF CONTENTS, Cont.

	Page
Air-Fluidized Particle Beds	48
Magnetic Separation	50
High-Gradient Magnetic Separation	50
Open Gradient Magnetic Separation	51
Electrostatic Separation	52
Corona Separation	54
Triboelectric Separation	57
Grain Size Characterization of Mineral Inclusions	61
Introduction	61
Background	62
Experimental Investigation	62
Scanning Electron Microscopy	62
Sample Description	62
Sample Preparation	62
Procedure	64
Results	64
Optical Microscopy	68
Results	69
Construction of Liberation Curves	73
Illinois No. 2 Coal	73
Indiana New Albany Shale	73
Grinding Techniques Used	73
Micropulverizer	78
Jet-Mill	79
Energy Consumption in Grinding	79
Particle Size Analysis	82
Triboelectrification	82
Introduction	82
Particle Charging Mechanisms	84
Conductive Induction	85
Ion Bombardment or C rona Charging	85
Contact Electrification	85

TABLE OF CONTENTS, Cont.

	Page
Metal-Metal Contacts	86
Metal-Insulator Contacts	87
Insulator-Insulator Contacts	87
Triboelectrification in Air	88
Work Functions	90
Theoretical Computation of Work Functions	91
Determination of Surface Charge From Work Functions	92
Gaussian Limit of Charge by Triboelectrification	95
Particle Charge Measurement	96
Charge Measurement Results	100
Effect of Temperature	100
Effect of Gas Velocity	100
Effect of Kerogen Content	101
Effect of Additives	103
Effect of Tribocharger Geometry	103
Discussion	105
Beneficiation of Illinois Coals	105
Introduction	105
Separation in a Continuous Electrofluidized Bed	106
Apparatus	106
Results	109
Separation in a Electrostatic Sieve Conveyor	115
Separation in a Batch Electrostatic Separator	119
Beneficiation of Eastern Oil Shales	120
Introduction	120
Background	120
Separation Tests in a Continuous Separator	122
Experimental System	123
Sample Description	123
Determination of Pyritic Sulfur	128
Determination of Kerogen	128
Desulfurization Tests	129
Beneficiation Tests in a Batch Separator	132

TABLE OF CONTENTS, Cont.

	Page
Parametric Studies	132
Determination of Kerogen Concentration Profiles	135
Effect of Inlet Geometry	136
Effect of Gas Velocity	146
Factors Limiting Separation	146
Discussion	148
Separation Tests With Model Mixtures	148
Introduction	148
Experimental	148
Parametric Studies	150
Effect of Gas Velocity	150
Effect of Applied Voltage	150
Effect of Inlet Geometry	150
Discussion	155
Modeling of a Batch Separator	155
Introduction	155
Governing Equation	155
Assumptions	155
Solution of the Equation	157
Determination of Particle Diffusivity	160
Comparison With Experimental Data	161
Effect of Electrodiffusion Number	162
Discussion	164
Conclusions and Recommendations	164
Nomenclature	168
Bibliography	170
Subtask 3.3. Microbial Desulfurization and Denitrification	178
Subtask 3.3.1. Culture Development	178
Objective	178
Background	178
Project Description	178
Results	182
Discussion	192
References Cited	197

TABLE OF CONTENTS, Cont.

	Page
Subtask 3.3.2. Microbial Process Development	200
Objective	200
Summary	200
Introduction	201
Technical Discussion	202
Experimental Equipment and Test Procedures	202
Desulfurization Cultures	202
Denitrification Cultures	202
Oil Shale	202
Desulfurization Studies	202
Denitrification Studies	204
Stimulation/Inhibition Shake Flask Experiments	204
Settling and Mixing Characteristic Experiments	204
Agitation Studies	205
Sulfur Bioassay	205
Protein Assay	205
Discussion	205
Desulfurization Studies	205
Denitrification Studies	211
Stimulation/Inhibition Shake Flask Studies	216
Settling and Mixing Characteristic Studies	216
Agitation Studies	220
Conclusion	223
References Cited	223
ACKNOWLEDGMENT	226
APPENDIX A. An Analytical Method for Determination of Forms of Sulfur in Oil Shale	A-1
APPENDIX B. Measurement of Cohesive Force Between Fine Particles Using a Cohetester	B-1

LIST OF FIGURES

Figure No.		Page
3-1	Flow Diagram of the Ambient-Pressure Thermogravimetric Analyzer Unit	7
3-2	Results of Duplicate Tests Conducted in the TGA Unit With Calcite	8
3-3	Effect of Reaction Temperature on Sulfidation Reaction Rate Involving Calcined Calcium-Based Sorbents	10
3-4	Effect of Sorbent Particle Size on Sulfidation Reaction Rate Involving Calcined Calcium-Based Sorbents	11
3-5	Comparison of Experimental Data With Diffusion-Controlled, Shrinking-Core Model	12
3-6	Effect of Reactor Pressure on Sulfur Capture	13
3-7	Schematic Diagram of Batch Laboratory-Scale PFH Unit	15
3-8	The Effects of Added Ca/Shale S Ratio and Operating Conditions on Sulfur Capture Efficiency	19
3-9	CaO Conversion of Calcined Limestone Batches	22
3-10	CaO Conversion of New Calcined Limestone Batches	23
3-11	Effect of Sorbent Type and Temperature on Sulfidation Reaction Rate	26
3-12	Effect of Calcination on the Sulfidation of Siderite	27
3-13	Schematic Diagram of Laboratory-Scale Continuous PFH Unit	30
3-14	Block Diagram of the Electrostatic Shale Beneficiation Process	37
3-15	Rotating Drum-Type Corona Separator	56
3-16	AED's Continuous UFC Belt Separator	59
3-17	PETC's Triboelectrostatic Separator	60
3-18	Photograph of IITRI's Scanning Electron Microscope Facility	63
3-19	Typical Scanning Electron Micrograph of Illinois No. 2 Coal Sample Specimen	65
3-20	Typical X-Ray Peaks Obtained With the SEM System	65

LIST OF FIGURES, Cont.

Figure No.		Page
3-21	Scanning Electron Micrograph of an Illinois No. 2 Coal Sample Specimen (Bright Spots Show Pyrite-Enriched Area)	67
3-22	Scanning Electron Micrograph of an Illinois No. 2 Coal Sample Specimen (Bright Spots Show Pyrite-Enriched Area)	67
3-23	Scanning Electron Micrograph of an Indiana-New Albany Oil Shale Sample Specimen (Bright Spots Show Pyrite- or Mineral-Enriched Area)	69
3-24	Optical Micrographs of an Illinois No. 2 Coal Sample Specimen	71
3-25	Optical Micrographs of an Illinois No. 6 Coal Sample Specimen	72
3-26	Optical Micrographs of an IN-NA Oil Shale Sample Specimen	74
3-27	Percent Pyrite Liberation as a Function of Particle Size for Illinois No. 2 Coal Sample	75
3-28	Percent Mineral Matter Liberation as a Function of Particle Size for Indiana-New Albany Shale Sample	77
3-29	Schematic Diagram of the Bantam-Micropulverizer	78
3-30	Schematic Diagram of the 4-Inch Micron-Master Laboratory Jet Mill	80
3-31	Theoretical Grinding Energy Required as a Function of Coal Size	81
3-32	Schematic Diagram of the Coulter-Counter System	83
3-33	Particle Size Distribution for the Ground IN-NA Shale	83
3-34	Charge on a Chromium Sphere After Contact With a Sphere of Another Metal Plotted Against the Contact Potential Difference Between the Metal and Chromium	88
3-35	Triboelectrification of a Series of Metals in Contact With an Insulator as a Function of Work Functions of Metals	90
3-36	Electronegativity of Various Elements in the Periodic Table	93
3-37	Schematic Diagram of the Faraday Cage System	97

LIST OF FIGURES, Cont.

Figure No.		Page
3-38	Principle of Operation of a Faraday Cage	98
3-39	Surface Charge of Oil Shale and Pyrites as a Function of Temperature	101
3-40	Surface Charge of Shale and Pyrites as a Function of Velocity	102
3-41	Surface Charge of Shales With Varying Kerogen Content	103
3-42	Various Triboc̲harger Configurations Used	104
3-43	Perspective View of IIT's Continuous Electrofluidized Bed System	107
3-44	Line Diagram of IIT's Continuous Electrofluidized Bed System	108
3-45	Removal of Pyritic Sulfur From Illinois Coals in the Electrofluidized Bed	112
3-46	Flow Rates of Inlet, Clean Coal and Pyrite-Enriched Streams in the Electrofluidized Bed Corresponding to Data in Figure 3-45	113
3-47	Schematic Diagram of the Continuous Electrostatic Sieve Conveyor	116
3-48	Removal of Pyritic Sulfur From Illinois No. 2 Coal as a Function of Gas Velocity in the Continuous Electrostatic Sieve Conveyor Shown in Figure 3-47	117
3-49	Coal Recovery as a Function of Gas Velocity in the Continuous Electrostatic Sieve Conveyor Shown in Figure 3-47	118
3-50	Schematic Diagram of the Batch Electrostatic Separator System	119
3-51	Experimental System for Oil Shale Beneficiation	124
3-52	Electrostatic Sieve Separator Used for Shale Desulfurization Tests	125
3-53	Schematic of Perkin Elmer CHN 2400 Elemental Analyzer	129
3-54	Stepwise Detection of Gases in PC CHN 2400 Analyzer	130

LIST OF FIGURES, Cont.

Figure No.		Page
3-55	Flow Split as a Function of Gas Velocity in Electrostatic Separator	131
3-56	Pyrite Removal as a Function of Gas Velocity	131
3-57	Effect of Particle Size on Kerogen Enrichment and Pyrite Removal	133
3-58	Effect of Surface Moisture on Kerogen Enrichment and Pyrite Removal	134
3-59	Effect of Inlet Gas Velocity on Kerogen Enrichment and Pyrite Removal	134
3-60	Effect of Solids Loading on Kerogen Enrichment and Pyrite Removal	135
3-61	Kerogen Concentration Profile of the Layers Deposited at Negative and Positive Electrodes	137
3-62	Weight Distribution Profile of the Layer Deposited at Negative Electrode	137
3-63	Weight Dist ibution Profile of the Layer Deposited at Positive Electrode	138
3-64	Pyrite Concentration Profile of the Layers Deposited at Negative and Positive Electrodes	138
3-65	Sample Locations Corresponding to the Sample Numbers in Tables 3-28 and 3-29	141
3-66	Schematic Diagram of the Batch Electrostatic Separator	141
3-67	Various Inlet Geometries Tested	142
3-68	Kerogen Concentration Profile of Layers Deposited on Negative and Positive Electrode in Batch Separator (Rectangular Channel Inlet and Air Flow of 20 cfm)	143
3-69	Kerogen Concentration Profile of Layers Deposited on Negative and Positive Electrode in Batch Separator (Rectangular Slit Jet and Air Flow of 20 cfm)	144
3-70	Kerogen Concentration Profile of Layers Deposited on Negative and Positive Electrode in Batch Separator (Circular Jet and Air Flow of 20 cfm)	145
3-71	Kerogen Concentration Profile of Layers Deposited on Negative and Positive Electrode in Batch Separator (Circular Jet and Air Flow of 24 cfm)	147

LIST OF FIGURES, Cont.

Figure No.		Page
3-72	Carbon Concentration Profile of Layers Deposited at Positive and Negative Electrodes	149
3-73	Carbon Concentration Profile of Layers Deposited at Negative Electrode as a Function of Gas Velocity	151
3-74	Carbon Concentration Profile of Layers Deposited at Positive Electrode as a Function of Gas Velocity	152
3-75	Carbon Concentration Profile of Layers Deposited at Negative Electrode as a Function of Applied Voltage	153
3-76	Carbon Concentration Profile of Layers Deposited at Positive Electrode as a Function of Applied Voltage	154
3-77	Carbon Concentration Profile of Layers Deposited at Negative Electrode for the Various Inlet Geometrical Configurations	156
3-78	Geometrical Configuration of an Electrostatic Separator Used in Modeling	158
3-79	Comparison of Experimental Data With the Calculated Values for the Separation of Carbon From a Model Mixture of Charcoal and Silica	163
3-80	Effect of Electrodiffusion Number	164
3-81	Systematic Approach to an Electrostatic Separator Development	165
3-82	Conceptual Design of a Continuous Electrostatic Separator	166
3-83	Scanning Electron Micrographs of Shale Particles Determined by Wet-Sieving to Be: (A) -100+200; (B) -200+325; and (C) -325 mesh (x 65, size bar = 100 μm)	184
3-84	Transmission Electron Micrographs Showing Various Microorganisms Associated With Freshly Ground Indiana New Albany Oil Shale. (A) x 3150, size bar = 2 μm; and (B) x 2500, size bar = 2 μm	185
3-85	Two Spectra Obtained Using an Energy Dispersive X-Ray Fluorescence Spectrometer to Analyze a Sample of -200 Mesh, Dry-Sieved Indiana New Albany Oil Shale Before (Unshaded Spectrum) and After (Shaded Spectrum) Pretreatment for 60 Hours With 5.0 M HNO_3	189

LIST OF FIGURES, Cont.

Figure No.		Page
3-86	Scanning Electron Micrograph of Pretreated Shale Particles Coated With Microorganisms Following Incubation With a Mixed Culture Inoculum (x 6000, size bar = 2 μm)	193
3-87	Spectra Collected of Samples From the Sewage A Flask Initially (Unshaded) and After 17 Days of Incubation (Shaded)	195
3-88	Standard Curve: Plot of Slurry Concentration Versus Wet Weight of Shale Pellet	206
3-89	Cell Counts on Oil Shale Slurries and Denitrifying Bacteria	213
3-90	Protein Determinations on Oil Shale Slurries and Denitrifying Bacteria	214
3-91	Effect of Various Oil Shale Concentrations on Cell Growth in the Presence of Glucose	218
3-92	Cell Growth in an 8 Weight Percent Oil Shale Slurry With and Without Glucose	219
3-93	Settling Characteristics of Slurries With Different Oil Shale Concentrations	221
3-94	Settling Characteristics of Oil Shale in the Presence and Absence of Microbes (IGTS7)	222

LIST OF TABLES

Table No.		Page
3-1	Feed Shale Sulfur-by-Type Analysis	4
3-2	Continuous PFH Test Sulfur Conversions	6
3-3	Elemental Analyses of the Sorbents Used for In-Bed Sulfur-Capture Tests	9
3-4	Analyses of Calcined Limestone	16
3-5	Sulfur Conversions Achieved in Batch PFH Tests With Indiana New Albany Shale	17
3-6	Sulfur Conversions Achieved in Tests Conducted With Calcined Limestone in the Batch PFH Reactor	18
3-7	Composition of Raw and Calcined Siderite for TGA and Batch PFH Sulfur-Capture Tests	24
3-8	Operating Conditions of Batch PFH Sulfur Capture Tests With Indiana Shale and Siderite	28
3-9	Sulfur Conversions Achieved in Tests Conducted With Indiana Shale and Calcined Limestone in the Batch PFH Reactor	28
3-10	Summary of Operating Conditions and Results of Continuous PFH Sulfur Capture Test	31
3-11	Industrial Separations Made by Electrostatics	36
3-12	Analyses of Coals in Illinois Basin Coal Sample Program	41
3-13	Physical Coal Beneficiation Processes (Wet Methods)	43
3-14	Physical Coal Beneficiation Processes (Dry Methods)	46
3-15	Physio-chemical Properties of Coal and its Mineral Admixtures	55
3-16	Typical Elemental Analysis of a Pyrite Particle Using the ZAP Software	66
3-17	Elemental Analysis of Mineral-Enriched Areas in an Indiana New Albany Shale Specimen Using the SEM	70
3-18	Summary of the SEM Analysis Results for Illinois No. 2 Coal Sample Done by ISGS	76
3-19	Work Functions of Various Crystal Faces	89

LIST OF TABLES, Cont.

Table No.		Page
3-20	Work Functions of Various Compounds	94
3-21	Surface Charge of Various Powders Measured Experimentally Using a Faraday Cage	99
3-22	Desulfurization Test With Illinois No. 2 Coal in Electrofluidized Bed	110
3-23	Desulfurization Test With Illinois No. 2 Coal in Electrofluidized Bed	111
3-24	Desulfurization Test With Illinois No. 6 Coal in Electrofluidized Bed	114
3-25	Electrostatic Beneficiation of Herrin No. 6 (IBC-104) Coal in a Batch Separator	121
3-26	Chemical Analysis of IN-NA Oil Shale	126
3-27	Major and Trace Elements in IN-NA Oil Shale	127
3-28	Kerogen Material Balance	139
3-29	Pyrite Material Balance	140
3-30	Gram Stain Reaction and Morphologies for 16 Microorganisms Isolated From Indiana New Albany Shale	183
3-31	Average Percentage of +200, -200, and -325 Mesh Fractions Collected After Dry- and Wet-Sieving Handground or Wet-Sieving Beneficiated Indiana New Albany Oil Shale	183
3-32	Enumeration of Microorganisms Found in Wet-Sieved Indiana New Albany Oil Shale by Direct Counting in a Transmission Electron Microscope	186
3-33	The Average Length, Width, and Area of Particles in Wet-Sieved Fractions of Ground Indiana New Albany Shale Determined Using Transmission Electron Microscopy	186
3-34	Average Sulfur Content in the +200, -200, and -325 Mesh Fractions Collected After Dry- and Wet-Sieving Handground or Wet-Sieving Beneficiated Indiana New Albany Shale	187
3-35	Effect of Chemical Pretreatment on Selected Elements in Dry-Sieved Handground Indiana New Albany Oil Shale	187
3-36	The Percent Change in the Sulfur Content of +200 and -200 Mesh (Dry-Sieved) Indiana New Albany Shale Before and After Incubations With a Mixed Culture Inoculum	190

LIST OF TABLES, Cont.

Table No.		Page
3-37	The Average Percent Sulfur Concentration of +200 and -200 mesh (Dry-Sieved) Indiana New Albany Shale Samples Determined in an EDXS Before and After Incubation With a Mixed Culture Inoculum	190
3-38	The Percent Sulfur in -325 Mesh (Wet-Sieved) Pretreated Indiana New Albany Shale Samples Before and After 18-Day Incubation With a Mixed Culture Inoculum in S-free Medium (pH 7) Altered With Respect to Carbon Source	191
3-39	The Average Percent Sulfur Concentration of Pretreated Wet-Sieved Indiana New Albany Shale Samples Determined in an EDXS Before and After Incubation With a Mixed Culture Inoculum	192
3-40	The Average Absorbance of Samples Containing Pyridine Collected From Uninoculated Flasks (Control A and B) and Flasks Inoculated With a Mixture of Oil Shale Isolates (Mix A and B), Isolate No. 6 (Micro A and B), and an Aliquot of Raw Sewage (Sewage A and B) After 0, 2, 3, 4, 15, and 16 Days Incubation	194
3-41	The Average Absorbance of Samples Containing Pyridine Collected From Uninoculated Flasks (Control A and B) and Flasks Inoculated With a Mixed Culture Developed From Raw Sewage After 0, 3, 5, and 7 Days Incubation	196
3-42	Ultimate Analyses of Raw and Beneficiated Indiana New Albany Oil Shale	203
3-43	Ultimate Chemical Analysis on Oil Shale Samples for Sulfur Removal	207
3-44	Sulfur by Type Analysis on Oil Shale Samples Treated With IGTS7M or OSU Mixed Culture	208
3-45	Sulfur by Type Analysis on Oil Shale Samples Treated with IGTS7M	210
3-46	Sulfur Removal From Oil Shale in the Presence of IGTS7M	211
3-47	Sulfur Analysis on Oil Shale Samples Treated With *Thiobacillus ferrooxidans*	212
3-48	Nitrogen Transformation in the Presence of IGTD1 and OSU Mixed Culture	215
3-49	Nitrogen Removal in the Presence of IGTD1 and OSU Mixed Culture	217

LIST OF TABLES, Cont.

Table No.		Page
3-50	Effect of Different Rates of Agitation on Settling and Growth in the Bioreactor	224

55WP/61090toc/RPP

INTRODUCTION

Shale oil containing less sulfur and nitrogen will reduce oil hydrotreating requirements, save significant capital costs, and reduce hydrogen consumption. Three novel approaches for desulfurization have shown good potential with coal and could be cost-effective for oil shales: electrodesulfurization, microbial desulfurization and denitrification, and in-bed desulfurization.

Electrostatic Desulfurization

The use of classic magnetic separation for the desulfurization of coal has not been very effective or economical. Many research programs have been conducted to improve the performance of magnetic separation by the use of high-gradient magnetic separation (HGMS), superconducting magnets, or pretreatment of coal to improve the magnetic properties of pyrite. HGMS has large energy requirements; superconducting magnets require a liquid helium temperature of 4.2 K; and coal pretreatment costs are very high.

The electrostatic method for desulfurization requires less energy, does not require any chemical pretreatment, and can be used at ambient conditions. This method is based on the principle that pyritic and non-pyritic components of shale develop either different levels of the same charge or dissimilar charges, depending upon the method of charging used. Some work on the desulfurization of coal in fluidized beds or conveying systems has been conducted with very encouraging results. The work at the Illinois Institute of Technology (IIT) has shown that as much as 70% of the pyrite can be removed by the electrostatic method. The results can be improved by changing the tribocharging system to one that can charge pyrite with one type of charge and non-pyritic material with the opposite charge.

The electrodesulfurization technique could be used as a stand-alone method or complementary to the beneficiation process for removing additional pyritic sulfur. In the past, electrostatic methods used expensive rotor-type machines, which involved scraping of solids that stuck to the electrodes. Using an electrostatic sieve concept, researchers at IIT have solved both the problems of sticking and the costly rotating machinery used in the past. The rate of pyrite and shale separation is determined by their electrophoretic mobility. The concept has been applied to continuous separation in pneumatic conveyors. This novel technique, which was utilized to separate pyrites from Illinois coal, was applied to Eastern oil shales.

Microbial Desulfurization and Denitrification

Beneficiation of oil shale reduces only pyritic sulfur and mineral matter; it cannot remove organic sulfur and nitrogen. Removal of these components requires either chemical or microbial processing. Generally, milder operating conditions improve thermal efficiency and economics. Microbial processing is conducted at milder conditions. The microbial approach has the potential to desulfurize and denitrify oil shales at ambient pressure and at a temperature of only 25° to 55°C. No other chemical cleaning approach that can remove organic sulfur and nitrogen operates at such mild conditions.

Under a continuing DOE program, Atlantic Research Corporation has shown that one of its proprietary cultures can reduce the organic sulfur content of coal by about 47%. In another DOE program, IGT has developed aerobic and anaerobic mixed cultures that can convert over 95% of dibenzylthiophene (DBT), a typical sulfur compound found in coal. These results are very exciting because this is the first time that mixed cultures and anaerobic systems, which are expected to be more economical than the single-culture aerobic systems, have been demonstrated to degrade DBT. The marginal cost of the microbial treatment step is expected to be very small because the cost of fine grinding the shale in a water slurry has already been incurred for the beneficiation step.

Samples of Eastern oil shale were used as the source of enrichment culture inocula for the isolation of both aerobic and anaerobic microorganisms under various growth conditions. Lab-scale batch tests were conducted to determine the effects of various culture development parameters, such as source of inocula, pH, temperature, and culture media, on culture growth. Culture development was accomplished at the shaker-flask scale of operation. The culture media used included non-shale carbon sources, various trace minerals, and vitamins, but omitted sources of sulfur and nitrogen. A similar test matrix was used to develop cultures that ultimately have shale as the only source of organic carbon, sulfur, and nitrogen. Those cultures that demonstrated the greatest removal of sulfur and nitrogen were selected for process development studies.

The effects of process operating conditions on the efficiencies and rates of organic sulfur and nitrogen removal from Eastern oil shale by the selected cultures were determined using batch and continuous reactors. Preliminary optimum operating conditions of oil shale concentration, microorganism concentration, and retention time were determined using batch reactors. These conditions were further refined in experiments using a reactor operating on a continuous feed mode.

In-Bed Desulfurization

Another desulfurization technique, in-bed sulfur capture, has been developed and successfully utilized for atmospheric combustion work with coal. The application of this technique for in-bed sulfur capture in a PFH retort was investigated. Desulfurization in the PFH reactor will mitigate, and perhaps eliminate, the need for downstream sulfur recovery and tail gas cleanup sections of the integrated PFH process facility. Tests included lab-scale batch and continuous tests to determine the effects of temperature, pressure, limestone-to-shale ratio, and feedstock on the efficiency of sulfur capture. Lab-scale batch testing was a cost-effective way to identify the most important process variables to be tested in continuous tests. Continuous tests were conducted at the laboratory scale to provide material balances and obtain process design data.

TASK 3. TESTING OF PROCESS IMPROVEMENT CONCEPTS

The overall objective of this task was to obtain data on novel process concepts that have the potential for improving the overall economics of PFH processing with Eastern oil shales. This task is divided into five subtasks corresponding to the five concepts being tested: In-Bed Sulfur Capture, Electrostatic Desulfurization, Microbial Desulfurization and Denitrification, Electroseparation of Fines From Shale Oil, and Restricted Pipe Discharge System (RPDS). This report focuses on process concepts related to sulfur control.

Subtask 3.1. In-Bed Sulfur Capture Tests

The objective of this subtask was to determine the effects of operating conditions (temperature, pressure, and sorbent-to-shale ratios) on the effectiveness of in-bed sulfur capture with limestone and presintered iron ore (siderite).

Discussion

Several series of tests were performed to meet the objectives of this subtask. The goals of the test series were to determine the reactivities of various calcium-based sulfur capture sorbents, to determine the reactivities of raw and calcined siderite sulfur capture sorbents, and to demonstrate the effectiveness of the sorbents in laboratory-scale PFH reactors. The following tests were conducted in this subtask.

- TGA tests to study the reactivity between hydrogen sulfide and limestone, calcined limestone, and dolomite
- Batch PFH tests with six Eastern shales and a calcined limestone sorbent
- One continuous PFH test with Indiana shale and a calcined limestone sulfur capture sorbent
- TGA tests to study the reactivity between hydrogen sulfide and raw and calcined siderite
- Batch PFH tests with Indiana shale using raw and calcined siderite sorbents
- TGA tests to study the reactivities of several Ca-based sorbents including the batches of calcined limestone used in the laboratory-scale PFH tests.

The sulfur contents and sulfur-by-type analyses of the six Eastern U.S. shales studied in this program are presented in Table 3-1. Total sulfur contents were found to range from 2.2% for the Ohio shale to 9.2% for the Alabama shale. A large fraction of the sulfur in these shales is in pyrite. During the hydroretorting of Eastern shales, up to half of the pyritic sulfur is converted to hydrogen sulfide (H_2S). Other sulfur species can also react with hydrogen to produce H_2S.

Table 3-1. FEED SHALE SULFUR-BY-TYPE ANALYSES

Shale	AL		IN		KY		MI		OH		TN	
PFH Test	C-54		C-53		C-15		C-40		C-39		C-19	
Sample	Feed	Res	Feed	Res	Feed	Res	Feed	Res	Feed	Res	Feed	Res
S Type, wt % dry												
Sulfide	0.04	4.42	0.02	1.41	0.02	2.50	0.01	1.84	0.01	1.11	0.04	2.73
Sulfate	0.29	0.09	0.18	0.12	0.39	0.16	0.70	0.35	0.58	0.13	0.95	0.66
Pyrite	3.47	0.14	2.23	0.10	4.06	0.13	1.85	0.09	1.26	0.10	4.21	0.12
Organic	5.44	0.93	0.67	0.44	0.84	0.59	0.61	0.66	0.35	0.45	1.66	1.62
Total	9.24	5.58	3.10	2.07	5.21	3.38	3.17	2.94	2.20	1.79	6.86	5.13
S Type, % total S												
Sulfide	0.4	79.2	0.5	68.1	0.4	74.0	0.3	62.6	0.6	62.0	0.5	53.2
Sulfate	3.1	1.6	5.8	5.8	5.6	4.7	22.1	11.9	26.4	7.3	13.8	12.9
Pyrite	37.6	2.5	72.3	4.8	77.9	3.8	58.4	3.1	57.3	5.6	61.4	2.3
Organic	58.9	16.7	21.4	21.3	16.1	17.5	19.2	22.4	15.7	25.1	24.3	31.6
Total	100.0	100.0	100.0	100.0	100.0	100.0	100.0	100.0	100.0	100.0	100.0	100.0
S Conversion, %												
Sulfate	74.0		43.0		53.1		55.6		80.5		39.9	
Pyrite	96.6		96.2		97.3		95.7		93.1		97.5	
Organic	85.7		43.8		40.3		4.0		~0.0		15.6	
Total	49.5		42.9		44.9		17.7		29.3		35.3	

55WP/61090t3-1/RPP

Continuous PFH tests in Subtasks 1.2 and 2.2 yielded sulfur conversions to H_2S of up to 50%. The sulfur conversions for all continuous PFH tests are presented in Table 3-2. The Indiana and Kentucky New Albany shales and the Alabama shale had sulfur conversions to H_2S of 40% to 50%. Sulfur conversions to H_2S were lower for the Tennessee, Ohio, and Michigan shales with Michigan shale showing the lowest conversion of sulfur to H_2S. An attempt was made to find a relationship between the PFH sulfur conversions and the shale sulfur analyses in Table 3-1. The shales with the lowest sulfur conversions have significant amounts of sulfate sulfur. Sulfate and organic sulfur conversions were lower for these shales. For all six shales, hydrogen sulfide is the predominant product from PFH processing of the pyritic sulfur, but sulfate, pyritic, and organic sulfur are all converted to some extent during PFH processing.

Work in this task was directed toward identifying in-bed sulfur sorbents that could capture sulfur from H_2S in the reducing environment of the PFH process.

TGA Tests With Ca-Based Sorbents

The first work completed in this subtask was a series of thermogravimetric analysis (TGA) tests to determine the reactivities of calcined and uncalcined limestone (calcite) and dolomite toward H_2S. Ten tests were conducted in an ambient-pressure TGA unit. The effects of sorbent type, particle diameter, and reaction temperature were investigated.

A schematic diagram of the TGA unit used in these tests is shown in Figure 3-1. During a test, a simultaneous recording is made of the sample weight, the rate of weight change, and the temperature of the furnace in close proximity to the sorbent being heated. The sample is contained in a platinum basket, while a metered flow of gas is introduced at the top of the furnace chamber. The platinum basket is suspended from a recording balance. Any movement of the balance arm, because of a change in sample weight, is sensed by a linear differential transformer on the left arm of the balance. A restoring force is applied to the right arm by an electromagnet proportional to the change in weight. The recording balance control unit senses the required force to maintain a null and converts this into a signal that is proportional to the weight of the sample. The sample weight signal and the temperature signals are recorded by a computer during the test.

The chemical compositions of the sorbents used in these tests are given in Table 3-3. The average particle diameters of the sorbents were -80+100 mesh (d_p = 0.0165 cm) and -20+30 mesh (d_p = 0.071 cm). The tests were conducted in the temperature range of 900° to 1050°F (482° to 565°C). The reactant gas contained 5 mole percent H_2S, 15 mole percent hydrogen, and 80 mole percent nitrogen. Duplicate runs were conducted to determine the accuracy and reproducibility of the measurements. The results of the duplicate tests with calcined limestone are presented in Figure 3-2.

Four tests were conducted to determine the reactivities of uncalcined sorbents (limestone and dolomite) toward H_2S at temperatures of 900° and 1050°F (482° and 565°C). The results of these tests indicate that uncalcined calcium-based sorbents do not react with H_2S in the range of temperature investigated.

Table 3-2. CONTINUOUS PFH TEST SULFUR CONVERSIONS

Test	Shale	Temperature, °F	Pressure, psig	Residence Time, min	Sulfur Conversion, % Res. Shale	H_2S	Oil
C-14	AL	919	598	30	50.1	47.0	2.9
C-24	AL	914	608	68	49.4	48.1	2.5
C-33	AL	920	619	53	50.2	46.8	3.0
C-37	AL	953	618	53	49.4	47.7	2.9
C-54	AL	934	605	17	50.5	46.9	
C-1	IN	1000	633	98	NA	NA	NA
C-7	IN	900	600	19	54.2	40.8	5.0
C-10	IN	898	407	50	54.0	41.6	4.5
C-21	IN	907	1001	28	55.0	40.0	5.0
C-22	IN	908	377	24	56.4	38.3	5.3
C-23	IN	916	603	9	56.7	38.5	4.8
C-43	IN	959	610	26	NA	NA	NA
C-44	IN	959	606	25	52.7	42.4	4.9
C-53	IN	916	597	12	57.1	38.5	4.4
C-15	KY	919	602	29	55.1	40.9	4.0
C-45	KY	937	606	40	57.0	40.7	2.3
C-28	MI	1049	621	21	72.5	24.1	3.4
C-40	MI	1050	609	47	82.3	15.8	1.9
C-46	MI	1069	607	46	80.9	17.6	1.5
C-16	OH	922	596	19	59.9	34.3	5.8
C-32	OH	917	619	62	67.7	25.7	6.6
C-39	OH	939	616	42	70.7	25.6	3.7
C-19	TN	918	599	27	63.8	33.5	2.7
C-27	TN	916	694	17	62.4	34.1	3.5

NA = Not Available.

55WP/61090t3-2/RPP

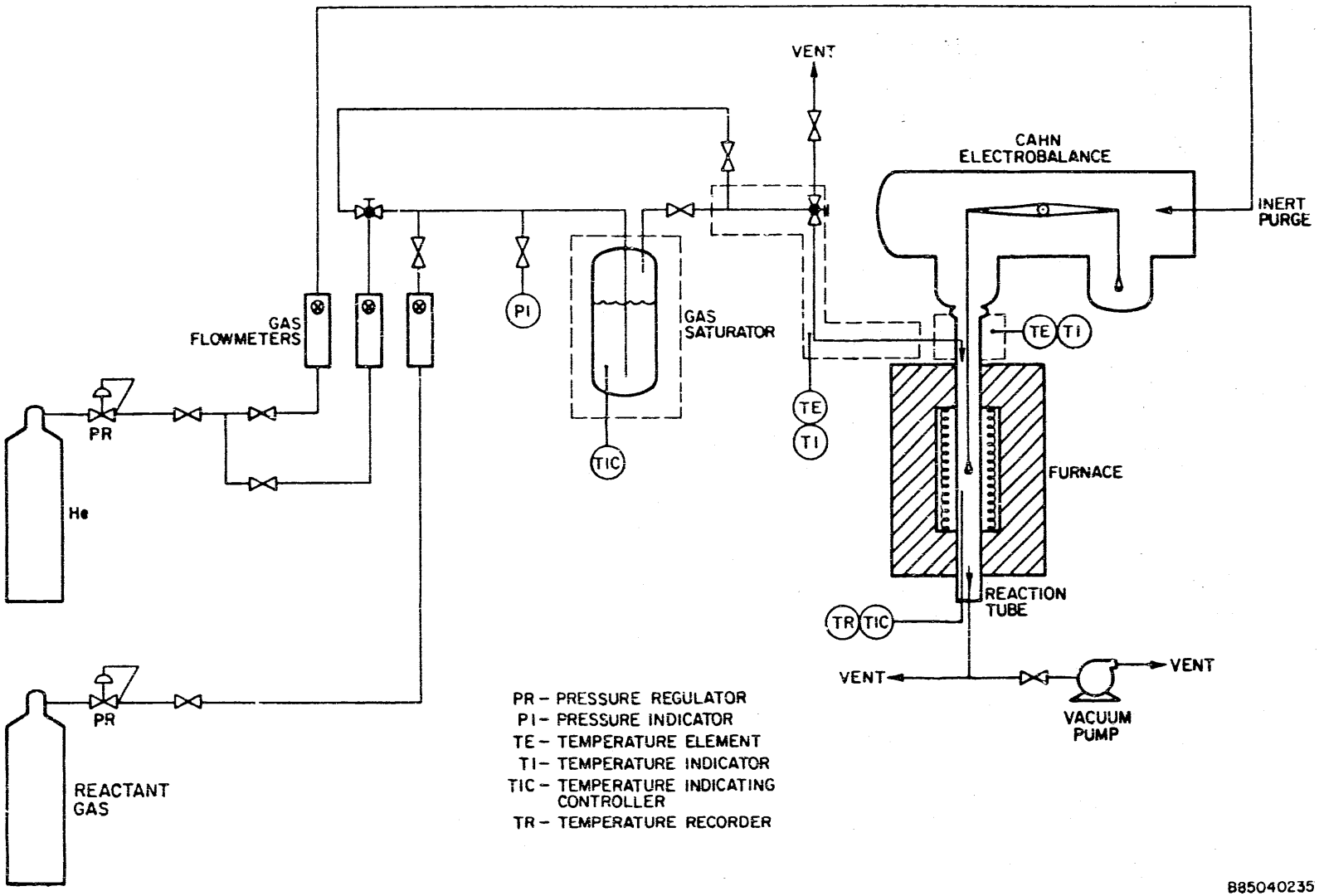

Figure 3-1. FLOW DIAGRAM OF THE AMBIENT-PRESSURE THERMOGRAVIMETRIC ANALYZER UNIT

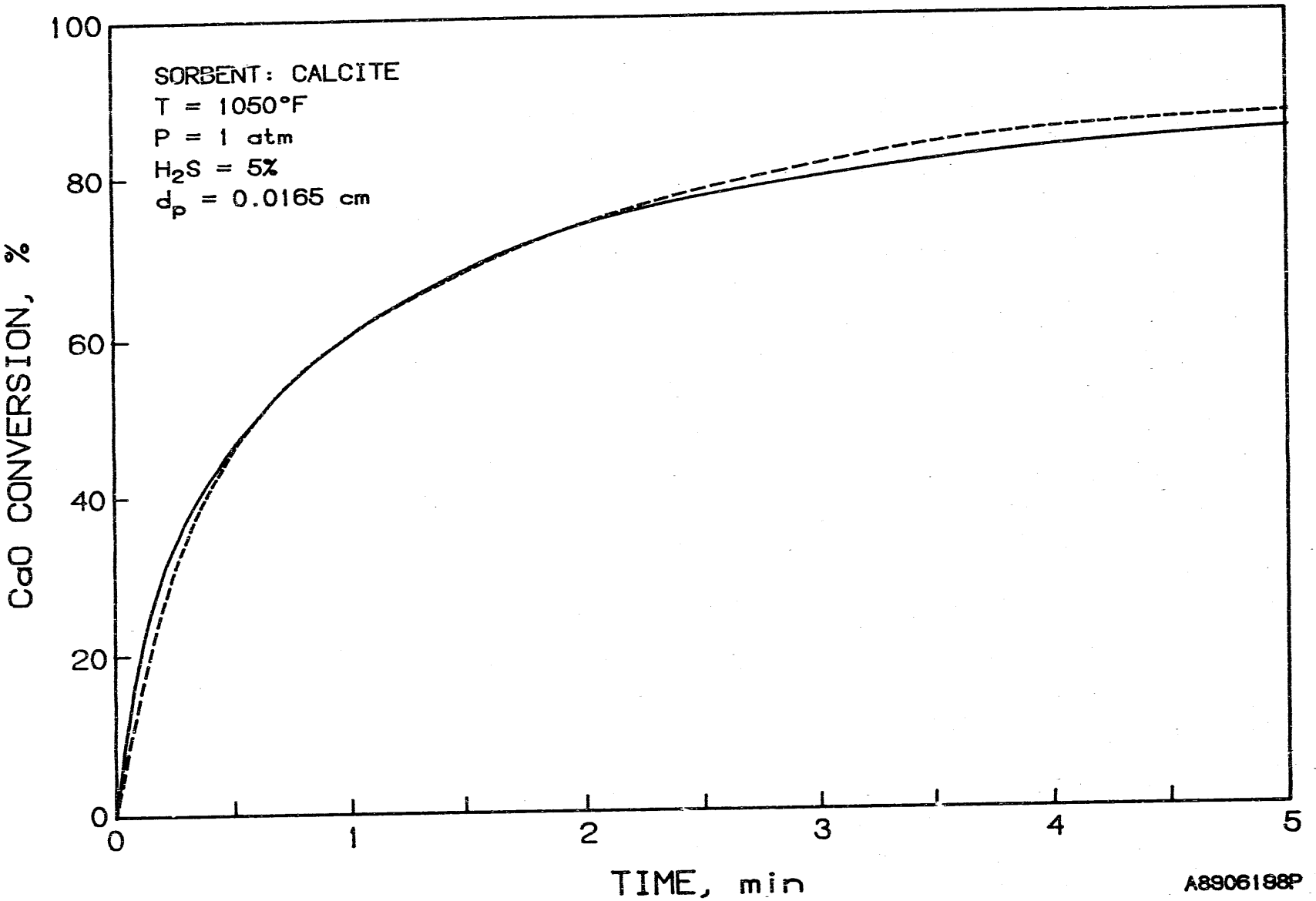

Figure 3-2. RESULTS OF DUPLICATE TESTS CONDUCTED IN THE TGA UNIT WITH CALCITE

Table 3-3. ELEMENTAL ANALYSES OF THE SORBENTS USED FOR IN-BED SULFUR-CAPTURE TESTS

Component	Limestone (Calcite)	Dolomite
	wt %	
Calcium	40.6	22.1
Magnesium	0.58	13.5
Silicon	0.22	0.36
Potassium	0.032	0.07
Iron	0.054	0.13
Strontium	0.016	0.006
Aluminum	0.051	0.12
Carbon Dioxide	43.50	46.5

The effect of temperature on the rate of reaction between H_2S and calcined limestone and dolomite is shown in Figure 3-3, indicating that the reactivities of the sorbent significantly increase with an increase in temperature. The data also indicate that dolomite was more reactive than limestone. Figure 3-4 shows the effect of particle size on the reaction rate from both sorbents. As expected, the reaction rate decreases with an increase in sorbent particle size.

To estimate the extent of desulfurization in a PFH reactor, the sulfidation reaction rate at elevated pressure should be determined by extrapolating the ambient pressure data using a kinetic model. Figure 3-5 shows good agreement between the experimental ambient-pressure data and the diffusion-controlled, shrinking-core model for spherical particles of unshrinking size at 1050°F (565°C). This kinetic model was used to extrapolate the ambient pressure data to elevated pressure.

The estimated sulfur capture in a 2-inch-diameter PFH reactor is presented in Figure 3-6. The results indicate that at a reactor pressure of 400 psia and a reactor temperature of 1050°F (565°C), about 85% of H_2S can be captured using -80+100 mesh particles of limestone with a Ca/S ratio of 2. These data were used to determine the operating parameters for the lab-scale batch and continuous tests.

Subtask 3.1.1. Lab-Scale Batch Tests

The objective of this subtask is to determine the effects of temperature, pressure, and sorbent-to-shale ratio on the in-bed sulfur capture for PFH of shales by conducting lab-scale batch tests. This subtask provided direction for selection of operating conditions for in-bed sulfur capture in continuous tests.

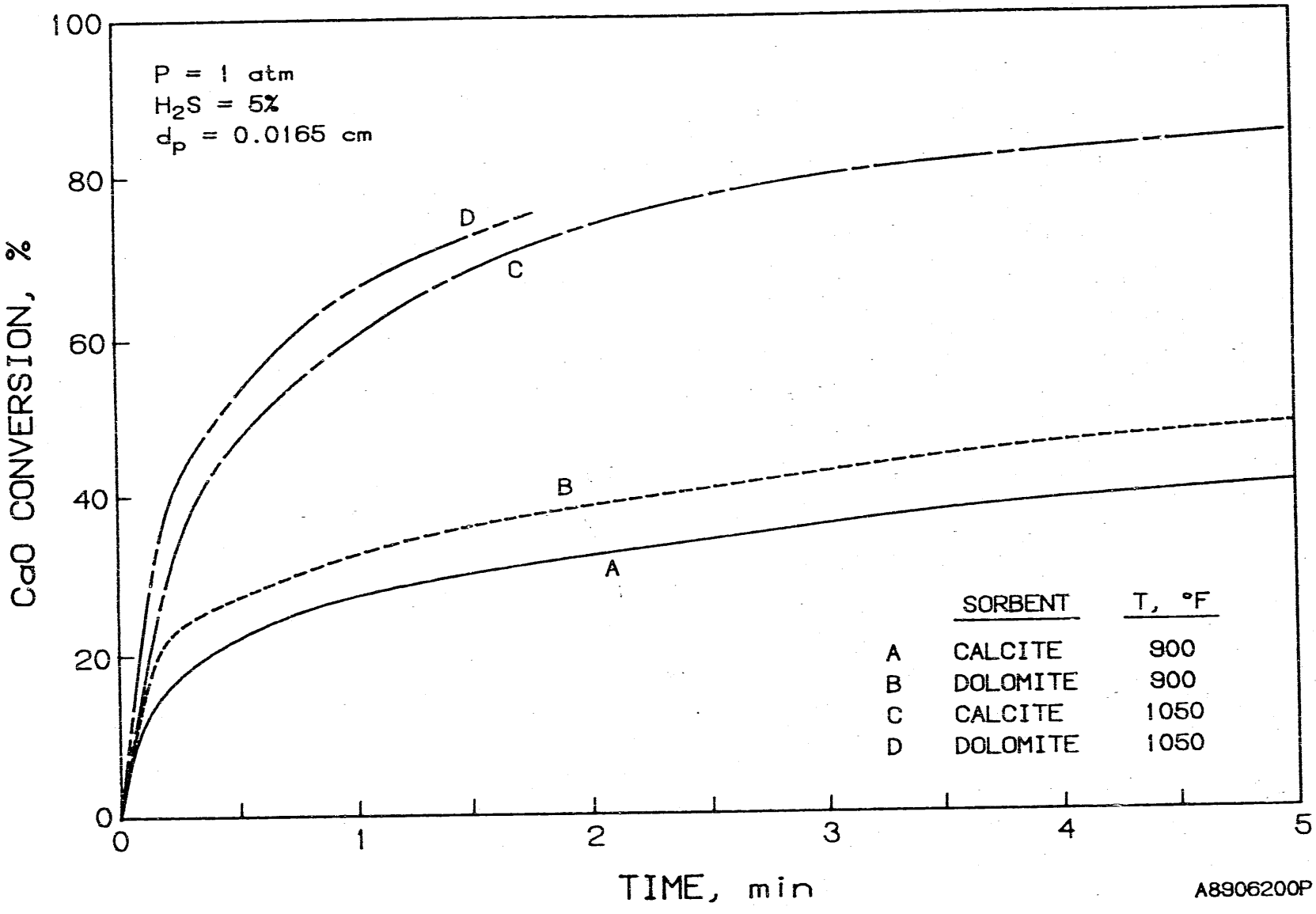

Figure 3-3. EFFECT OF REACTION TEMPERATURE ON SULFIDATION REACTION RATE INVOLVING CALCINED CALCIUM-BASED SORBENTS

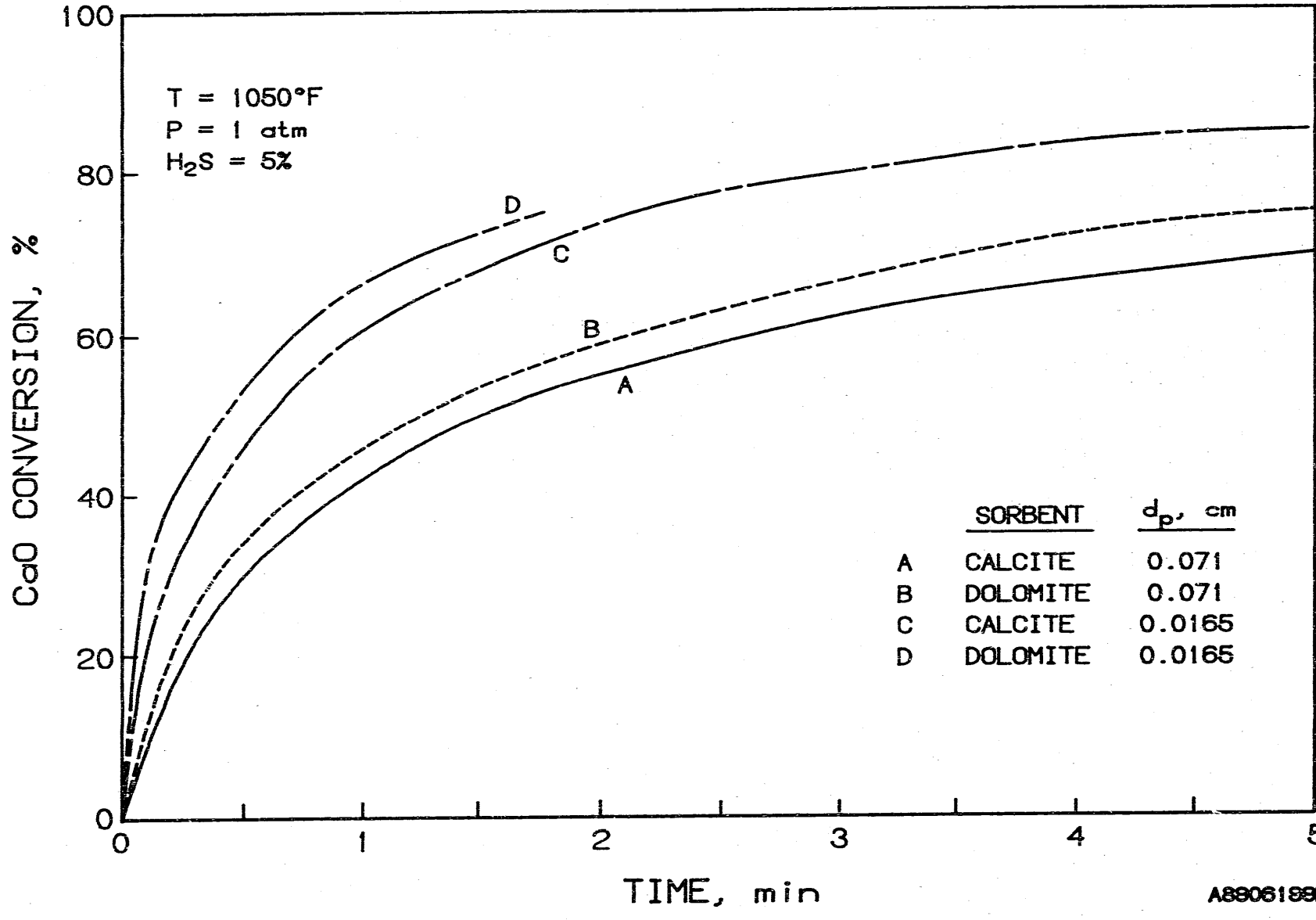

Figure 3-4. EFFECT OF SORBENT PARTICLE SIZE ON SULFIDATION REACTION RATE INVOLVING CALCINED CALCIUM-BASED SORBENTS

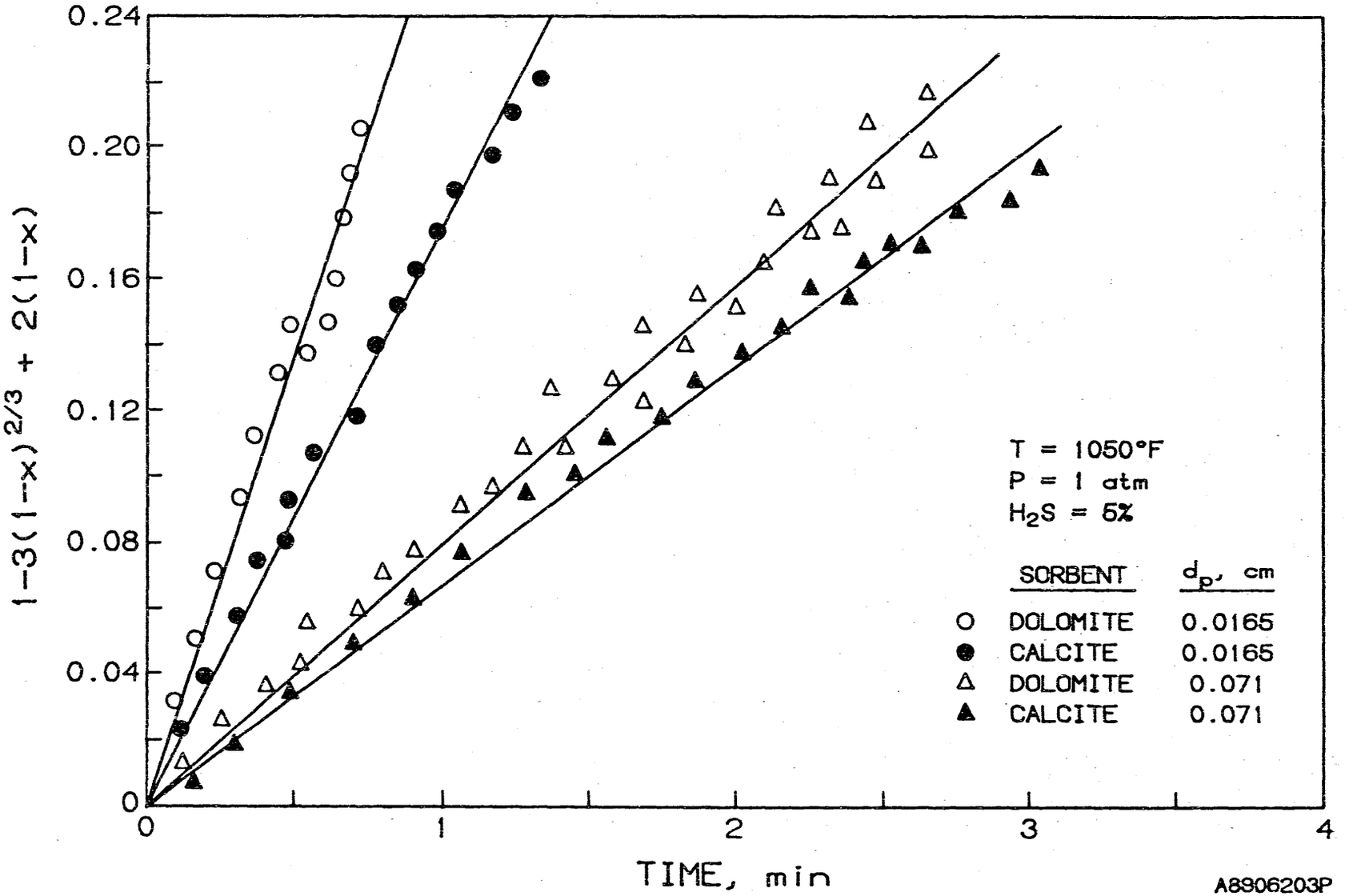

Figure 3-5. COMPARISON OF EXPERIMENTAL DATA WITH DIFFUSION-CONTROLLED, SHRINKING-CORE MODEL

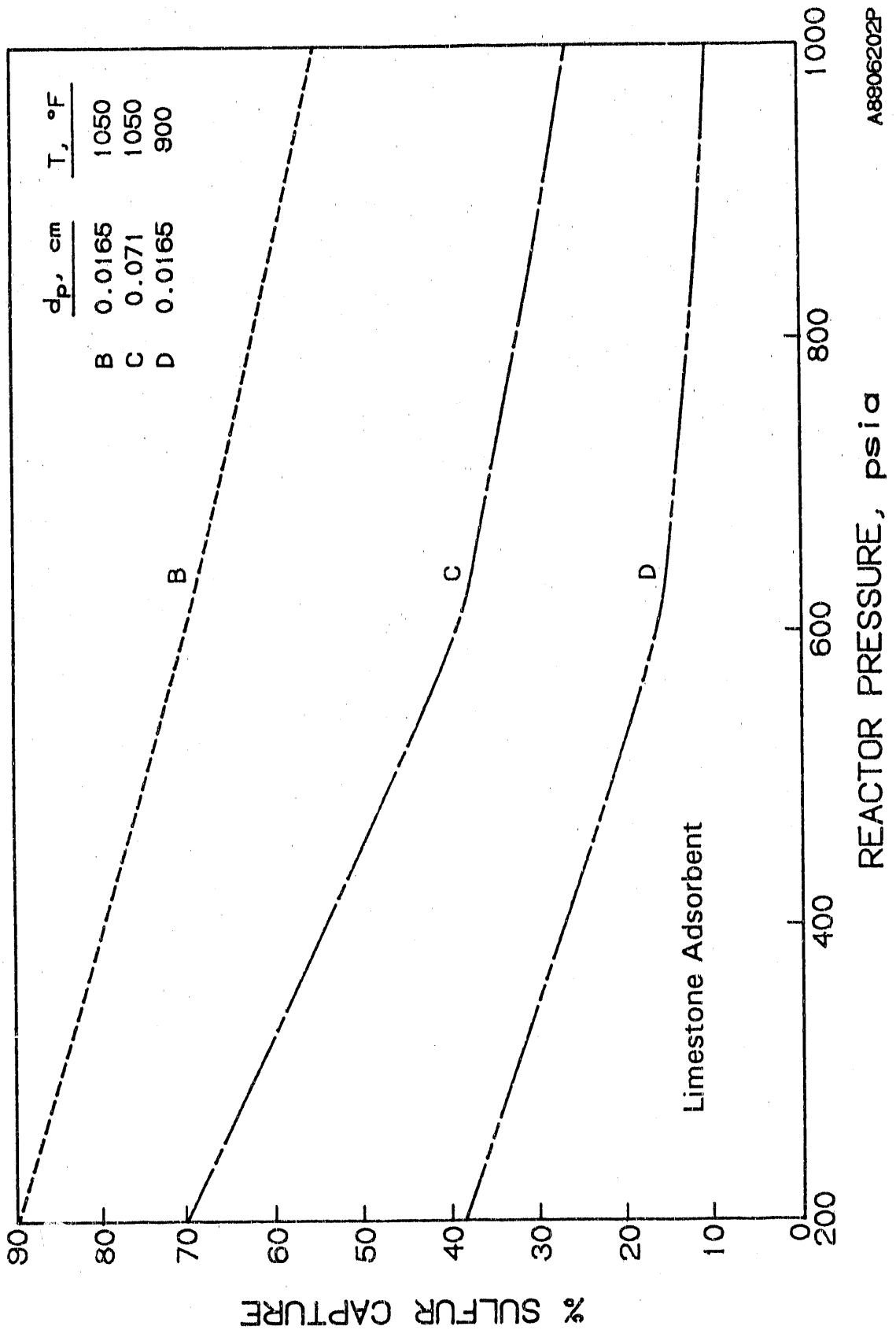

Figure 3-6. EFFECT OF REACTOR PRESSURE ON SULFUR CAPTURE

Experimental Equipment

A schematic diagram of the batch laboratory-scale PFH unit is shown in Figure 3-7. Major pieces of equipment that comprise the batch PFH system are a feed hopper with a preheat furnace, reactor, liquid collection vessel, recycle compressor, reactor and gas preheat split-tube furnaces, mass flow controllers, and a computer data acquisition and control system. In a typical test, 200 grams of sized shale is charged to the feed hopper and 200 ml of the same sized sand or sorbent is charged to the reactor. The system is pressurized with hydrogen, the reactor is heated to the desired retorting temperature, and the gas is circulated at fluidization velocities using the recycle compressor. A small flow of make-up hydrogen is also established. Shale is preheated in the feed hopper for the desired time and then dropped into the preheated fluidized sand or sorbent bed, which is already at retorting conditions. Reactor conditions of temperature, pressure, and gas flow are maintained throughout the PFH tests. After the test, the furnaces, are shut off and opened. All product solids, liquids, and gases are carefully collected and analyzed.

Three batches of calcined limestone were prepared for batch and continuous PFH sulfur capture tests. It was not possible to prepare enough sorbent for all of the PFH tests in a single batch in the calcination reactor. Limestone from the same Michigan quarry was used for all three batches of calcined limestone. The first batch of sorbent was prepared from one sample of limestone, and the second and third batches of sorbent were prepared from a second limestone sample collected a year later. The same calcination procedure was used to prepare each batch of sorbent. Limestone was sized to -60+100 mesh, fluidized in nitrogen, heated to 1600°F (871°C), and then held at that temperature for 30 minutes. The calcined limestone was removed from the reactor and screened to -60+100 mesh to obtain the sorbent for the PFH tests. Analyses of the three batches of calcined limestone are presented in Table 3-4. The table also shows the PFH tests in which each batch of sorbent was used.

A total of 24 batch PFH tests were conducted using calcined limestone. Indiana shale was used for nine tests. Three tests were made with each of the other five shales. Sulfur analyses were performed on samples of feed and residue shale from the batch PFH tests with limestone and from a number of tests without limestone, but at similar conditions. Sulfur contents of a number of the product oils were also determined.

The effects of PFH operating conditions on the sulfur capture efficiency of calcined limestone were studied in Indiana shale tests. Indiana shale sulfur conversions with calcined limestone and with no sorbent are presented in Table 3-5. Sulfur conversions from tests with the other five shales are presented in Table 3-6.

Batch PFH Tests With Calcined Limestone and Indiana Shale

With no sorbent added, the average sulfur conversions to oil and gas (except for Test 92) were 3.5% and 44.5%, respectively. There is no apparent correlation between sulfur conversions and temperature [843° to 1084°F (450° to 584°C)], pressure [400 to 1000 psig (2.8 to 7.0 MPa)], or residence time (3 to 23 minutes).

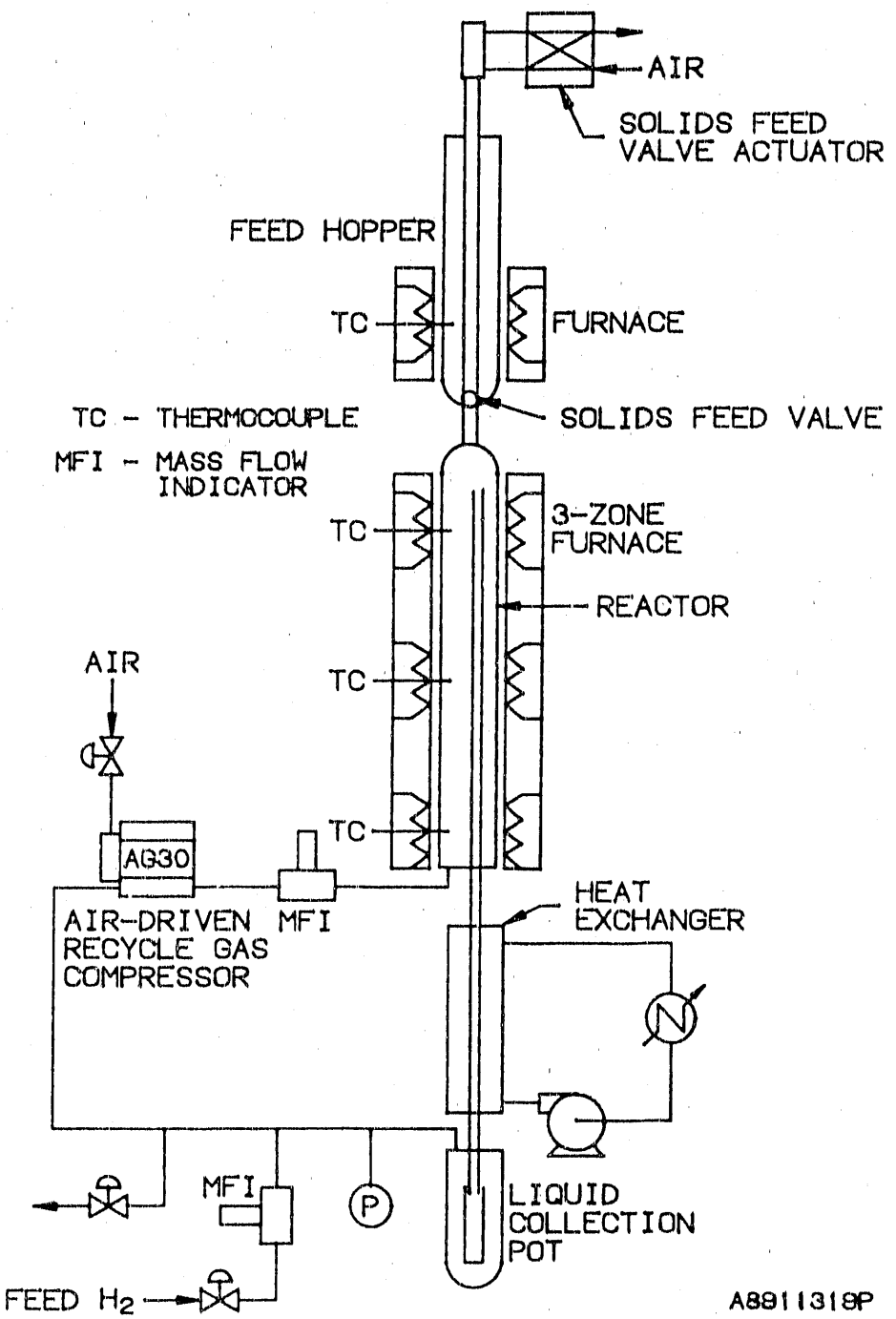

Figure 3-7. SCHEMATIC DIAGRAM OF BATCH LABORATORY-SCALE PFH UNIT

Table 3-4. ANALYSES OF CALCINED LIMESTONE

Batch No.	1	2	3
Batch PFH Test No.	103-124	125-137	138-142
Continuous PFH Test No.		C-41	
Composition, wt %			
CaO	96.2	84.1	92.5
$CaCO_3$	2.5	2.8	3.6
Others	1.3	13.1	3.9
Total	100.0	100.0	100.0
Distribution, % of feed Ca			
CaO	98.6	98.2	96.3
$CaCO_3$	1.4	1.8	3.7
Total	100.0	100.0	100.0

Calcined limestone from Batch 1 was added to the feed shale in Tests 103, 106, 107, 108, 111, and 112. Since the results of earlier batch tests conducted without limestone addition showed that the sulfur conversion reactions were completed in 3 to 5 minutes, a 5-minute residence time was chosen for all batch PFH sulfur capture tests. Test operating conditions were varied to study the effects of pressure, temperature, and feed calcium-to-sulfur ratio on the sulfur capture efficiency when using the sorbent. Sulfur capture efficiency is defined as the percent reduction in sulfur conversion to gas (as H_2S). Temperatures and pressures of 900° and 1050°F (482° and 565°C), and 400 and 600 psig (2.8 and 4.2 MPa), respectively, were tested. Sufficient sorbent was included to provide 0.5, 1.0, or 1.5 moles of calcium for every mole of feed sulfur. Since 50% of the sulfur is converted to H_2S during hydroretorting, the ratios of calcium to H_2S were 1:1, 2:1, or 3:1.

The use of the calcined limestone sorbent did not significantly affect the sulfur conversion to oil. With no sorbent added, the product oil contained 0.9% to 1.3% sulfur (3.0% to 3.9% of the feed sulfur). The addition of sorbent did not change the amount of sulfur in the oil (1.2% to 1.3%).

The effects of batch PFH test conditions on the sulfur capture efficiency is summarized in Figure 3-8. At 900°F and 600 psig (482°C and 4.2 MPa), with a calcium to H_2S ratio of 3:1, about 16% of the calcium is converted to calcium sulfide resulting in a sulfur capture efficiency of 48%.

Increasing the reactor temperature from 900° to 1050°F (482° to 565°C) increased the calcium conversion to calcium sulfide at 600 psig (4.2 MPa), from 16% to 29%. At 1050°F and 600 psig (565°C and 4.2 MPa), a Ca/H_2S ratio of 3:1 resulted in a sulfur capture efficiency of 87%.

The effects of pressure were studied by conducting a series of tests using a Ca/H_2S ratio of 3:1. At 900°F (482°C), sulfur capture efficiency was 48% at 600 psig (4.2 MPa) and 58% at 400 psig (2.8 MPa). At 1050°F (565°C), the sulfur capture efficiency increased from 87% at 600 psig (4.2 MPa) to 96% at 400 psig (2.8 MPa).

Table 3-5. SULFUR CONVERSIONS ACHIEVED IN BATCH PFH TESTS WITH INDIANA NEW ALBANY SHALE

Test No.	Temp., °F	Press., psig	Residence Time, min	Sorbent	Ca/S[2] mol. Ratio	Gas Recycle	Sulfur,[3] wt % Residue	Sulfur,[3] wt % Oil	Sulfur Conversion, % of Feed Sulfur Oil	Sulfur Conversion, % of Feed Sulfur Gas[5]	Sulfur Capture Efficiency,[7] %
70	843	1009	14	No	0	Yes	1.92	NA[4]	NA	44.5[6]	—
89	908	409	18	No	0	Yes	1.70	0.92	3.0	49.7	—
90	894	602	4	No	0	Yes	1.87	NA	NA	44.8[6]	—
84	917	615	22	No	0	Yes	1.98	NA	NA	42.4[6]	—
79	906	1003	4	No	0	Yes	1.99	NA	NA	43.4[6]	—
91	896	1020	23	No	0	Yes	1.71	0.96	3.5	50.8	—
93	1037	420	23	No	0	Yes	2.05	1.29	3.9	40.5	—
92	1084	597	13	No	0	Yes	2.49	1.08	3.6	29.4	—
55	1053	1002	6	No	0	Yes	2.10	NA	NA	40.4[6]	—
47	1060	988	13	No	0	Yes	2.05	NA	NA	42.9[6]	—
103	1051	599	3	CaO[1]	1.5	Yes	3.19	1.24	3.7	5.6	87.4
106	898	634	5	CaO	1.5	Yes	2.36	1.17	3.7	23.3	47.5
107	918	600	3	CaO	1.0	Yes	2.79	1.25	4.3	28.7	35.3
108	922	590	5	CaO	0.5	Yes	1.91	1.28	4.1	40.4	9.0
111	1062	412	5	CaO	1.5	Yes	3.11	1.20	4.1	1.7	96.2
112	934	418	3	CaO	1.5	Yes	2.50	1.28	4.0	18.8	57.6
135	1110	618	3	CaO	1.5	No	2.15	1.34	NA	31.7	32.6
136[9]	1102	622	7	CaO	1.5	No[8]	2.56	0.93	NA	20.8	55.7
137[9]	1114	621	5	CaO	1.5	No	1.59	1.04	NA	49.7	0

[1] Calcined limestone.
[2] Added Ca/feed shale S.
[3] Feed shale sulfur = 3.07 wt % (dry).
[4] NA = not available.
[5] By difference.
[6] Using average sulfur conversion to oil = 3.5%.
[7] Decrease in H_2S production.
[8] High gas velocity; 1.5 x u_{mf}.
[9] Sorbent mixed and preheated with sand.

55WP/61090t3-5/RPP

Table 3-6. SULFUR CONVERSIONS ACHIEVED IN TESTS CONDUCTED WITH CALCINED LIMESTONE IN THE BATCH PFH REACTOR

Test No.	Shale	Temp., °F	Press., psig	Residence Time, min	Sorbent	Sorbent Batch	Gas Recycle	Sulfur, wt %			Conversion % of Feed Sulfur		Sulfur Capture Efficiency,[4] %
								Shale	Residue	Oil	Oil	Gas[2]	
58	OH	1064	979	22	No	—	Yes	2.25	1.22	NA[1]	NA	28.1[3]	—
62	OH	905	1003	24	No	—	Yes	2.25	1.27	NA	NA	27.8[3]	—
121	OH	1077	593	4	CaO[6]	1	Yes	2.25	2.73	1.47	4.4	0.0	100.0
122	OH	942	590	4	CaO	1	Yes	2.25	2.07	1.22	3.8	10.1	63.9
138[7]	OH	1066	613	6	CaO	3	No[8]	2.25	0.75	1.48	4.4[5]	64.9	0.0
63	MI	1044	1005	23	No	—	Yes	3.05	1.86	NA	NA	22.3[3]	—
66	MI	912	402	23	No	—	Yes	3.05	1.35	NA	NA	40.2[3]	—
123	MI	1079	599	5	CaO	1	Yes	3.05	2.81	1.55	2.6	8.7	78.4
124	MI	959	596	3	CaO	1	Yes	3.05	2.18	1.36	2.3	27.3	32.1
139[7]	MI	1072	640	8	CaO	3	No[8]	3.05	1.93	1.58	2.6[5]	36.1	10.2
68	KY	1051	1003	24	No	—	Yes	5.37	2.78	NA	NA	36.0	—
118	KY	957	398	18	No	—	Yes	5.37	3.58	NA	NA	41.7[3]	—
125	KY	1079	573	4	CaO	2	Yes	5.37	4.04	1.28	2.0	23.2	40.3
126	KY	938	605	4	CaO	2	Yes	5.37	3.50	1.19	2.4	31.4	19.2
140[7]	KY	1068	612	6	CaO	3	No[8]	5.37	2.94	1.58	2.5[5]	45.3	0.0
80	TN	1061	1001	22	No	—	Yes	7.08	3.36	NA	NA	38.2[3]	—
85	TN	910	398	22	No	—	Yes	7.08	3.49	NA	NA	35.8[3]	—
127	TN	1073	615	4	CaO	2	Yes	7.08	5.55	1.79	1.9	15.7	57.6
128	TN	945	589	5	CaO	2	Yes	7.08	4.62	1.63	1.9	28.9	21.9
141[7]	TN	1074	609	6	CaO	3	No[8]	7.08	4.02	1.98	2.1[5]	38.9	0.0
73	AL	1067	1013	24	No	—	Yes	8.93	3.95	NA	NA	41.2[3]	—
78	AL	899	400	24	No	—	Yes	8.93	4.10	NA	NA	43.3[3]	—
129	AL	1086	614	6	CaO	2	Yes	8.93	6.83	1.95	2.3	17.3	59.1
130	AL	946	600	4	CaO	2	Yes	8.93	5.90	1.96	2.4	27.4	35.1
142[7]	AL	1074	599	6	CaO	3	No[8]	8.93	4.10	2.51	2.6[5]	49.4	0.0

[1] NA = not available.
[2] By difference.
[3] Using average sulfur conversion to oil.
[4] Decrease in H_2S production.
[5] Estimated.
[6] Calcined limestone, molar Ca/S = 1.5.
[7] Sorbent mixed and preheated with sand.
[8] High gas velocity, 1.5 X u_{mf}.

55WP/61090t3-6/RPP

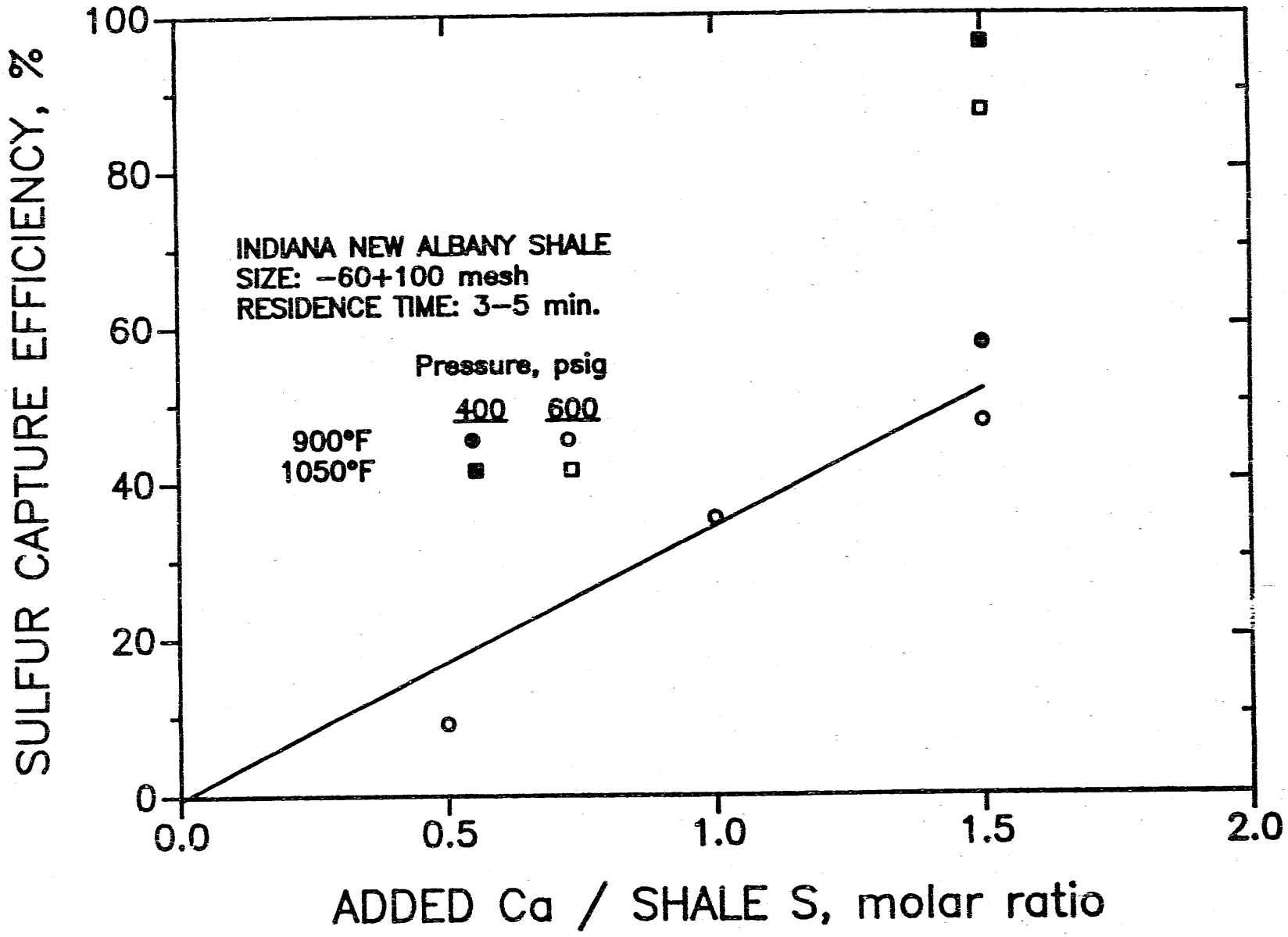

Figure 3-8. THE EFFECTS OF ADDED Ca/SHALE S RATIO AND OPERATING CONDITIONS ON SULFUR CAPTURE EFFICIENCY

The calcined limestone sorbent has been found to be very effective at capturing H_2S. The highest sulfur capture efficiency observed was at reactor conditions of 1050°F and 400 psig (565°C and 2.8 MPa) using a Ca/H_2S ratio of 3:1. At this condition, 32% of the calcium was converted to calcium sulfide, and a sulfur capture efficiency of 96% was achieved. Analysis of test results suggests that a high level of sulfur capture efficiency could be obtained at other temperatures and pressures by increasing the Ca/S ratio.

The first batch of calcined limestone proved to be an effective sulfur capture sorbent in the first six Indiana shale tests. The second batch of limestone did not show the same high sulfur capture efficiency when used with other shales. In order to compare the first and second batches of sorbent, three final batch PFH tests were conducted with Indiana shale.

The short shale residence times were chosen to allow sufficient time for the product gas to pass only once through the reactor. A 'single pass' of feed gas was used in Tests 135, 136, and 137 to ensure that no product gas was recycled to the reactor. All three tests were conducted at 1050°F (565°C) (or higher) and 600 psig (4.2 MPa) with a residence time of 3 to 7 minutes and a calcined limestone to sulfur ratio of 1:5.

Test 135 was conducted with a shale-sorbent mixture introduced to the bed from the feed hopper. A sulfur capture efficiency of 33% was achieved compared to an expected value of 80% to 90%. The lower than expected sulfur capture efficiency in Test 135 may be attributed to the product H_2S being generated and swept from the reactor before the sorbent is at a high enough temperature to be effective.

In Tests 136 and 137 the sorbent and the sand were mixed and loaded in the reactor. The shale was introduced after the mixture was preheated and fluidized. Operating conditions for the tests were similar, except Test 137 was fluidized at the minimum fluidization velocity, and Test 136 had a feed gas flow rate 1.5 times the minimum fluidization velocity.

At minimum fluidization (Test 137), no sulfur capture was achieved. This indicates the bed was not well mixed. The product H_2S was generated in the top of the bed and left the reactor before contacting the sorbent. At 1.5 times minimum fluidization (Test 136), a sulfur capture efficiency of 57% was achieved. Good solids mixing resulted in much greater sulfur capture, but the sulfur capture efficiency was lower than expected based on results from batch tests conducted previously using the first batch of calcined limestone. Results from Tests 135 to 137 indicated the second batch of sorbents was not as effective as the first batch.

Batch PFH Tests With Calcined Limestone and Other Shales

Calcined limestone was used as a sorbent for 15 tests with the Alabama, Kentucky, Michigan, Ohio, and Tennessee shales. The same operating conditions were used for three tests with each of the five shales. Residence times were 3 to 5 minutes for all tests since Indiana shale tests showed H_2S production was complete in this amount of time. The pressure was 600 psig and the Ca/S molar ratio was 1.5 for all tests. The first two tests with each shale used feed gas recycle, and the temperatures were 900° and 1050°F (482° and 565°C). In the final test with each shale, a temperature of 1050°F (565°C) was again

used, but a 'single pass' of feed hydrogen was used instead of a recycle feed gas. The sorbent was mixed and preheated with the sand in the last test with each shale, and a gas velocity of 1.5 times the minimum fluidization velocity was used to ensure good solids mixing and exposure of the sorbent to the product H_2S.

The sulfur capture efficiency of the calcined limestone increased with increasing temperature in PFH tests with all five shales. This result agrees with earlier Indiana shale PFH tests at the same 900° and 1050°F (482° and 565°C) temperatures. Analyses of the oils from Indiana shale tests and tests with the other five shales showed no apparent effect of the sorbent on the amount of sulfur in the oil. The sulfur contents of the product shale oils ranged from 1.2 to 2.0 weight percent (or 2% to 4% of the feed sulfur).

The first two sulfur capture tests with Ohio and Michigan shale were performed using sorbent from the first batch of calcined limestone. The second batch of calcined limestone provided sorbent for the first two tests with Kentucky, Tennessee, and Alabama shales. The third batch of sorbent was used for the final test with all five shales. Higher sulfur capture efficiencies were obtained in the Ohio and Michigan shale tests than in tests with the other three shales. These results agree with the Indiana shale tests, which indicate that the first batch of sorbent was more reactive than the second batch.

Almost no sulfur capture was achieved in the 'single pass' tests using the third batch of calcined limestone. This suggests that the third batch of sorbent was even less reactive than the second batch.

TGA Tests With Calcined Limestone Used in PFH Tests

The first batch of calcined limestone appeared to be more reactive than the other two batches. After completion of the batch and continuous PFH tests, a series of tests were conducted in a TGA to quantify the relative reactivities of the three sorbent batches. Additional TGA tests were conducted to identify a more reactive calcium-based sulfur sorbent.

In the TGA tests, samples were exposed to a reactant gas containing 5 mole percent H_2S at a temperature of 1050°F (565°C). The CaO conversions versus time for the three samples are shown in Figure 3-9. The TGA results confirm the batch and continuous PFH results. The first batch of calcined limestone was much more reactive than the second and third batches. A screen analysis showed that the sorbent from the first batch was less than 100 mesh, but size alone can not explain the difference in reactivity between the batches of sorbent.

Four additional calcined limestone samples were tested for reactivity. The first sample was from the original batch of limestone used in the batch PFH tests. The second sample was obtained a year later from the same quarry. The third sample was obtained from a quarry in Alpena, Michigan. The fourth was from the original limestone sample, which was calcined and then partially hydrated. The three calcined limestones and one hydrated calcined limestone were also sulfided at 1050°F (565°C) in a reactant gas containing 5 mole percent H_2S. Calcium conversions-versus-temperature curves for all four samples are presented in Figure 3-10.

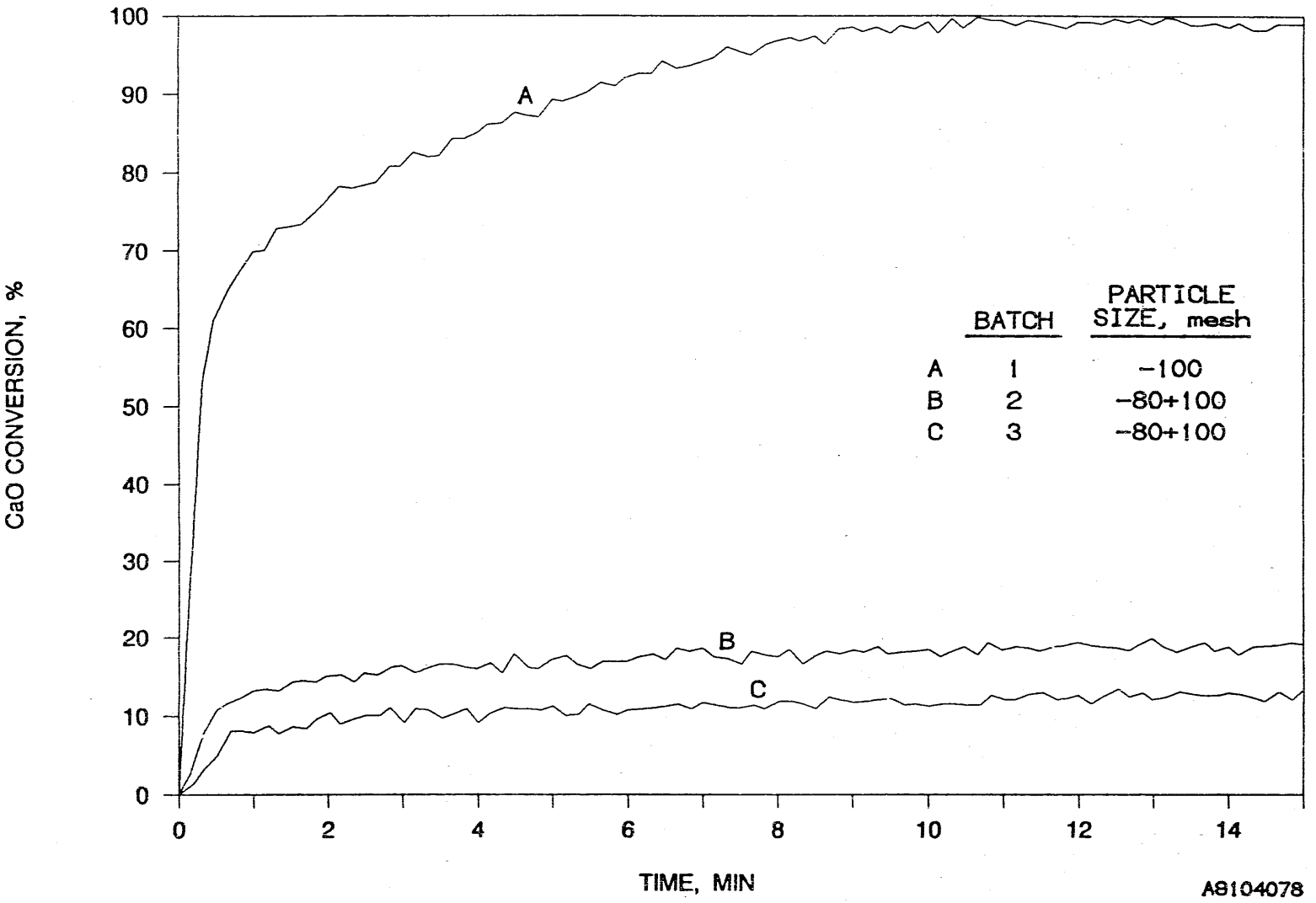

Figure 3-9. CaO CONVERSION OF CALCINED LIMESTONE BATCHES

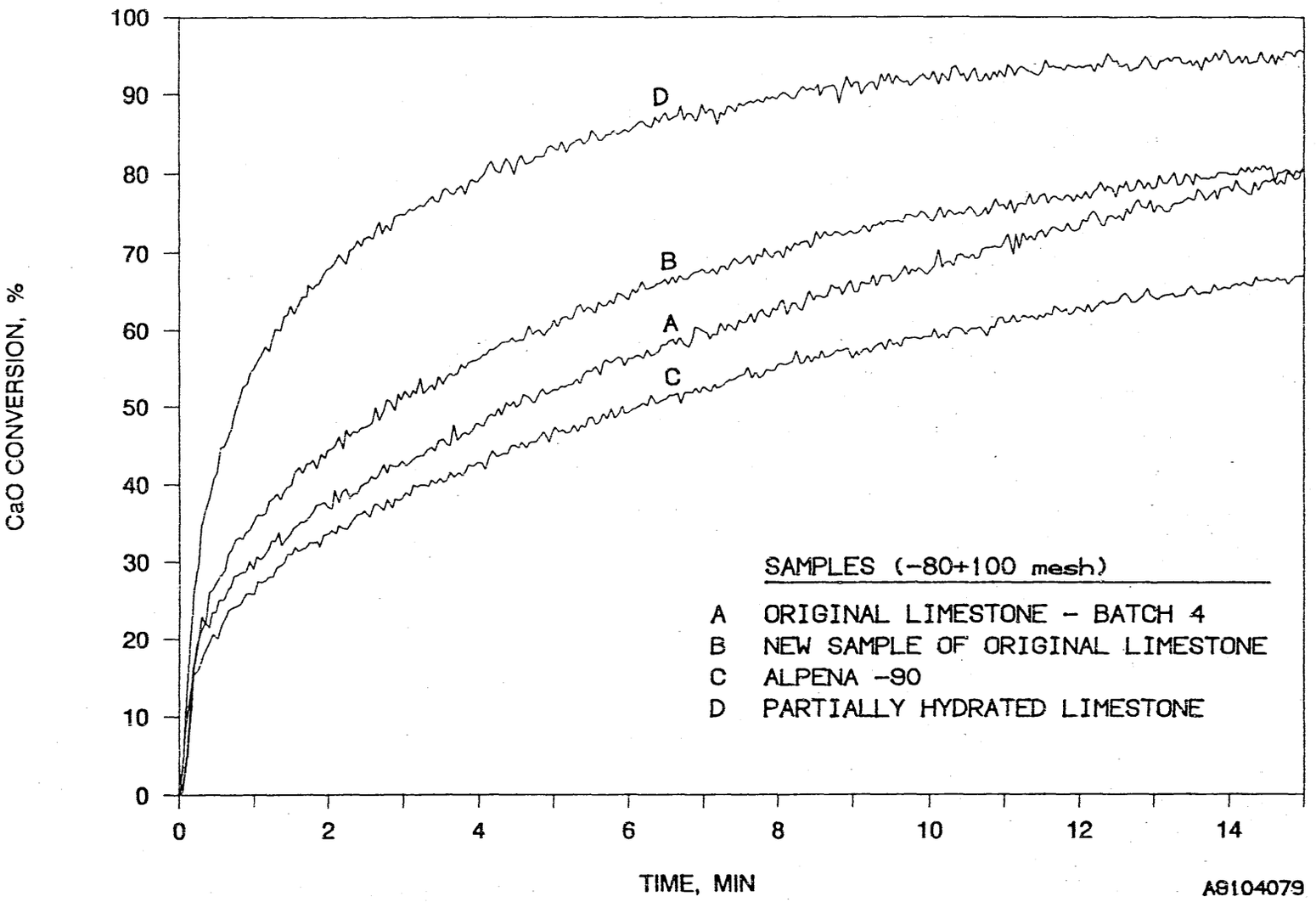

Figure 3-10. CaO CONVERSION OF NEW CALCINED LIMESTONE BATCHES

The results showed that the two batches of the original limestone and the Alpena limestone have similar reactivities. All three calcined limestones were more reactive than the second and third batches and limestones used in the batch PFH tests, but less reactive than the first batch of limestone used in the PFH tests. The partially hydrated calcined limestone was more reactive than any of the calcined limestones tests. Except for the increase in the reactivity of the hydrated lime due to a large increase in surface area after hydration, the reasons for different reactivities among the calcined limestones were not determined.

TGA Siderite Tests

Siderite ($FeCO_3$) was considered as a second potential in-bed sulfur capture sorbent for the PFH process. The two-stage reaction path consists of the calcination of $FeCO_3$ to produce FeO and the reaction of FeO with H_2S to form FeS and H_2O. The sulfur capture efficiency of naturally occurring siderite was evaluated since economics would prohibit the use of pure, manufactured siderite in a commercial PFH process.

A sample of high-grade natural siderite from Nova Scotia was crushed and screened to a particle size consist of -60+100 mesh. Analysis (Table 3-7) of the raw, sized siderite sample showed that it contained about 43% iron and 33% carbon dioxide present as carbonate. Based on the assumption that the sulfur was originally present as FeS_2, the iron carbonate content of the raw sample was estimated to be about 60%.

Table 3-7. COMPOSITION OF RAW AND CALCINED SIDERITE FOR TGA AND BATCH PFH SULFUR-CAPTURE TESTS

	Siderite	
Sample	Raw	Calcined
Composition, wt %		
Calcium	1.70	6.50
Copper	0.31	0.10
Iron	43.40	70.00
Magnesium	2.50	4.50
Manganese	0.46	0.86
Zinc	0.16	0.13
CO_2 (as carbonate)	33.20	1.95
Sulfur	7.19	0.54
Others by diff. (mostly O_2)	11.08	15.42
Total	100.00	100.00

Two calcination and 3 sulfidation tests were conducted in an ambient pressure TGA at temperatures of 900° and 1050°F (482° and 565°C) to allow direct comparison with earlier tests conducted with the calcined-limestone sorbent.

Calcination tests conducted in a nitrogen atmosphere demonstrated that decomposition of siderite begins at about 900°F (482°C). The times required for complete calcination at 900° and 1050°F are 60 and 5 minutes, respectively.

The composition of the calcined siderite sample is also presented in Table 3-7. Calcination reduced the carbonate content to <2 weight percent. The higher calcium content of the calcined siderite sample compared with the raw sample is attributed to variations between the samples used for analysis.

In the sulfidation tests, fully calcined sorbents were reacted with a reactant gas containing 5 mole percent hydrogen sulfide, 20 mole percent hydrogen, and 75 mole percent nitrogen. At 1050°F (565°C), an estimated 65% of the iron oxide (in the calcined siderite) was converted to iron sulfide in 1 minute. The sorbent was fully sulfided in about 15 minutes. At 900°F (482°C), the estimated extent of sulfidation was about 45% after 1 minute, and a maximum conversion of 60% was achieved. The rate of reaction of calcined siderite with H_2S at 1050°F (565°C) is about the same as that of calcined limestone tested earlier. At 900°F (482°C), the rate of the sulfidation reaction is higher with calcined siderite than with calcined limestone. The sorbent conversions during the sulfidation tests for calcined siderite and calcined limestone at 900° to 1050°F (482° to 565°C) are presented in Figure 3-11.

Two tests were conducted in a high-temperature, high-pressure thermobalance reactor to determine the effect of elevated pressure on the reactivity of siderite and sulfur. The tests were conducted at 1050°F and 300 psig (565°C and 2.2 MPa). In one test, the sorbent was first calcined and then reacted with H_2S simulating a PFH reactor with calcined siderite injection. In the second test, uncalcined siderite was exposed to the reactant gas containing H_2S at 1050°F (565°C).

The rates of sulfidation at 1050°F and 300 psig (565°C and 2.2 MPa) are shown in Figure 3-12. At these conditions, the rate of sulfidation for precalcined siderite is more than double the sulfidation rate for raw siderite. Comparison of the rates of calcined siderite sulfidation at 0 psig (Figure 3-11) and 300 psig (Figure 3-12) shows that the reaction is faster at low pressure. Increasing the pressure decreases the global rate of sulfidation because the rate of gas diffusion decreases with increasing pressure.

Batch PFH Siderite Tests

Four batch PFH tests were performed with Indiana shale and siderite in-bed sulfur capture sorbents. The sorbent for the first two tests was calcined siderite, and raw siderite was used as the sorbent in the other two tests. For all four tests, the iron (added)-to-shale sulfur molar ratio was 1.5, corresponding to an iron-to-H_2S molar ratio of 3. The sorbents and feed shale were mixed and introduced to the fluidized bed together. Operating conditions, sulfur conversions, and sorbent sulfur capture efficiencies for Tests 131 to 134 are presented in Tables 3-8 and 3-9.

The tests with calcined siderite were performed at 1050°F and 600 psig (565°C and 4.2 MPa) with residence times of 5 and 30 minutes. Sulfur capture

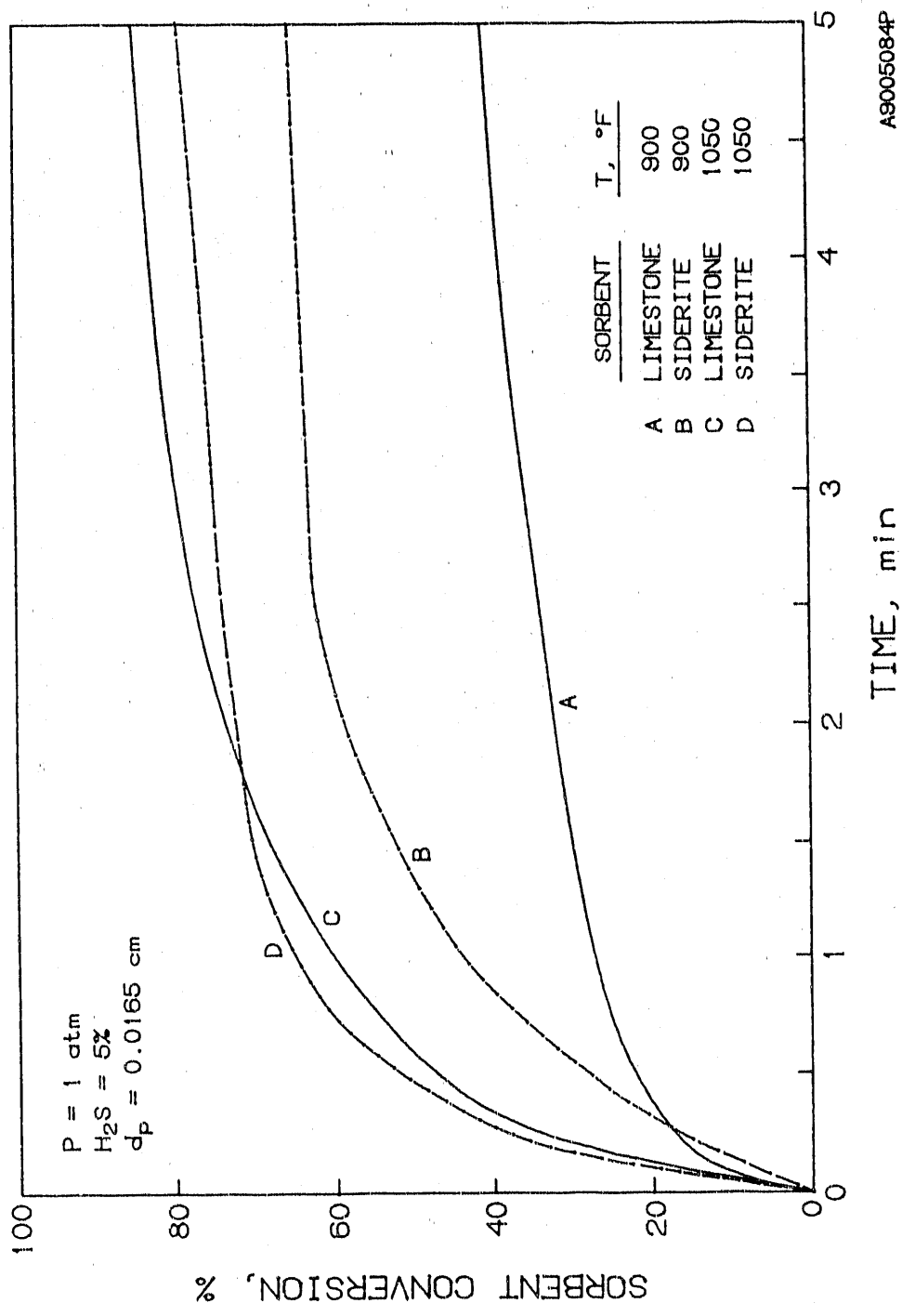

Figure 3-11. EFFECT OF SORBENT TYPE AND TEMPERATURE ON SULFIDATION REACTION RATE

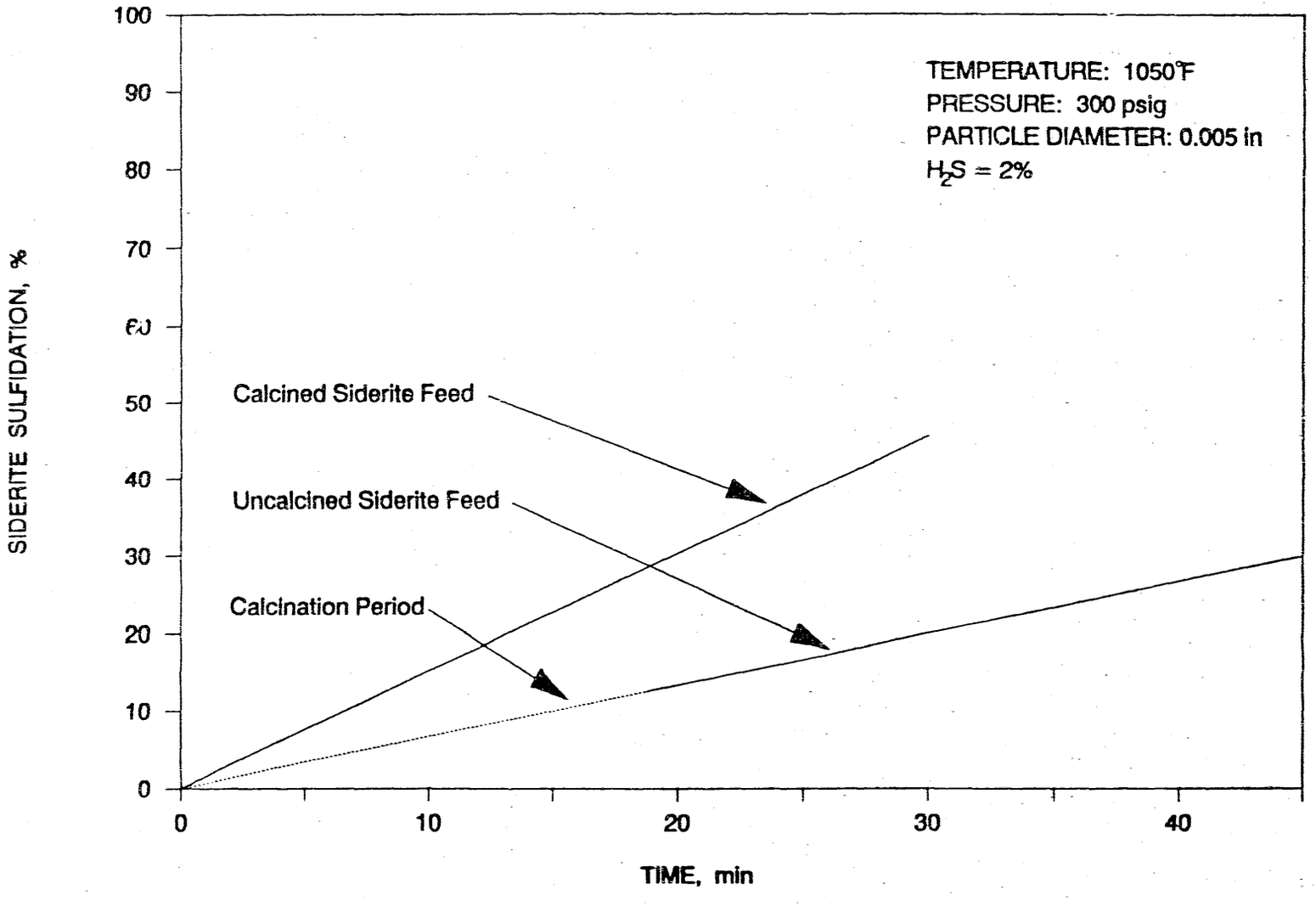

Figure 3-12. EFFECT OF CALCINATION ON THE SULFIDATION OF SIDERITE

Table 3-8. OPERATING CONDITIONS OF BATCH PFH SULFUR CAPTURE TESTS WITH INDIANA SHALE AND SIDERITE

Test	Temp, °F	Press., psig	Residence Time, min	Sorbent	Fe/S Mole Ratio
47	1060	986	13	No	0
89	907	401	18	No	0
131	1097	588	28	FeO[1]	1.5
132	1088	595	5	FeO	1.5
133	1084	583	30	$FeCO_3$[2]	1.5
134	949	607	28	$FeCO_3$	1.5

[1] Calcined siderite.

[2] Siderite.

Table 3-9. SULFUR CONVERSIONS ACHIEVED IN TESTS CONDUCTED WITH INDIANA SHALE AND CALCINED LIMESTONE IN THE BATCH PFH REACTOR

	Sulfur, wt %				Conversion, % of Feed Sulfur		
Test	Shale	Sorbent	Residue[1]	Oil	Oil	Gas[4]	Sulfur Capture Efficiency,[5] %
47	3.07	--	2.05	NA[2]	4.0[3]	42.4	0
89	3.07	--	1.70	0.92	3.0	49.7	0
131	3.07	0.54	3.47	1.55	4.0[3]	0	100.0
132	3.07	0.54	3.06	1.01	4.0[3]	2.1	95.5
133	3.07	7.19	3.67	1.25	4.0[3]	21.7	53.9
134	3.07	7.19	3.03	1.25	4.0[3]	20.1	57.2

[1] Shale and sorbent.

[2] NA = Not available.

[3] Average of 8 batch PFH oil samples.

[4] By difference.

[5] Decrease in H_2S production.

efficiencies of 95% and 100% were achieved in the two tests. This level of sulfur capture is comparable with the best values achieved with the most reactive calcined limestone (first batch).

Tests using raw siderite sorbent were conducted at 950° and 1050°F (510° and 565°C) using a pressure of 600 psig (4.2 MPa) and a shale residence time of 30 minutes. The raw siderite did not prove to be as effective a sorbent as calcined siderite. At similar conditions, raw siderite captured 53% and 57% of sulfur from the product H_2S, while calcined siderite removed essentially all of the product H_2S. Results of the batch PFH tests with raw and calcined siderite are in good agreement with the TGA tests conducted with these sorbents.

Subtask 3.1.2. Lab-Scale Continuous Tests

The objectives of this subtask were to obtain steady-state data for characterizing gas, liquid, and solids products and to perform material balances for in-bed sulfur-capture tests at selected conditions of temperature, pressure, and limestone-to-shale ratio as determined in Subtask 3.1.1.

Experimental Equipment

The continuous PFH unit includes a feed hopper, reactor, unsteady state and steady-state solids and liquids receivers, feed and residue screws, a recycle compressor, split-tube furnaces, mass flow controllers for the recycle and makeup hydrogen gases, a dry gas meter, and a computer-based data acquisition and control system (Figure 3-13). The feed hopper can hold 4000 grams of raw shale permitting tests of up to 5 hours with a feed rate of 700 g/h.

At the beginning of a test, the temperatures, pressure, solids feed and discharge rates, and the gas recycle rate are established. Steady-state data collection is started after at least three bed turnovers at steady-state conditions. Steady-state residue solids and product liquids are collected in separate vessels, and gas samples are taken at the beginning, middle, and end of steady-state operation. All residue solids and product liquids and gases are analyzed for each test. Weights and sample analyses are used for carbon balance, oil yield, and sulfur conversion calculations. Operation in the continuous unit generates larger quantities of effluents for characterization than batch unit operation.

Results and Discussion

One sulfur capture test (C-41) was performed in the continuous PFH unit with Indiana shale and calcined limestone from the second batch. (See Table 3-4.) The operating conditions were a temperature of 1069°F (576°C) and a pressure of 613 psig (4.3 MPa) with a 39-minute average shale residence time. Shale and sorbent were mixed in a calcium-to-sulfur molar ratio of 1.5 and placed in the feed hopper. Solids were charged to the reactor from the ambient temperature feed hopper. A single pass of feed hydrogen was used to prevent recycle of product H_2S back to the reactor. Operating conditions and sulfur conversions for Test C-41 are presented in Table 3-10.

Sulfur capture efficiency in Test C-41 was 30%. This demonstrates in-bed sulfur capture in a continuous unit is possible. However, the level of sulfur

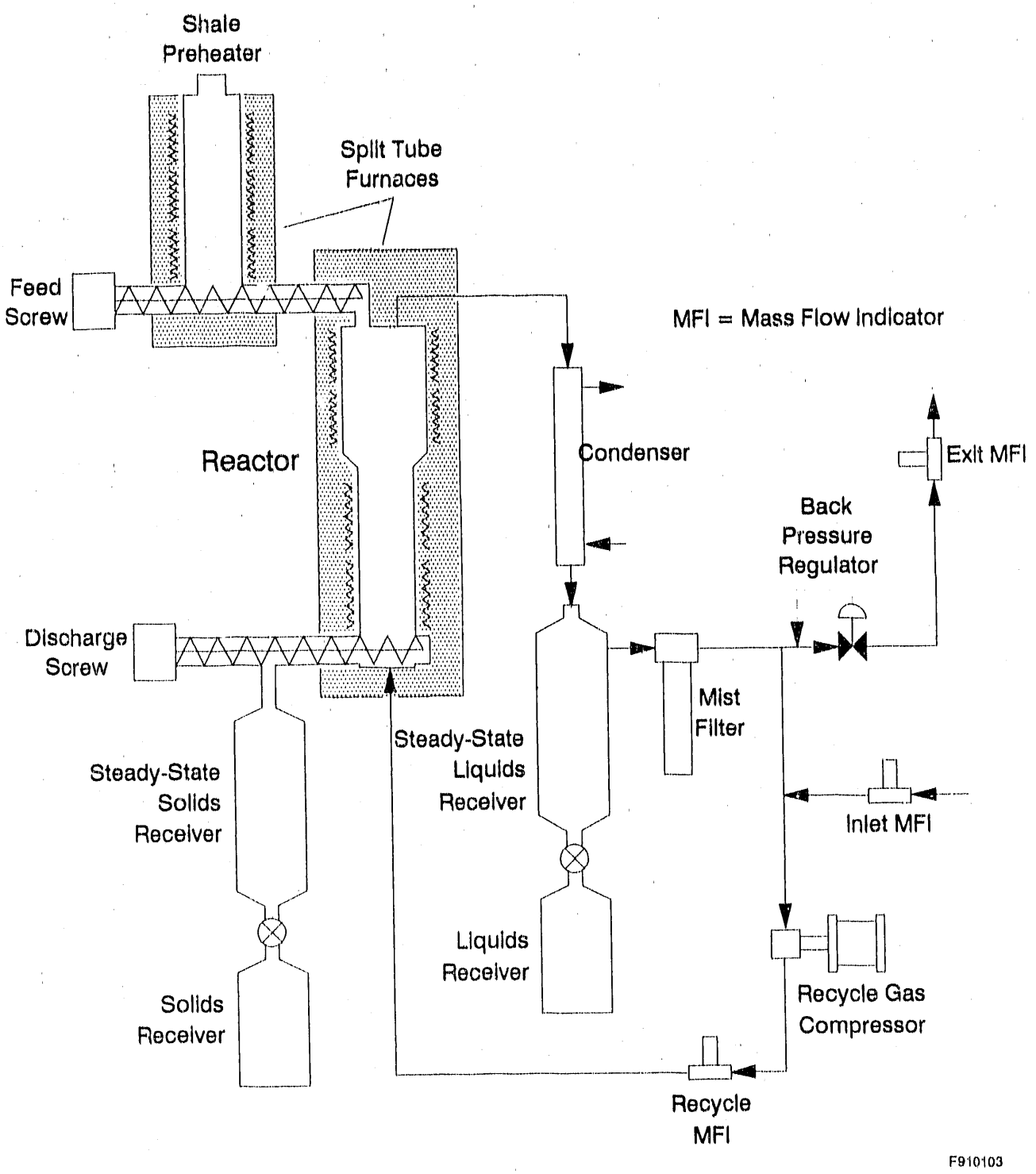

Figure 3-13. SCHEMATIC DIAGRAM OF LABORATORY-SCALE CONTINUOUS PFH UNIT

Table 3-10. SUMMARY OF OPERATING CONDITIONS AND RESULTS OF CONTINUOUS PFH SULFUR CAPTURE TEST

Test No.	C-41
Shale	Indiana New Albany
Sorbent[1]	CaO
Feed Ca/S, mole ratio	1.5
Operating Conditions	
Average Feed Hopper Temperature, °F	78
Feed Hopper Shale Residence Time, min	--
Average Reactor Temperature, °F	1069
Reactor Shale Residence Time, min	39
Pressure, psig	613
Shale Particle Size, mesh	-60+100
Superficial Gas Velocity ft/s	0.099
Minimum Fluidization Velocity, ft/s	0.056
Operating Results	
Product Distribution, % feed sulfur	
Spent Shale	63.3
H_2S[2]	4.0
Oil	32.7
Total	100.0
Sulfur Capture Efficiency,[3] %	30

[1] Calcined limestone.

[2] By difference.

[3] Fraction of product H_2S captured by sorbent.

capture achieved with the second batch was lower than expected based on batch tests with the first batch of sorbent.

Subtask 3.1.3. Bench-Scale Tests

The objective of this subtask was to conduct in-bed sulfur-capture tests in a bench-scale unit to determine the effects of scale-up from laboratory-scale tests and to provide data for environmental mitigation analyses.

Discussion

A suitably active sorbent was not identified for retorting conditions; therefore, this task was not conducted.

55WP/61090T3/RPP

Subtask 3.2. Dry Electrostatic Desulfurization of Eastern Oil Shales

Preface

The electrostatic process investigated in this study for desulfurization and/or beneficiation of Eastern oil shales was also tested for Illinois coals. The results of tests with Illinois coals are included here to provide an overall picture of the process and to compare the efficacy of the process for coal and shale beneficiation. The coal desulfurization work was performed with matching funds from the Illinois Institute of Technology (IIT).

Summary

This report presents the work performed by IIT, from October 1, 1987, through April 30, 1990, under Subcontract No. S1-14062 with IGT for Subtask 3.2. "Dry Electrostatic Desulfurization of Eastern Oil Shales" of the overall program on "Pressurized Fluidized-Bed Hydroretorting of Eastern Oil Shales." This program was funded by DOE/METC under prime Contract No. DE-AC21-87MC11089.

The basis of the electrostatic shale desulfurization or beneficiation method is the observation that carbonaceous matter present in shale can be made to acquire a positive charge, while mineral matter, including pyrites, can be charged negatively with a copper tribocharger. Hence, the application of a direct high-voltage electric field results in a clear separation, once the pyrites and minerals have been liberated from the organic matrix by grinding or by other means.

The grain size of mineral inclusions present in coal and shale was determined using scanning electron and optical microscopes. The pyrite and mineral particles occurred in the particle size range of 5 to 10 μm in an Eastern oil shale (Indiana New Albany) sample, making it necessary to grind the particles to these fine sizes for the liberation of mineral inclusions.

In view of the requirement of grinding the shale particles to 5 μm that fall into the Geldart type "C" classification (cohesive powders), the use of an electrofluidized bed for separating particles was not feasible. Hence, the work under this contract involved only the use of pneumatic electrostatic conveyor.

The electrostatic force principally responsible for the separation, is the product of the surface charge of the particles and the applied electric field strength. The surface charge on the particles was imparted using a copper tribocharger. The magnitude and polarity of charge was found to depend primarily on the work functions and, to a lesser degree, on elastic and electrical properties of the particle and the material of the tribocharger. A semi-empirical approach was developed to correlate the charge with these properties and to choose a suitable material for the tribocharger. The surface charge of the particles was measured using a Faraday cage, and a parametric study was conducted to investigate the effect of various process variables on particle charging.

The surface charge measurements of various shales containing different kerogen contents and ground to an average particle size of 5 μm showed that

charge becomes more positive with an increase in the kerogen content. This observation in conjunction with charge measurements for a low-ash coal and charcoal confirmed that the kerogen in the shale acquires a positive charge with the copper tribocharger. On the other hand, the measured value of the charge acquired by mineral matter and pyrite particles was negative with mineral particles carrying a charge about 2.5 times that of pyrites. This observation made it difficult to separate only the pyrites from the shale without separating mineral matter. Hence, the process resulted in a beneficiation technique, rather than a desulfurization technique.

IIT's electrostatic pneumatic conveyor, which had performed very well with Illinois No. 2 coal, was used in this study. This separator had perforated aluminum electrodes. In the case of finely ground shale, which exhibited a very strong cohesive nature, severe flow problems were encountered. Hence, experiments were restricted to batch units.

The separation tests in a batch separator showed an 80% ash and a 70% pyrite removal from the Illinois No. 6 coal. Also, the tests with synthetic mixtures of silica and charcoal showed a clear separation. Furthermore, for the separation of the synthetic mixture into its components, the effect of various hydrodynamic variables, such as electric field strength, particle velocity, and geometry of the separator, was investigated to determine the optimum operating conditions most conducive for the separation.

IIT conducted about 50 tests with an Indiana New Albany shale sample. The best kerogen enrichment achieved with this shale was 34% (feed had a kerogen content of 12%). A systematic parametric study showed that the separation efficiency increased with an increase in gas/particle velocity and with a decrease in particle loading in a gas stream. Furthermore, the kerogen and the pyrite concentrations at both electrodes were found to vary with the position in the separator. A maximum and a minimum in the kerogen concentration were observed at the negative and the positive electrodes, respectively.

Kerogen enrichments better than 34% could not be achieved due to the agglomeration of finely ground shale particles. These agglomerates were difficult to break, since the cohesive force between the shale particles, measured experimentally using a cohetester, was very large. Also, an analytical procedure for determination of various sulfur forms in the Eastern oil shales was developed. The ASTM method available for determination of various forms of sulfur in coal was found to be inapplicable for the oil shales.

A simple mathematical analysis of the batch electrostatic separator showed that the efficiency of the separation can be enhanced by increasing a) the inter-electrode spacing, b) electric field strength, and c) the surface charge of the particles.

Finally, a conceptual design of a continuous separator to beneficiate shale was proposed. The unique feature of this device is a specially designed baffle, made of a material having similar electrical properties to that of air, with preferential perforations. In this separator, the kerogen particles migrate to the negative electrode where they are removed with the help of a vibrator. The bulk stream, which contains mineral matter and pyrites, is disposed of.

Program Objectives

The overall objective of this program was to establish the feasibility of separating pyrites from Eastern oil shales by a dry electrostatic process. The principle of operation was that pyritic and non-pyritic constituents of shale can be made to acquire different surface charges, so they can be separated in the presence of an electric field.

During the course of this study, it was found that both pyrites and minerals present in shale acquire very similar surface charges, while carbonaceous matter (kerogen) present in shale assumes an opposite charge from that of the minerals and pyrites. This observation made it difficult to just remove pyrites without removing mineral matter. Therefore, this process results in shale beneficiation as well as shale desulfurization process.

Introduction

The Devonian oil shales of the Eastern United States are a significant domestic energy resource; yet until the recent attention to alternative fuel oil and petroleum resources, interest in the mineral shales, which contain the earth's most abundant organic matter, kerogen, has been sporadic. In the United States and throughout the world there are vast shale reserves, but the technology to exploit them and extract the oil from kerogen by heating and refining the volatiles produced has been slow to develop, which has primarily been due to economic and environmental factors.

Oil shale, unlike coal, contains a large fraction of inert material, typically about 80%. During hydroretorting, a process by which the kerogen in the shale is converted to shale oil at high pressure and temperature and in the presence of hydrogen, this inert fraction causes significant energy losses. Hence, removal of this inert material from the oil shale prior to the retorting process would improve the process efficiency. Furthermore, operating the hydroretort with beneficiated shale reduces the hydrogen consumption and pressure vessel requirements. Also, removal of sulfur prior to hydroretorting results in a reduced consumption of hydrogen because of less production of H_2S and reduction in the size of H_2S removal and recovery systems. There are, therefore, incentives for removing mineral matter and pyritic sulfur before hydroretorting.

Coal or shale beneficiation processes can be classified into physical, chemical and biological techniques. Physical and mechanical methods can be further classified into dry and wet methods. A detailed literature review of various physical beneficiation processes is given in the next section.

Wet methods, such as froth flotation, have gained a commercial status. However, there are problems associated with the use of wet methods. These problems include fresh water supply, handling of corrosive slurries, drying the particles before further processing, pollution and disposal of refuse.

A desirable process would be a dry process, which would avoid many of the problems associated with a wet process without introducing other problems. Two dry processes that have been extensively used to beneficiate coal are magnetic and electrostatic, with magnetic methods being used in both dry and wet processing modes. There are, however, problems associated with magnetic

methods when coal is ground to ultra-fine sizes for liberation of finely dispersed mineral matter and pyrites. These problems include difficulties in making the fine powder flow through the magnet, the need to maintain cryogenic conditions (a liquid helium environment) and a reduced driving force for the separation for the finer particle sizes with the latter die to the fact that the magnetic susceptibility is directly proportional to particle volume. A detailed description of the magnetic separation method is presented in the next section.

The other promising class of dry separation processes is known as electrostatic separation. The processes under this category separate materials based on one or more of their electrical properties such as the dielectric constant, electrical conductivity, and work function. In this method, charged particles are separated based on the differential attraction or repulsion under the influence of an electrical field. A partial list of commercial applications of electrostatic separation is presented in Table 3-11 (Lawver and Dyrenforth, 1973). It is estimated that about 14 million tons (12.7 million metric tons) of product per year in the world are produced by electrostatic separation (Knoll et al. 1984) and mineral beneficiation accounts for about 95% of the entire production. This electrostatic process investigated for shale beneficiation was originally developed for desulfurization of Illinois coals with a sponsorship from the Department of Energy and Natural Resources of the State of Illinois and the Center for Reserach on Sulfur in Coal (CRSC, Carterville, IL). Further work on coal desulfurization was conducted with matching funds from the Technology Commercialization Center at IIT. These results are included in this report to present an overall picture of the process. The basis of the electrostatic coal or shale beneficiation method is the fact that the surface charge of the organic matter in coal or shale can be made positive relative to a copper tribocharger, while the surface charge of pyrites and minerals found in coal becomes negative. Hence, application of a high voltage electrical field causes a clear separation, once the pyrites and mineral matter have been liberated by grinding or by other means.

A simple block diagram in Figure 3-14 illustrates the various steps involved in an electrostatic shale beneficiation process. First, the shale is ground to a particle size at which most of the mineral inclusions are liberated from the organic matrix. A scanning electron microscope was used to determine the grain size of associated minerals and pyrites. For Illinois coals, this grain size was found to be in the range of 5 to 10 μm. In the Indiana New Albany shale, the mineral inclusions also occur in a size range of 5 to 10 μm. Thus, both coal and shale must be finely ground.

The second, and the most important step in this process, is the triboelectrification or imparting of a surface charge on particles by rubbing, friction or contact. The efficacy of this beneficiation method depends on the extent of the charge differential created between the inorganic and organic constituents of the shale. Until recently, very little was known about triboelectrification, because little fundamental work had been done which directly relates the surface charge of coal and other minerals present with their structural properties. Therefore, a comprehensive literature review was conducted in the area of triboelectrification to understand the role of various process variables on the surface charge of particles in gaseous media. A complete description of the fundamentals of particle charging with methods

Table 3-11. INDUSTRIAL SEPARATIONS MADE BY ELECTROSTATICS

Arsenopyrite-feldspathic gangue	Mica-feldspars/silicates
Asbestos-silicates	Molybdenite-silicates
Barite-silicates	Monazite-beach sands
Chromite-ilmenite-magnetite-monazite	Nickel-copper ores-metasilicates
Coal-pyrite	Rutile-beach sands
Coal-shale	Scheelite-pyrite
Cobalt-silver silicates	Silicon carbide-alumina/silicates
Coke-iron	Spodumene-cassiterite
Copper ore-silicates	Stibnite-silicates
Copper wire-insulation	Wire-thermoplastics/rubber
Diamonds-silica	Wolframite-pyrite
Feldspar-mica gangue	Zircon-beach sand
Feldspar-quartz	Bark-sand
Fluorites-silicates	Barley-rodent excrement
Fly ash-carbon	Cocoa beans-shell
Gold/platinoids-beach sand	Cotton seeds-stems
Gold/platinum-jewelry sweeps	Movie film-paper
Graphite-silicates	Nut meats-shells
Halite-sylvite	Peanuts-shells
Ilmenite-garnet	Plastic-lint
Ilmenite-beach sand	Polyvinals-polyesters
Iron (specular hematite)-silicates	Rice-rodent excrement
Kaolin-iron contamination	Seeds-foreign material
Kyanite-rutile and iron gangues	Soap-detergent
Limestone-silicates	Soybeans-rodent excrement
Magnetite-silicates/rutile	Walnuts-shells
	Wheat-garlic seeds

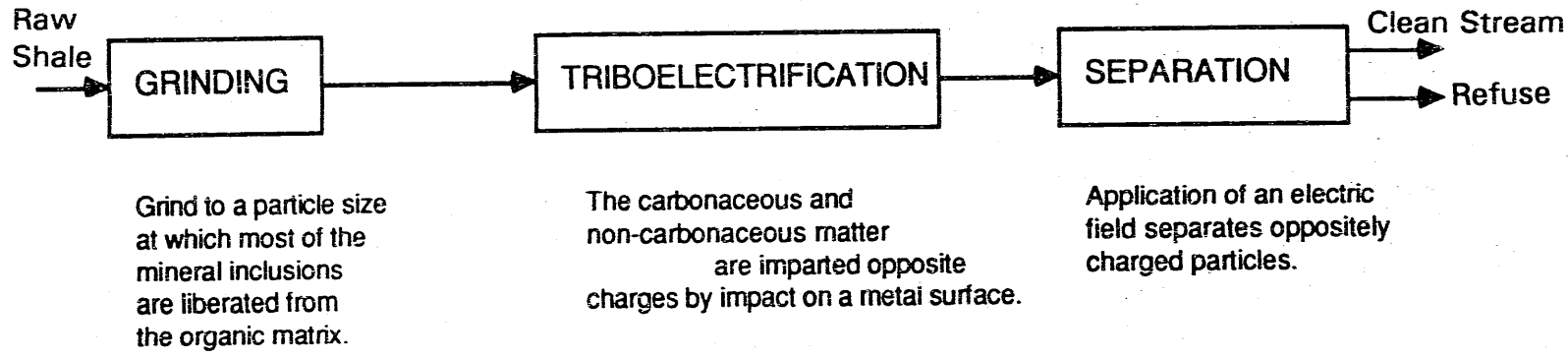

Figure 3-14. BLOCK DIAGRAM OF THE ELECTROSTATIC SHALE BENEFICIATION PROCESS

to calculate the surface charge from elastic and electrical properties of the particles and tribocharging surface is presented here. An effort has been made to correlate the work function values to the surface charge that was measured experimentally.

The last step in this process is the design of a separator. The dominant force inside this separator is electrical, which is the product of the surface charge and the applied electrical field gradient ($F_e = q \cdot E$). Normally, inside an electrostatic separator, there exists a very delicate balance between the electrostatic force and hydrodynamic forces (for example, gas-particle drag and momentum forces), making the design of the separator a difficult task.

A number of devices were designed, built and tested to separate pyrites and ash-forming minerals from coals and shales. These devices included an electrofluidized bed, an electrostatic sieve conveyor and a batch electrostatic separator, operating either in continuous or in batch mode. Perforated aluminum electrodes were used to withdraw the mineral inclusions from coal.

At a later stage, the idea of using perforated electrodes for operating the separator in continuous mode was found to be unsuitable for the fine particles for beneficiating both coal and oil shale. The primary reason for the poor performance was that the perforations in the electrode significantly reduced the extent of the applied electrostatic force and they provided an air circulation path. Both of these factors were later found to be detrimental for the efficient separation. Eventually, the perforated aluminum electrodes were replaced with solid copper plates. Since there was no provision for continuously collecting the particles, the system now operated in a semi-batch mode. In this semi-batch system, particles were found to stick with the electrodes in the form of a layer, the chemical composition of which was found to vary along the position in the separator. Concentration profiles for the kerogen were obtained on both electrodes and the kerogen concentration in the shale was determined using a Perkin-Elmer Elemental Analyzer. Also, an analytical scheme was developed for determining the forms of sulfur in the shale (Appendix A). As discussed earlier, the design of an efficient electrostatic separator for shale beneficiation requires the value of the surface charge of both kerogen and mineral matter. It was not possible to obtain either pure kerogen or pure mineral matter for the measurement of the surface charge. Therefore, IIT measured the charge of shales with varying kerogen contents and extrapolated the value to pure kerogen. This method gave unsatisfactory results. Therefore, they tested some model mixtures of well-characterized silica and charcoal particles in the semi-batch separator.

Mukherjee (1987) and Gidaspow et al. (1989) tried simulating this separator using a multiphase hydrodynamic code, which required the use of a supercomputer. Their code was not able to predict the formation of the layer observed experimentally. The major flaws in their method were the absence of primary forces in the model, such as the force of adhesion which is responsible for sticking of the particles to the electrodes, the unaccountability of distortion in the electrical field due to perforations in the electrodes, etc. Also, their model was so complex that simple order of magnitude analysis was not possible. A simple mathematical model was developed to describe electrostatic separation in a batch separator. This model is essentially an extension of the diffusion model developed by Soo (1989) for the design of electrostatic precipitators.

Since the equations used in this model are based on simplified assumptions such a plug flow, steady state, etc., the match between experimental results and the model predictions cannot be expected to be perfect. However, for the separation of the model mixtures, the model predictions are in reasonable agreement with the experimental data. Therefore, this simplified model can be used as a valuable tool for design and scaleup of the batch electrostatic separator.

The cohesive force between the fine shale particles was also measured using a Cohetester. Details of the measurement are described in Appendix B.

Finally, a conceptual design of a continuous separator to extract kerogen from shale was proposed.

Literature Review

Introduction

The market distinguishes two main types of coal; coking (or metallurgical) coal, used mainly in the iron and steel industry, and steaming (or thermal coal), used mainly in electric power generation. Coal is also used in smaller quantities for special purposes such as chemical feedstock for gasification, liquefaction, the manufacture of graphite and electrode carbon, and in coal-oil or coal-water slurries. For use as a feedstock or for admixing with oil, coal should generally be rather pure -- from 3% to less than 1% ash with very little sulfur. Specifications for coking coals generally range from 6% to 10% ash. Power station fuels should also be low in sulfur. Also, with increasing awareness of the slagging and fouling of boilers and other problems caused by abrasive mineral particles, such as erosion of heat exchanger tubes inside the combustors, the high mineral matter content of many run-of-mine (ROM) steaming coals is now seen as a liability. Thus, the beneficiation of thermal coals, as well as traditional cleaning of coals for coking, is becoming important. Even where beneficiation of coal is not essential technically, it helps to reduce the volume of the product and to increase its value so that the impact of freight charges is minimized.

Coal beneficiation, also referred to as coal preparation or coal cleaning, is a generic term used to designate various operations performed on ROM coal to prepare it for specific end-uses, such as feed for a coke oven or coal-fired boiler, or use in a coal conversion process. Over the years, coal beneficiation has come to encompass the entire spectrum of operations ranging from relatively simple crushing and size-classification operations to rather elaborate chemical or microbiological processes that are used (or being developed) to render ROM coal more suitable for the end use.

Coal beneficiation offers a significant, though often overlooked, means of reducing the sulfur and mineral matter content of several coals and thereby offering a plausible and, in many cases, economic solution to the problem of burning high-sulfur coals in an environmentally accepted manner. Moreover, beneficiating coal also results in 1) lower transportation costs per unit of energy delivered; 2) lower disposal costs at the user facility; 3) improved coal handling capabilities; 4) higher combustion efficiency in the furnace; and 5) reduced slagging in the furnace, which translates into reduced downtime for the furnace.

An up-to-date review of various physical coal beneficiation processes including commercially used froth-flotation and oil-agglomeration processes is presented below. Also, the importance of electrostatic separation with special emphasis on its application in coal beneficiation is discussed.

Sulfur Distribution in Coal

The sulfur in coal is commonly classified into organic and inorganic sulfur. The organic sulfur is chemically bonded to the hydrocarbon matrix of coal while the inorganic sulfur is imbedded in the coal, mainly as loose pyrites and sulfates. IGT has prepared a Coal Conversion Systems Technical Data Book which lists the composition and properties of selected U.S. coal samples (IGT Data Book, 1982) along with the forms of sulfur. The total sulfur content of coal samples varies from 0.37% to a high of 7.27%. For Illinois coals, the sulfur contents range from 2.15% to 4.63%. The pyritic sulfur content of Illinois coal varies from 1.03% to a high of 2.55%, while the organic sulfur content varies from a low of 0.92% to a high of 3% as shown in Table 3-12. Usually, organic sulfur levels much greater than 2% or much less than 0.3% are uncommon. Some Illinois coals, such as Illinois No. 2 coal, has a relatively low organic sulfur of 0.92%. If all the pyritic sulfur is removed from this coal, it can be burned as a compliance fuel, meeting the NSPS standards of 1.2 pound SO_2 per million Btu.

Coal Beneficiation Methods

The coal beneficiation methods can be generally classified as physical, chemical, and biological. Physical methods have been extensively used to remove ash with a fraction of the pyrite, depending on the extent of grinding. Coal beneficiation, as defined earlier, is essentially a process of separating raw coal into ash-rich and ash-lean fractions by virtue of the difference in physical properties of ash in relation to the hydrocarbon matrix. These physical properties include specific gravity, surface activity, magnetic susceptibility, work function, electrical conductivity, dielectric constant, etc. The chemical and biological methods are primarily used to remove organic sulfur, generally after most of the inorganic sulfur and ash has been removed from the coal by physical methods.

Physical beneficiation methods can be effective in removing mineral matter, including pyritic sulfur from the coal. These processes take advantage of the differences in physical properties between coal and mineral matter to achieve the separation.

In a typical physical cleaning operation, raw coal is crushed to about a 50 mm (2-inch top size). It is then screened into coarse, intermediate and fine sizes. Crushing the coal liberates some of the ash-forming minerals, including a portion of pyritic sulfur. The percentage of impurities freed from the coal matrix generally increases as coal particle size decreases. The coarse and intermediate-sized coals are typically subjected to a cleaning process based on the differences in the specific gravity between the coal particles and the associated impurities. Such cleaning processes use jigs, dense-medium baths, cyclone systems and concentrating tables (Wilson, 1977). The fine-sized (typically less than 500 μm) coal, if beneficiated, is typically cleaned using a froth-flotation technique based on the differences in surface properties of coal and its associated impurities. At fine sizes,

Table 3-12. ANALYSES OF COALS IN ILLINOIS BASIN COAL SAMPLE PROGRAM

Sample	#1[2]	#2[3]	#3[4]	#4[5]	#5[6]
Moisture	14.14	13.62	5.36	10.21	9.47
Volatile Matter	44.12	43.34	39.20	30.56	40.38
Fixed Carbon	45.62	49.92	52.48	31.36	41.61
H-T Ash	10.28	6.66	8.36	38.10	18.00
Carbon	67.66	73.31	73.82	45.97	63.26
Hydrogen	4.86	5.21	4.94	3.46	4.40
Nitrogen	1.18	1.47	1.68	0.80	1.23
Oxygen	11.63	10.09	8.75	7.43	8.39
Sulfatic Sulfur	0.06	0.10	0.09	0.10	0.00
Pyritic Sulfur	1.20	2.34	1.03	2.33	2.55
Organic Sulfur	3.00	0.92	1.16	1.76	2.08
Py/Org S Ratio	0.40	2.53	0.89	1.32	1.23
Total Sulfur	4.26	3.23	2.27	4.19	4.63
Chlorine	0.13	0.03	0.18	0.05	0.09
Btu/lb	12,606	13,526	13,437	8,492	11,522
Free Swelling Index	4.5	4.3	5.2	2.1	3.8

1. Moisture Free Basis.
2. Preparation plant Illinois #6 coal sample collected from West Central Illinois (IBC-101).
3. Preparation plant Illinois #2 coal sample collected from Central Illinois (IBC-102).
4. Preparation plant 80% IL #5 & 20% IL #6 coal sample collected from Southern IL (IBC-103).
5. Run-of-mine Illinois #6 coal sample collected from Southwestern Illinois (IBC-104).
6. Channel Illinois #6 coal sample collected from Southwestern Illinois (IBC-105).

greater potential for cleaning exists because a greater portion of the impurities are released from the coal matrix. However, this potential is not fully realized owing to inefficiencies in separating fine particles using state-of-the-art flotation technology.

Table 3-13 lists the various wet coal beneficiation processes with their sulfur and ash removal capabilities. In this table, the wet processes are further classified into 3 broad categories, namely froth flotation, oil-agglomeration, and heavy liquid cycloning.

A major effort is underway to improve froth flotation of coals. The Center for Research on Sulfur in Coal (CRSC, Carterville, IL) has been sponsoring research to develop an advanced flotation process which is essentially a combination of conventional froth flotation with oil agglomeration processes. This process called an "aggregate flotation", is being developed at the Illinois State Geological Survey (ISGS), Urbana, in collaboration with Dr. J. Fitzpatrick of Northwestern University (Lytle, 1989). The ISGS researchers have claimed development of some reagents, now being patented, which selectively float the coal with minimal mineral entrainment. The laboratory-scale testing of this process showed about 80% ash removal and 50% to 60% reductions in pyritic sulfur with a Btu recovery of 80% to 90% at the average particle size of 37 μm (400 mesh). The poor pyritic sulfur removals in this process can be attributed to the fact that at 37 μm particle size, only about 70% to 80% pyrites are liberated. For complete removal of pyrites by any physical process, coal needs to ground to a particle size of about 10 μm. Unfortunately, at a particle size of 10 μm, the dewatering of the coal becomes a very difficult task, both in terms of the energy consumption and in the ease of operation.

In view of the difficulties with ultra-fine sizes, the U.S. Department of Energy (DOE) has been sponsoring research to develop advanced technologies under the clean coal technology program. One of the techniques, "static tube flotation," is being developed at Michigan Technological University (MTU). This technology utilizes a controlled in-line reagent dispersion system with a packed-bed column design, thus permitting a controllable froth bed height (Yang, 1988). In laboratory tests, MTU has achieved clean coal products in the range of 1% to 30% ash at weight recoveries of 46% to 94%. The preliminary economic estimates indicate that the capital and operating cost of the static tube flotation process is roughly equivalent to a conventional process.

Another advanced flotation technology (under a contract from the DOE) is "microbubble flotation," which is being developed at Virginia Polytechnic Institute and State University (VPI) (Yoon, 1987). Microbubbles are defined as those having a Reynolds number less than one which, by definition, will not develop any wake as they rise through the column. The advantages of using microbubbles are increased bubble-particle collision efficiency and minimal entrainment of fine mineral matter (refuse) in the concentrate due to quiescent conditions.

The DOE, in collaboration with the Electric Power Research Institute (EPRI) has also contracted, with Bechtel National Inc., to test a German-developed microbubble flotation process (Bechtel, 1988). In this process, product ash contents of less than 5% were obtained for the three coals tested at weight recoveries ranging between 30% to 68%.

Table 3-13. PHYSICAL COAL BENEFICIATION PROCESSES (Wet Methods)

	Process	Performance			Organization	Comments	References
		Ash Removal	Sulfur Removal	Btu Recovery			
FLOTATION PROCESSES							
1.	Aggregate Flotation	>90%	35%	80%	Illinois State Geological Survey, Urbana	Process uses a combination of alcohol, surfactant and kerosene as surface-active reagents. Process under pilot-plant scale testing at EPRI[1]'s CQDC[2].	Lytle (1989)
2.	Static Tube Flotation	>90%	-	60-95%	Michigan Tech. University	Proprietary System. A packed bed column with controlled inline dispersion system is utilized.	Yang (1987, 1988)
3.	Microbubble Flotation	90%	30%	42-80%	Virginia Poly-technic & State University	Microbubbles with Re#<1 are generated. These microbubble increase bubble-particle collision efficiency and minimize entrainment of fine-sized refuse.	Yoon (1987)
4.	Bechtel's Micro-bubble Flotation	72%	47%	30-68%	Bechtel National, Inc.	German-developed microbubble flotation process being tested at EPRI's CQDC. Special microbubble flotation cells are used.	Bechtel (1988)
5.	Air-sparged Hydrocyclone	63%	-	72%	University of Utah	Specially designed hydrocyclone with 2 concentric tubes is used. Residence time<1 s. Particle size of 60% minus 400 mesh is used.	Miller (1987)
6.	Reverse Coal Pyrite Flotation	79%	50%	64-87%	Pittsburgh Energy Technology Center	Two stage flotation process in which pyrites are floated with xanthate while coal is dispersed with a hydrophillic colloid.	Miller (1987) Holt (1981)

1. Electric Power Research Institute 2. Coal Quality Development Center, Homer City, PA

Table 3-13, Cont. PHYSICAL COAL BENEFICIATION PROCESSES (Wet Methods)

Process	Performance: Ash Removal	Performance: Sulfur Removal	Performance: Btu Recovery	Organization	Comments	References
SELECTIVE AGGLOMERATION PROCESSES						
1. Otisca Process	75-92%	50%	97%	Otisca Industries Limited	Process uses Freon-113 as agglomerant. Removes almost all the pyritic sulfur with good coal recoveries.	Simmons and Keller (1988)
2. LICADO Process	50-78%	50%	78%	Westinghouse and University of Pittsburgh	Uses liquid CO_2 at about 6000 kPa and 25°C. Works well for a particle size range of 150 to 300 microns.	He, et al., (1989) & Morsi, et al., (1988)
3. Spherical Agglomeration	51-73%	24-38%	92%	Bechtel National, Inc.	Originally developed by National Research Council of Canada. Ultrafine coal is slurried in heptane. High shear reactor is used to agglomerated. Particle size used: 10-15 µm.	Bechtel (1988)
4. Aglofloat Process	50-89%	10-50%	63-94%	EPRI[1] and Alberta Research Council	Fine coal (25-290 µm)is slurried in water and heavy crude oil is added as wetting agent. High shear mixing forms agglomerates.	Ignaisk, et al., (1988)
HEAVY LIQUID CYCLONING (HLC) PROCESSES						
1. Heavy Liquid Cycloning Process	55%	50%	75%	Pittsburgh Energy Technology Center	Coal is slurried in Freon-113 and fed in a specially designed cyclone at very high pressures. Good pyrite rejections obtained.	Maronde (1988)
2. Methylene Chloride based HLC Process	79-94%	40-60%	46-68%	Process Technology Inc.	Process under testing at EPRI's CQDC[2]. Methlene chloride is used as a heavy liquid. Particle Size used: 45-150 µm.	Hucko, et al., (1989)

1. Electric Power Research Institute 2. Coal Quality Development Center, Homer City, PA.

Dry Beneficiation Methods

Although the wet cleaning processes have gained commercial acceptance, there are some inherent problems associated with them. These problems include the requirement of a source of water of suitable purity and a facility to treat water from the process for reuse or discharge. The biggest problem is to dewater the coal slurry after cleaning. Currently, there are no proven technologies available for dewatering, although both the DOE and the CRSC have sponsored research in this area (Parekh, 1987). The complexity of the problem increases when coal is fine ground to liberate the impurities (Dahlstorm and Klepper, 1982). The only potential substitute for the dewatering process is thermal drying preceded by mechanical filtration, which leads to high economic penalties (Gidaspow et al. 1987).

In view of these difficulties, a desirable solution would be a dry process that avoids the problems associated with the wet processes without introducing serious problems of its own. Most coal mined today in the world is burned as a dry, pulverized powder of about 70% -200 mesh (74 μm) in pulverized coal combustors and technologies for using dry coal powders as fuel are more developed than are the technologies for burning coal-water slurries. The dry powders, however, present potential problems in storage, transportation and handling.

Generally, dry separation is carried out using mechanical, magnetic and electrical techniques. Mechanical beneficiation of coal is probably effective down to 1 mm particle size, while electrical and magnetic techniques are most applicable to fine coal below 1 mm. Table 3-14 lists various dry coal beneficiation processes that were either developed or are presently being developed around the world.

Mechanical Methods

Mechanical separation of mineral inclusions from coal generally involves the response of particles to gravitational, inertial and centrifugal forces, while under the influence of another force (usually the viscous drag of water or air). The particle size, shape, and density, the fluid density and viscosity, and the solids concentration in air or liquid suspension, all have a bearing on mechanical separation.

Both air [specific gravity (SG) = 0.0012] and water (SG = 1.0) are less dense than coal (SG = 1.3 to 1.4) or mineral matter (SG = 2.5 to 5.0), therefore separation cannot be made based on terminal velocities. However, when a fluid with a density intermediate to the components involved is used, the separation becomes absolute and will, in principle, become independent of particle size since all particles 'see' an intermediate density around them and they float or sink accordingly. This type of separation works only for coarse particles, because the rate of floating or sinking (terminal velocity) for fine particles is very low (≈1 cm/s), although this can be increased using a cyclone or a centrifuge. Not surprisingly, dense-media separation using magnetic suspensions is popular in coal preparation, and float-sink testing using heavy liquids is a standard procedure. This philosophy also underlies in most of the heavy liquid cycloning processes indicated in Table 3-13 including the Otisca process which have started using Freon-113 as a heavy liquid.

Table 3-14. PHYSICAL COAL BENEFICIATION PROCESSES (Dry Methods)

Process	Performance			Organization	Comments	References
	Ash Removal	Sulfur Removal	Btu Recovery			
MECHANICAL PROCESSES						
1. Centrifugal Separation	-	50%	75%	US Bureau of Mines (METC[1])	Factors influencing separation efficiency: particle size and shape, density, air velocity and equipment design.	Singh & Peterson (1979).
2. Microwave Coal Cleaning Process	-	40-50%	-	G.E. Laboratories	Microwave heating is used to separate pyrites and organic sulfur from coal. Removal of organic sulfur is facilitated by treating the coal with NaOH.	Coal Age (1977)
3. Dry Table Separation	30%	<40%	75%	FMC Corporation	Separation by gravity and vibration forces. Strongly dependent on the type of processed coal.	Wilson (1977)
4. Air Fluidized Bed	-	30%	60%	Lehigh University	An air fluidized bed was used with particles ground to 100 μm. Density difference between coal and pyrites resulted in separation.	Levy et al. (1987)
MAGNETIC PROCESSES						
1. Magnex Process	67%	45%	73%	Hazen Research Inc.	Iron carbonyl vapors are used to render the pyrite and ash impurities magnetic. Low intensity magnetic field (8-12 kGauss) is used for separation.	Kindig and Turner (1976)
2. High Gradient Magnetic Separation	52%	45%	80%	ORNL[2] and Auburn University	Fluidized bed of pulverized coal is subjected to a high intensity (20 k-orsted) magnetic field.	Liu (1982)

1. Morgontown Energy Technology Center, Morgantown, WV. 2. Oak Ridge National Laboratories, Oak Ridge, TN.

Table 3-14, Cont. PHYSICAL COAL BENEFICIATION PROCESSES (Dry Methods)

Process	Performance			Organization	Comments	References
	Ash Removal	Sulfur Removal	Btu Recovery			
MAGNETIC PROCESSES continued						
3. Open Gradient Magnetic Separation	60%	40%	40%	Argonne National Laboratory	Superconducting quadrupole magnet was used. Dry pulverized coal of particle size 75 μm was used. System worked only under cryogenic conditions.	Doctor et al. (1987)
ELECTROSTATIC PROCESSES						
1. Rotating Drum Electrostatic Separator	-	40%	90%	U S Bureau of Mines	This process combined centrifugal and electrostatic separations. Particle charging by ion bombardment.	Abel et al.(1973)
2. UFC Electrostatic Process	55%	25%	60-80%	Advance Energy Dynamics	A lab scale vertical belt type separator was used. Particle charging by tribofication. Pre-wased coals gave better results.	AED (1987)
3. TriboElectrostatic Separation	90%	30-60%	45%	Pittsburgh Energy Technology Center	A semi-batch lab scale unit with copper tribocharger was used. Particles were scrapped from the electrodes. A number of tribocharger materials were investigated.	Link (1987, 1988)
4. Electrostatic Beneficiation	65%	-	78%	Fuji Electric R&D Center, Japan	Cyclone tribicharger was used. Particle size used: 74 μm. Effect of cyclone wall was investigated.	Masuda et al. (1981)
5. Dilute Electrostatic Separation Loop	78%	50%	40-80%	University of West-Ontario, Canada	Dilute phase transporation of fine coal (size < 180 μm) in electrostatic loop. Effect of various carrier gases investigated.	Inculet (1984)
6. Electrocyclojet	60%	-	72%	University of Cagliari, Italy	A specially designed cyclone was used for triboelectrification.	Carta et al. (1989).

The earlier mechanical methods for coal beneficiation (also known as dry concentration methods) used an airflow cleaner. Since air is very light a medium of sufficient density has to be built with the material itself. Hence, there must be some device to impart to the bed the necessary mobility for proper classification. Historically, most air cleaning devices used a vertical upward current of air through the bed of material. They differ by the method of imparting mobility to the bed and the method of removing the refuse. In general terms, the air machines were divided into three categories:

1. Pneumatic jigs where the air current was pulsated.

2. Pneumatic tables where the refuse was deviated from the direction of flow of the clean coal by a system of riffles fixed to the deck.

3. Pneumatic launders where the products flowed in the same direction and the cleaned coal was skimmed off the top of the bed and/or the refuse was extracted from the bottom in successive stages.

In recent years, however, the two latter types of units have declined in popularity. The only type of unit currently used by coal mining companies is a pneumatic jig, based on pulsating air current.

One of the commercially used devices based on above principle is a Super-Airflow Cleaner manufactured by Roberts and Schaeffer Company (McCulloch et al. 1979). In this cleaner, coal and refuse particles enter by means of pulsating air. A bed of hutch material, which is generally fine refuse, is used to migrate the refuse material from the coal through it. This process, also called "jigging," is highly versatile and economical for preparing a clean coal product. There are a number of commercially available jigs, such as Baum jigs and Batac jigs. Baum jigs are generally used for cleaning coarse coal, whereas Batac jigs are used for both coarse and fine coal cleaning. Also in Batac jigs, when cleaning fine coals, feldspar beds are used in place of a bed of fine refuse used as hutch material in Baum jigs. A complete description of these jigs and tables can be found in the review of dry mechanical coal cleaning process by Butcher and Symonds (1981).

The FMC Corporation has developed a dry table (Wilson, 1977) that is different from conventional jigs and tables because it uses no air flow. It operates by vibration and gravitational forces, with the feed material acting somewhat like an autogenous medium. The FMC table has an inclined deck with a wedge shape, tapering from the feed to the discharge end. The coal apparently moves in a spiral path to the discharge lip, while the denser shale and rock move in a smaller spiral to the back wall. At the discharge lip, mineral particles that are still present in the coal tend to be conveyed back up the deck because of a lower resiliency and greater surface roughness. Butcher and Symonds (1981) assess this device as less efficient than air tables or jigs but it has the advantage of a simple design and few ancillaries.

Air-Fluidized Particle Beds

As mentioned earlier, the air-fluidized particle bed, where the apparent fluid density $(\rho_b)^*$ reflects the density of the solid particles (ρ_s) and their volume fraction (ε_s) seems to be the best dry mechanical separation device.

$$\rho_b = \varepsilon_s \cdot \rho_s \qquad (3\text{-}1)$$

In a typical fluidized bed, a bed of particles resting on a grid is held in place by a fine mesh screen at the bed surface. A fluid is passed upward at low velocity and it encounters frictional resistance exhibiting a pressure drop as it flows through the interstices. This pressure drop, expressed per unit length, increases with increase in fluid throughput. If the bed of particles is not restricted at the surface, however, then at a sufficiently high fluid velocity (at which the pressure drop or resistance to flow is equal to or greater than the weight of the bed resting on the grid), the bed will be lifted. Since particles are not bonded together and merely rest upon each other (though this is certainly not true for fine and cohesive particles), they will move farther apart and open up the interstices which allow easy passage of the fluids resulting in a decrease in the bulk density and an increase in the bed volume.

The velocity at which the particles begin to behave as a fluid is called the minimum fluidization velocity (U_{mf}). A number of correlations have been proposed for determining of U_{mf} in the literature (Zenz and Othmer, 1960). However, Gidaspow (1990) developed the following equation using a momentum balance. According to his formula, the minimum fluidization velocity U_{mf} is estimated by --

$$U_{mf} = \varepsilon_{mf} \cdot V_{mf} = \frac{d_p^2(\rho_s - \rho_g)g}{1650\mu} \qquad (3\text{-}2)$$

This correlation is very similar to the formula used to determine the terminal settling velocity of a single sphere settling in a fluid. From Equation 3-2, it is evident that if a fluidizing medium is chosen of narrowly sized particles which are appreciably finer than the feed material to be separated, then the segregation seems to depend largely on density. The feed can span a wide range with the limits being determined by the difficulty in maintaining the air velocity above the U_{mf} of the largest particles yet still below the terminal settling velocity of the finest particles, which would otherwise be entrained out of the bed.

There is a lot of literature available on practical fluidized-bed devices working on this principle (Iohn, 1971). Their use, however, seems to be limited to a very coarse particle size, typically in the range of 50 to 3 mm. Carta et al. (1963) has reported good results for coal cleaning down to 0.2 mm size using a "Dry Flo (pneumatic sluice) separator." In a recent study by Levy et al. (1987), in which a bed of magnetite particles (-80+10 mesh) was fluidized with air at room temperature, they reported that pyrites and minerals segregate from the coal. Their air flow rates were close to the minimum bubbling velocities. They determined the effects of various operating variables, such as superficial gas velocity, magnetite particle size and coal-to-magnetite feed weight ratio on sulfur removal efficiency. Their results indicate that about 50% to 60% pyritic sulfur removal is possible with relatively low coal recoveries at an average particle size of 80 mesh (about 200 μm).

---

* Other nomenclature for this section is included on Pages II-170 to II-172.

Magnetic Separation

The principles of magnetic separation have been applied commercially for nearly 100 years. Applications range from the removal of coarse tramp iron to more sophisticated separations, such as elimination of weakly magnetic iron-stained particulates from paper-coating clays. The application of magnetic separation methods to weakly magnetic particles has been made possible by recent advances, such as development of the technology to generate high gradient and open gradient magnetic fields.

High-Gradient Magnetic Separation (HGMS)

The high-gradient magnetic separation (HGMS) technology was developed around 1969 for the wet separation of feebly magnetic contaminants from kaolin clay (Lin and Liu, 1977). Kolm and Marston at the Massachusetts Institute of Technology (MIT) developed a method for generating very high magnetic field gradients. In combination with high field intensities, this method provided a magnetic force density (intensity multiplied by gradient of intensity) more than two orders of magnitude above that previously available, sufficient to attract very weakly diamagnetic materials or very fine particles of ferromagnetic or paramagnetic materials. HGMS now supersedes earlier devices in many existing applications, as well as being capable of separations not previously possible.

The key to HGMS is the placement of a fine filamentary structure of ferromagnetic material, such as ferritic stainless steel wool, knitted wire mesh, or expanded metal discs, within a fairly uniform magnetic field. With this design, a strong field intensity of 20 kOe can be generated and distributed uniformly throughout the working volume. Furthermore, by placing the ferromagnetic packing material that increases and distorts the field in their vicinity in a uniform magnetic field, large field gradients of the order of 1 to 10 kOe/μ can be produced. At the same time, while the fibers in the matrix have a high surface area, there is overall still around 95% open space. Therefore, there can be a high trapping efficiency with only a low pressure drop and little tendency towards plugging, with the result that high throughputs are possible (as long as mechanical entrapment does not interfere).

The earlier emphasis of HGMS was on wet separations. Dry HGMS of coal was probably studied after penalties associated with wet HGMS became apparent. Both dry and wet HGMS studies on coal and coal products have been concerned primarily with removal of pyritic sulfur because of the importance of sulfur reduction in U.S. coals. Coal is basically diamagnetic at room temperature, but the diamagnetism varies from sample to sample. The diamagnetic susceptibility of coals ranges from -0.78×10^{-6} to -0.06×10^{-6} cgs·mu/g (Yergey *et al.* 1976), with a variation of 0.7×10^{-6} cgs·emu/g. The magnetic susceptibility χ_m (based on particle volume) is the ratio of magnetic moment, $\vec{M}$ created on a magnetic material when placed in an external magnetic field to the magnetic field intensity $\vec{H}$ as given by the equation --

$$\vec{M} = \chi_m \vec{H} \qquad (3\text{-}3)$$

Generally, diamagnetic materials have a negative value of χ_m and furthermore, for diamagnetic materials, χ_m does not depend on temperature and field intensity (Tsai, 1982). If the magnetic susceptibility of a material is

positive, and on the order of 10^{-6} to 10^{-3} cgs·emu/g, the material is called paramagnetic. Most mineral inclusions in coal are paramagnetic as their magnetic susceptibility values range from 0.3 X 10^{-6} cgs·emu/g for pyrites to 4.5 X 10^{-5} cgs·emu/g for clays and shales. The magnetic susceptibility is a bulk property and cannot be varied significantly except by chemical change or by attachment of magnetic material. Electrical properties, on the other hand, cover a wide range and can be varied rather easily, especially at the particle surface.

HGMS depends strongly on particle size, partly because the magnetization of particles is proportional to their volume and partly because the size of the region where the high field gradient exists is about the same as the size of the fiber that generates the gradient. For coal, the maximum size studied was about 700 μm, although efforts are underway to use HGMS for finer sizes since mineral inclusions are very finely dispersed in most U.S. coals. A pilot-plant scale study, done by Sala Magnetics, Inc. for EPRI (Weschler et al. 1980), indicated that, for an average particle size of 100 μm and under the best operating conditions, pyritic sulfur reductions in the range of 49% to 82% with coal yields ranging from 54% to 83% are possible. As one would expect, the highest level of sulfur removal corresponds to the lowest value of the coal yield and vice-versa.

In order to avoid the expensive, and operationally difficult step of dewatering and thermal drying after wet HGMS, desulfurization of dry pulverized coal was initiated in 1976 by Luborsky, of General Electric Company, in collaboration with MIT. Further studies were carried out at Oak Ridge National Laboratory (ORNL) and at Auburn University (Liu and his colleagues). Researchers both at ORNL and MIT adapted gravity feeding of coal to the HGMS matrix, assisted by vibration or low velocity air flow to handle the fine particles, while Auburn researchers devised a fluidized-bed matrix technique. A detailed description of all these dry magnetic techniques can be found in the book on physical cleaning of coal by Y. A. Liu (1982) and in a review paper by Lockhart (1984).

Results for the conventional HGMS technique vary considerably, with pyritic removals from 14% to 94%, ash removals from 15% to 85%; with higher removals associated with low coal recoveries as pointed earlier. It was argued that better liberation through finer grinding would improve the process performance; however, all the researchers reported that fine particles were detrimental to the performance of dry HGMS of coal, apparently because fines adhere to the surfaces of larger particles and promote agglomeration. Later on, it was concluded that dry HGMS in conventional form certainly cannot be relied on to beneficiate coal crushed to pulverized fuel specification (for example, 70% -74 μm).

Open Gradient Magnetic Separation (OGMS)

The alternative to trapping particles in a magnetized structure is to spread particles in a falling stream into a spectrum according to their magnetic characteristics. Since there is no particle trapping, OGMS can run continuously, splitting a stream of particles into appropriately located exit channels. In OGMS, solenoids are arranged such that the magnetic field has 'cusps' where there is a strong non-uniformity. The magnetic force acting on a particle in an OGMS process is much smaller than in HGMS but the distance

over which the force acts is greater. This is because the separation achieved depends on the product of force and distance at any point integrated over the path length of particles falling through the field region.

The first work on OGMS was started at ORNL from laboratory tests on the Frantz Isodynamic Separator to pilot-size (300 kg/h) studies (Hise et al. 1982). The feed coals and the test results seem to be much the same as in the HGMS program. Later on, researchers at the Argonne National Laboratory (ANL) further developed this process for the high-sulfur Illinois coals. The ANL OGMS apparatus employs a superconducting quadrupole magnet capable of operating between 10 to 100 lb/h (4.5 to 45 kg/h) and is based on free-fall conditions. The force of the particles closest to the magnetic poles is about 36,000 Gauss. A feed annulus controls the fall of the particles in an effort to prevent them from dropping directly into the center of the magnet or along the inner walls of the unit. As a result, the pyritic (mineral) fractions of the feed passing through the unit adhere to the magnetic poles, while the coal particles are pushed out of the magnetic field, and fall through the center of the unit for collection (Doctor et al. 1987).

ANL researchers have conducted several tests with an Illinois Basin coal to verify the performance of their OGMS unit. Their best results with Illinois No. 6 coal show a removal of 60% ash and 60% to 70% pyritic sulfur with about 50% coal recovery. An economic evaluation of their process, conducted by the CRSC, shows that the process is extremely capital-intensive and, also, the operating costs are very high due to the need to maintain cryogenic temperatures to cool the superconducting magnet (Carter, 1989).

Electrostatic Separation

Electrical separation in mineral processing is an old unit operation dating back to the turn of the century. There have been no comprehensive books on this subject, other than one by Ralston in 1961 and lately a monograph by Inculet in 1984.

Dry electrostatic separation involve charging and discharging of the particles. Charging can be achieved by ion-bombardment, contact or friction (triboelectrification), conductive induction or some combination of these processes. A detailed description of all the charging mechanisms and their role in electrostatic separation is discussed in the section on Triboelectrification.

In a typical electrostatic process, materials get separated based on one or more of their electrical properties such as dielectric constant, electrical conductivity and work function. Charged particles are separated based on the differential attraction or repulsion under the influence of an electrical field.

A mixture of particles can be separated by an electrostatic method under the following conditions.

a. Positively charged particles from the negatively charged particles,

b. Uncharged particles from charged particles, and

c. Particles with different charge to mass ratio irrespective of the polarity of the charge.

For an electrostatic separation to be effective, one of the above conditions must be met.

The force acting on a particle (F_e) in an electrostatic field is the product of the charge on the particle (q) and the electrical field strength --

$$F_e = q \cdot E \tag{3-4}$$

The surface charge of a particle can be normalized over its surface area, as it is a surface property, thus,

$$q = \pi d_p^2 \sigma \tag{3-5}$$

where d_p is the particle diameter (m), σ is surface charge per unit area (C/m^2). Therefore, the force acting on a particle becomes --

$$F_e = \pi d_p^2 \sigma E \tag{3-6}$$

The gravitational force (F_g) on a particle is --

$$F_g = \frac{\pi}{6} d_p^3 \rho_p g \tag{3-7}$$

where ρ_p is the particle density and g is the acceleration due to gravity.

The ratio R of electrostatic force to gravitational force determines the efficacy of an electrostatic separation. Thus,

$$R = \frac{F_e}{F_g} = \frac{\pi d_p^2 \sigma E}{\frac{\pi}{6} d_p^3 \rho_p g} = \frac{6\sigma E}{d_p \rho_p g} \tag{3-8}$$

Equation 3-8 indicates the following:

a. Smaller particles (d_p is small) can be separated more effectively.

b. Particles having high charge density (σ) will separate more easily.

c. An application of high electric field (E) will facilitate the separation. However, there is an upper limit on this value, that is, breakdown strength of air $E_{bk} = 3 \times 10^6$ volt/m.

d. In outer space, where the acceleration due to gravity, g, is small compared to its value at the earth's surface, will result in a much more effective separation than on the earth.

e. Particles with smaller densities will separate more efficiently than heavier particles.

The practical upper size limit for an electrostatic separation is about 10 mesh or 1 mm. The lower size limit is about 20 μm.

Coal is a combination of a number of petrographic ingredients, such a fusain, durain, clarain, vitrain, etc., which are minerals differing in their internal structure and their physiochemical and technical properties. Table 3-15 lists the values for these properties for various coal and its admixtures. Coal is generally less conducting than mineral matter. Pyrite is the most conducting material that is found in coal. Vitrain is less conducting that fusain and durain.

Electrostatic methods employed for separation in the past could be very broadly classified into two categories.

1. Electrodynamic or corona separation

2. Triboelectric separation

As pointed out earlier, although there are separators working on the conductive induction and other charging mechanisms, the above two categories account for more than 95% of the commercially used separators.

Corona Separation

In the corona technique, a rotating drum (which is earthed) is used together with a small diameter, pointed electrode that provides the corona discharge. Feed particles enter at the top of the drum and become charged by ion bombardment and are pinned to the drum surface. When they leave the corona region they give up charge to the earthed drum and fall off. The particles with higher conductivity lose charge faster and fall off first, and are thereby separated from the more insulating particles. Modern machines usually include a large diameter non-ionizing electrode after the corona electrode, which lifts the particles off the drum and deflects them, and therefore improves the selectivity of the separation (see Figure 3-15). Generally, fine particles separate more effectively with high rotor speeds and lower voltage, while larger particles give better separation at lower rotor speeds and high voltages.

The corona-rotating drum separator has been widely used to separate metals from glass, ceramics, plastics, and polymers, plastics from paper and from other plastics, and for removing contaminants from grains and processed foods. In mineral processing, the major commercial applications are in concentration of heavy minerals (rutile, zircon, illmenite, monazite) from beach sands and alluvial deposits, beneficiation of various ores and separation of tin ores from gangue materials (Ralston, 1961; Knoll and Mitchell, 1984; Boron and Grodzicki, 1976; Mugeraya, 1985). At the University of Florida, Dr. Moudgil's group is developing various reagent coatings capable of enhancing particle separation efficiencies. They have developed some polymer coatings to effectively separate quartz from phosphate ore using this corona-drum technique.

The corona-drum separation of coal was started as early as in 1915 when F.W.C. Schniewind received two patents to separate various petrographic constituents of coal, such as clarain, durain, vitrain, and fusain from each

Table 3-15. PHYSIO-CHEMICAL PROPERTIES OF COAL AND ITS MINERAL ADMIXTURES

Description	Density (gm/cm^3)	Elect. Resistivity (ohm/cm^3)	Dielectric Constant[a] (ϵ_{20})	Work Function (eV)
Bituminous & Brown Coal	1.3	10^7 - 10^{10}	4.58[b]	4.0[c]
Coal dust & mineral inclusions	2.5	10^9 - 10^{12}		
Vitrain, Clarain and Durain	1.20 - 1.36	10^8 - 10^9		
Fusain (mineralized)	1.37 - 1.52	10^2 - 10^4		
Quartz sand & argillaceous shale	2.6	10^6 - 10^7	6.53	5.0
Pyrite	4.8	10^3	33.7 - 81	5.5
Calcite	2.5	10^9	6.36	1.8

a. Values taken from Ralston (1961).
b. Available only for diamond.
c. Value for graphite.

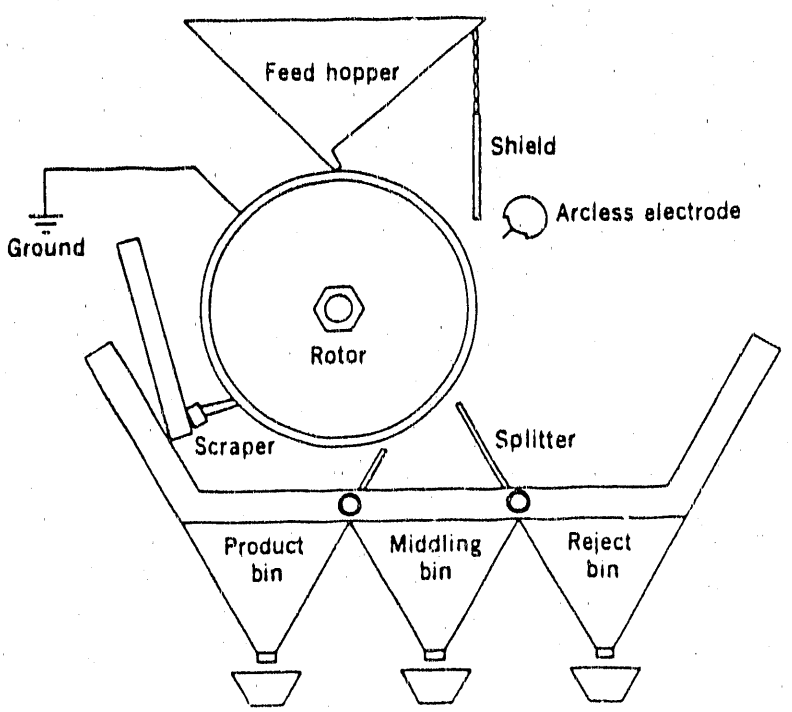

Figure 3-15. ROTATING DRUM-TYPE CORONA SEPARATOR

other, using an electrostatic method. Ralston (1961) has reviewed the state-of-the-art then existing in this area. Gray and Whelan (1956) studied a variety of coals differing in rank, particle-size over the size range of 2 mm to 125 μm, and water contents using different electrodes, different drum materials, different drum speeds and various voltages. They illustrated the diversity of conditions under which good separation of coal and shale was achieved. Ralston (1961) mentioned that all ranks of coal from German brown coal to Pennsylvania anthracite had been studied, both to obtain low ash, low sulfur products and to fractionate the macerals. Olofinskii's 1957 book refers to the use of corona techniques for size classification of coal; the beneficiation was incidental. He reported that for coal beneficiation, the best results were obtained in a chamber type corona separator with coal particle size ranging from 5 to 1/2 mm. Furthermore, he found that the corona-separation products obtained were selective in composition and contained particles within very narrow particle-size range.

Advanced Energy Dynamics (AED) of Natick, MA, has developed a number of units to beneficiate coals. Their earlier units (Rich, 1981, 1984) were based on corona-rotating drum method to cope with coal particles below 150 μm. AED used a knife blade and plastic shields to strip off the boundary gas layer just ahead of the particle feed stream, thereby allowing adhesion of fine coal particles. Also, spurious charges (presumably of triboelectric origin), which caused clumping and agglomeration of fine particles in the feed, were eliminated by an a.c. corona discharge.

AED tested the technology at the Picway Station Power Plant at Columbus, Ohio at up to 10 t/h of feed. The drums were about 14 inches in diameter and 10 feet long (35.6 cm by 3.05 M) spinning at 360 rpm and dividing the feed (particle-size ~74 μm) into three streams: clean coal that goes to the burners, intermediate coal for recycling and rejected ash and pyrites.

Arthur D. Little, Inc. of Cambridge, Massachusetts, is investigating the enhancement of electrostatic separation by charging the particles by triboelectrification and separating them on a rotary-drum type electrostatic unit. No results are available so far.

Triboelectric Separation

Triboelectric separation involves charging of particles via contact or friction with other particles or with a surface (called tribocharger) followed by transport or free fall through an electric field whose intensity is below the air breakdown voltage (corona discharge). The electric field deflects the particles according to the magnitude and sign of their charge. Most of the research reported in the literature assumed that deflection step is relatively simple, therefore, the emphasis was concentrated on obtaining adequate selectivity and a sufficient degree of charge in the charging step. Unfortunately, this is only true for the coarser sizes ($d_p \geq 100$ μm). For finer sizes, aerodynamic problems of charging and transporting the particles become acute and the hydrodynamics of flow plays a vital role.

Early triboelectric separators used the charges generated by particles sliding down, or transported through, chutes, pipes or nozzles. As mentioned before, the rotating-drum-type separators have also been used for triboelectrified particles (without the corona discharge); these are pinned to or repelled from the drum according to the sign of their charge. However, free-fall and other arrangements that preferentially deflect the triboelectrified particles are more common. Besides, cyclones and fluidized-beds are now popular for improving the charge as a result of more frequent and better particle-particle and/or particle-wall contacts. The variety of charging arrangements is reflected in the variety of triboelectrostatic separation devices that have been used.

The most important application of triboelectric separation is undoubtedly that in the potash mineral salt industry of West Germany (Singewald, 1982). Deflecting electrodes about 10 meters long are used to separate mixtures of salts at 200 to 300 ton/h with approximately 100 kV applied and currents of about 1 mA. The salt grains become charged through heating and mutual contact; conditioning agents are also used to modify the surface charges.

Carta's group at the University of Cagliari in Sardina, Italy, has been working for the last 25 years on triboelectric separation for beneficiating barite, feldspars, fluorspar and several coals. They developed a variety of devices, such as triboelectric cyclone separator and electrocyclojet and extended their applications to pilot scale. Apparently, they can handle particle sizes in the range 20 to 30 μm (Alfano et al. 1985; Ciccu et al. 1989).

The other category of triboelectric separators involved fluidized beds for tribocharging. Historically, the work on fluidized bed techniques mostly

involved corona charging. Inculet's group at the University of Western Ontario (UWO), Canada, modified this technique to handle fine particles by combining very low gas flow rates with mechanical vibration. However, the UWO group concentrated their efforts more on the triboelectric charging functions of fluidized beds in order to obtain better selectivity of charging, especially when dealing with mixtures of relatively insulating particles such as coal (Inculet, 1984). Two configurations involving fluidized beds were used by the UWO group for beneficiating coal, namely fluidized-bed apparatus and dilute-phase loop. Descriptions of each of these is given below.

In one apparatus, a fluidized bed was used to precharge the particles triboelectrically. The particles were then allowed to flow downwards into a region between vertical high voltage deflecting electrodes, at the bottom of which were a number of containers for collecting the deflected fractions. This type of apparatus was used for the narrow size range of 80 to 180 μm (Inculet et al. 1979).

The other apparatus was a dilute-phase loop for particles below 50 μm. The loop was 8 meters tall and involved complete entrainment of particles into a gas suspension where they formed thin streamlines. The particles were deflected from one streamline to another by an electric field within the loop, according to their charge characteristics. The actual charging step in this system was apparently open to choice -- a fluidized or vibrated feeding device for pre-charging the particles prior to entrainment into the loop; charging through contact with copper-wall of the loop or a copper honeycomb within the loop; charging by corona electrodes within the loop; or some combination of these methods. The loop is similar in principle to the cyclone devices used by Carta and others (Inculet, 1984).

Japanese researchers (Masuda et al. 1981) later combined both loop and cyclone tribocharging to beneficiate Japanese coals. They reported, that with a cyclone tribocharger, they were able to obtain a product of 7.5% ash content from a feed of 17% ash content with about 85% recovery. The particle size in their tests was in the range of 50 to 70 μm. They also investigated the effect of cyclone wall material and found that copper was the best suited.

Triboelectric separation of coal has also been studied in Poland (Ciesla et al. 1978), but few details or practical results are available. Nonetheless, Ciesla et al. (1978) conducted a detailed study of characterization of surface charge of coal and associated minerals as a function of air flow rate, cyclone material, particle concentration and humidity, to determine the best operating conditions for the separation.

More recent work on beneficiation using triboelectric separation was done by AED (1987). AED developed a Vertical-Belt Separator (VBS) device that separated coal from its liberated mineral impurities by utilizing the differences in their work functions. In the VBS device, particles were charged by triboelectrification. The VBS device (Figure 3-16) is composed of several stationary, flat, parallel electrodes, charged so as to maintain an electric field between them. Between the electrodes are two sections of open mesh transport belt. The two sections of belt move in opposite directions and transport particles adjacent to opposite electrodes in opposite directions. The motion of the belt agitates the particles and generates a highly turbulent, high-shear zone between the electrodes. This produces vigorous

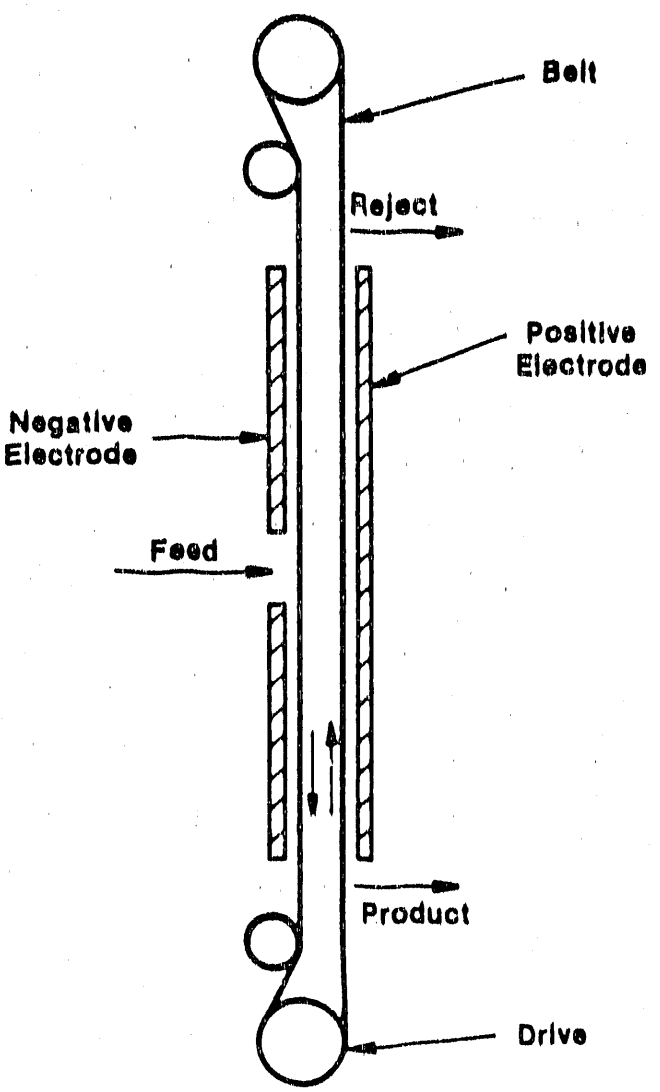

Figure 3-16. AED'S CONTINUOUS UFC BELT SEPARATOR

particle-to-particle contact and leads to high electrostatic charging. The electric field moves the positively charged coal and negatively charged mineral particles toward opposite electrodes, where they are transported by the belt in opposite directions, and results in a countercurrent flow of coal and refuse particles. As the particles are transported, they are subjected to continued agitation, particle contact, and charging. This renewed charging results in continued separation as the particles are transported toward the product- and reject-removal sections at opposite ends of the separator. The VBS is similar to a distillation column with countercurrent flow of the separating streams, and multistage contacting and separation leading to a separation much greater than that achievable with a single stage.

The performance of AED's VBS system for Lower Kittaning and Illinois No. 6 coals ground to 90% -44 μm was reported to be satisfactory. Ash and pyritic removals were in the range of 50% to 65%, and 20% to 75%, respectively, with 62% to 81% Btu recoveries. This system was found to be unsuitable for Upper Freeport coal although reasons for this poor performance are still not well-understood.

The in-house laboratory at PETC has also been developing a continuous, integrated, dry electrostatic beneficiation system for processing of ultrafine coal. Their system relies on triboelectrification for placing charges on coal and the liberated mineral matter. Unlike the AED process, in which the motion of the belts placed within an electric field is used to bring particles in contact and induce electrostatic charges, the PETC process uses a copper surface to triboelectrically charge the coal and mineral matter particles. The work at PETC has shown that this is a novel and viable means for selectively placing positive charges on coal and negative charges on its associated mineral matter, including pyrite.

PETC's Triboelectrostatic Separator (Figure 3-17) consists of two sections, namely, the triboelectric charger and the electrostatic separator. Ultrafine coal ranging in size from -75 μm to -38 μm is fed into a current of air that imparts to the particles a velocity of 30 to 300 m/s. The particles are charged as they pass through the copper triboelectrification section and are then separated in the electrostatic separator that operates with a potential difference of 50,000 volts. The positively charged clean-coal particles are separated from the negatively charged mineral matter and are collected on the negatively charged plate of the electrostatic separator.

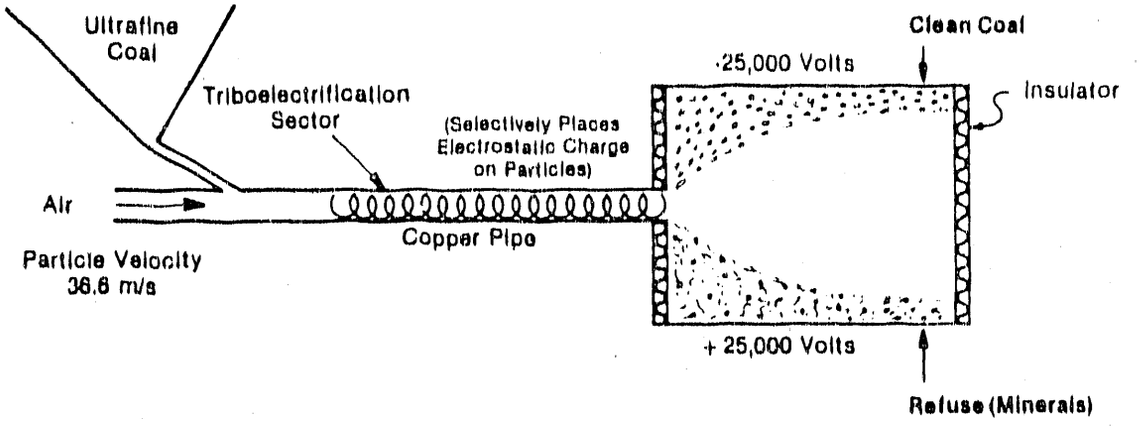

Figure 3-17. PETC'S TRIBOELECTROSTATIC SEPARATOR

Considerable development work in selection of tribocharging materials (Teflon, nylon, copper, stainless steel, aluminum, Inconel, and Monel), aerosolizing medium for coal (air, carbon dioxide, nitrogen, and argon) and system design was done at PETC in 1987 and 1988. This development work culminated in the testing of a new copper tribocharger configuration and an integrated-system concept (Link, 1987, 1988). The new tribocharger unit provides increased turbulence of the aerosol stream and improves particle-charging efficiency. The volume of air required has been reduced by one-third, and a 33% increase in the aerosol solids concentration was realized. Three coals (Upper Freeport, Illinois No. 6, and Pittsburgh seam) were ground to 37 μm top size and subjected to two-stage cleaning in the new tribocharger second-generation Triboelectrostatic Separator configuration. The results indicate that the ash and pyritic sulfur content of Illinois No. 6 coal in two-stage cleaning are reduced from 13.6% to 1.6% (88.2% reduction) and from 2.42% to 0.18% (92.6% reduction), respectively (Link, 1987) and the clean-coal weight yield was 45.3%. Similar results were obtained for the Pittsburgh seam coal (two-stage cleaning, 87.4% ash reduction, 91.3% pyritic sulfur reduction, and 42.6% clean-coal weight yield) and the Upper Freeport Coal (two-stage cleaning, 93.1% ash reduction, 95.3% pyritic sulfur reduction, and 40.6% clean-coal weight yield).

PETC researchers are developing a continuous unit using mesh type electrodes. Their recent results, however, indicate that the open area in the electrodes is detrimental to the effective separation.

Grain Size Characterization of Mineral Inclusions

Introduction

In any physical coal or shale beneficiation process, mineral inclusions from the organic matrix need to be liberated before they can be physically separated. Generally, this is accomplished through fine grinding with the extent of grinding dependent upon the grain size of these mineral inclusions. In coals and shales, these mineral inclusions are either iron pyrites or the ash-forming minerals -- silica, quartz, clay, alumina, etc. The characterization of iron pyrite grain size is of vital importance, since this determines the efficacy of a physical desulfurization process.

Typically, more than half the sulfur in high-sulfur coals is present as pyritic sulfur which can, theoretically, be removed with sufficiently rigorous physical cleaning. However, since the amount, size and distribution of pyrite and other mineral particles can vary widely among coals, they can greatly affect the response of coal to cleaning. Thus, it is imperative that the mineral content of raw coal be characterized for effective and efficient design of coal cleaning processes. Yet, conventional analyses only provide results on the bulk ash content and elemental composition; they do not address the issue of how pyrite and other ash-forming mineral particles are associated with and distributed throughout the coal matrix.

Scanning Electron Microscopy (SEM), in conjunction with energy-dispersive X-ray (EDX) analysis, is able to provide the required in-situ characterization of pyrite and other minerals in coals and shales for size, shape, chemical identity and their relation to the organic matrix. SEM offers a way to

visualize features that are hundreds and thousands of angstroms in diameter by direct observation in three dimensions -- not possible by any other technique.

Background

The SEM technique is not new in the area of coal cleaning as it has been around for the last 20 years. Raymond Geer (1977), at Ames Laboratory in Iowa, did the pioneering work in this area. He found that pyrites in coal occur in various forms, such as in frambodial, amorphous and in crystalline forms. He also studied the distribution of the forms of pyrites over an extended size range. Later on, from the same laboratory, Straszheim et al. (1987) automated this procedure with the use of an Automated-Image Analysis (AIS) technique. Huggins' group, at the University of Kentucky, used this technique to characterize a wide range of coals (Huggins et al. 1982). Kneller and Maxwell (1985), at the University of Toledo, used this technique to determine the size, shape and distribution of pyrites in 6 Ohio coal beds and their findings indicated that the maximum pyrite concentration is detected in the particle-size range of 8 to 16 μm. For Illinois coals, researchers at the ISGS conducted this analysis using SEM technique and found that most of the pyrite particles occur in a size less than 10 μm. The IIT findings were consistent with the results of ISGS researchers. Also, in Eastern oil shales, specifically in Indiana New Albany shale, pyrite particles were found to occur in the range of 2 to 15 μm.

Experimental Investigation

Two techniques, SEM and optical microscopy were used independently to establish the size and distribution of mineral matter, specifically iron pyrites, in coals and shales. A detailed description of both the techniques is presented below.

Scanning Electron Microscopy

All these tests were conducted at the IIT Research Institute's (IITRI) Surface Engineering Center with the help of Drs. Verma and Panda. IITRI has a JEOL JSM Model 35CF Scanning Electron Microscope with computerized ORTEC QUAN-2 EDX and ORTEC JEOL WDX energy-dispersive spectrometers. Figure 3-18 shows a photograph of IITRI's SEM system. This SEM system allows examination of samples with a magnification of 10,000 without loss of resolution.

Sample Description

Two coal samples, Colchester No. 2 and Illinois No. 6 (IBC-102 and IBC-104, respectively) were obtained from the Illinois Basin Coal Sample Bank operated by the ISGS. Also, one Eastern oil shale sample was obtained from IGT. These samples were thoroughly washed with water and dried under nitrogen for 24 hours. The sulfur and ash content of all the samples were determined using standard ASTM techniques.

Sample Preparation

For each sample, two types of sample specimens were prepared using standard metallographic techniques. In the first type, the samples were ground in a Bantam Micropulverizer to an average particle size of 53 μm.

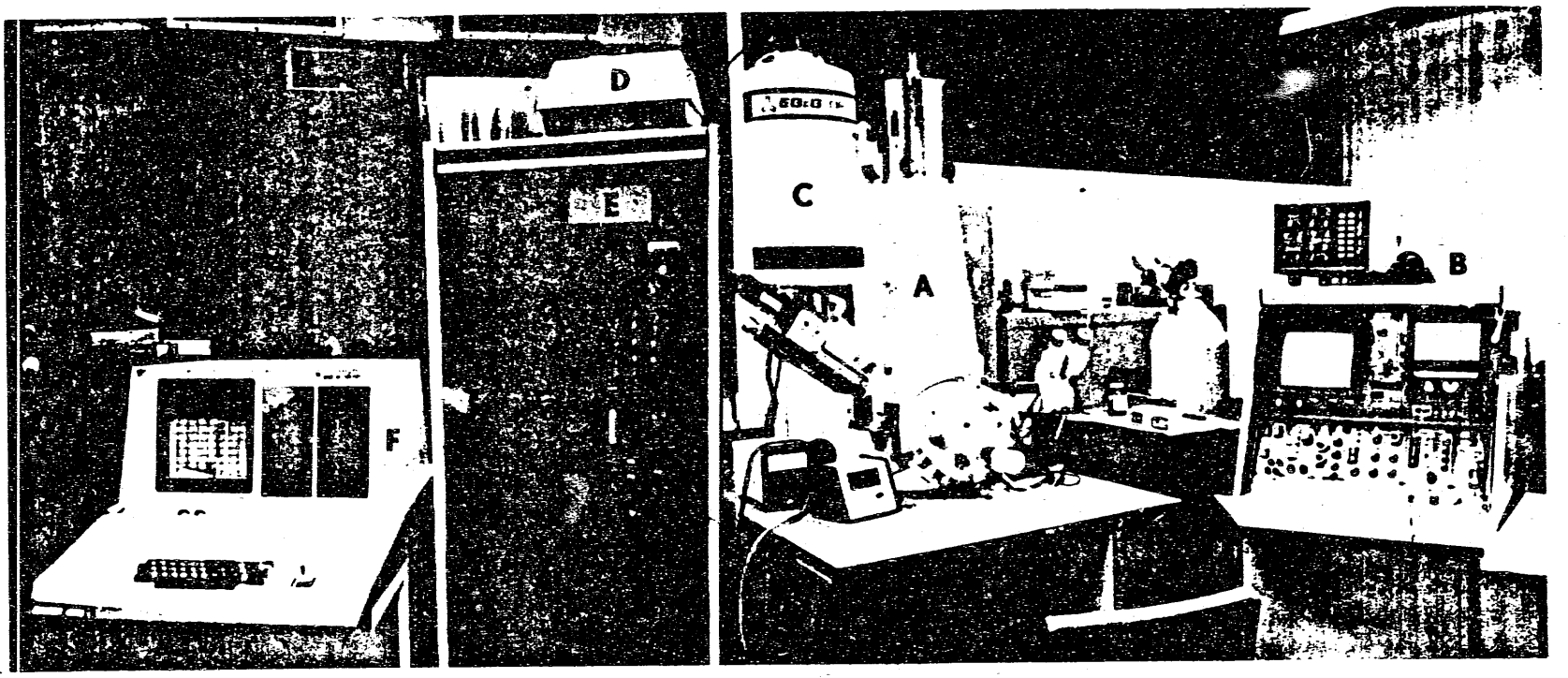

A - JEOL JSM 35CF SEM

B - Control Cabinet for SEM

C - ORTEC QUAN-II Energy-Dispersive X-Ray Spectrometer

D - Printer for EDX Unit

E - Control Cabinet for JEOL 4-Crystal Wavelength-Dispersive X-Ray Spectrometer

F - Display and Computer for EDX Unit

Figure 3-18. A PHOTOGRAPH OF IITRI'S SCANNING ELECTRON MICROSCOPE FACILITY

Ground samples were sealed in a glass bottle under nitrogen to prevent them from absorbing any atmospheric moisture, Then, about 0.1 gm of sample was mounted and these samples received a vacuum-deposited coating of about 200 Å gold. In the second type, 2 to 3 pieces of coal or shale, about 1 mm in size, were mounted using a cold mounting compound (an epoxy in a mold) with a hardener and left overnight for setting. These samples were polished using SiC grit papers from 280 to 600 grade, successively. These samples were further polished using a diamond paste until a mirror polish (6 μm, 1 μm, and 0.25 μm) was achieved using kerosene oil as a lubricant. The specimens prepared by this method were also used for a study under an optical microscope.

Procedure

Samples were analyzed in the SEM with an accelerating potential of 15 kV and a beam current of 1-4 nA, using both secondary electron and back-scattered electron signals. When an electron beam hits the surface of the specimen, secondary electrons from the surface are generated. These electrons are channelled by photomultipliers within the microscope system to produce a scanning or a back-scattered electron image. Thus, the SEM is able to print a micrograph with a resolution of 50 μm (and less) size range.

The back-scattered electron signal from a phase in a polished cross section is proportional to its average atomic number (Robinson et al. 1984). Therefore, since most minerals have a much higher average atomic number than coal (10 to 15 vs. 6) they stand out much brighter in a back-scattered electron image. Similarly, pyrites (with an average atomic number of 21) are very bright and are easily distinguished from other minerals. Furthermore, the pyrites and the minerals in coal are more conductive than the organic matter. This difference in electrical conductivities, in conjunction with atomic number difference, produces contrast on a micrograph as shown in Figure 3-19. In this micrograph, bright white spots show pyrites, while light gray spots show minerals, and coal particles appear to be dark grayish-blackish. With this SEM system, one can use either the energy or wave length of these back-scattered X-rays to identify the various elements which are present in the specimen. In this study, however, energy of X-ray signals, which were generated in the microscope, was used after correcting it for 1) the atomic weight of the elements, 2) the fluorescence of the elements and 3) the atomic adsorption characteristics of the elements, to identify the various elements present. These X-ray signals are channelled to produce peaks and typical X-ray peaks obtained are shown in Figure 3-20. The elements present in the specimen were analyzed for their composition using software available with the microscope. Table 3-16 shows the typical composition results obtained using this software.

Results

The following sections describe the results of SEM analysis for Illinois coals and for Eastern oil shales.

Illinois Coals. Figures 3-21 and 3-22 show the scanning electron micrographs for a specimen of Illinois No. 2 coal sample, at magnifications of 180 and 60 times, respectively (the length scale is indicated by a bar). The bright, light gray, and dark gray spots, respectively represent pyrites,

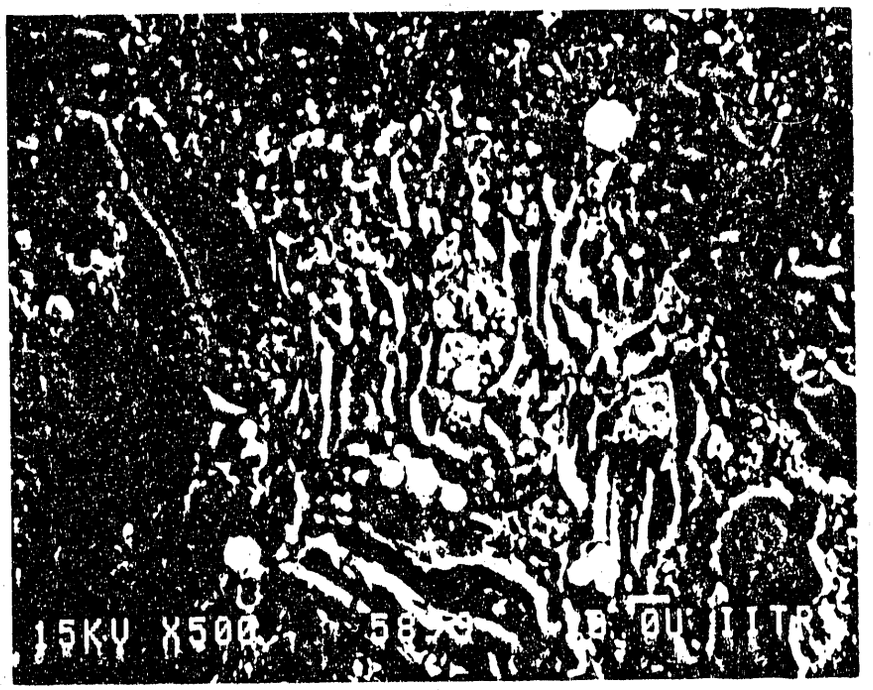

Figure 3-19. A TYPICAL SCANNING ELECTRON MICROGRAPH OF ILLINOIS NO. 2 COAL SAMPLE SPECIMEN

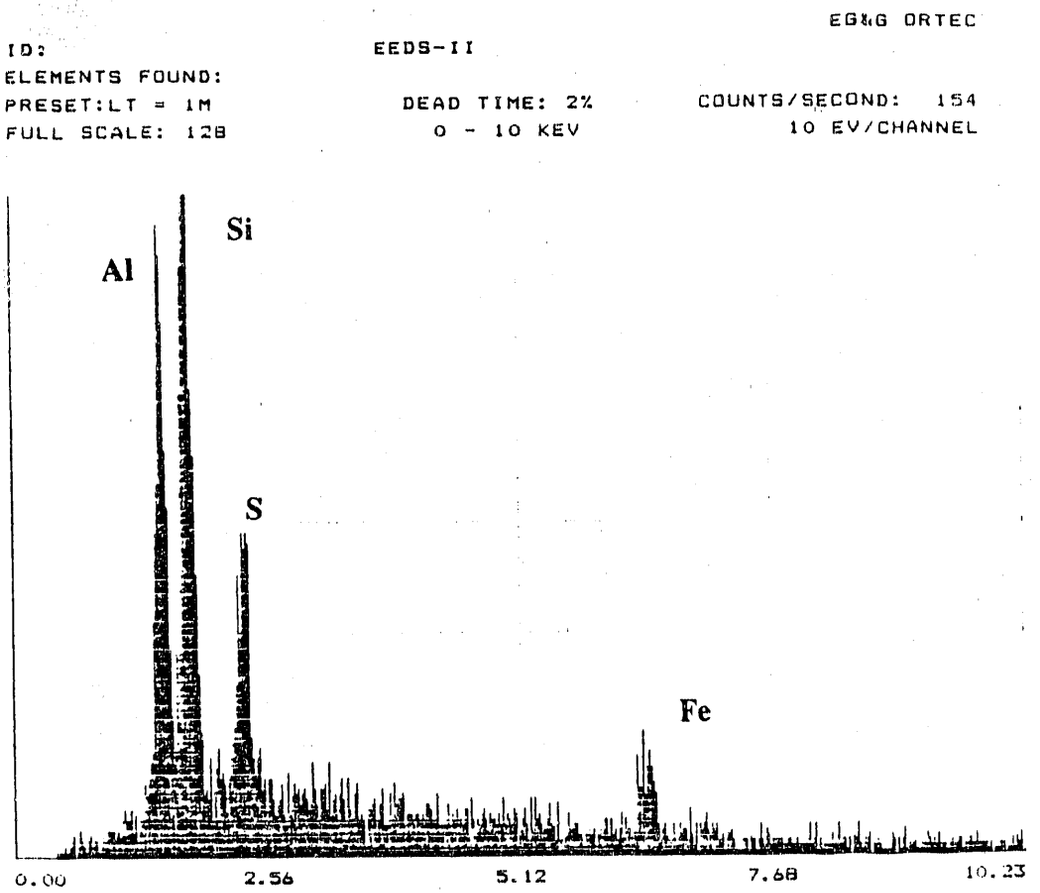

Figure 3-20. TYPICAL X-RAY PEAKS OBTAINED WITH THE SEM SYSTEM

Table 3-16. TYPICAL ELEMENTAL ANALYSIS OF A PYRITE PARTICLE USING THE ZAP SOFTWARE

EG&G ORTEC
ZAP MICROANALYSIS REPORT
V02.14 17-JUL-87 10:02

ID:006,SMALL PARTICLE

ELEMENT	WEIGHT PERCENT	ATOMIC PERCENT	INTENSITY (CPS)
AL KA	0.00	0.00	-7.51
SI KA	0.00	0.00	-5.82
S KA	43.23	57.01	244.65
FE KA	56.77	42.99	100.94

ACCELERATING VOLTAGE:	15.0	KV
SPECIMEN TILT X-AXIS:	0.0	DEGREES
Y-AXIS:	0.0	DEGREES
INCIDENCE ANGLE :	90.00	DEGREES
TAKEOFF ANGLE :	40.00	DEGREES
SAMPLE DENSITY :	3.56	G/CC

Figure 3-21. SCANNING ELECTRON MICROGRAPH OF AN ILLINOIS NO. 2 COAL SAMPLE SPECIMEN (Bright Spots Show Pyrite-Enriched Area)

Figure 3-22. SCANNING ELECTRON MICROGRAPH OF AN ILLINOIS NO. 2 COAL SAMPLE SPECIMENT (Bright Spots Show Pyrite-Enriched Area)

minerals, and carbon in the specimen. In Figure 3-21 the bright white section on top seems to be pyrite enriched since this micrograph represents a large particle. Similarly in Figure 3-22, most of the bright spots are either of a cubical or of an orthorhombic shape, indicative of the shape of the pyrites in the coal. This observation was confirmed with the SEM data of Straszheim et al. (1987). It is evident that most of the pyrite particles, as individual entities, occur in the particle-size range of 2 to 10 μm.

Similar observations were made with a specimen of Illinois No. 6 coal with a pyrite grain size ranging from 2 to 10 μm and mineral matter grain size in the 10 to 50 μm range. These ranges are consistent with the findings of ISGS researchers (Rapp, 1987).

Eastern Oil Shales. Figure 3-23 shows a typical scanning electron micrograph (1500 times magnification) for the Indiana New Albany oil shale sample specimen. Various areas on the specimen were analyzed for their elemental composition using X-ray peaks. Table 3-17 shows the elemental analysis of 7 mineral enriched areas. The following inferences can be drawn from the data.

1. The average grain size of pyrite particles in this shale sample is in the range of 4 to 15 μm.

2. Silica is a major constituent of the shale mineral matter.

3. The weight ratio of iron to sulfur indicates that besides pyrites, iron is present in other forms also, such as iron oxides, iron silicates, iron sulfide, etc. This observation has a bearing on the applicability of the conventional ASTM chemical analysis method to determine the pyritic sulfur content, as discussed in Appendix A.

4. Pyrite particles are approximately of cuboid shape.

Hence, based on the above observations, it became imperative to grind the Illinois coal and the Eastern oil shale particles to finer sizes. Since grinding coal to micron-sized particles is energy-intensive, most electric utility industries are reluctant to do so. They operate their power plants at typical particle size of 70% -200 mesh (74 μm). Hence, in order to evaluate the performance of any physical desulfurization process, it becomes necessary to determine the percentage of pyrite liberation as a function of particle size for various coals. In the case of shale, fine grinding is necessary for removal of mineral matter because hydroretorting the beneficiated shale over the raw shale (without removal of any mineral matter) results in economic incentives (Section on Beneficiation of Eastern Shales).

The SEM information obtained above was not enough to determine the liberation curve. Therefore, these results were used in conjunction with the results obtained using an optical microscope.

Optical Microscopy

A Nikon S-2000Y optical microscope (Leitz-Metallograph) at IITRI was used for this study. Samples of coals and shales were prepared as described earlier. Only the specimens prepared by the second type, that is, by cold mounting and polishing, were used for this analysis.

Figure 3-23. SCANNING ELECTRON MICROGRAPH OF AN INDIANA-NEW ALBANY OIL SHALE SAMPLE SPECIMEN
(Bright Spots Show Pyrite- or Mineral-Enriched Area)

Samples were examined using a pointed source of light (both polarized as well as columnized beam). The optical reflectivity of various petrographic constituents present in coal is different. This difference in optical reflectivity (or contrast) was used to differentiate various mineral fractions.

Results

The results of this analysis for various specimens are described below. All the micrographs shown below were taken using bright light at a magnification of 200, indicating that 1 cm on the micrograph represents 5μm.

Illinois No. 2 Coal. Figure 3-24 shows the optical micrographs of Illinois No. 2 coal specimen taken at different locations. The bright spots were used to identify the pyrite association. The pyrites are not dispersed uniformly and occur at cleavage planes. Since this coal sample has very low ash content, it was relatively easy to identify the pyrite particles.

Illinois No. 6 Coal. This coal sample (Figure 3-25) has a very high ash content (about 35% to 40%) and the dominance of mineral matter makes it very difficult to clearly identify the pyrites. These micrographs show a very interesting distribution pattern of ash minerals in this coal as the grain

Table 3-17. ELEMENTAL ANALYSIS OF MINERAL ENRICHED AREAS IN AN INDIANA-NEW ALBANY SPECIMEN USING THE SEM

Sample I.D.	40-001[2]	40-002[3]	40-003[4]	10-004[5]	10-005[6]	10-006[7]	10-007[8]
Si	96.43	39.05	39.29	76.35	0.00	55.00	75.76
Al	0.00	8.85	0.00	0.00	0.00	0.00	0.97
S	2.44	17.28	51.36	0.00	23.32	0.00	0.00
Ca	0.00	0.00	0.00	20.46	0.00	0.00	0.00
K	0.00	7.13	0.00	0.00	0.00	7.41	2.25
Fe	1.13	27.70	9.34	3.19	76.68	36.79	21.11
Na	0.00	0.00	0.00	0.00	0.00	0.00	0.00

1. Compositions are in weight percent on a carbon-free basis.
2. A typical silica cluster with traces of pyrites.
3. A mineral matter particle containing silica, alumina and pyrites.
4. Another mineral matter particle predominantly containing sulfur.
5. A pyrite-free mineral matter particle containing calcite.
6. A pure pyrite particle. Please note that the ratio of Fe/S = 3.3 > 0.875 (in pyrite).
7. A typical ash particle having silica, K and Fe.
8. Another pyrite-free mineral cluster.

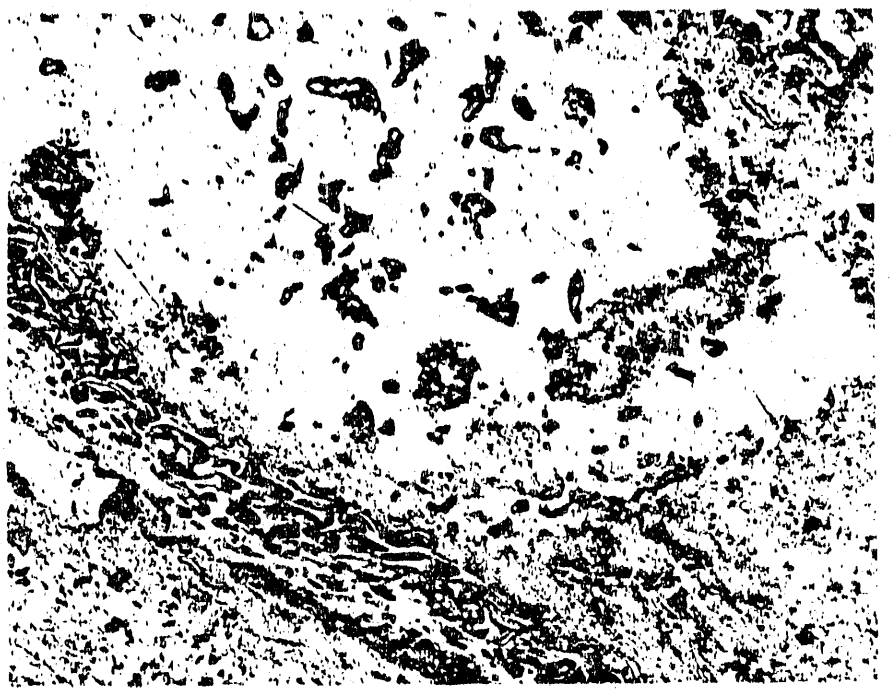

(a)

(b)

Figure 3-24. OPTICAL MICROGRAPHS OF AN ILLINOIS NO. 2 COAL SAMPLE SPECIMEN

(a)

(b)

Figure 3-25. OPTICAL MICROGRAPHS OF AN ILLINOIS NO. 6 COAL SAMPLE SPECIMEN

size of mineral matter particles is fairly coarse while pyrites are dispersed in very fine grains.

The mineral matter in oil shales is generally in the range of 70% to 85% and it is the dominating constituent of shale. Clear ident cation of pyrites in the shale matrix becomes very difficult due to the dominance of mineral matter. Figure 3-26 shows the optical micrographs of this shale specimen. Most of the area in these micrographs is covered by light gray spots representative of mineral matter, and to a small extent, by the bright spots representing pyrites, consistent with chemical composition determined by ASTM methods. Unlike the coal, the distribution of mineral matter in the shale is quite uniform. However, the kerogen seems to occur in streaks, as can be seen from Figure 3-26 (b).

Construction of Liberation Curves

Illinois No. 2 Coal

Based on the results obtained from SEM and optical microscopy analyses, a curve was constructed showing pyrite liberation as a function of particle size (Figure 3-27). This curve shows an inverse relationship between the percent pyrite liberation and particle size. This finding is consistent with investigations of Carlston (1985) who determined this curve using float-sink analysis and whose curve was a best-fit straight line rather than a smooth curve. Furthermore, for nearly complete liberation of pyrites, the coal sample must of ground to an average particle size of 2 μm. However, at a particle size of 20 μm, about 90% of the pyrites are liberated from the organic matrix. At 74 μm, which is typically used in pulverized coal burners, only 65% to 70% pyrites are liberated. Hence, the best pyrite removals at this particle size cannot be better than 70%. The ISGS researchers have also determined the pyrite grain size for this coal sample (Rapp, 1987). Their findings (summarized in Table 3-18) show that the mean diameter of free pyrite grain is 3.36 μm.

Indiana New Albany Shale

Figure 3-28 shows the liberation curve for Indiana New Albany oil shale sample, which was constructed using the same procedure described in the previous section for Illinois No. 2 coal. For nearly complete liberation of mineral matter from the organic matrix, the particles must be ground to less than 5 μm.

Grinding Techniques Used

Having determined the particle size required for the separation, it would be appropriate to briefly describe the techniques used for grinding the particles. Both the coal and shale samples were ground in 2 stages. In the first stage, they were ground in a Bantam Micropulverizer from an average particle-size of 12-20 mesh to 270 mesh (53 μm). In the second stage, they were ground in a jet mill to an average particle size of 5 to 10 μm. A brief description of both these techniques is given below.

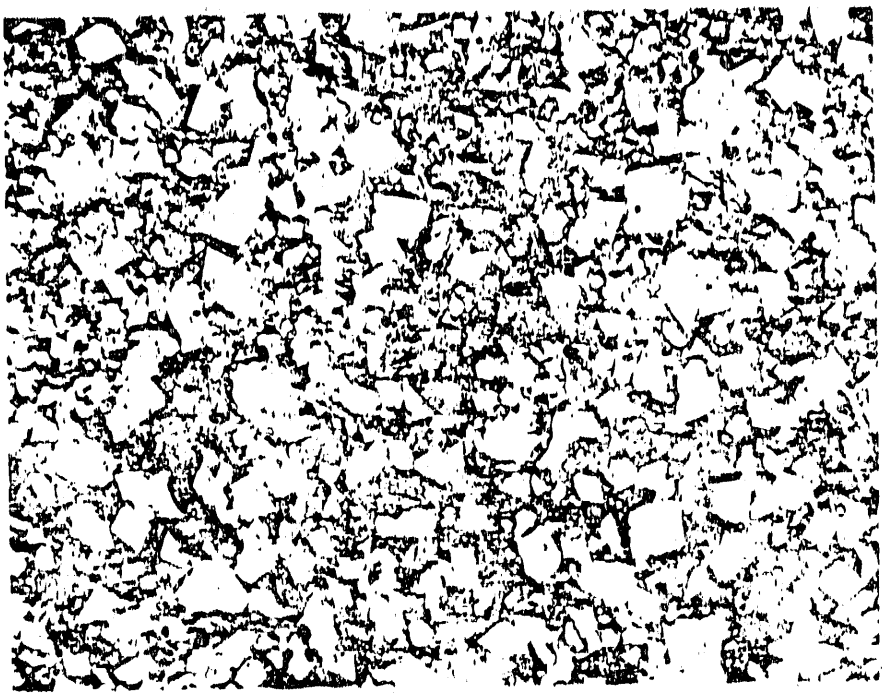

(a)

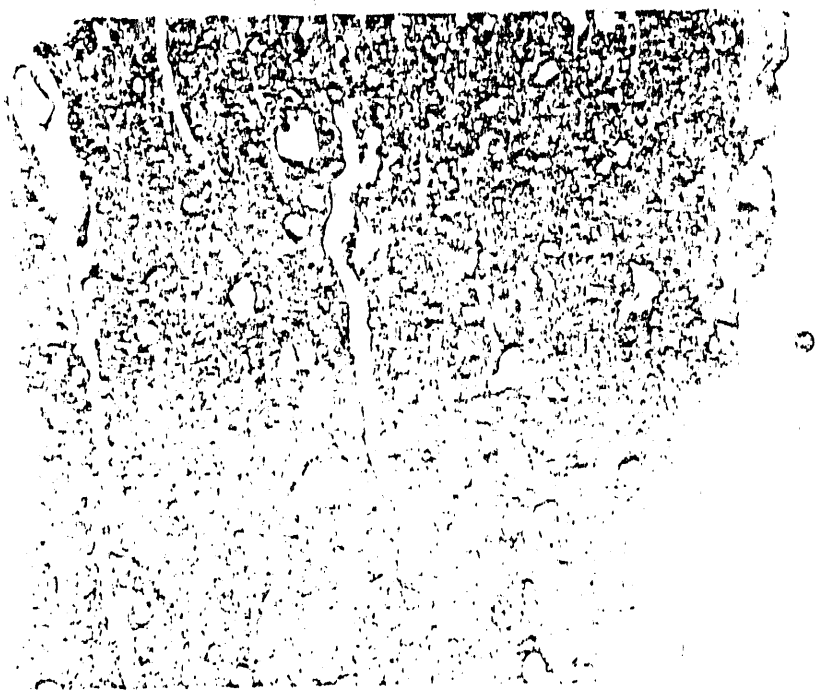

(b)

Figure 3-26. OPTICAL MICROGRAPHS OF AN IN-NA OIL SHALE SAMPLE SPECIMEN

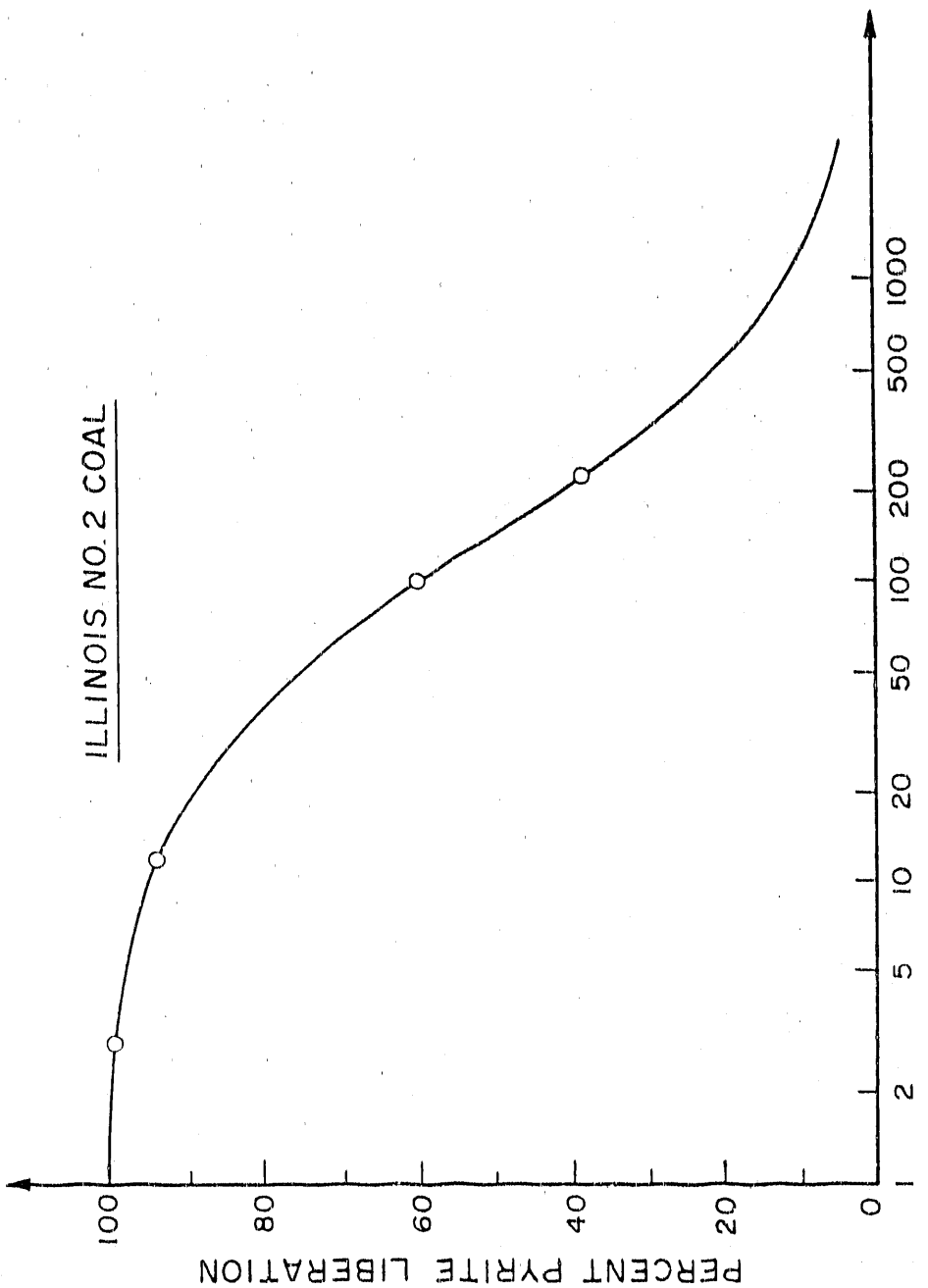

Figure 3-27. PERCENT PYRITE LIBERATION AS A FUNCTION OF PARTICLE SIZE FOR ILLINOIS NO. 2 COAL SAMPLE

Table 3-18. SUMMARY OF THE SEM ANALYSIS RESULTS FOR ILLINOIS NO. 2 COAL SAMPLE DONE BY ISGS

Particle Type	# of Grains	Mean Diameter (μm)	% Diameter
Vitrite	197	4.50	34.77
Inertite	1	2.41	0.09
Trimacerite	160	4.67	29.31
Carbominerite	97	6.46	24.58
Pyritic Coal	17	11.34	17.56
Free Pyrite	28	3.36	3.69
Total	500	5.10	100.00

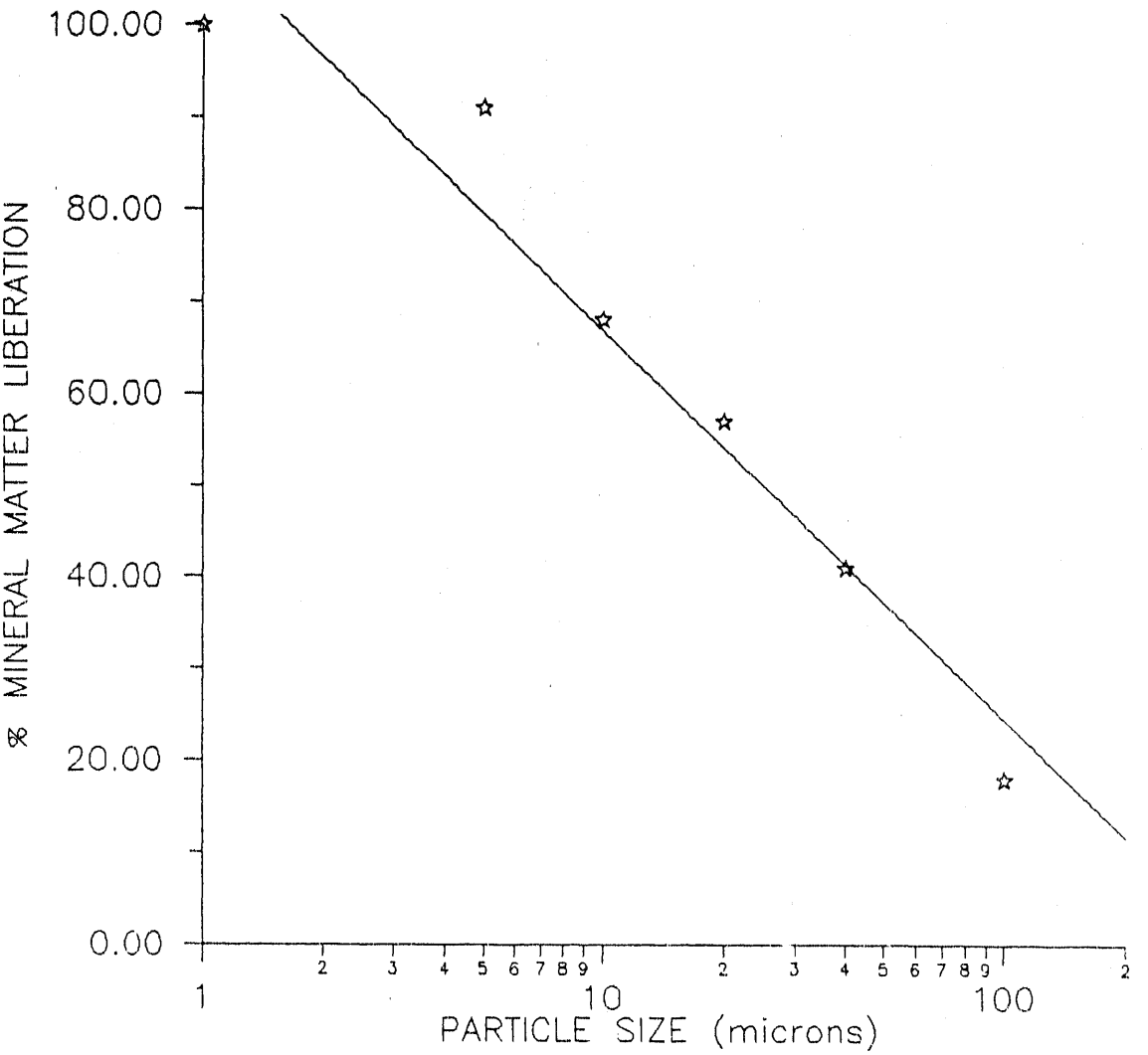

Figure 3-28. PERCENT MINERAL MATTER LIBERATION AS A FUNCTION OF PARTICLE SIZE OF INDIANA-NEW ALBANY SHALE SAMPLE

Micropulverizer

Figure 3-29 shows a schematic diagram of the micropulverizer manufactured by the Pulverizing Machinery Company (New Jersey). This machine is a close-clearance, high-speed, controlled sealed-feed hammer mill, which can be used for a wide range of non-abrasive materials with the major applications being sugar, carbon-black, chemicals, pharmaceuticals, plastics, dye-stuffs, dry-colors and cosmetics. Speeds, types of hammers, feed-devices, housing variations and screen perforations are all varied to fit applications, with the result that finenesses and character of grind cover a wide range. Feed material should usually be 1.5 inches (3.8 cm) or finer.

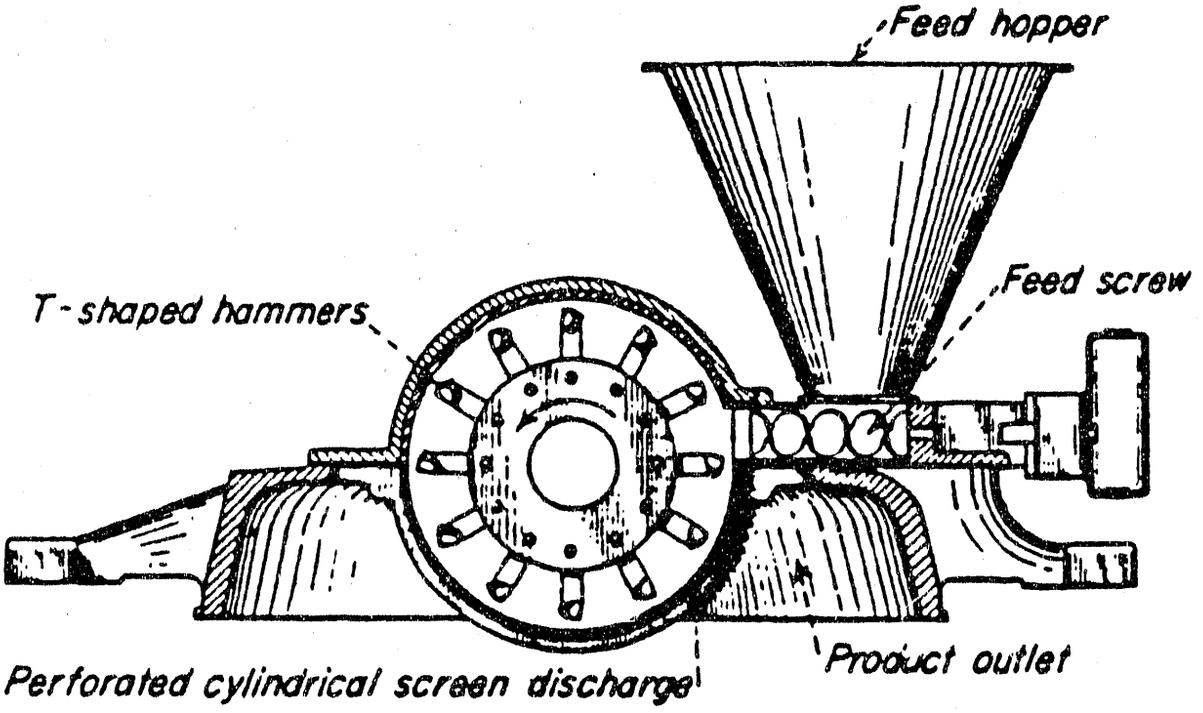

Figure 3-29. SCHEMATIC DIAGRAM OF THE BANTAM-MICROPULVERIZER

A replaceable liner for the mill housing cover is made with multiple serrations, which are designed to promote head-on-breakage of particles thrown against the wall by the rotating hammers.

These mills can be fitted with a variety of screens, with round holes, transverse slots, or herringbone slots in a wide selection of opening sizes. However, the round perforated screen is the strongest and is the one generally used. The grinding capacity of our mill is about 50 lb/h (22.7 kg/h) and the typical grind size obtained using this pulverizer is in the range of 40 to 90 μm.

Jet Mill

For ultra-fine grinding to sizes up to 1 to 5 μm, a Micron-Mas jet mill manufactured by the Jet Pulverizing Company (New Jersey) was used. This 4-inch pulverizer (Figure 3-30) can grind friable or crystalline material to an average particle size of 1 to 5 μm. It is fabricated entirely of 18-8 stainless steel and consists of a feed injector, grinding chamber and an efficient built-in cyclone collector. This mill uses air compressed to 100 psig (0.8 MPa), or of superheated steam at 150 psig and 550°F (1.14 MPa and 288°C). All surfaces contacting the product are lined with Teflon bonded-in-place.

This jet mill, also called fluid-energy mill, has a shallow grinding chamber wherein the material to be pulverized is acted upon by a number of gaseous fluid jets issuing through orifices space around the periphery of the chamber. The rotating gas must discharge at the center, carrying the fines with it, while the coarse particles are thrown towards the wall where they are subjected to further size reduction by impact from particles in the incoming jet. The outlet from the grinding chamber leads directly into a centrifugal product collector. These mills are constructed in sizes from 2 inches to 42 inches (5.1 to 107 cm) in diameter with grinding capacities up to 200 ton/h (182 metric ton/h).

This jet mill was used to grind both coal and shale to the fine sizes (5 to 10 μm). The oil shale was ground using high pressure nitrogen at IGT's Energy Development Center to prevent any oxidation that could possibly occur in air. The particle-size analysis of ground shale was done using a Coulter Counter.

Energy Consumption in Grinding

Grinding can be visualized as a process of increasing the surface area per unit mass of particles. As particles become finer, the surface area per unit mass increases. Based on this observation, several laws have been proposed to relate size reduction to a single variable, that is, the energy input to the mill. One of the laws is Bond's law, which is generally used to estimate the energy required in grinding from a particle size d_{pa} to a size d_{pb}. According to this law, the energy required in kWh per ton of material (McCabe and Smith, 1976) is --

$$\frac{P}{\dot{m}} = 0.3162\ W_i \left[\frac{1}{\sqrt{d_{pb}}} - \frac{1}{\sqrt{d_{pa}}} \right] \qquad (3\text{-}9)$$

Here, P is power in kilowatts, $\dot{m}$ is mass flow-rate in ton/h, d_{pa} is feed particle size in mm, d_{pb} is product particle size in mm, and W_i is the work index, which is defined as the gross energy in kWh per ton of feed needed to reduce a very large feed to such a size that 80% of the product passes a 100 μm screen. The values of W_i for various materials are tabulated in many handbooks (Perry et al. 1984). The value of the work index for coal is 13, and for oil shale it is 15.87.

Using Equation 3-9 the theoretical energy required in grinding a feed particle size of 28 mesh (1168 μm) to a desired product particle size (1 μm to

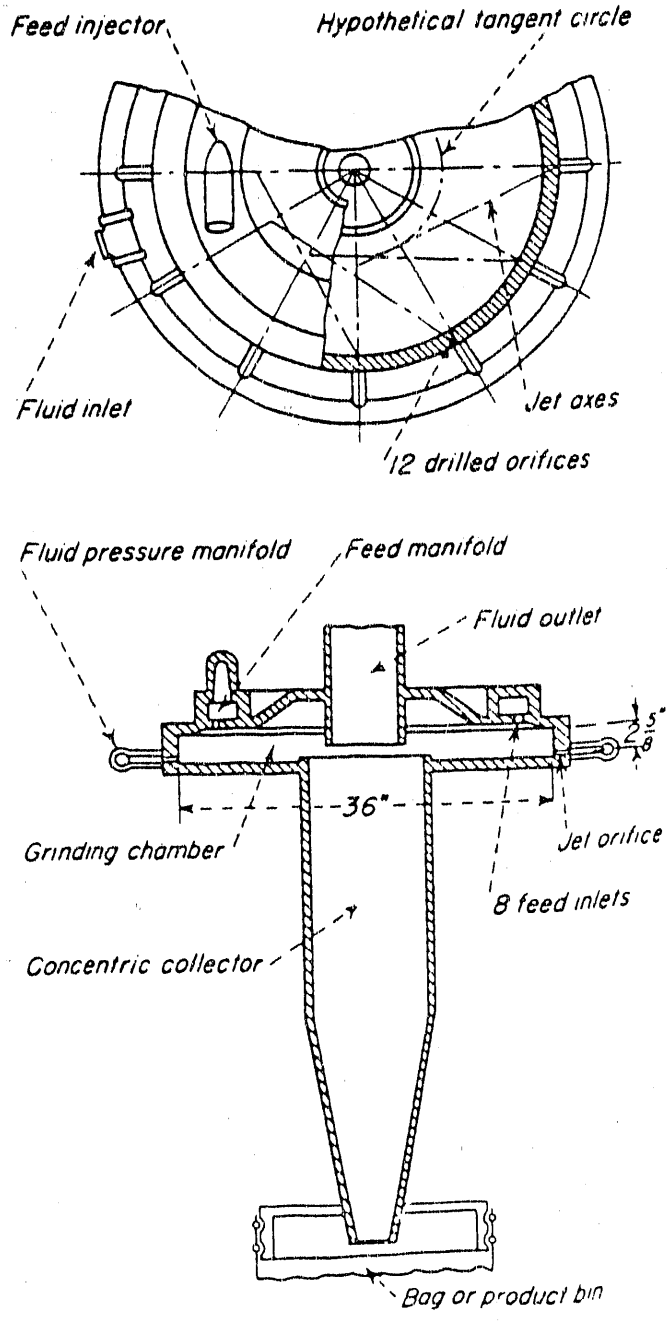

Figure 3-30. SCHEMATIC DIAGRAM OF THE 4-INCH MICRON-MASTER LABORATORY JET MILL

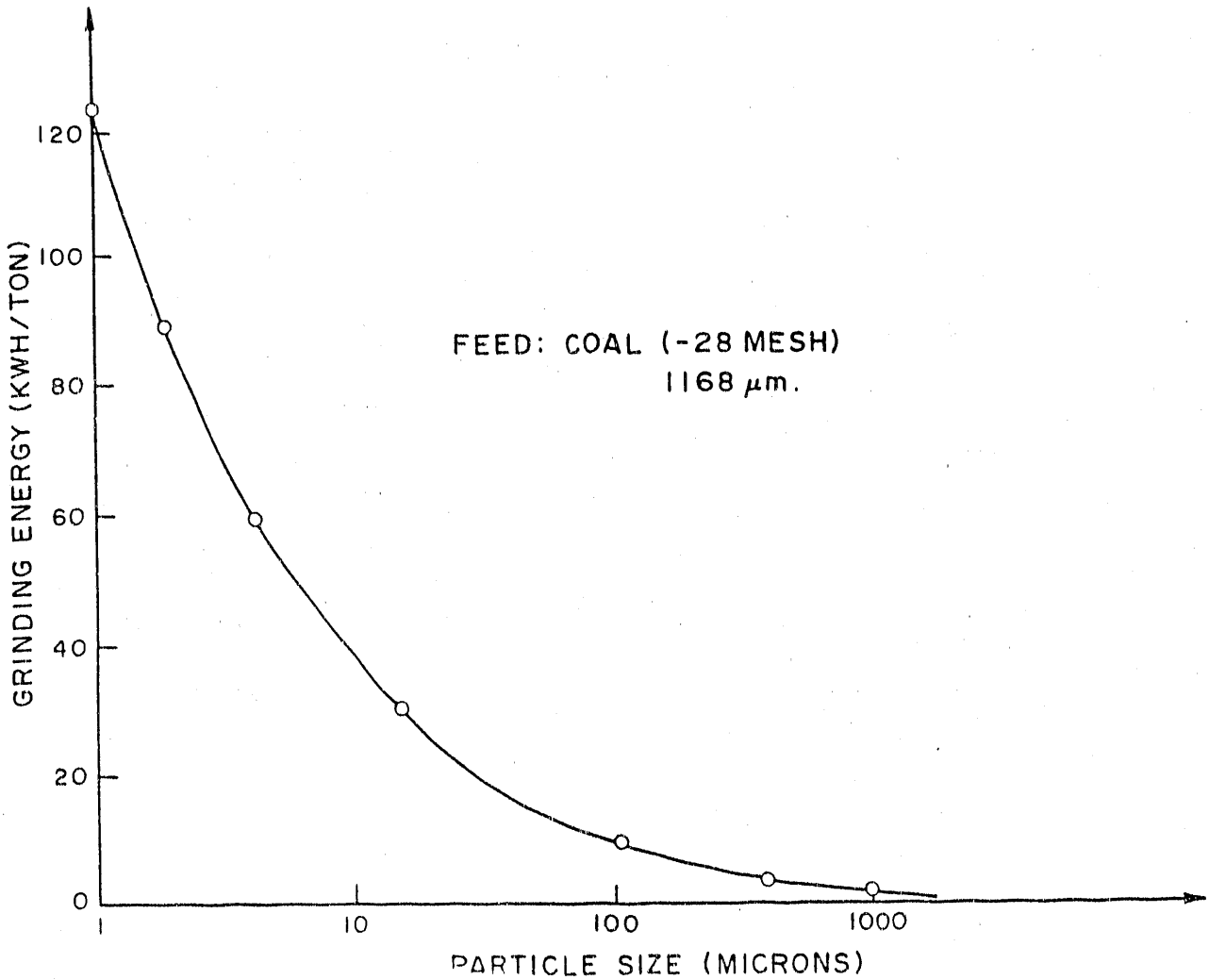

Figure 3-31. THEORETICAL GRINDING ENERGY REQUIRED AS A FUNCTION OF COAL SIZE

1000 μm) was estimated for coal. Figure 3-31 shows the curve for the required grinding energy as a function of particle size. The energy requirement increases at an exponential rate when grinding the particles to very fine sizes.

Also, a comparison was made between the theoretical energy required and actual energy used in grinding the oil shale from a particle size of 1.82 to 0.04 mm. The energy required when using the equation was about 22 kWh/t, while actual energy consumed was about 44 kWh/t. The actual energy consumed in grinding was calculated by measuring the output current and multiplying it to the circuit voltage for the measured feed rate. Thus, the ratio of actual energy consumed to theoretical energy required is 2 and for economic evaluation purposes, this provides a rough method of estimating the actual grinding energy required.

The energy consumption in the jet mill is very high as the complete pressure head of the air at a very high flow rate is used in the grinding operation. Since total power consumption equals the drop in pressure head times the flow rate, this value becomes very high compared to the energy consumed in a hammer mill operation thus showing that grinding by a jet mill is a very energy-inefficient process.

Particle-Size Analysis

In order to determine the particle-size distribution of finely ground oil shale or coal particles, a Coulter Counter (Model TA II) was used. The Coulter Counter technique is basically a method of determining the number and size of particles suspended in an electrolyte by causing them to pass through a small orifice on either side of which is immersed an electrode. The changes in resistance as particles pass through the orifice generate voltage pulses whose amplitudes are proportional to the volumes of the particles. The pulses are then amplified, sized and counted, and, from the derived data, the size distribution of the suspended phase is determined.

Figure 3-32 shows a schematic diagram of a Coulter Counter. A controlled vacuum initiates flow through a sapphire orifice let into a glass tube and imbalances a mercury siphon. The system is then isolated from the vacuum source by closing tap A and flow continues due to the balancing action of the mercury siphon. The advancing column of mercury activates the counter by means of start and stop probes so placed that a count is carried out while a known volume of electrolyte passes through the orifice (0.05, 0.5, or 2.0 mL). The resistance across the orifice is monitored by means of immersed electrodes on either side. As each particle passes through the orifice it changes the resistance, thus generating a voltage pulse that is amplified, sized and counted to determine the particle-size distribution. A more complete description of this technique is given in Allen (1968).

Figure 3-33 shows the particle-size distribution of ground shale particles. The volume mean size is about 7 μm. Fine shale particles are extremely cohesive and form agglomerates which is very detrimental to an efficient separation. The cohesive force between the fine shale particles was measured using a cohetester (details of the force measurements are described in Appendix B).

Triboelectrification

Introduction

Electrostatic processes can separate particles based on one or more of their electrical properties such as dielectric constant, electrical conductivity, and work function and all of these properties play a role in the charging process. The role of dielectric constant in charging can be explained using Cohen's Law, which states that on contact and separation of two solids, the material with higher dielectric constant charges positively (Ralston, 1961). There are, however, always some exceptions to the law. The role of electrical conductivity can be seen in terms of the charge retention time. Charged particles with higher conductivity (metals) tend to loose their charge quickly as compared to particles with lower conductivity (insulators). The role of the third property, that is, work function is of prime importance

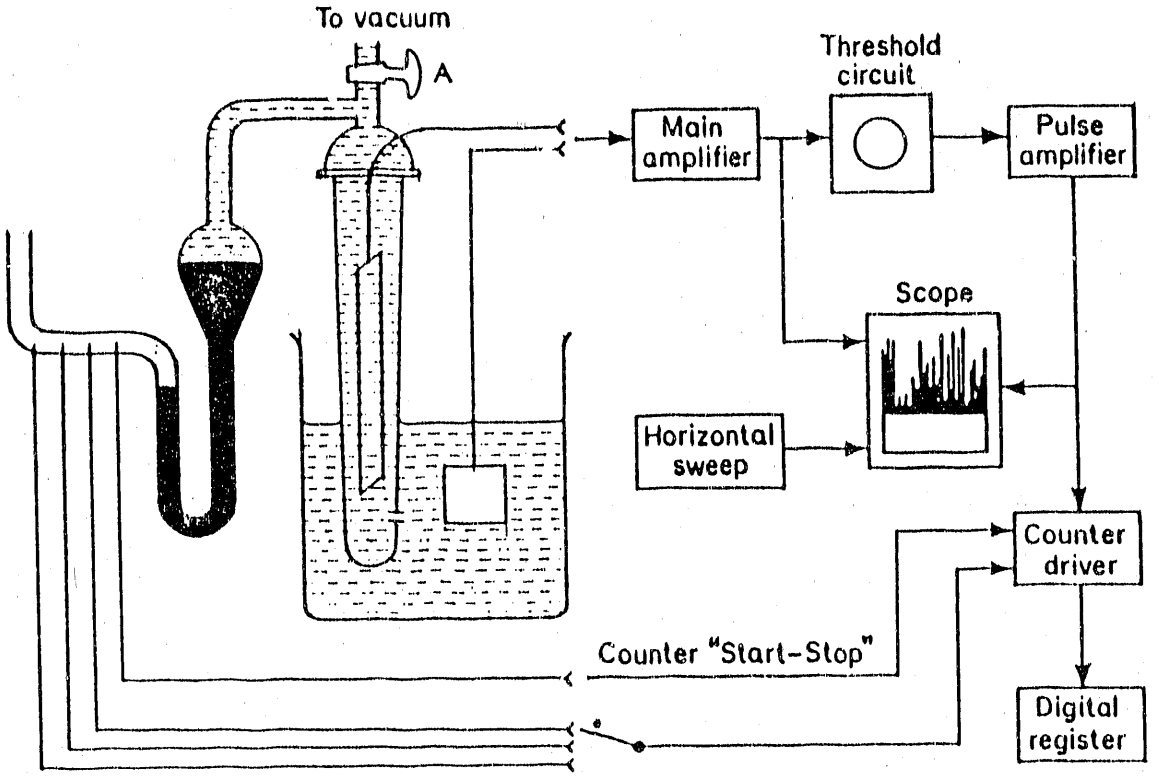

Figure 3-32. A SCHEMATIC DIAGRAM OF THE COULTER-COUNTER SYSTEM

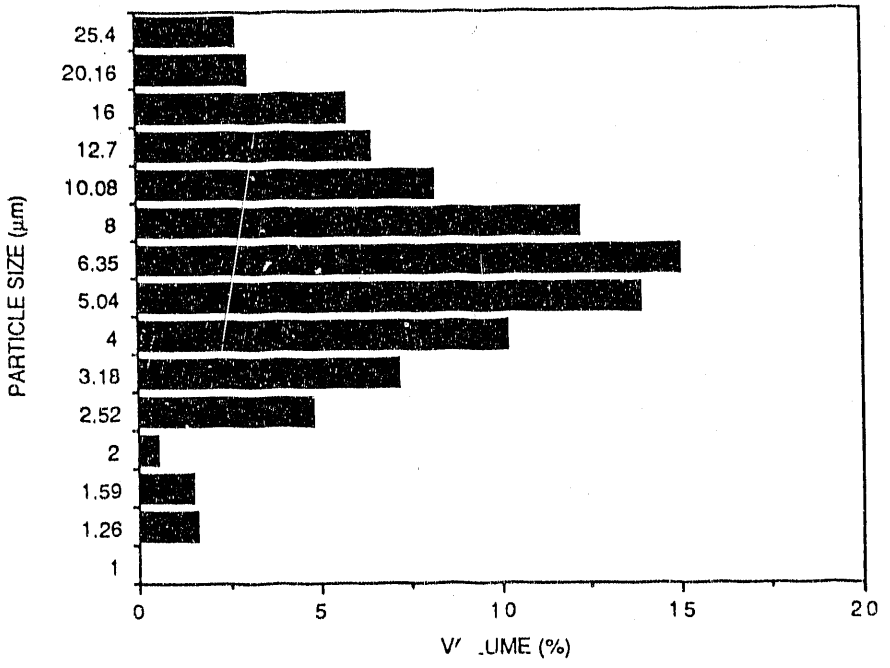

Figure 3-33. PARTICLE SIZE DISTRIBUTION FOR THE GROUND IN-NA SHALE

due to the fact that the electrostatic separation techniques investigated are based on triboelectrification as a means of charging the particles. According to the available theories of particle charging, the triboelectrification phenomenon is directly related to the work functions and, all of these electrical properties are inter-related either directly or indirectly with each other.

Particle Charging Mechanisms

There are a number of ways by which a charge can be generated on the particles so they may be separated in an electrostatic field. Following is a partial list of the various ways.

1. Charging by conduction

2. Charging by induction

3. Charging by dielectric hysteresis

4. Charging by contact and separation of poor conductors (contact potential)

5. Charging by spray, corona or other electric leakage

6. Charging by thermo-ionic emission of electrons or ions

7. Charging by photoelectric methods

8. Pyroelectric polarization, piezoelectric polarization or other naturally occurring dipoles in solid state

9. The dielectric medium separating process (does not require charging of the particles but an electric field must be set up).

Some of the processes depend not on differences in charging, but in dissipation of charge, since many of the processes involved in loss of charge are the reverse of the charging process. Charged bodies usually loose their charges through leakage and every finite solid has, at least, microscopic points (called sharp points) that can cause such leakage. Even when every effort is made to obtain perfect insulation, leakage occurs through these sharp points, which are the center of highly concentrated electrostatic fields leading to a corona discharge. Other processes depend on the shape of the field used for separation. Needless to say, the variety of forms of apparatus which effect these separations is very great.

Despite many ways in which to cause solids to acquire an electrical charge, only three charging mechanisms are used in commercial electrostatic separation, namely:

1. Charging by conductive induction

2. Charging by ion or electron bombardment (corona charging)

3. Charging by contact and frictional electrification (triboelectrification).

It should be mentioned here that these charge mechanisms are by no means mutually exclusive. Although several charging mechanisms are often active in an electrostatic separation (for example, particles sliding over a grounded chute or electrode in the presence of a high electric field), it is always desirable to design a separator in which only one charging mechanism predominates. The design of a separator usually depends on the type of charging mechanism used to effect the separation. A brief description of these charging mechanisms is presented here.

Conductive Induction

In this process, an initially uncharged particle that comes into contact with a charged surface assumes the polarity and, eventually, the potential of the surface. A particle of a good electrical conductor will assume the polarity and potential of the charged surface very rapidly. However, a dielectric particle will become polarized so that the side of the particle away from the charged surface develops the same polarity as the surface. Electrostatic separation of the conductor and non-conductor (dielectric) particles can be accomplished by the movement of the conductors in the electric field.

The electrostatic separators exploiting this principle use various electrode designs, such as plate separators, screen-plate separators, rotating electrode separators and electrostatic sieves. In all these designs, the feed material is introduced onto a ground metal slide in front of which is placed a static electrode. This static electrode may be a plate, a screen, a roller or a combination of plate and screen, depending upon the nature of application and feed particle size.

Ion Bombardment or Corona Charging

Charging of particles by means of a corona discharge is a very effective and sure way of placing a charge of known polarity on particles. Both types of particles (assuming a particle mixture of two types) are bombarded by ions of atmospheric gases which have been generated by an electrical corona discharge from a high voltage electrode (usually a fine tungsten wire at 20 to 30 kV with respect to ground and several centimeters away from the particles). When ion bombardment ceases, the conductor particle looses its acquired charge to ground very rapidly and experiences the electrostatic force tending to hold it to the conducting surface. This mechanism is used in industrial electrostatic precipitators. Rotating drum type separators used in the past to beneficiate ores, also work on this mechanism. There are, however, some major drawbacks in this process, namely:

1. It requires relatively high voltage equipment capable of delivering the required current.

2. Placing the same polarity charge on both types of the particles makes achieving the necessary selective deflection in an electrical field impractical.

Contact Electrification

When two dissimilar materials are brought into contact and then separated, they are found to be charged; this is the phenomenon of contact

electrification. This phenomenon, also referred as triboelectrification, is from the Greek word "tribein," meaning to rub. This is one of the most practical and inexpensive processes by which we can achieve selective charging of particulate matter in preparation for electrostatic separation. Tribo, or frictional, or contact electrification involves at least two physical phenomena which are important in determining electrification. The phenomena are the electronic charge transfer across the interface at the point of contact of the two materials and the electronic charge back-flow which takes place as solids are separated. The present state-of-the-art knowledge of electron transfer, between materials of different work function under rigidly controlled conditions, permits the prediction of the polarity of the charge. However, the magnitude of the charge transfer which remains on the surface after the separation is still not quantitatively predictable.

This subject of contact electrification naturally falls into three divisions:

a. Electrification of metals by metals

b. Electrification of insulators by metals

c. Electrification of insulators by insulators.

A metal is defined as having high electrical conductivity which decreases with rise in temperature and which, normally, also decreases if impurities are added. An insulator has very low conductivity (resistivity $\rho > 10^{11}$ $\Omega \cdot cm$) and a semiconductor has intermediate values; the conductivity increases with temperature, and also normally increases with added impurity. A brief description of the present state of understanding for each of these is presented below.

Metal-Metal Contacts

Contact electrification is often thought of as a phenomenon associated with insulators. In fact, charge transfer across the interface between two metals may be greater than the charge transfer between a metal and an insulator. However, the charging of metals is not usually noticeable because first, they act an as infinite ground and, secondly, they cannot accumulate charge.

The extent of the contact electrification in a metal-metal contact is governed by the charge transfer as to bring the combination to a thermodynamic equilibrium, or cause the electrochemical potential to be the same throughout the two metals (Lowell and Rose-Innes, 1980). The work function, which has a similar meaning to the electrochemical potential, is defined as the energy required to remove an electron from its Fermi level. The Fermi level is defined as the level from which the probability of finding an electron is 0.5.

Suppose two metals having work functions ϕ_A and ϕ_B are brought into contact so that the electrons between them are exchanged and come into thermodynamic equilibrium. The difference in the surface potentials of the metal will then be --

$$V_c = \frac{\phi_B - \phi_A}{e} \qquad (3\text{-}10)$$

here e is the electron charge. V_c is called the contact potential difference. The charge Q on the metal while they are in contact is given by the product of V_c and the effective capacitance between them.

$$Q = C_o \hat{} V_c \qquad (3\text{-}11)$$

where C_o is a constant that depends on the nature of contact. Figure 3-34 shows the charge on a chromium sphere after a contact with a sphere of another metal and plotted against the contact potential difference between the metal and Cr (Lowell and Rose-Innes, 1980). Harper (1967) developed a model to predict the constant C_o in Equation 3-11 based on the tunnelling effect. His experiments confirmed that the charge transfer between two metals is proportional to their contact potential differences or work functions. The work function of metal is sensitive to the presence of oxides, surface contamination and other factors and Table 3-19 shows the work function of a few metals. A complete list of work function values can be found in the works of Fomenko (1966, 1972) and the CRC Handbook (Michaelson, 1989).

Metal-Insulator Contacts

This type of contact is of prime importance in electrostatic separation. The charge acquired by an insulator from a metal that touches it may depend not only on the nature of the insulator but also, in some circumstances, on the particular metal, and type and duration of contact. Davies (1967) showed that the total charge transferred to polyethylene by contact to a metal increases with the time of contact and reaches an apparently constant value after about 15 minutes while Gonsalves (1953) found that the increase in the charge with time of contact was due to the increase in the area of contact.

As discussed in the metal-metal contact section, the charge transfer premise of thermodynamic equilibrium may be applied here. Figure 3-35 shows the triboelectrification of a series of metals in contact with an insulator (Inculet, 1984), and the inter-relationship appears linear. This indicates that the work function theory provides a good tool to analyze and predict the polarity of the charge on clean surfaces and in controlled ambients. The values for work functions of various insulators are tabulated in several monographs on electrostatics (Cross, 1987; Moore, 1973).

There are a few examples that do not exhibit a linear relationship between work function and triboelectrification that should be discussed. According to Akande and Lowell (1985), who conducted the experiments by contacting a series of metals with both Nylon-66 and PTFE, charge was not influenced by the work function for PTFE, while, with Nylon-66, it showed a perfect linear relationship and had work functions similar to the one shown in Figure 3-35. They attributed this to the existence of the non-equilibrium state of electrons in the insulators where the theory of work function breaks down.

Insulator-Insulator Contacts

Most of the contact electrification studies were concentrated on the problem of metal-insulator contacts. Contacts between two insulators have not been so intensively studied, and relatively little is known about them.

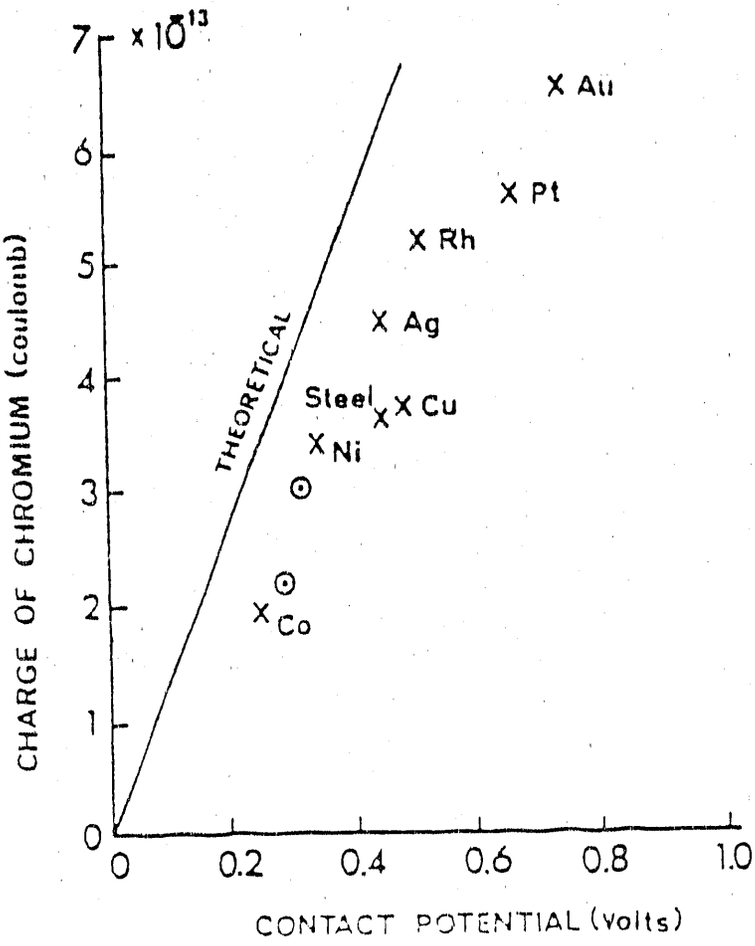

Figure 3-34. CHARGE ON A CHROMIUM SPHERE AFTER CONTACT WITH A SPHERE OF ANOTHER METAL PLOTTED AGAINST THE CONTACT POTENTIAL DIFFERENCE BETWEEN THE METAL AND CHROMIUM
(Lowell and Rose-Innes, 1980)

Triboelectrification in Air

Experiments with clean surfaces, simple elements and controlled environments to maintain the surface clean, such as vacuum, have helped apply some of the theoretical explanations to the triboelectrification phenomenon. When dealing with complex materials at ambient conditions, any prediction as to the polarity or magnitude of charge can only be guess work. However, if large numbers of experiments can be conducted to provide a statistically valid sample and, at the same time, reproducibility of the materials and ambient conditions can be maintained, practical applications may be designed on the basis of such obtained values. A good example of reliable data for triboelectrification in air is beneficiation of coal in an electrostatic separator; where the carbonaceous material in coal acquires a positive charge

Table 3-19. WORK FUNCTIONS OF VARIOUS CRYSTAL FACES

Material	Crystal Face	Work Function (eV)
Single Crystal Molybdenum	100	4.35 - 4.40
	110	4.90 - 5.10
	111	4.10 - 4.15
	112	4.55
	114	4.18
	116	4.00
Single Crystal Copper	100	5.60
	111	4.87
Single Crystal Rhenium	1000	5.53
	1010	5.05
	1011	5.04
	1100	5.15
	1120	4.80
	1121	4.70
	1124	4.72
	2110	5.07
	2111	4.82
	2112	5.27
	2113	4.84
Nickel Single Crystal	100	4.89 - 5.10
	110	4.64
	111	5.22
Aluminum Single Crystal	100	3.38
	110	3.80
	111	3.11
Chromium Single Crystal	100	3.88
	110	4.70
	111	3.88
	112	4.05
	116	3.75

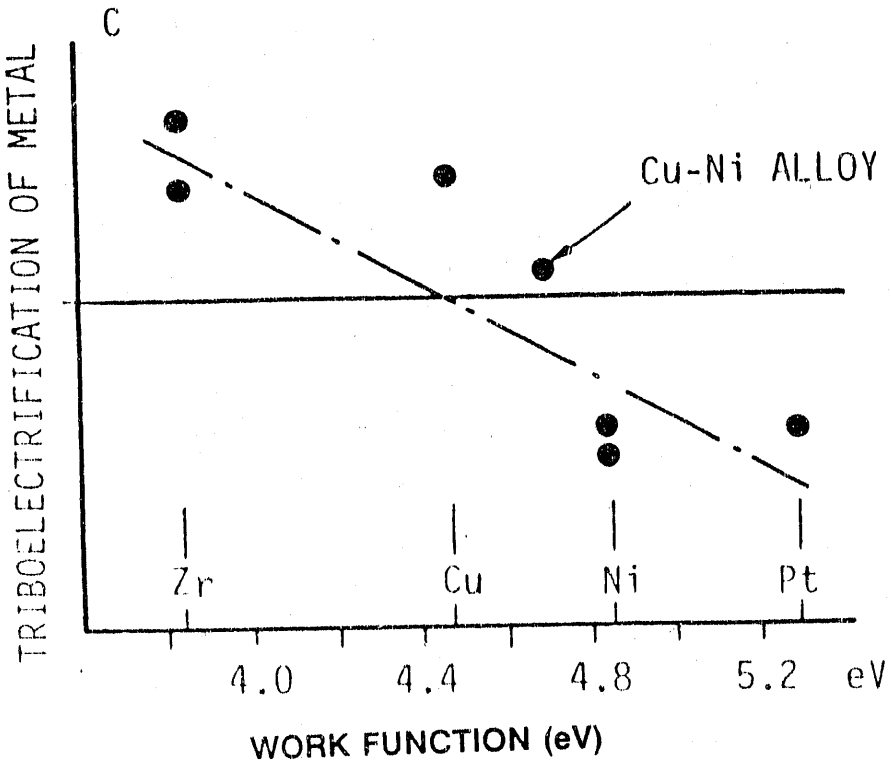

Figure 3-35. TRIBOELECTRIFICATION OF A SERIES OF METALS IN CONTACT WITH AN INSULATOR AS A FUNCTION OF WORK FUNCTIONS OF METALS

while minerals and pyrite charge negatively when coal is contacted with a copper surface. A more widespread application of this phenomena could be separating a solid mixture into its components. A suitable surface can be chosen whose work function falls between the work function of mixture components. When powder is brought into contact with that surface, the component with the highest work function charges negatively while other components acquire a positive charge thus enabling them to be separated using an electric field.

Work Functions

As defined earlier, the work function is the difference between the energy of an electron at the Fermi level inside the surface of a solid and an electron at rest in vacuum outside the solid. This value of the work function depends both on the internal structure of the material and its surface conditions. Work functions were studied extensively to determine the reliability of cathode materials used in electronic devices.

There are several methods available for the experimental determination and theoretical calculation of the work function of a particular material (Davies, 1969; Cross, 1987) and a detailed description of all these methods can be found in a book chapter by Riviere (1969). A short description of the measuring techniques is given here.

The thermionic method. The work function is found from the temperature behavior of the emission current appearing in response to heating the substance. The measurement results are interpreted with the aid of the Richardson Equation.

$$J = \frac{I}{S} = (1 - r_e) \cdot T^2 \cdot \exp\left(-\frac{e\phi}{kT}\right) \qquad (3\text{-}12)$$

where J is the current density of the current I emitted from area S at cathode temperature T, r_e is the zero-field reflection coefficient for the incident electrons, A is the Richardson constant, e is the electron charge, ϕ is the work function and k is Boltzmann's constant.

The photoelectric method. The work function is determined by the long-wavelength edge of the photoelectric effect.

The field emission method. The work function is determined by the current flowing when a high accelerating field ($>10^6$ volts/cm) is set up at the surface of the cathode.

The effusion method. The equilibrium pressure of the electron gas over the emitter at different temperatures is used to determine the work function.

The calorimetric method. The work function is computed by using the relationship between the quantity of the heat supplied to heat the cathode and the quantity of heat carried off by the electrons participating in the emission process.

The contact potential difference method. The work function is determined by measuring the contact potential difference between the material and a second electrode having a known work function. This method has been widely used for measuring the contact potential of various minerals.

Ciccu et al. (1989) have successfully used this contact potential difference method to measure the work function of various minerals. They used gold as a stable reference electrode in their experiment. In this method, the work function of material A, ϕ_A can be determined using the equation --

$$\phi_A = e \cdot V_c + \phi_o \qquad (3\text{-}13)$$

where ϕ_o is the work function of the reference (gold in their case) which is known, V_c is the measured contact potential difference and e is the charge on the electron.

Theoretical Computation of Work Functions

Empirical relationships linking the work function to various physical characteristics are utilized to calculate the work functions. The values of the work functions are correlated with atomic number, atomic volume, compressibility factor, crystal lattice energy, first ionization potential of the atom, packing density of the atoms on the facets of the crystal, surface tension, electronegativity, zero-charge potential, and atomic radius. The dependence of the kinetic characteristics of the processes, such as hydrogen

overvoltage and energy of activation of high temperature oxidation of metals on the electron work functions, was also determined. The most widely used correlation is given by Gordy-Thomas (1956):

$$\phi = 2.27\chi + 0.34 \qquad (3\text{-}14)$$

where χ is the electronegativity in Pauling units.

Electronegativity is defined as the tendency evinced by an atom in a molecule to attach or release electrons, and is usually represented as the half sum of the first ionization potential I of the atom and its electron affinity E.

$$\chi = \frac{1}{2}(I + E) \qquad (3\text{-}15)$$

Figure 3-36 shows electronegativities of various elements in the periodic table. Equation 3-14 can be used to calculate the work function of the elements in the periodic table.

To determine the work function of binary compounds, such as oxides or chlorides of various metals, the Gordy-Thomas Equation was extended by Yamamoto et al. (1974). They proposed that the work function ϕ_{AB} of a binary compound formed by reaction of elements A and B would be --

$$\phi_{AB} = \phi_A + \frac{1.41}{d_A}\left|\frac{2\phi_A - \phi_B - 0.34}{\phi_A + \phi_B - 0.68}\right| \qquad (3\text{-}16)$$

where ϕ_A and ϕ_B are the work functions of elements A and B, respectively, d_A is the single covalent bond length of element A. Table 3-20 shows the values of work functions of various compounds mainly oxides of various metals (Fomenko, 1971).

Determination of Surface Charge From Work Functions

The knowledge of work functions can now be used to estimate the resulting surface charge of the materials after contact with a surface. Professor Soo, who did the pioneering work (Soo, 1967; Soo, 1983; Soo, 1989) on the phenomenon of particle charging, analyzed the charging of dust particles by impact (Cheng and Soo, 1970). He based his analysis in terms of the dynamics of impacting bodies. Justification for such a viewpoint came from the fact that, because of the irregular nature of the contacting surface, two bodies brought into contact will touch each other at a few discrete points. However, with high impact velocities or large impact pressures, deformation immediately occurs thus allowing these discrete points to develop into contact areas. For this reason, Soo argued that the mechanical properties of the particles (for example, Poisson's Ratio, Young's Modulus, etc.) must enter into the equation in some form and he developed the following basic relationship.

The charge on a particle by impact on a wall by a turbulent suspension can be given by --

H 2.20																	
Li 1.0	Be 1.5											B 2.0	C 2.60	N 3.05	O 3.50	F 3.90	Ne
Na 0.9	Mg 1.2											Al 1.5	Si 1.90	P 2.15	S 2.60	Cl 3.15	Ar
K 0.8	Ca 1.0	Sc 1.3	Ti 1.5	V 1.6	Cr 1.6	Mn 1.5	Fe 1.85	Co 1.8	Ni 1.8	Cu 1.95	Zn 1.6	Ga 1.6	Ge 1.9	As 2.0	Se 2.45	Br 2.85	Kr
Rb 0.8	Sr 1.0	Y 1.3	Zr 1.6	Nb 1.6	Mo 1.8	Tc 1.9	Ru 2.2	Rh 2.2	Pd 2.2	Ag 1.9	Cd 1.7	In 1.7	Sn 1.85	Sb 2.05	Ta 2.30	I 2.65	Xn
Cs 0.7	Ba 0.9	La *	Hf 1.3	Ta 1.3	W 1.7	Re 1.9	Os 2.2	Ir 2.2	Pt	Au 2.4	Hg 1.9	Tl 1.8	Pb 1.8	Bi 1.9	Po 2.0	At 2.20	Rn
Fr 0.65	Ra 0.9	Ac 1.1															

Ce *	Pr *	Nd *	Pm *	Sm *	Eu *	Gd *	Tb *	Dy *	Ho *	Er *	Tm *	Yb *	Lu *
Th 1.3	Pa 1.5	U 1.7	Np **	Pu **	Am **	Cm **	Bk **	Cf **	Es **	Em **	Md **	No **	Lr

* La - Lu 1.1 - 1.2

** Np - No 1.3

Figure 3-36. ELECTRONEGATIVITY OF VARIOUS ELEMENTS IN THE PERIODIC TABLE

Table 3-20. WORK FUNCTIONS OF VARIOUS COMPOUNDS

Compounds	Work Function (eV)
BeO	3.80 - 4.70
(Ba, Sr)CO_3	1.25
Carbon (graphite)	4.00
La_2O_3	2.80
MgO	4.70
CeO_2	3.21
Al_2O_3	4.70
SiO_2	5.00
CaO	1.60 $\pm$ 0.20
TiO_2	6.21
FeO	3.85
SrO	1.27
Y_2O_3	2.00
ZrO_2	5.80
MoO_3	4.25
CS_2	0.99 - 1.17
BaO	1.10
Pr_6O_{11}	2.80
Nd_2O_3	2.30
Sm_2O_3	2.80
Eu_2O_3	2.60
Gd_2O_3	2.10
Tb_2O_3	2.10
Dy_2O_3	2.10
Ho_2O_3	2.10
Er_2O_3	2.40
ThO_2	2.54
UO_2	3.15

$$Q_{21} = 5.43 d_p^2 |V_1|^{0.6} \left[\frac{1 - \nu_1^2}{E_1} + \frac{1 - \nu_2^2}{E_2} \right]^{0.8} \rho_1^{0.8} \left[\frac{\sigma_1 \cdot \sigma_2}{\sigma_1 + \sigma_2} \right] (V_2 - V_1) \cdot \left(\frac{(1 + r^*)}{2} \right)^{0.8} \quad (3\text{-}17)$$

Here, the particle is referred to as species 1 and the surface is species 2, d_p is the particle diameter, V_1 is the velocity of impact, ν is Poisson's Ratio, E is the Modulus of Elasticity, ρ_1 is the particle density, V is the contact potential and r^* is the ratio of rebound speed to incoming speed.

In the case of coal particles (d_p = 16 μm) flowing in a brass pipe at a velocity of 35 m/s, and the charge value on the coal particle was estimated using this equation to be 1.6 X 10^{-3} C/kg as compared to the measured value of 2 X 10^{-3} C/kg. The duration of contact in the experiment was of the order of 10^{-5} s, which was much smaller than the relaxation time of the particle cloud. Therefore, this equation can be used for estimating the value of the charge for the case of particle flow in a metal or plastic tube.

The charge value for coal particles, measured experimentally with a tube charger was found to be in close agreement with the value predicted by this equation. For the case of minerals, pyrites and kerogen, it was difficult to obtain values of the elastic and electrical properties from handbooks, so rigorous comparisons could not be made. This equation predicts the polarity of the charge correctly, as is evidenced from charge measurements for coal particles impacting with copper and plastic surfaces. In the first case, coal particles acquired a positive charge; while in contact with the plastic, they charged negatively, because the work function value for the coal (ϕ = 3.93 eV) was smaller than for the copper (ϕ = 4.38 eV) and greater than for the plastic (ϕ = 3.5 eV).

Harper (1967), proposed a semi-empirical correlation to estimate the charge of metallic powders by triboelectrification.

$$\left(\frac{q}{m}\right) = 2.66 \text{ X } 10^{-13} \frac{\phi_1 - \phi_2}{\rho R^2} (8.85 + 1.115 \log R) \quad (3\text{-}18)$$

where ϕ_1 and ϕ_2 are the contact potentials, R is the particle radius in centimeters and ρ is the particle density in g/cm^3. For example, a 5-μm antimony (Sb) particle (ϕ = 4.08 volts) will acquire a charge of +6 X 10^4 C/kg on contact with a copper surface (ϕ = 4.38 volts), while an aluminum particle (ϕ = 5.42 volts) will acquire a -2 X 10^{-3} C/kg charge with a copper surface. Therefore, a scheme can be designed to charge the particles selectively in order to be able to separate them in an electrostatic separator.

Gaussian Limit of Charge by Trioboelectrification

The maximum charge q_m that can be acquired by a particle in air by triboelectrification is given by the Gaussian limit (Cross, 1987), that is,

$$q_m = \pi d_p^2 \varepsilon_o E_b \quad (3\text{-}19)$$

or maximum charge-to-mass ratio

$$\left(\frac{q}{m}\right)_m = \frac{6E_b\varepsilon_o}{\rho_p d_p} \qquad (3\text{-}20)$$

where E_b is the breakdown voltage of the air, ε_o is the permittivity of space. It can be seen from Equation 3-20 that a 20-μm diameter particle charged to the Gaussian limit has a maximum charge of 8×10^{-3} C/kg.

Particle Charge Measurement

The standard method for measuring charge is through the use of a Faraday cage or "pail" coupled to a suitable monitoring circuit (Secker and Chubb, 1984; Nieh and Nguyen, 1987, 1988; Fasso et al. 1982, Soo et al. 1964; Mukherjee et al. 1987; Gajewski, 1989) and Figure 3-37 shows a schematic diagram of a Faraday cage. It is a double-walled vessel of any suitable shape with the outer wall being grounded to form an electrical screen that prevents stray external charges from affecting the measurement. The inner wall is connected to an electrometer that measures charge by detecting the voltage build-up across a known capacitance. The principle of operation of the Faraday cage is illustrated in Figure 3-38, If a charged object of any form or conductivity is placed in the container, an equal and opposite charge is induced on the inner wall. This charge leaves behind an equal and opposite charge on the capacitor of the electrometer, which can be measured to give the charge inside the container. It does not matter whether charge flows between the object and the inner wall of the Faraday cage so that the object is neutralized, or whether the charges remain separate but paired. The Faraday cage can, therefore, be used to measure charge on either conductors or insulators. The insulation between the inner and outer container of the Faraday cage must be extremely high, that is, there should be no decay of charge when a charged particle is left in the cage.

Obviously, the Faraday cage is not able to be used when the charge is stored on a moving belt or a large particle, but it is useful for estimating the charge on liquid or powder samples. Care must be taken, however, that the means by which the liquid or powder is introduced into the chamber does not produce additional charge. The sample must enter the cage directly and not through a tube or funnel which is not a part of the inner container. When powder is collected from a gas stream, the inner can is provided with the holes to allow the air to escape and is lined with a filter to collect the powder. It is unimportant whether the filter is insulating or conducting. Figure 3-37 also shows the details of isokinetic collection of particles inside the Faraday cage. Here, a sampling tube is necessary, but it is connected electrically to the inner vessel so if charge separation occurs at its walls, both charges are measured and there is no net affect. The sampling tube is covered with an earthen shield to prevent measurement of frictional charge from collision of dust particles with the outside of the sampling tube, and with uniform sampling, the charge can be directly measured by an electrometer. The weight of the particles collected inside the inner chamber of the Faraday cage is then determined, giving an estimate of an average charge-to-mass ratio of the particle. The typical range of the charge measurement using a Faraday cage is 10^{-3} to 10^{-6} C/kg, and Table 3-21 shows the surface charge of various mineral particles measured using a Faraday cage at the IIT laboratory.

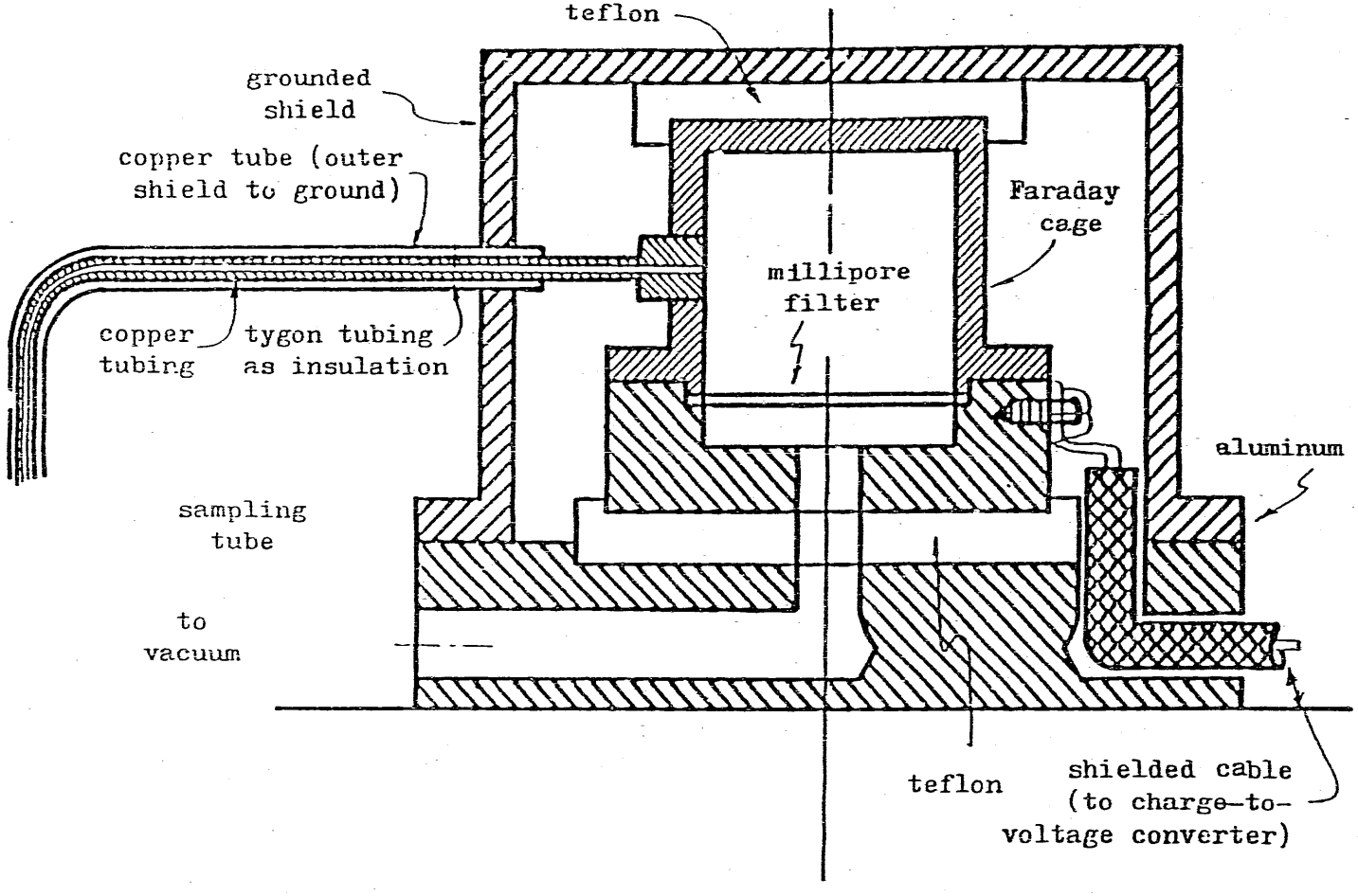

Figure 3-37. SCHEMATIC DIAGRAM OF THE FARADAY CAGE SYSTEM

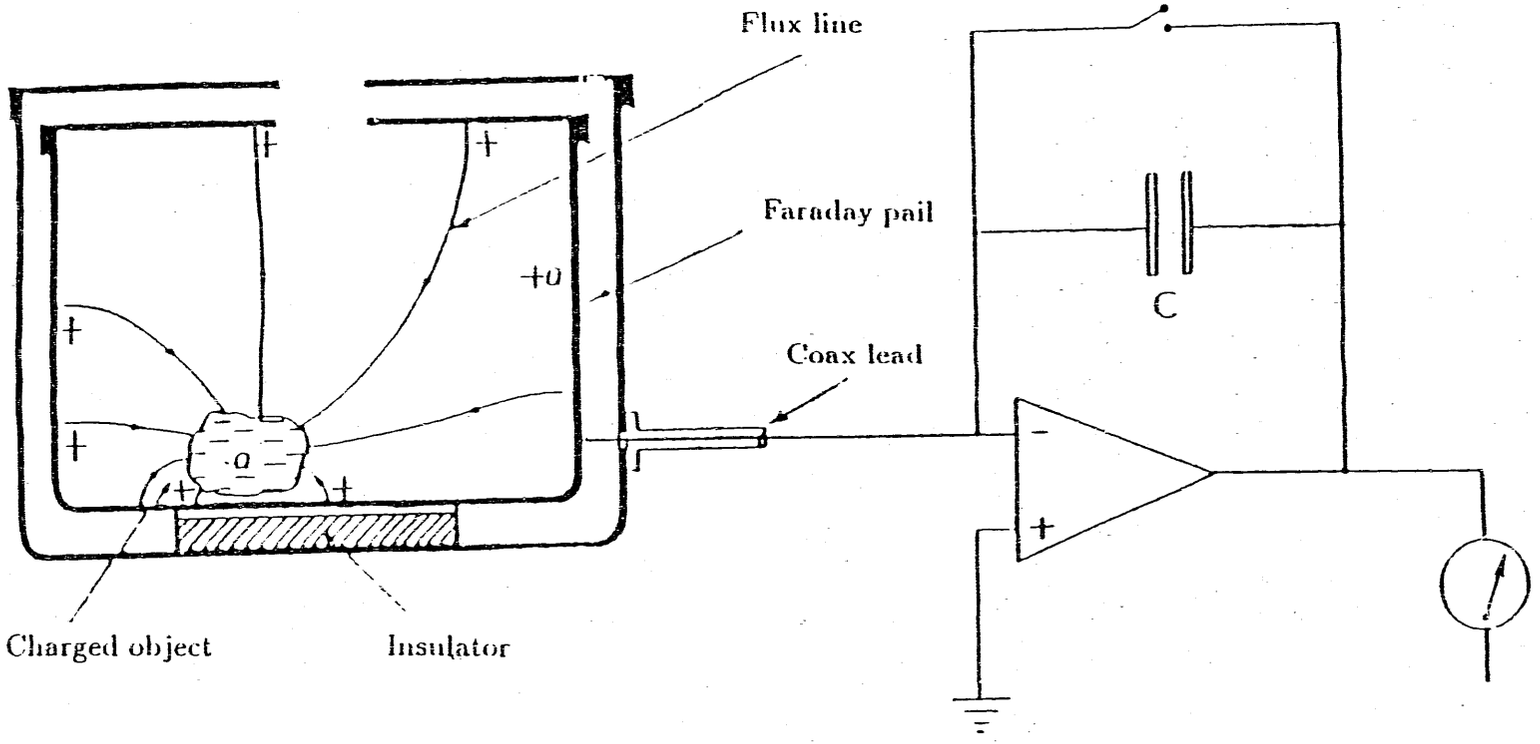

Figure 3-38. PRINCIPLE OF OPERATION OF A FARADAY CAGE

Table 3-21. SURFACE CHARGE OF VARIOUS POWDERS MEASURED EXPERIMENTALLY USING A FARADAY CAGE

Particles	Charge (C/kg)	Remarks
Pyrites	-7.00×10^{-4}	Chemically pure pyrites were used for the charge measurements.
Minerals	-1.85×10^{-3}	Spent shale from IGT was used as a mineral resource.
Shale	-6.30×10^{-5}	Indiana-New Albany Shale was used.
IL #2 Coal	$+1.34 \times 10^{-5}$	This was an Illinois Basin Coal sample.
Kerogen	$+7.00 \times 10^{-3}$	Obtained by extra-polation (see Fig 4.8)
Alabama Beneficiated Shale (ABS)	$+2.00 \times 10^{-3}$	Obtained from IGT.
ABS + Tullanox	-4.00×10^{-5}	Tullanox was added to improve the flowability.
ABS + Alumina	-1.50×10^{-4}	Degaussa alumina is also a flow smoothoner.
Charcoal	$+1.90 \times 10^{-3}$	Wood Charcoal used.

All these charge measurements were made at a particle size of 5 microns and at a gas velocity of 5 m/s with no applied electric field.

Other charge measuring techniques include a ball probe developed by Soo (Soo, 1967) and perfected by Mukherjee (1987). This ball probe is a very simple device and makes dynamic measurements possible. However, there are some drawbacks associated with this technique, which restricts its use.

Charge Measurement Results

The surface charge of various powders was experimentally determined using the Faraday cage. The effect of various variables was studied on the particle charging. A brief description of these variables and their influence on the triboelectrification is discussed below.

Effect of Temperature

Figure 3-39 shows the charge-to-mass ratio of oil shale and pyrite particles as a function of gas temperature. Charge on both shale and pyrite is negative but the charge on oil shale is one order of magnitude higher than the charge on pyrites. Furthermore, the charge increases with an increase in temperature, as one would expect. The increase in air temperature can be correlated with a decrease in humidity,; it is well known that surface charge increases with a decrease in humidity (Mukherjee, 1987).

Effect of Gas Velocity

Figure 3-40 shows the surface charge of shale and pyrites as a function of gas velocity. The charge of both shale and pyrites increases with increase in velocity. However, the rate of charge increase of pyrites is much higher than that of shale. This results in a crossover of charges of pyrites and shale at a gas velocity of 5.8 m/s. Therefore, gas velocity plays a vital role in the process of particle charging. Below the crossover velocity, the surface charge on pyrites is less than that on the shale particles, therefore, shale particles will move preferentially towards the positive electrode. However, if the system is operated at a velocity greater than 5.8 m/s, a reverse trend should be observed. These observations were supported when shale beneficiation tests were conducted at different velocities. At a velocity of 5 m/s, the pyrite-rich stream was detected at the negative electrode, whereas at a velocity of 8 m/s, the pyrite-rich stream was collected at the positive electrode.

According to Equation 3-17, the charge is proportional to the 0.6 power of the velocity. If this were true, both lines in Figure 3-40 would be parallel. A possible explanation is that the velocity plotted in this figure is the conveying velocity, while the equation uses the velocity of impact. These two velocities are not the same. Also, while deriving Equation 3-17, the area of contact for the charge transfer was determined using the elastic properties of the particles and the surface. However, this area of contact might not depend linearly on the velocity, as Equation 3-17 assumes. Furthermore, Japanese researchers (Masuda et al. 1976) calculated a dependency of charge on the velocity of impact to the 1.4 power, which was based on their observation of scar formation on the metal surface during impact.

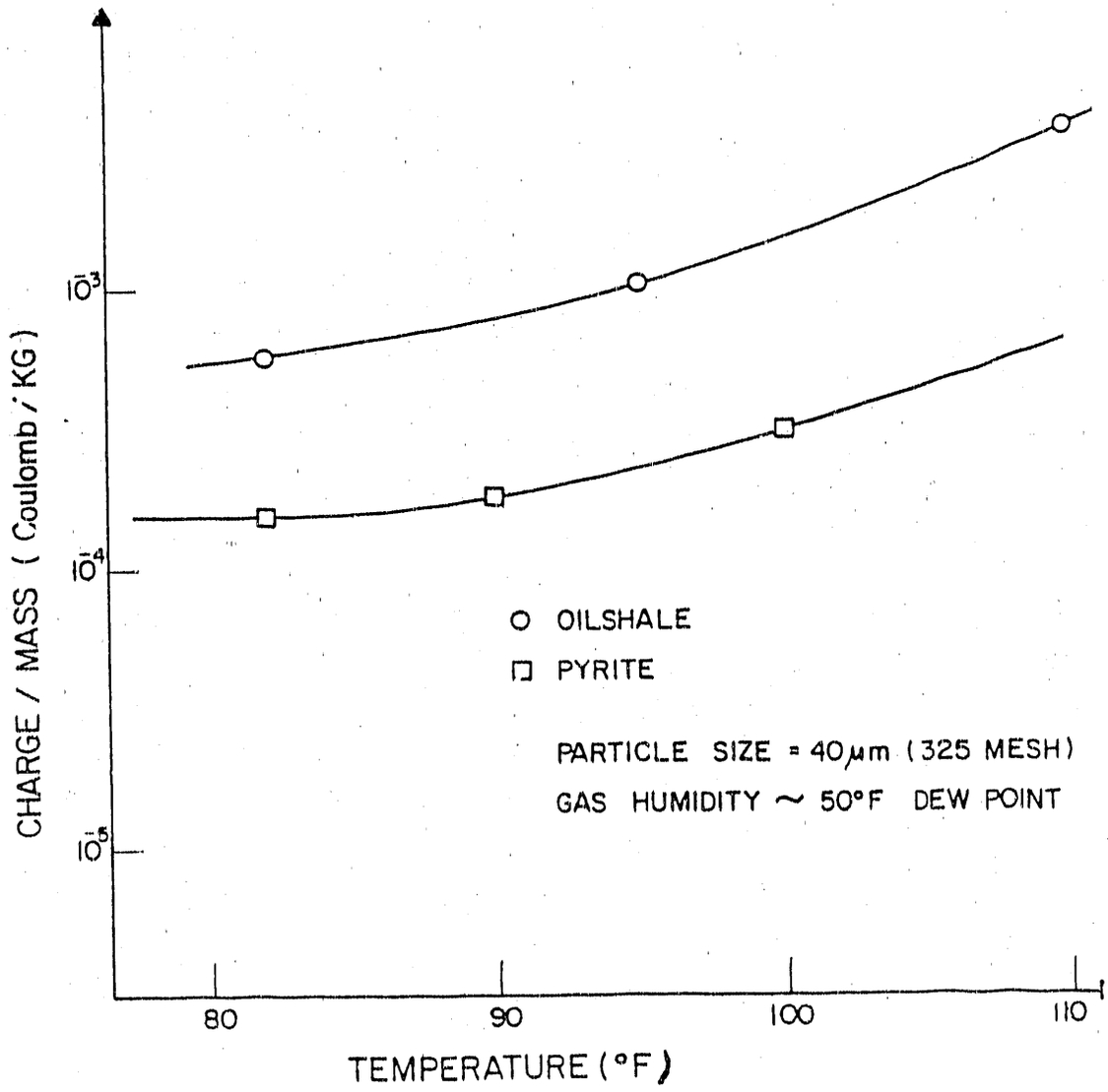

Figure 3-39. SURFACE CHARGE OF OIL SHALE AND PYRITES AS A FUNCTION OF TEMPERATURE

Effect of Kerogen Content

Figure 3-41 shows the surface charge of oil shale particles as a function of kerogen content. For these measurements, three shales of kerogen content 12%, 34% and 50% were obtained from IGT. The first shale was the Indiana New Albany shale used extensively for beneficiation tests. The second and third shales were beneficiated shales that IGT obtained from the Mineral Research Institute (MRI), Alabama. These shales had been beneficiated using the froth flotation technique.

The results show that with an increase in kerogen content, the surface charge, which is negative for raw shale, becomes positive. This is expected, since the carbonaceous matter in coal also acquires a positive charge, although kerogen has very different chemical properties than carbon in coal.

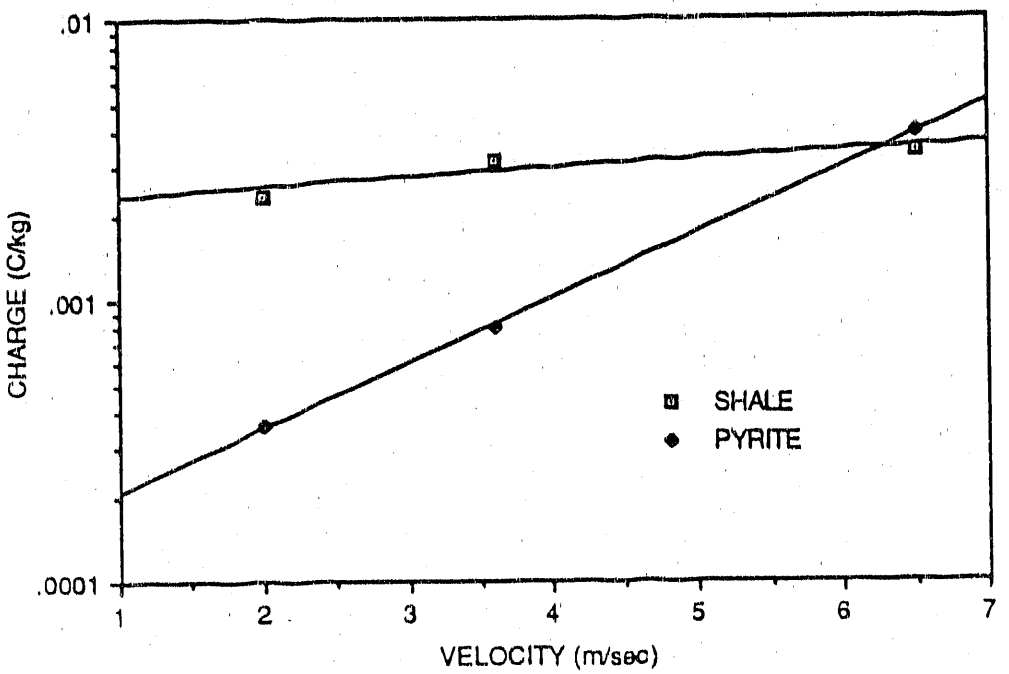

Figure 3-40. SURFACE CHARGE OF SHALE AND PYRITES AS A FUNCTION OF VELOCITY

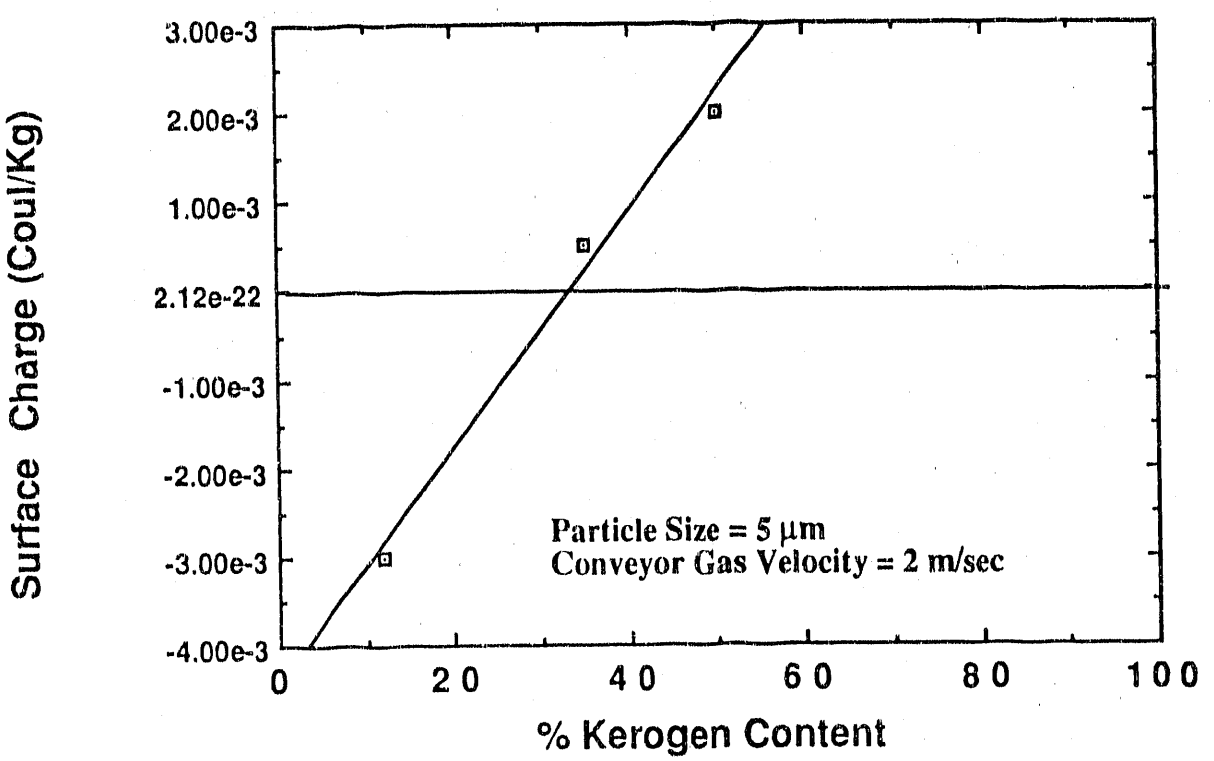

Figure 3-41. SURFACE CHARGE OF SHALES WITH VARYING KEROGEN CONTENT

These values of surface charge may not be used to extrapolate in order to determine the charge for the pure kerogen, because:

1. The relationship may not be linear. Three data points in Figure 3-41 are not sufficient to fit a curve.

2. The surface charge of beneficiated shale might be altered by the addition of surfactants added while beneficiation in a froth flotation method.

The only correct way to determine the surface charge of kerogen would be to obtain pure kerogen and measure its charge, which is not possible. Another possibility might be to beneficiate the shale by a dry electrostatic method in various stages to obtain the highest purity shale and then measure the charge. The only problem with this alternative is that it is generally not possible to obtain enough sample so that it can be run for conducting experiments in stages and finally to measure the surface charge.

Similarly, the surface charge of mineral matter present in the shale was determined by measuring the surface charge on a spent shale sample having a carbon content of less that 0.5%. This shale was produced as a refuse material after the raw shale was hydroretorted. Since this was subjected to high pressure and high temperature conditions, it may not represent the true mineral matter and, therefore, may not provide the correct estimate of the charge.

Effect of Additives

Since finely ground shale particles are extremely cohesive, some flow enhancing agents are added to these cohesive powders to make them flow better. Tullanox and alumina are two of these agents. Tullanox is a fused silica of submicron size. Addition of both the agents to shale improved the flowability. However, the surface change of shale after adding of these agents changed drastically as shown in Table 3-21. The Alabama beneficiated shale without addition any of these agents had a surface charge of $+2 \times 10^{-3}$ C/kg. With addition of Tullanox, this charge decreased to -4×10^{-5} C/kg. That is why these agents reduce cohesion. Dutta *et al.* (1989) have used these agents to improve the flowability of cohesive powders. They report that addition of these powders reduces the inter-particle forces, but they do not mention anything about surface charge. Therefore, measurement of surface charge may provide an insight in selecting a flow enhancing agent that can then be added in a right proportion to improve the flowability of the powders.

Effect of Tribocharger Geometry

Various tribocharger geometries were tested as shown in Figure 3-42. The very first tribocharger was an aluminum honeycomb, typically used in air conditioners. A schematic diagram of the honeycomb charger is shown in Figure 3-42 (a). The major drawback with this charger was that due to limited contact of particles with the metal surface, the charge acquired was very small.

The second configuration tried was a cyclone tribocharger used in the past by many researchers (Alfano *et al.* 1985; Masuda *et al.* 1981, Inculet, 1984). This cyclone was especially designed to provide maximum particle-to-

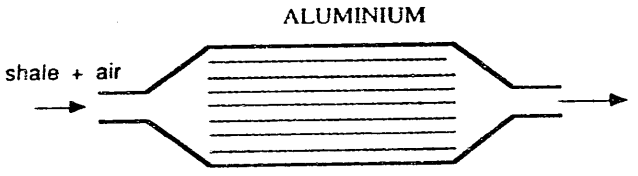

(a) HONEYCOMB

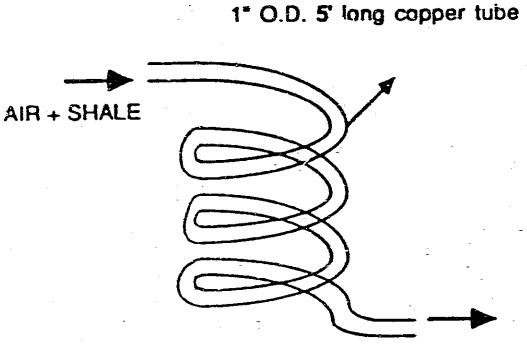

(c) TUBE CHARGER

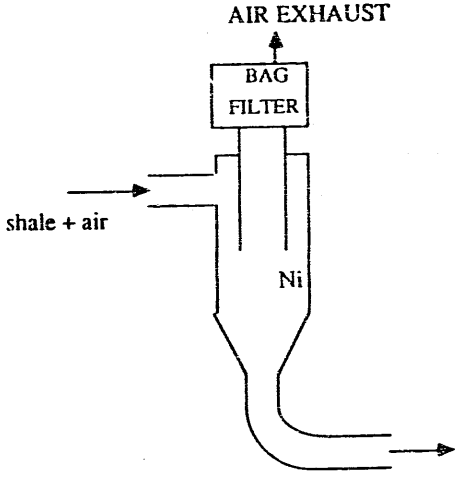

(b) CYCLONE TRIBOCHARGER

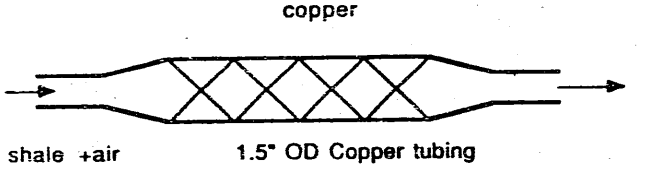

(d) MOTIONLESS MIXER TYPE CHARGER

Figure 3-42. VARIOUS TRIBOCHARGER CONFIGURATIONS USED

wall contact with a special feed inlet and was custom built at B. G. Wickberg & Company (Massachusetts). The material of construction was stainless steel with the inner surface lined with nickel. The work function of nickel lies between the work function of carbon and mineral matter. Figure 3-42 (b) shows the schematic of this cyclone tribocharger. With this device, kerogen and minerals present in the shale were found to electrify positively and negatively, respectively, which was essential for efficient separation. However, a significant charge neutralization occurred due to attraction between the oppositely charged species resulting in poor separation. The main reason for the charge neutralization was that particles were exiting from the cyclone at very low velocities and there was a high probability of oppositely charged species coming into contact with each other.

In view of the problem of charge neutralization in a cyclone tribocharger, a tube charger was designed and built [Figure 3-42 (c)]. This was a 1-inch (2.54-cm) O.D. copper tube in the form of a spiral to provide maximum particle-to-wall contact. This device worked reasonably well. The only problem with this configuration was that significant pressure drops were observed that resulted in back flow.

Finally, based on the work of researchers at PETC, an impeller type charger was designed and built and is shown in Figure 3-42 (d) (Link, 1988). This device consists of an 1.25-inch (3.2-cm) OD copper tube into which, an impeller-type copper construction is housed. Proper design of the impeller is very important because 1) enough open area is needed for particles to flow through it and 2) at the same time, there should be enough contacts between the particles and the tribocharger surface so that they could charge effectively.

This tribocharger configuration turned out to be the best, as it was simple to build, inexpensive, easy to operate and clean, and most importantly, it charged particles very effectively. The tribocharger was tested for both coal as well as for shale particles. Also, the model mixtures of silica and charcoal were separated after triboelectrifying the particles with this tribocharger.

Discussion

The role of triboelectrification in the electrostatic separation has been discussed. An effort has been made to quantify the surface charge imparted on a particle by triboelectrification. It has been shown that the polarity of the charge acquired by a particle depends primarily on the work function values of the particle and the tribocharging surface. Also, the effect of various process variables on particle charging has been presented with special emphasis on charging coal and shale particles for beneficiation. Various tribocharging configurations were investigated and their advantages and disadvantages were discussed.

Beneficiation of Illinois Coals

Introduction

A comprehensive literature review of various coal beneficiation processes, including electrostatic separation techniques either presently in

use, or being developed, was presented previously. Also, the merits of the electrostatic methods (based on triboelectrification) over other wet and other dry beneficiation methods were identified and discussed. The fluidized-bed type electrostatic separators have been used in the past for coal cleaning (Inculet, 1984). However, IIT's technique is unique in the sense that the fluidized bed is used as the means for separating the charged particles rather than using it as a device to charge the particles.

In previous work, IIT used a batch electrofluidized bed to determine the feasibility of separating iron pyrites from coals. Synthetic mixtures of coal and iron pyrites were prepared and tested in a batch-electrofluidized bed. The details of these tests are reported by Saxena (1985). These batch tests indicated that pyrites could be removed from coal by applying an electric field. However, the drawback with the batch-type electrofluidized bed was that the process of removal was not continuous. Therefore, a continuous electrofluidized bed was designed and constructed as described in the next section.

Separation in a Continuous Electrofluidized Bed

Apparatus

Figures 3-43 and 3-44 are schematic diagrams of the continuous electrofluidized bed. This device was a transparent, two-dimensional bed made of 1/2-inch (1.27-cm) thick plexiglas. The bed dimensions were 1/2-inch (1.27-cm) deep, 7-inches (17.8-cm) wide and 40-inches (102-cm) high. It consisted of two sections, the top section and the bottom section, joined together with flanges and screws. The top section of the bed was the actual fluidization section in which coal was continuously fed from the top, through a hopper and a vibratory feeder, and the pyrite-enriched stream and the clean coal stream were taken out through 1/4-inch (0.64-cm) diameter openings near the bottom of this section on either side of the bed fitted with tubes.

The bottom section of the bed was mainly used as a passage for nitrogen that was used as the fluidizing medium. It was a 7-1/2-inch (19.1-cm) high, 1/2-inch (1.27-cm) deep and 7-inch (17.8-cm) wide section containing two metal tubes for gas flow to the distributor and a rectangular slit acting as a 3 mm X 1 cm rectangular jet for nitrogen flow. Dry nitrogen was supplied from a high pressure tank and was metered by two rotameters; one measuring the total gas flow while the other measured the nitrogen flow through the rectangular jet. The nitrogen flow was regulated using a pressure regulator and the gas pressure was maintained at 20 psig (0.24 MPa).

The gas distributor was a porous, glass wool strip put between flanges joining the top and bottom sections of the bed, that maintained a homogeneous gas flow throughout the bed. Two perforated (ϕ = 3 mm) aluminum plates (with dimensions 1/2-inch X 40-inches) were separated from each other by 10 cm and supported by thin plexiglas pieces glued to the top section of the bed. These plates were referred to as electrodes when connected to the voltage generator.

A d.c. voltage generator (Universal Voltronics) capable of generating up to 36 kV, was used to generate the electric field. The distance between the electrodes was kept at 10 cm. Since, a spark between the electrodes around the distributor (support plate) was observed beyond 12 kV, the applied voltage in all the experiments was kept below 12 kV.

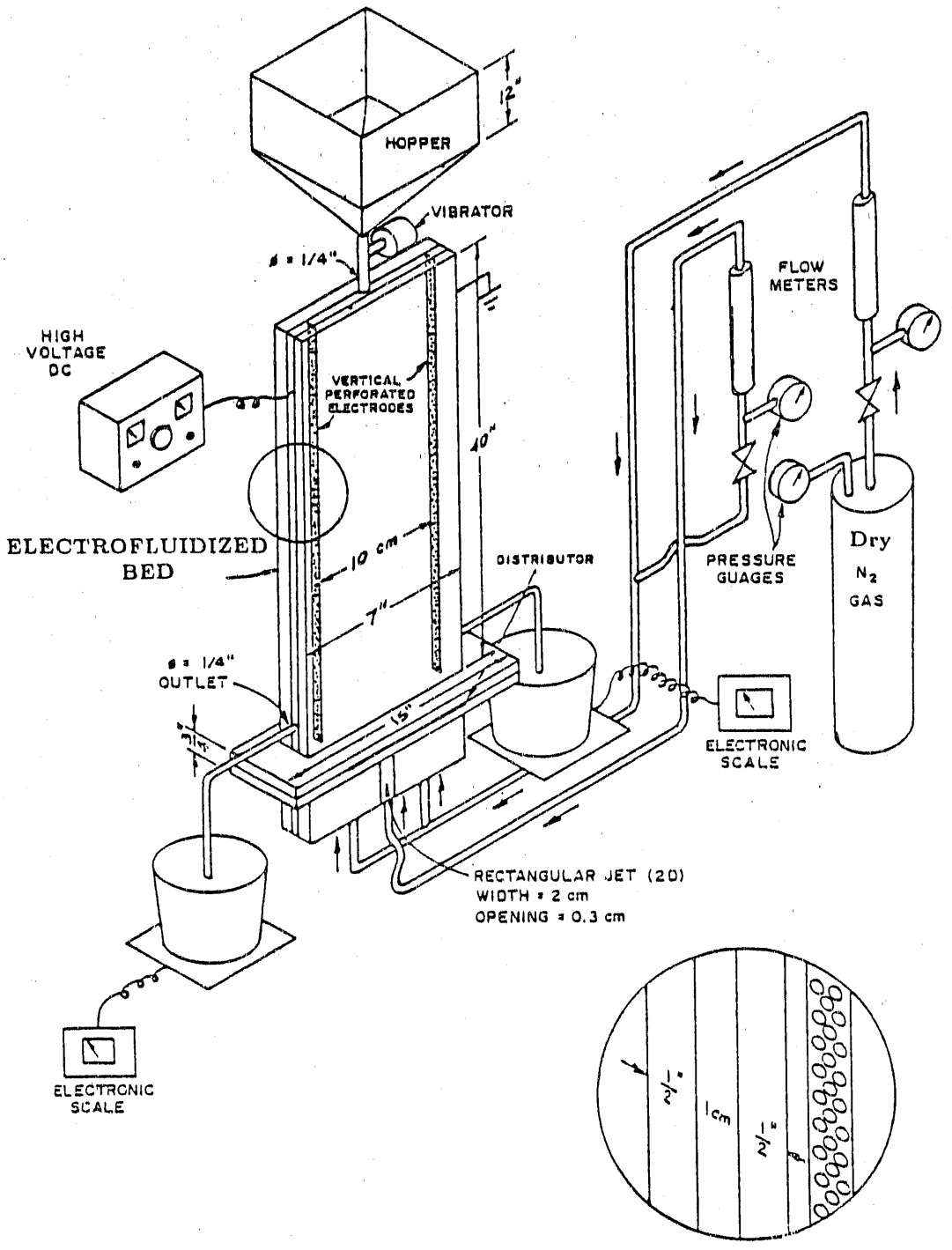

Figure 3-43. PERSPECTIVE VIEW OF IIT'S CONTINUOUS ELECTROFLUIDIZED BED SYSTEM

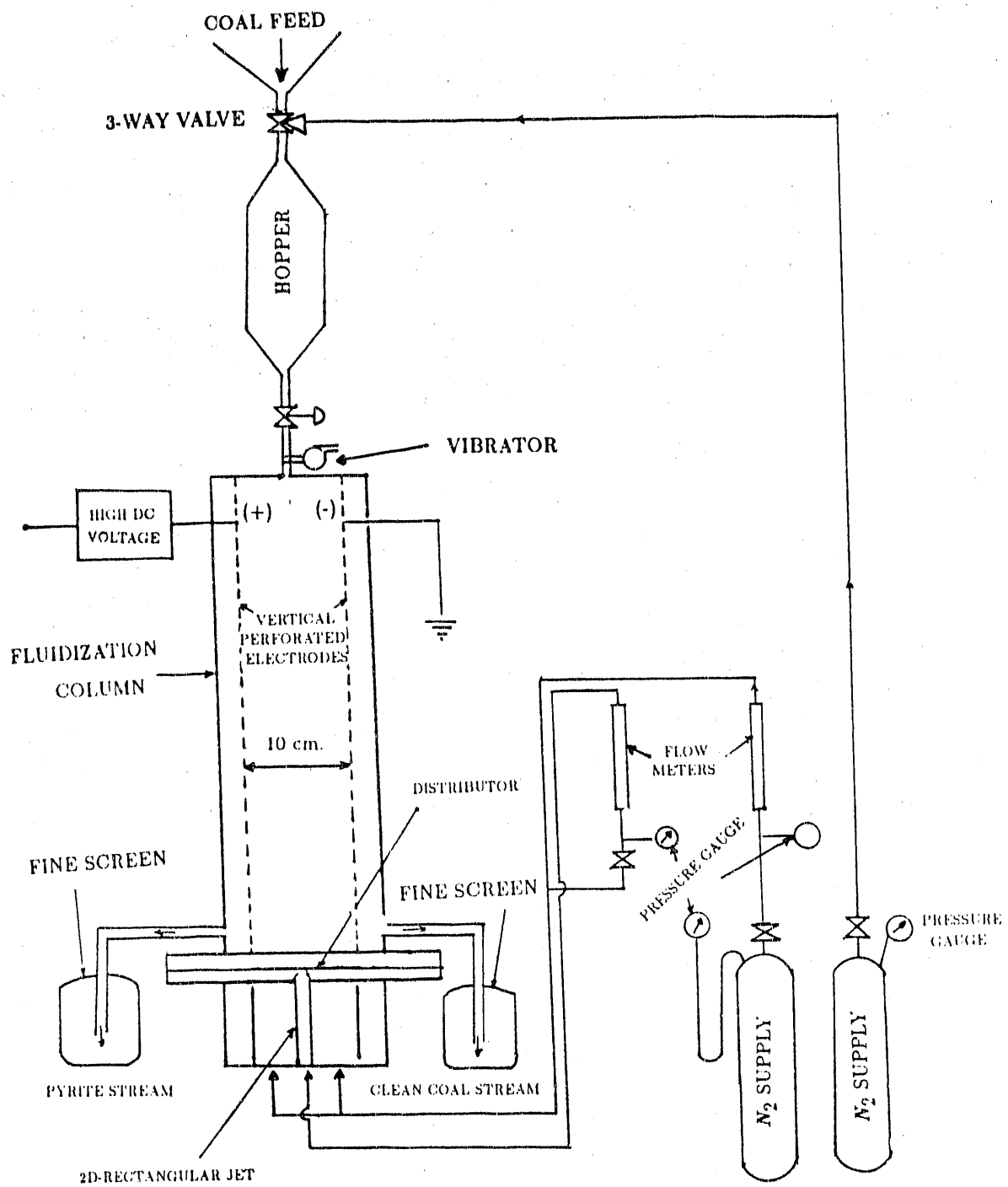

Figure 3-44. LINE DIAGRAM OF IIT'S CONTINUOUS ELECTROFLUIDIZED BED SYSTEM

The operating principle of the bed is simple. Coal particles, ground to a particle size in the range of 100 to 150 μm, were loaded in the hopper. They were then continuously fed from the hopper through a vibratory feeder actuated by air pressure and a high d.c. voltage was applied. While coal was fluidized using nitrogen gas, pyrites having negative charges migrated toward the positive electrode while pyrite-free coal particles (possibly carrying a positive charge) went to the negative electrode. Since the electrodes were perforated, both coal and pyrite particles passed through the electrode, fell in the channel and were collected through openings and weighed by digital electronic balances. Illinois No. 2 and Illinois No. 6 coal samples were tested in this unit and the results of the pyrite separation from these coal samples are described below.

Results

Following are the results for three Illinois coal samples. An Illinois No. 2, stripmined coal sample was obtained from Mr. Larry R. Camp of the ISGS. The initial pyrite content of this sample was 5.2% by weight and average particle size was 60 μm.

Six pounds of the coal sample were loaded in the hopper. Nitrogen gas was then introduced in the bed through the rectangular jet as well as through the distributor. The total flow of nitrogen to the bed was kept very small [0.22 cfm (6.23 L/min)] because the coal particles were very fine, having a minimum fluidization velocity of less than 1 cm/s. At the same time, a potential of 12,000 V was applied to the electrodes. During the test, coal started coming out through the outlets on both (positive and ground) sides and was collected. When all the coal in the hopper was used up, and no more material was observed to be coming out of the channels, the high voltage source and the nitrogen supply were cut off and materials collected on both sides were weighed. Samples of feed, pyrite-lean and pyrite-rich coal were sent to IGT for determination of pyrites by the ASTM method.

Table 3-22 shows the pertinent experimental data. In the first stage, the pyrite content of the coal was reduced from 5.2% to 3.33%. The stage number here indicates that pyrite-enriched coal obtained from the previous run was used as the feed in this run. The typical flow ratio of the pyrite-enriched steam and the pyrite-lean steam was about 4. The pyrite material balance matched within 90%.

Another test was made with Illinois No. 2 coal ground to a particle size of 150 μm. This coal sample was obtained from Mr. David Rapp of the ISGC. Table 3-23 shows the experimental data for this sample. In three stages, the pyrite content of this coal sample was reduced from 4.05% to 2.02% at a particle size of about 150 μm. However, coal recoveries were poor.

Figure 3-45 shows the pyrite removal as a function of stage number. The data suggest that the pyrite levels have the potential of being reduced sufficiently low to obtain compliance coal from Illinois No. 2 coal. This figure also shows finer ground coal gives a better separation.

Table 3-22. DESULFURIZATION TEST WITH ILLINOIS NO. 2 COAL IN ELECTROFLUIDIZED BED

Sample Used	:	Illinois #2 Coal
Average Particle Size	:	60 μm
Applied Voltage	:	12,000 Volts
Nitrogen Flow Rate		
(a) through jet	:	52 cm^3/sec
(b) through distributor	:	52 cm^3/sec

	Feed		Clean Coal Stream		Pyrite-rich Stream	
Stage #	Flow Rate (lb/hr)	Pyrite Content (wt.%)	Flow Rate (lb/hr)	Pyrite Content (wt.%)	Flow Rate (lb/hr)	Pyrite Content (wt.%)
1	6.00	5.20	2.00	3.33	3.80	5.87
2	3.80	5.87	1.00	4.30	2.50	6.25
3	2.00	6.25	0.50	3.65	1.25	8.40

Note: The output flow rates do not add up to the feed flow rate due to the holdup of some coal in the bed.

Table 3-23. DESULFURIZATION TEST WITH ILLINOIS NO. 2 COAL IN ELECTROFLUIDIZED BED

Sample Used	:	Illinois #2 Coal (IBC-102)
Average Particle Size	:	150 μm
Applied Voltage	:	10,000 Volts
Nitrogen Flow Rate		
(a) through jet	:	65 cm^3/sec
(b) through distributor	:	45 cm^3/sec

	Feed		Clean Coal Stream		Pyrite-rich Stream	
Stage #	Flow Rate (lb/hr)	Pyrite Content (wt.%)	Flow Rate (lb/hr)	Pyrite Content (wt.%)	Flow Rate (lb/hr)	Pyrite Content (wt.%)
1	6.00	4.05	3.00	3.41	2.40	4.23
2	4.00	3.41	2.20	2.70	1.40	3.75
3	2.00	2.70	1.00	2.02	0.60	3.00

The output flow rates do not add up to the feed flow rate due to the holdup of some coal in the bed.

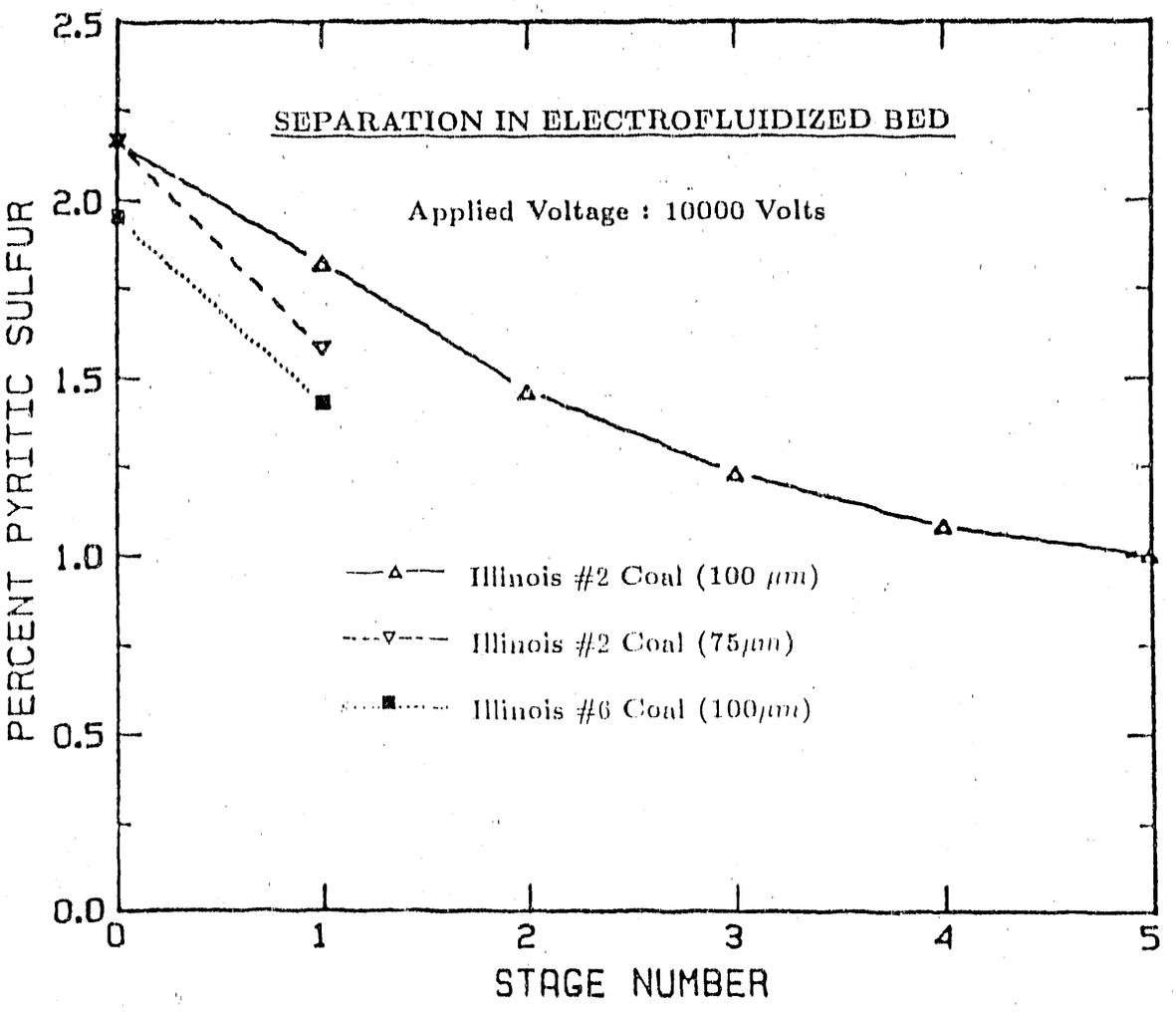

Figure 3-45. REMOVAL OF PYRITIC SULFUR FROM ILLINOIS COALS IN THE ELECTROFLUIDIZED BED

Figure 3-46 shows the mass flow rates for the streams in the electrofluidized bed for this coal sample. The inlet flow is split approximately equally into a clean-coal stream and a pyrite-enriched stream.

Experiments were done with an Illinois No. 6 (IBC-104) coal sample using the same procedure described above. This coal sample had an ash content in the range of 35% to 40%. Table 3-24 shows the experimental data for this sample. The poor separation results can be attributed to the presence of ash minerals, which possibly hindered the migration of pyrite particles towards the electrode.

In order to eliminate the need for staging, a multi-stage fluidized bed was designed and built. Unfortunately, the particles would not flow properly through the cavities connecting the clean product outlet to feed-inlets of successive stages. Therefore, further testing of this multistage unit was abandoned.

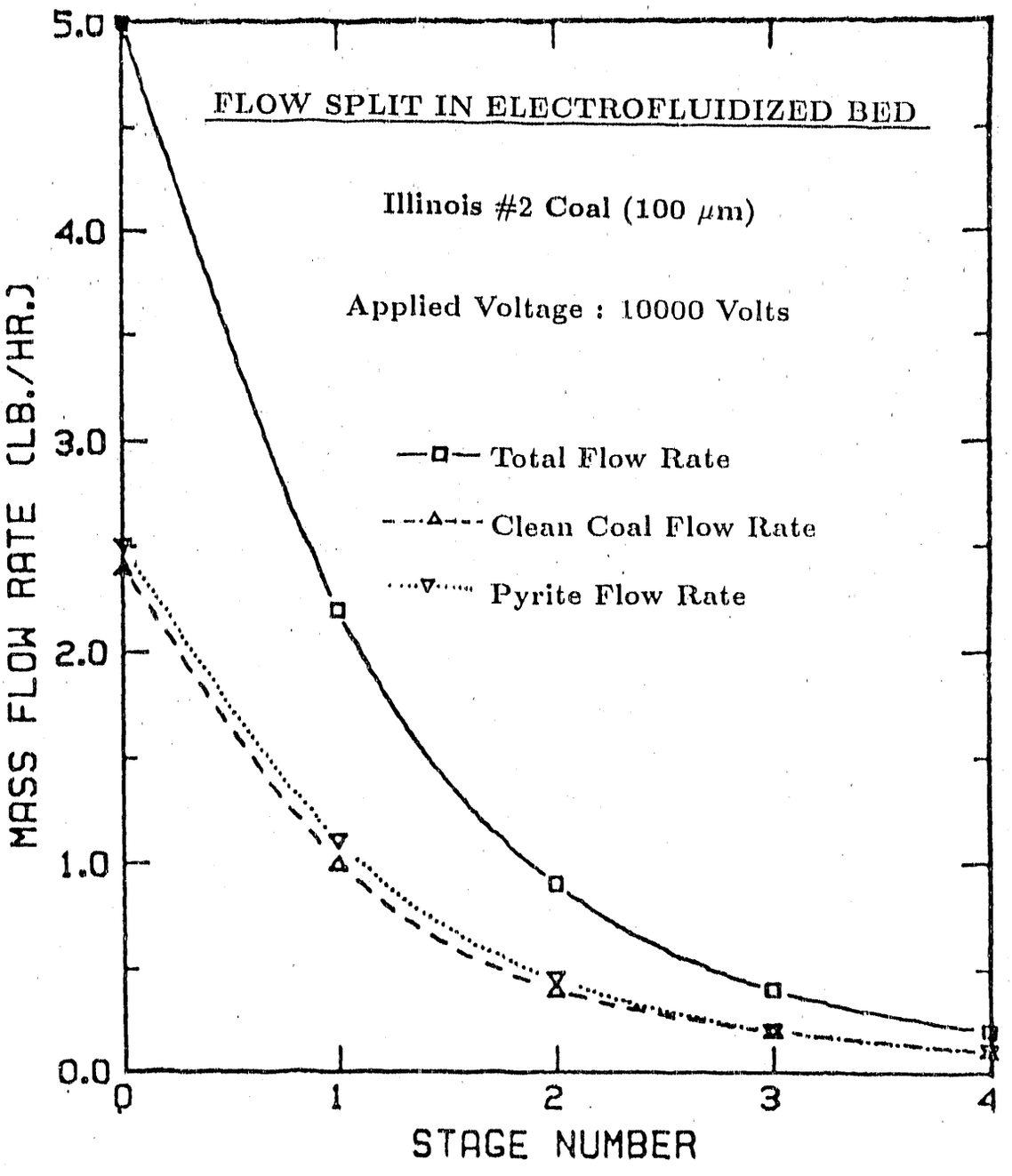

Figue 3-46. FLOW RATES OF INLET, CLEAN COAL AND PYRITE-ENRICHED STREAMS IN THE ELECTROFLUIDIZED BED CORRESPONDING TO DATA IN FIGURE 3-45

Table 3-24. DESULFURIZATION TEST WITH ILLINOIS NO. 6 COAL IN ELECTROFLUIDIZED BED

Sample Used	:	Illinois #6 Coal (IBC-104)
Average Particle Size	:	120 μm
Applied Voltage	:	5,000 Volts
Nitrogen Flow Rate		
(a) through jet	:	68 cm^3/sec
(b) through distributor	:	34 cm^3/sec

	Feed		Clean Coal Stream		Pyrite-rich Stream	
Stage #	Flow Rate (lb/hr)	Pyrite Content (wt.%)	Flow Rate (lb/hr)	Pyrite Content (wt.%)	Flow Rate (lb/hr)	Pyrite Content (wt.%)
1	6.30	3.05	3.40	3.01	2.70	3.09
2	3.00	3.01	1.40	2.92	1.30	3.03
3	2.50	2.92	1.20	2.89	1.20	2.95

The output flow rates do not add up to the feed flow rate due to the holdup of some coal in the bed.

IIT also attempted to run the fine particles (d_p = 40 μm or less) in the electrofluidized bed to improve pyrite removal. However, at these fine sizes the inter-particle forces become dominant. The particles cannot be fluidized by conventional methods as they fall into Geldart type "C" particle classification (Geldart, 1973). A phenomenon called "jet penetration" was observed in which the gas flow through the jet penetrates the bed without fluidizing the particles. At extremely high distributor gas velocities, particles were found to elutriate in the gas and the system could no longer be operated with the result that the fluidized-bed separation was found to be restricted to fairly coarse particle sizes (70 μm).

Separation in a Electrostatic Sieve Conveyor

Since the fluidized-bed system was restricted to coals ground to no less than 70 μm and since, for nearly complete liberation of pyrites, Illinois coals must be ground to less than 20 μm, a new separator called an electrostatic sieve conveyor was invented, as shown in Figure 3-47. Mukherjee (1987) worked on this device extensively and showed that, for the fine particles, this device could be very effectively. He conducted tests with Illinois No. 2 coal sample ground to a particle size of 40 μm. The results (shown in Figures 3-48 and 3-49) indicate pyrite removals in the range of 40% to 75% with coal weight recoveries ranging between 18% to 50%. The highest level of pyritic sulfur removal corresponds to the lowest value of coal recovery and vice-versa.

A test with a relatively coarse particle size Pittsburgh seam coal showed 30% ash removal, indicating that the system could also remove ash along with pyrite.

The poor coal recoveries in Mukherjee's experiments were found to be due to detrimental hydrodynamic flow conditions inside the separator. It became necessary to determine the optimum flow conditions to achieve maximum separation with reasonably good coal recoveries. To better understand the flow behavior of particles inside in the separator and to simulate his experimental data, Mukherjee used the hydrodynamic model of Gidaspow et al. (1987). His computations are shown by dotted lines in Figures 3-48 and 3-49. The model is in reasonable agreement with the experimental data.

Later on, Gidaspow et al. (1989) using a refined version of their model, with addition of a solids viscosity terms, which is believed to be needed for proper boundary-layer development, to design a commercial-scale electrostatic separator operating on the conditions of a typical pulverized coal combustion system. They came up with a design that had preferential perforations in the positive electrode to remove the pyrites at selected locations and they claimed that their system could recover 99% of the coal with about 90 to 95% of liberated pyrite removal. However, their findings were not verified experimentally. Furthermore, in the hydrodynamic code used in the simulations, there was no provision to account for the following factors:

a. The code does not have an adhesive or sticking force term that makes the charged particles stick to the electrode as observed by researchers at PETC (Link, 1988) and in these experiments in a batch unit.

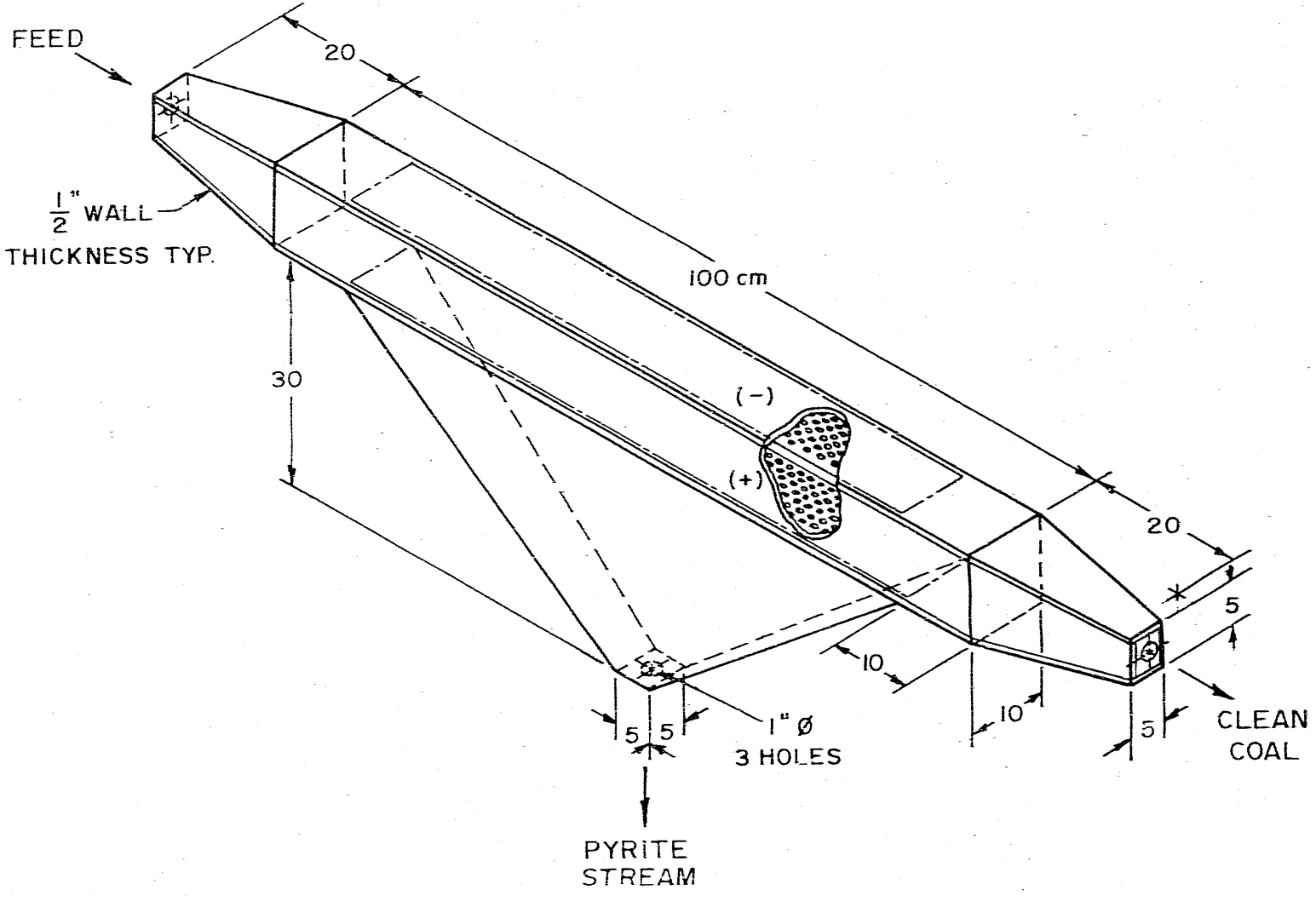

Figure 3-47. SCHEMATIC DIAGRAM OF THE CONTINUOUS ELECTROSTATIC SIEVE CONVEYOR

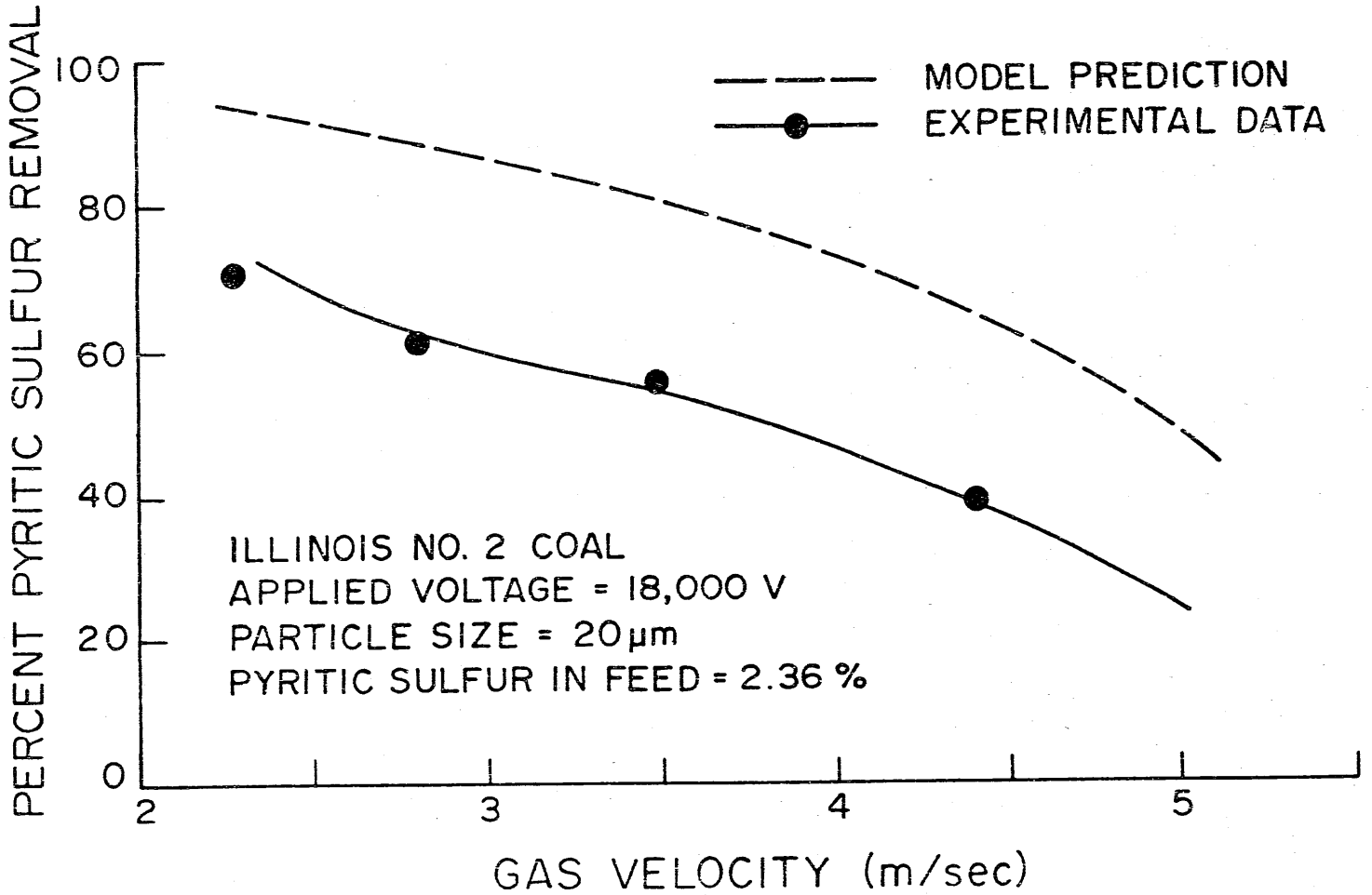

Figure 3-48. REMOVAL OF PYRITIC SULFUR FROM ILLINOIS NO. 2 COAL AS A FUNCTION OF GAS VELOCITY IN THE CONTINUOUS ELECTROSTATIC SIEVE CONVEYOR SHOWN IN FIGURE 3-47

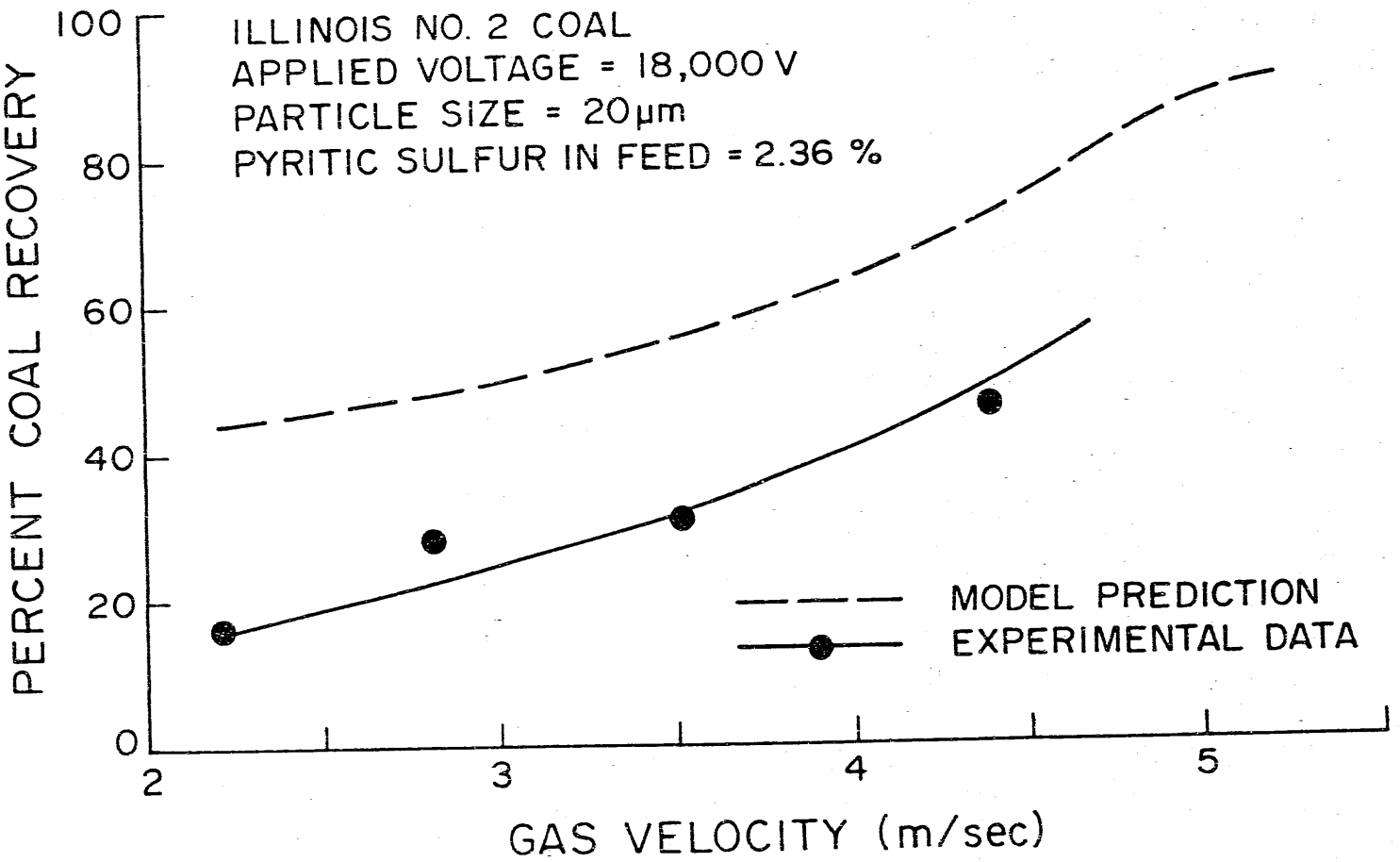

Figure 3-49. COAL RECOVERY AS A FUNCTION OF GAS VELOCITY IN THE CONTINUOUS ELECTROSTATIC SIEVE CONVEYOR SHOWN IN FIGURE 3-47

b. There is no provision in the code to account for distortion created in the electric field by the perforations in the electrodes. A recent study ar PETC indicates that the efficacy of separation decreases with the increase in open area in the electrode plate.

c. The coulombic force between the positively charged coal particles and negatively charged pyritic and mineral particles may be needed to accounting for charge neutralization.

d. In the code, a guessed value of solids viscosity is used -- some reliable measurements of this property are needed.

e. They use a very coarse grid in their numerical computations; use of a very fine computational mesh is needed for the prediction of layer formation.

The adaptability of this hydrodynamic code has been demonstrated in a variety of applications involving gas-solid flows (Gidaspow, 1990). In this case, however, the model can only be used to determine the order of magnitude estimates, but, in principle, the code should be able to simulate the experimental data, once all the basic forces are incorporated into it.

Separation in a Batch Electrostatic Separator

In view of the problems encountered with the perforated electrodes in the continuous sieve separator, and based on the PETC experimental data (Link, 1988), IIT designed and built a batch system (Figure 3-50). The electrodes in this unit do not have perforations. The positively charged coal particles stuck to the negative plate while negatively charged mineral matter including pyrites deposited on the positive electrode.

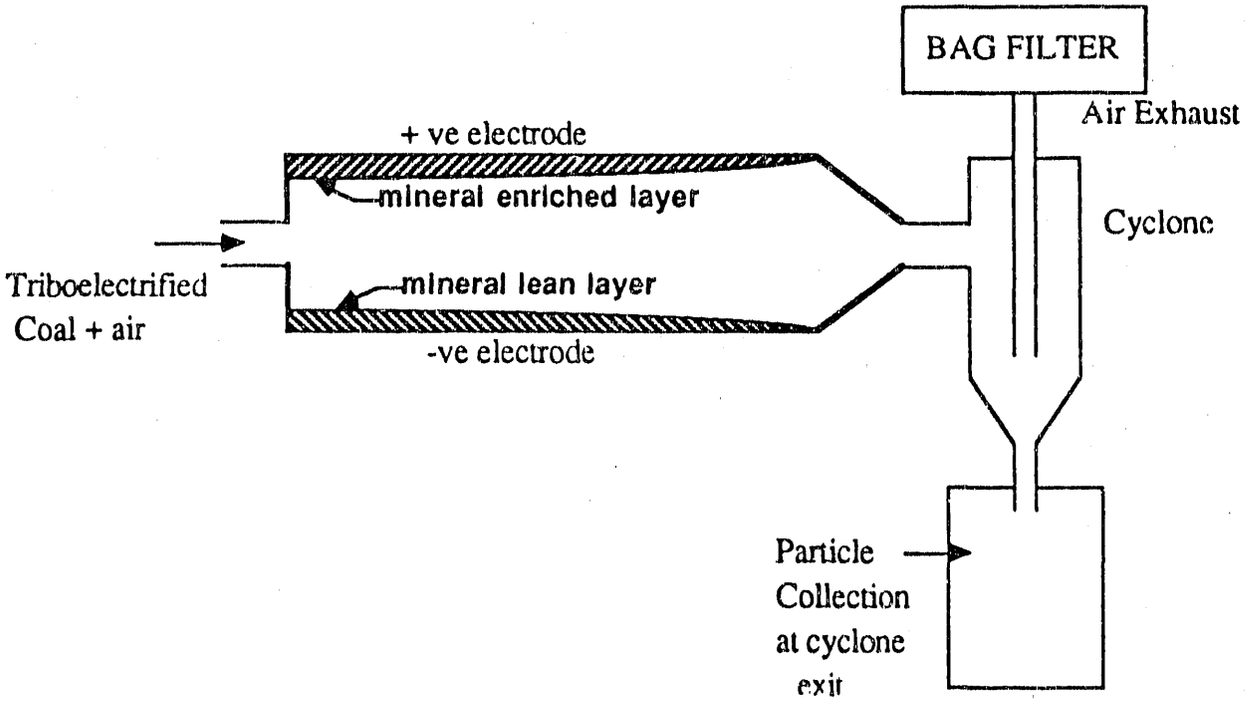

Figure 3-50. SCHEMATIC DIAGRAM OF THE BATCH ELECTROSTATIC SEPARATOR SYSTEM

A test was made in this unit with a high-ash content Illinois No. 6 coal, ground to an average particle size of 53 μm. For the reasons described previously, the carbonaceous matter present in the coal acquired a positive charge while minerals and pyrites charged negatively when brought in contact with a copper tribocharger. When the triboelectrified particles were introduced into the separator in the presence of an electric field, the positively charged particles deposited on the negative electrode and the negatively charged minerals and pyrite particles migrated towards the positive electrode, resulting in a clear separation. After 10 minutes of operation, the separator was opened and particles deposited on the positive and the negative electrodes were scraped off and collected. The particles accumulated at the cyclone exit were also collected. These collected samples were then weighed and analyzed for their pyritic sulfur and ash contents.

The results, with pertinent experimental data, are shown in Table 3-25. About 65% ash and 70% pyrites were removed with a Btu recovery of 92%. Note that at a 53-μm particle size, only about 75% of the pyrites are liberated from the organic matrix. Therefore, without any process optimization, therefore, more than 90% of the liberated pyrites were removed in one stage.

Beneficiation of Eastern Oil Shales

Introduction

Oil shale is comprised of 70% to 85% inert material. During thermal processing all of the inert material must be heated to retorting temperatures. Hence, removal of this inert material from the oil shale prior to the retorting process (beneficiation) would significantly improve process efficiency. Furthermore, removal of sulfur prior to hydroretorting results in reduced hydrogen consumption because less H_2S is formed. There are, therefore, incentives for removing mineral matter and pyritic sulfur before hydroretorting.

Background

Heavy-medium separation, originally developed for coal beneficiation, is one method used for upgrading shale feed. Crushed shale is put into an aqueous suspension of finely ground magnetite and atomized ferrosilicon particles. Shale rich in kerogen floats, while pieces heavier than the medium sink. This process may be carried out either in a tank or cyclone. The processing of shale is very similar to that of coal, the only difference being the specific gravity of shale is higher -- about 2.1 versus 1.6 for coal. Thus, the heavy medium must contain about 75% ferrosilicon and magnetite by weight, compared with about 60% for coal separation. This method, however, works for relatively coarse particle sizes.

Because of the need for fine grinding to liberate the mineral matter, the froth-flotation process being used commercially for the beneficiation of fine coals has been extended for the beneficiation of oil shales. Researchers at the University of Alabama's MRI (at Tulscaloosa) have developed a flotation process which could recover more than 95% of the organic carbon content (Hanna et al. 1983). In their process, wet ultrafine grinding to a particle size less than 10 μm is followed by a flotation process. MRI has been able to increase the kerogen content from 12% to 52% of an Eastern shale. The

Table 3-25. ELECTROSTATIC BENEFICIATION OF HERRIN NO. 6 (IBC-104) COAL IN A BATCH SEPARATOR

Sample Used	: IL #6 Coal (IBC-4)
Inlet Gas Velocity	: 15 meter/sec.
Applied Electric Field	: 2500 volts/cm
Particle Size	: 53 μm
Solids Loading	: 0.2 lb. coal/lb. air

Stream	*Weight (gms)*	*Ash (wt. %)*	*Pyr. S (wt. %)*	*Btu/lb*
Feed	200	34.38	2.16	7843
Negative Electrode	100	11.93	0.64	11210
Positive Electrode	30	77.68	1.76	1348
Cyclone exit[a]	60	48.22	2.99	5767

a. This stream can be recycled back and mixed with the feed to the separator.

BTU Recovery =92.00%
Ash Removal =65.30%
Pyritic Sulfur Removal =70.40%*

**This value represents about 95% of the liberated pyrites removal.*

beneficiation results for Western shales, however, are not as good as for Eastern shales with a kerogen enrichment of only 12% to 24%. This is probably due to the presence of dolomite in Western shales that tends to float with organic material (Parkinson, 1982).

Ultrafine grinding is required to liberate the mineral inclusions from the organic matrix and historically, conventional ball mills were used for wet grinding to these fine sizes. However, ball mills are energy-inefficient devices. As a result, new energy-efficient grinding approaches, such as ultrasonic grinding, pressure cycle comminution, stirred ball mill grinding, etc. are being investigated to wet-grind the shale for a froth flotation operation.

Other advanced flotation techniques developed for coal beneficiation are also being investigated for beneficiation of oil shales. These techniques include column flotation and the LICADO process. Basically, in all these methods, the finely ground shale particles, which are essentially a mixture of kerogen and mineral matter (including pyrites), are allowed to separate into two immiscible phases with the aid of various mechanical forces and reagent injections. The kerogen-bearing particles, being hydrophobic, attach to the bubbles in the presence of a surfactant (for example, kerosene) and float, while mineral-rich refuse, being hydrophilic, remains in water, sinks and collects at the bottom of the tank.

The principle of the operation of the LICADO process is slightly different than conventional flotation processes. In this process, liquid CO_2 at about 870 psia and room temperature is used. The operation is carried out by contacting a shale-water slurry with liquid CO_2. The hydrophobic kerogen particles are preferentially attached to the liquid CO_2-water interface and then transferred to the liquid CO_2 phase, while the hydrophilic mineral particles remain dispersed in the aqueous phase. By separating the non-aqueous (liquid CO_2) phase from the aqueous phase, a kerogen-rich shale/liquid CO_2 slurry is obtained. The organic-rich product in the form of dry particles is then obtained by first deliquoring the slurry to remove as much liquid CO_2 as possible and then recovering most of the remaining CO_2 as a gaseous phase by reducing the pressure of the coal/liquid CO_2 filter cake. This process has been successfully applied for the ultrafine-coal cleaning (He et al. 1989). However, tests with Eastern oil shales are reported in a Topical Report entitled "Beneficiation" (to be published).

Dry beneficiation methods for upgrading shale have been used rarely except for a corona-charging method investigated by T. A. Ring of the University of Kentucky with disappointing results. Magnetic methods have not been tried due to their inability to handle ultrafine particle sizes. In this study, an electrostatic method for the beneficiation of oil shales was investigated. The driving force for the separation is the difference between the surface charge of carbonaceous and non-carbonaceous matter present in the shale and the surface charge is imparted on the particles by impacting them against a copper surface.

Separation Tests in a Continuous Separator

Based on the surface charge measurements, and on initial experimental tests, it became clear that shale mineral matter, due to its dominance,

governs the triboelectrification process. Hence, pyrites alone could not be removed without also removing mineral matter since both pyrites and mineral matter acquire a negative charge. This process, therefore, resulted in a "beneficiation" process in place of a "desulfurization" process.

Experimental System

Figure 3-51 shows the experimental system for shale beneficiation. This system consists of 3 parts:

1. A measurement and control system for air humidity, temperature, pressure and flow rate.

2. A conveying and triboelectric charging system for charging the finely ground particles before feeding them to the separator.

3. The electrostatic separation and particle collection system.

A schematic diagram of an electrostatic sieve separator, used in initial tests, is shown in Figure 3-52. This geometrical configuration was obtained, after some computer modelling for the separation of iron pyrites from coal, by Mukherjee (1987) and was discussed previously. This separator had two aluminum electrodes with the bottom electrode being perforated while the top electrode was a flat aluminum sheet. A high d.c. voltage power supply was used for generating voltages of up to 36,000 volts with the output current being in the range of a few microamperes.

Using a tribocharger, an additional charge on both kerogen and mineral particles was imparted and various tribocharging configurations were investigated. Triboelectrically charged particles were introduced in the separator and a high d.c. voltage was applied. The inlet velocity of the particles to the separator was controlled by the air flow using a pressure regulator and a rotameter. Since air humidity plays a vital role in the particle-charging process, it was carefully controlled, as shown in Figure 3-51, by measuring it by a Dew Point Hygrometer and passing the air through a bed of activated silica gel and/or heating.

This process caused kerogen particles carrying a positive charge to migrate toward the negative electrode, while mineral particles including pyrites fell through the perforations in the electrode thus resulting in a clear separation.

Sample Description

The shale sample used in all the tests was an Indiana New Albany Shale obtained from IGT. The chemical analysis of this shale sample is shown in Table 3-26. The sulfur is present as pyrites, sulfates, sulfides and organic sulfur with the pyrites accounting for 80% of the total sulfur. Table 3-27 shows various major and trace elements in the Indiana Albany Shale. The most abundant element is silicon. The SEM analysis for this shale sample also showed that mineral matter and pyrites are very finely dispersed in the organic matrix with the average grain size of mineral particles being about 5 μm. This shale sample was fine ground in 2 stages, first in a hammer mill and then in a jet mill.

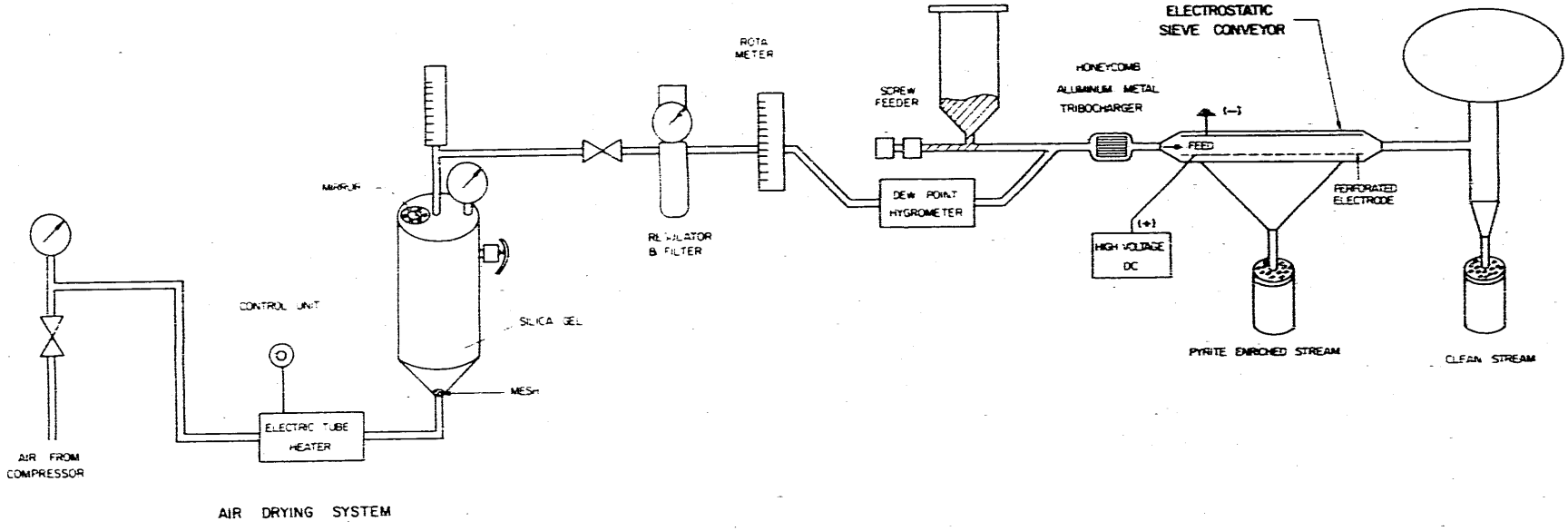

Figure 3-51. EXPERIMENTAL SYSTEM FOR OIL SHALE BENEFICIATION

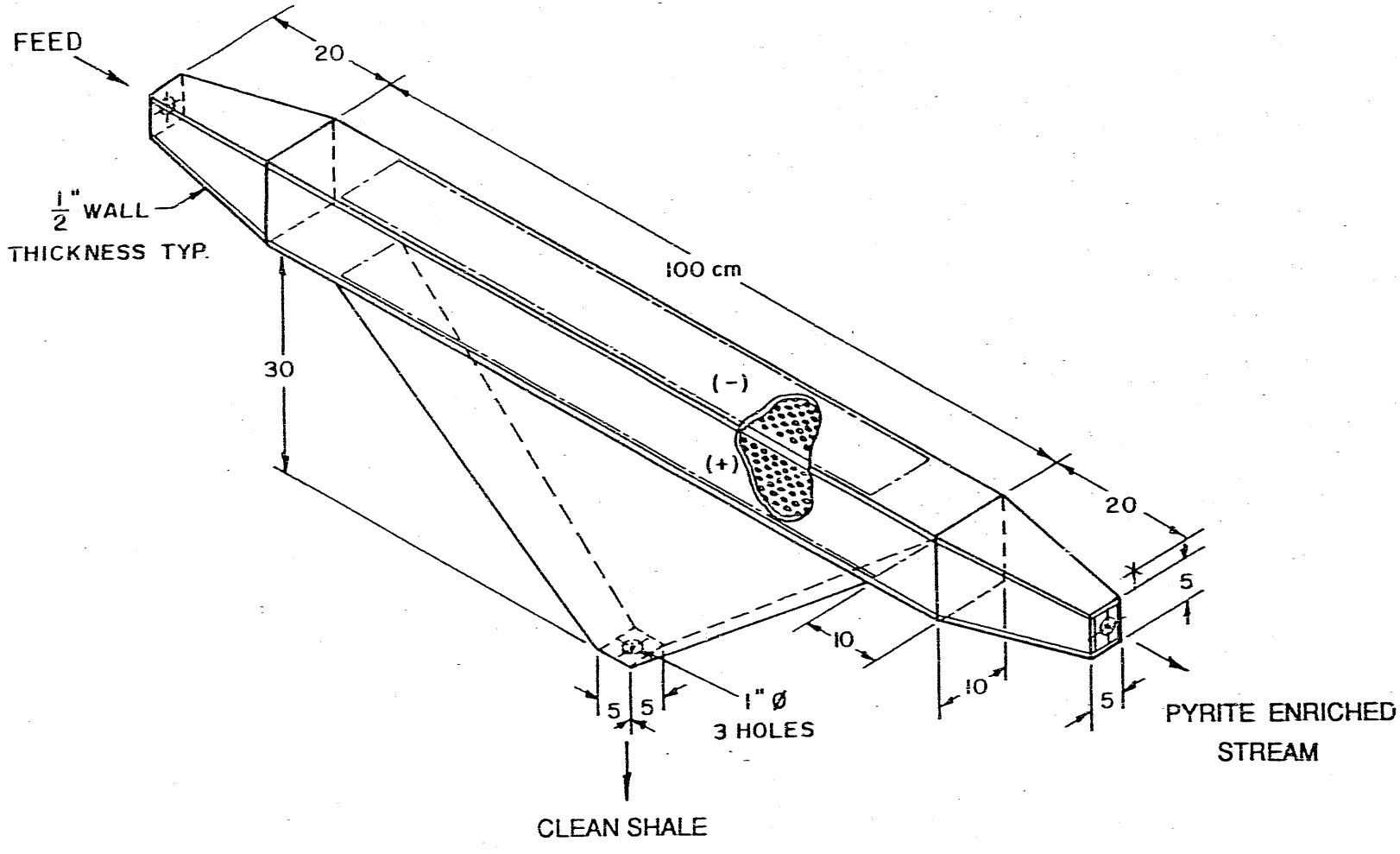

Figure 3-52. ELECTROSTATIC SIEVE SEPARATOR USED FOR SHALE DESULFURIZATION TESTS

Table 3-26. CHEMICAL ANALYSIS OF IN-NA OIL SHALE

Modified Ultimate Analysis		Wt.% Feed (Dry Basis)
Ash		78.47
Residual Mineral Oxides in Ash	75.33	
Organic Carbon		12.33
Organic Hydrogen		1.09
Sulfur		4.06
Nitrogen		0.43
Carbon Dioxide		1.20
High Temperature Water		3.88
MOX Oxygen		0.87
Oxygen (by difference)		1.09
TOTAL		**100.00**
Gross Heating Value (Btu/lb)		2437
Bulk Density (lb per cubic ft)		79.2
Helium Density (g/cc)		2.28
Mercury Density (g/cc)		2.11

1. This analysis was obtained from the Institute of Gas Technology (Project 65072 Task 1.3 BSU Tests)

Table 3-27. MAJOR AND TRACE ELEMENTS IN IN-NA OIL SHALE

Elements	Composition in ppm (by wt) except as noted
C	12.37%
H	1.54%
O	4.03%
N	0.45%
S	4.67%
CO_2	1.80%
Ash	75.14%
Ag	<20
Al	5.43%
As	57.1
B	42
Ba	310
Be	<5
Ca	0.79%
Cd	<4
Cl	260
Cr	33.6
Cu	68.4
F	260
Fe	5.25%
Hg	0.2
K	2.2%
Li	25.2
Mg	0.78%
Mn	301
Mo	160
Na	270
Ni	120
P	380
Pb	25
Sb	<4
Se	<4
Si	24.64%
Sr	110
Ti	0.4%
V	185
Zn	150

Determination of Pyritic Sulfur

The ASTM analysis procedure used to determine the forms of sulfur in coal cannot be used for oil shales. According to the ASTM procedure for coal, pyritic sulfur is analyzed by determining the iron in the sample and then stoichiometrically converting it into the pyritic sulfur with the assumption that the iron in the coal is present only in the form of iron pyrites. This assumption, however, is not valid for the case of oil shales, since in addition to iron pyrites, iron is present in other forms, for example, iron silicates, iron oxides, etc., as can be seen from the weight ratio of Fe to S from Table 3-27 and from the findings of SEM analysis. Therefore, a new technique was needed to determine the forms of sulfur in the shale.

Based on Tuttle's paper (Tuttle et al. 1986) and with the help of Dr. Chausak Chaven of the ISGS, a procedure was developed to determine the forms of sulfur in the shale (a complete description of this procedure is given in Appendix A). Basically, in this method, when shale is made to react with the concentrated HCl in a reducing atmosphere, pyritic sulfur is converted into H_2S. The H_2S is then determined by absorbing it into a $CdSO_4$ solution and titrating the resultant H_2SO_4 against a standardized NaOH solution. The results obtained from this procedure were checked with other techniques and were found to be consistent.

Determination of Kerogen

The organic carbon or kerogen in the shale was determined using an elemental analyzer. The initial results were based on analyses done with a LECO analyzer. Later, a Perkin Elmer Elemental Analyzer, PE CHN 2400, was used. A brief description of the principle of operation of the Elemental Analyzer is given below.

The PE 2400 CHN Elemental Analyzer is used for the rapid determination of carbon, hydrogen and nitrogen content in organic and other types of materials. Samples are combusted in a pure oxygen environment with the resultant combustion gases measured in an automated fashion. In addition to the carbon, hydrogen and nitrogen determinations, an accessory kit is available that allows the measurement of oxygen content of organic materials.

Figure 3-53 shows a schematic diagram of the PE 2400 CHN Elemental Analyzer. The system is comprised of 4 major zones: Combustion Zone, Gas Control Zone, Separation Zone, and Detection Zone. Operating gases include oxygen, for combustion of sample materials, and a carrier gas, either helium or argon. Samples (encapsulated in tin or aluminum vials) are inserted in the combustion zone either manually or automatically, from an integral 60-position auto sampler. In the presence of oxygen and combustion reagents, samples are combusted completely to CO_2, H_2O and N_2. These combustion products are then passed to the gas control zone of the system where the gases are contained in a mixing chamber. Here, the gases are rapidly mixed and precisely maintained at controlled conditions of pressure, temperature and volume which results in the thorough homogenization of product gases.

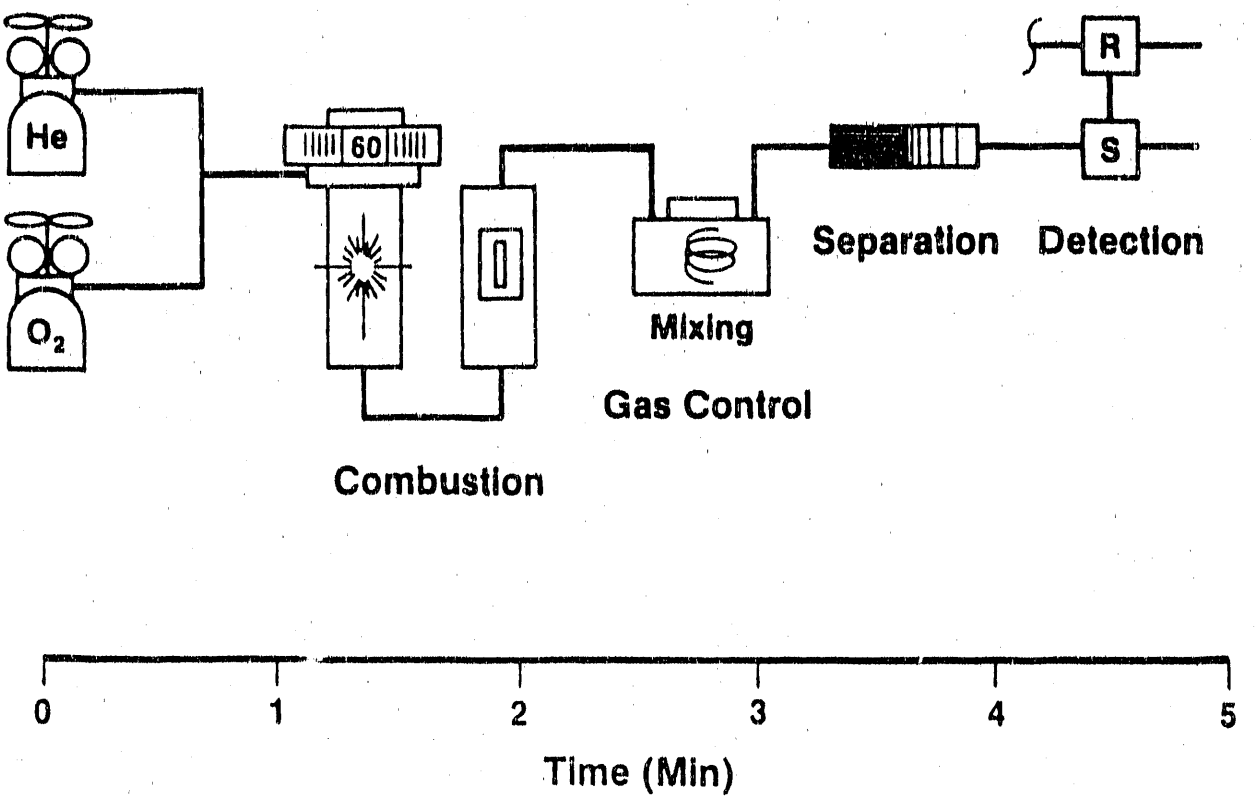

Figure 3-53. SCHEMATIC OF PERKIN ELMER CHN 2400 ELEMENTAL ANALYZER

After the product gases are homogenized in the gas control zone, the mixing chamber is depressurized through a column in the separation zone of the instrument. The approach used here is not a standard chromatography, but a technique known as frontal chromatography. In this method, there is a selective retention of the gases to produce a steady-state, stepwise signal rather than a peak signal which allows for a simpler, more reliable and accurate determination of the combustion gases.

The stepwise series of gases, illustrated graphically in Figure 3-54, is then passed through a thermal conductivity detector system in the detection zone of the analyzer. Since measurements are made as stepwise changes from the carrier gas baseline in this design, the variations associated with the quantitation of peak signals in the standard chromatography techniques are eliminated. All the steps described above are accomplished in under 5 minutes of analytical time after the weighed sample is first introduced in the system.

Desulfurization Tests

The initial tests were made in the continuous separator shown in Figure 3-52. In this separator, the top electrode was a flat aluminum sheet while the bottom electrode sheet had uniform perforations 3 mm in diameter. When the finely ground shale particles, aerosolized in the air, were introduced in the separator, most of the particles flowed with the air through

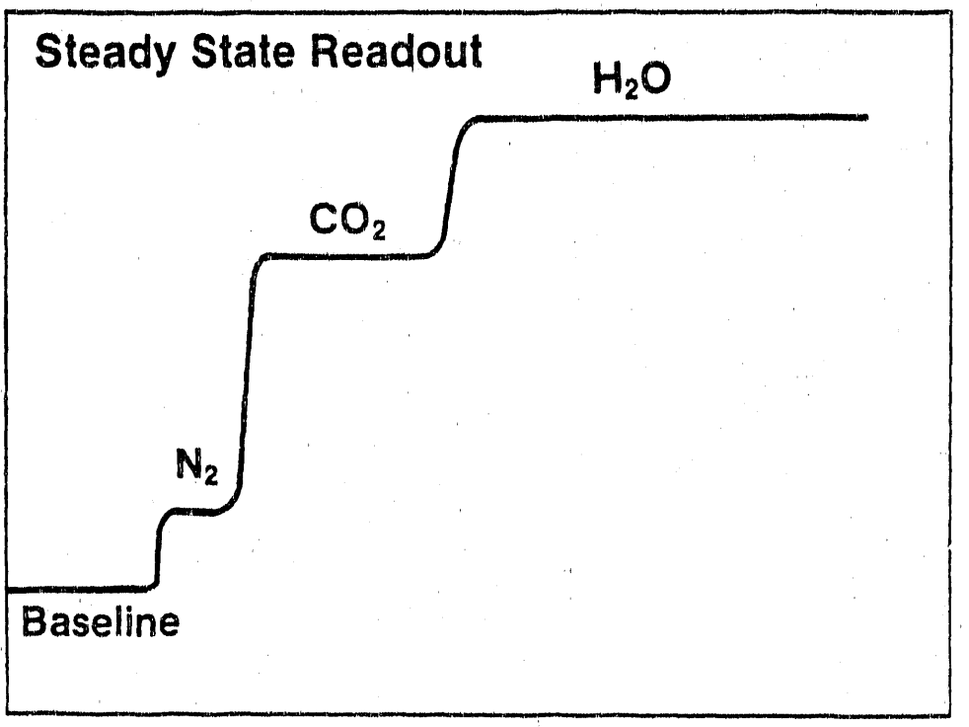

Figure 3-54. STEPWISE DETECTION OF GASES IN PC CHN 2400 ANALYZER

the perforations in the electrode. This was the main reason behind the poor coal recoveries obtained by Mukherjee (1987) as discussed previously. In order to solve this recirculation problem, the operation of this system was modified. By restricting the outflow from the positive electrode and closing the outlet below the conical section (Figure 3-52) to prevent the air from escaping, the particles were collected intermittently beneath the electrode in the conical section.

A systematic study was conducted to investigate the effect of gas velocity on the flow split in this modified system. Figure 3-55 shows the ratio of particle weight collected at the positive electrode compared to the particles collected at the negative electrode with an applied electric field strength of 18,000 volts. This ratio is a strong function of inlet gas velocity. At a velocity of 7 m/s, approximately equal split of particles between the positive and the negative electrode was observed.

Another systematic study was conducted to study the effect of gas velocity on the separation of pyrites. Figure 3-56 shows the percent of pyrite separation as a function of inlet gas velocity. With an increase in gas velocity, the pyrite separation becomes less effective. Similar trends were also observed by Mukherjee (1987) for desulfurization of Illinois coal in the same separator.

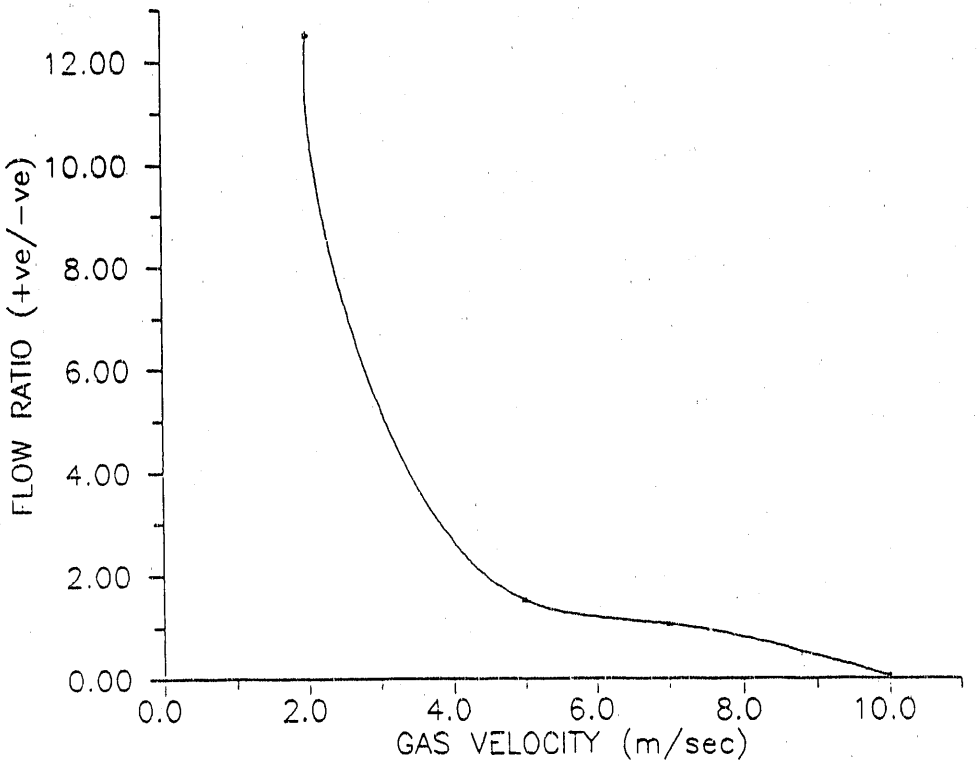

Figure 3-55. FLOW SPLIT AS A FUNCTION OF GAS VELOCITY IN ELECTROSTATIC SEPARATOR

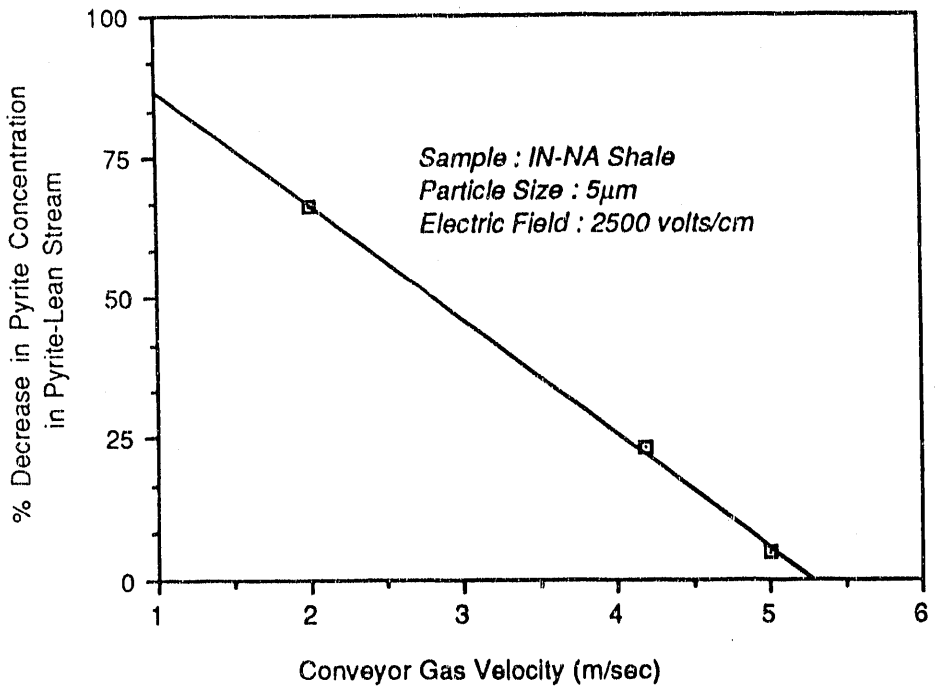

Figure 3-56. PYRITE REMOVAL AS A FUNCTION OF GAS VELOCITY

Beneficiation Tests in a Batch Separator

In view of the problems encountered in making the particles flow properly through the perforations in the electrodes, the perforated aluminum electrode was replaced by a copper screen with a mesh size of 600 μm and the top aluminum plate was replaced by a flat copper sheet. Introduction of particles into the cyclone-tribocharger was also modified to achieve better control of solid and gas flow rates. This system could no longer operate in a continuous mode because of the sticking of the particles with the electrode surface.

A test in this modified separator with shale ground to a particle size of 5 μm and in which particle layers were found to deposit on both the electrodes, showed significant kerogen enrichments, from a value of 12.37% in the feed to 20.50% in the layer deposited at the negative electrode with an applied electric field strength of 20,000 volts. Kerogen material balance matched within 92%.

Parametric Studies

A detailed parametric study was conducted to study the effect of the following process variables on kerogen enrichment and pyrite removal: Particle Size, Surface Moisture, Gas Velocity, and Solids Loading.

Two factors, the Kerogen Enrichment Factor and the Pyrite Removal, which are used to interpret the results, are defined as follows.

$$\text{Kerogen Enrichment Factor} = \frac{\%\ \text{organic carbon in clean shale}}{\%\ \text{organic carbon in feed}}$$

$$\text{Pyrite Removal, \%} = \left(1 - \frac{\text{pyritic sulfur in clean shale}}{\text{pyritic sulfur in feed}}\right) \times 100$$

For these studies, oil shale particles were ground to an average particle size of 5 μm. Tube charger was used to impart an additional surface charge on particles. A very dilute suspension of triboelectrically charged particles was conveyed pneumatically into the separator. Solid loadings were kept at 0.2 lb solid/lb air and a constant voltage of 2,000 volt/cm was applied. The kerogen particles, being positively charged, deposited on the negative electrode while a kerogen-lean, or a mineral-rich layer, deposited on the positive electrode. The experiment was run for a duration of about 2 to 5 minutes. At the end of the experiment, the separator was opened and the layers were collected, weighed and analyzed for their kerogen and pyritic sulfur contents. As discussed in an earlier section, the kerogen in the sample was analyzed by determining the organic carbon content using a LECO analyzer and analysis for pyritic sulfur was done using the procedure described above.

Figure 3-57 shows the effect of particle size on the kerogen enrichment factor and percent pyrite removal. Both kerogen enrichment and pyrite removal are better for shale ground to a particle size of 5 μm than the shale having a particle size of 53 μm. This is primarily due to the fact that at 53 μm, most of the mineral inclusions are not liberated from the shale matrix. Thus, for efficient kerogen extraction, the particles must be ground to finer sizes.

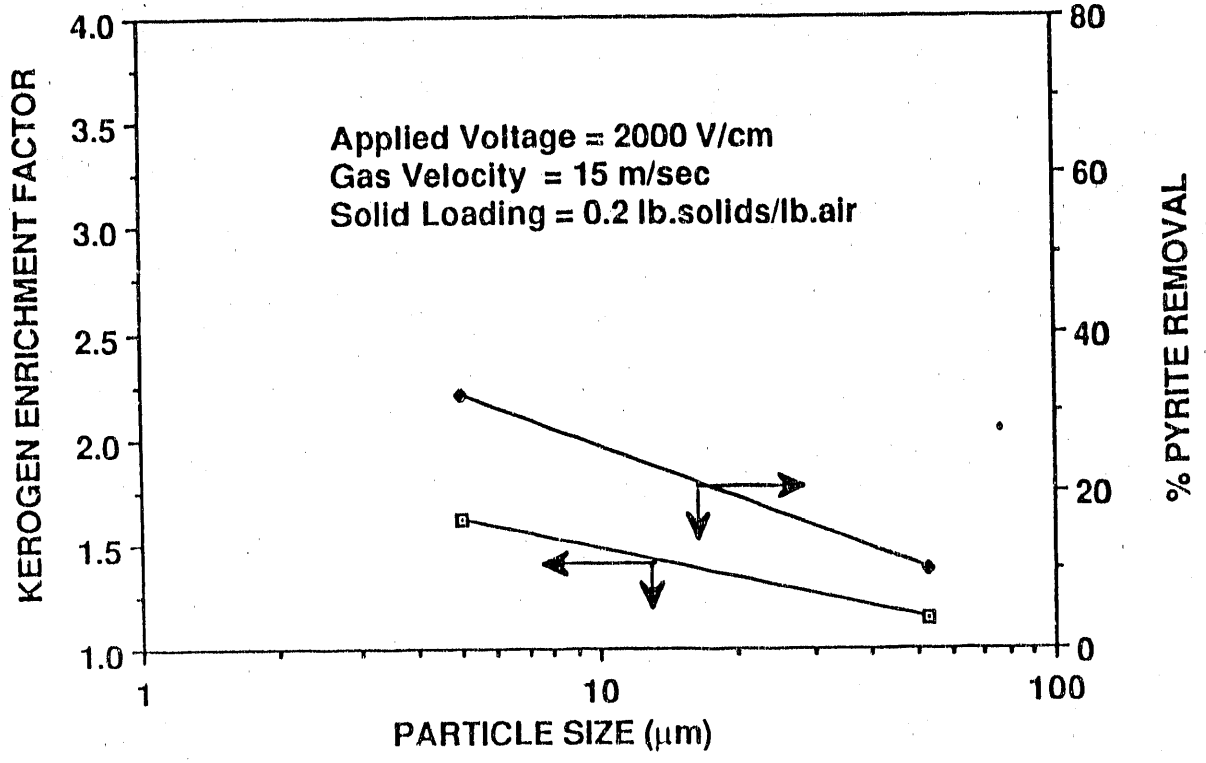

Figure 3-57. EFFECT OF PARTICLE SIZE ON KEROGEN ENRICHMENT AND PYRITE REMOVAL

To study the effect of surface moisture, experiments were conducted with undried freshly ground shale (referred to as undried) and the sample dried in a vacuum oven for 24 hours (referred to as dried). Figure 3-58 shows the kerogen enrichment factor and pyrite removal as a function of surface moisture. There was no significant difference in the results with dried and undried shale. However, kerogen enrichment and pyrite removal for dried samples are slightly better. Apparently, it is better to dry the sample before separation.

Experiments were conducted to study the effect of gas velocity on kerogen enrichment and pyrite removal to determine an optimum flow velocity. The results (Figure 3-59) show that both kerogen enrichment and pyrite removal are better at 25 m/s compared to 15 m/s. The increase in gas velocity resulted in an increase in kerogen enrichment from 12% to 24% with around 35% pyrite removal. The reasons for better separation at high gas velocity may be (1) less probability of agglomeration (2) higher charge acquired by particles as charge is a function of velocity and (3) less probability of charge-neutralization for positively charged kerogen and negatively charged minerals. Hence for better separation, the system should be operated at a high velocity.

Prior work by IIT indicated that the particle concentration in the gas stream (or solid loading) plays a vital role in separation. A series of tests

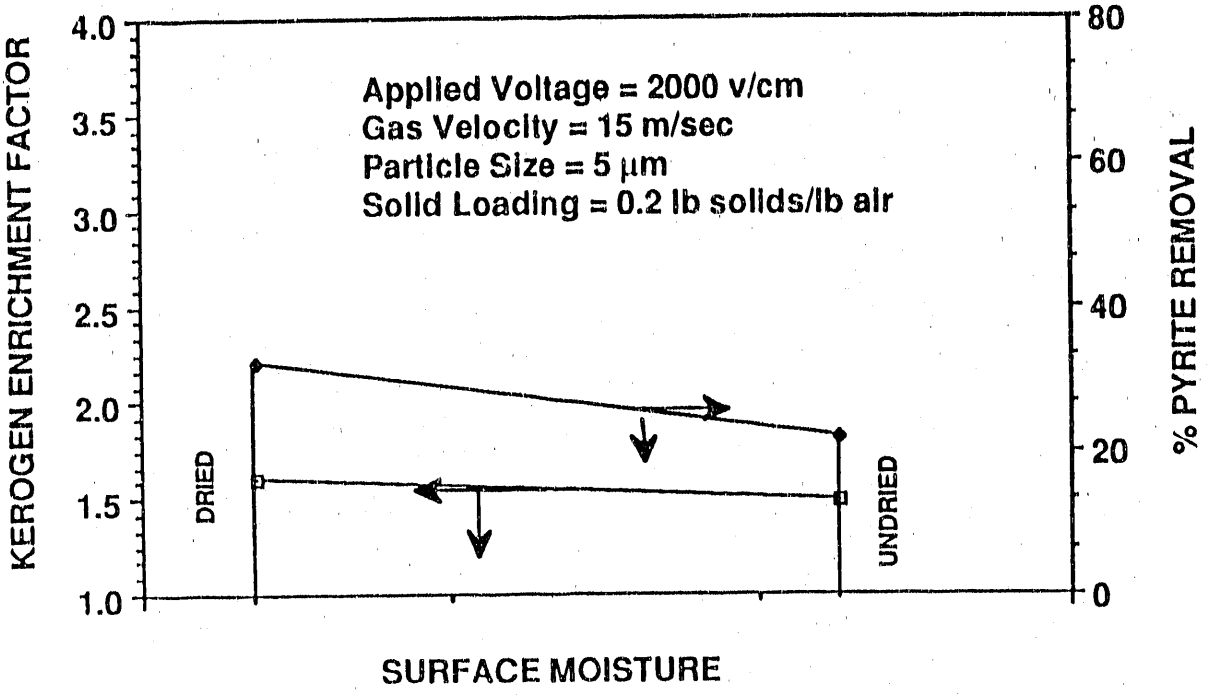

Figure 3-58. EFFECT OF SURFACE MOISTURE ON KEROGEN ENRICHMENT AND PYRITE REMOVAL

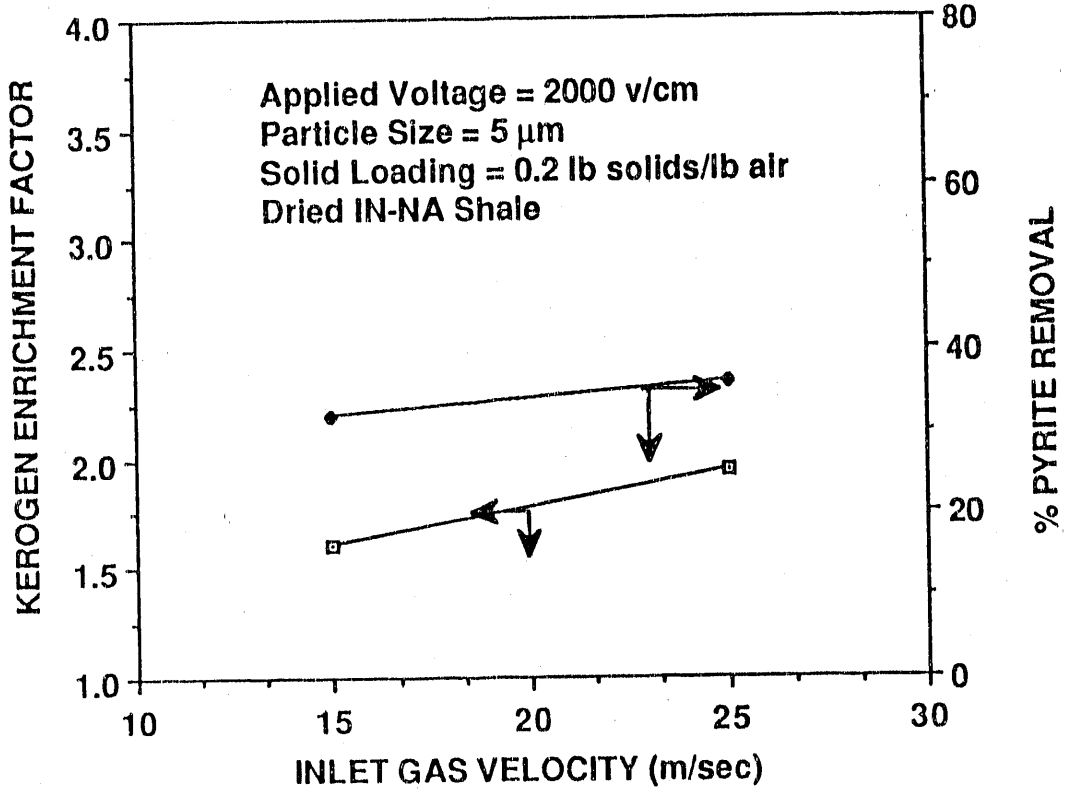

Figure 3-59. EFFECT OF INLET GAS VELOCITY ON KEROGEN ENRICHMENT AND PYRITE REMOVAL

were conducted to study the effect of solid loading on kerogen enrichment and pyrite removal. The results (Figure 3-60) show an unexpected high kerogen enrichment. The feed shale with 12.44% kerogen was enriched up to 33.5% kerogen with a kerogen enrichment factor of 2.7. At the same time, there was significant increase in pyrite removal. The primary reason for better separation (for the very dilute flow case) is that particle-particle interactions are significantly reduced and the suspension behaves as an aerosol. Additionally, particle motion due to the electrical field is less hindered by particle proximity.

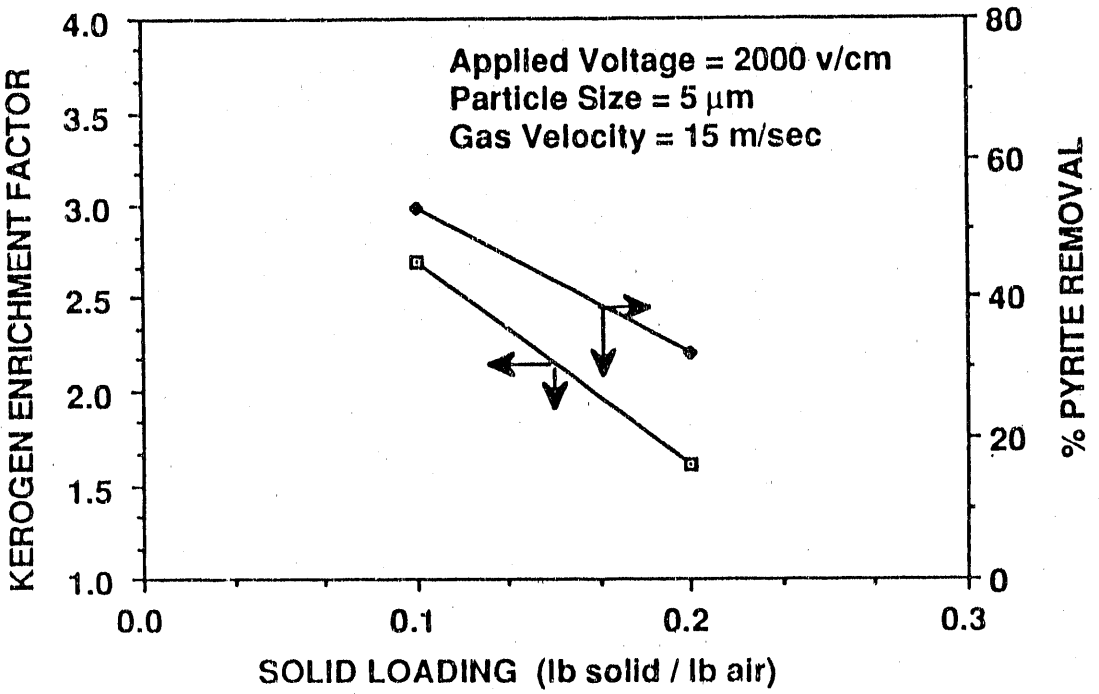

Figure 3-60. EFFECT OF SOLIDS LOADING ON KEROGEN ENRICHMENT AND PYRITE REMOVAL

The dilute phase transport is certainly beneficial to the separation with the only disadvantage being that it requires more energy in pumping the air. However, this energy consumption is small when compared to the upgrade in Btu output from the product.

Determination of Kerogen Concentration Profiles

A systematic study was conducted to determine the kerogen and pyrite concentration profiles in the layers deposited at both pyrite electrodes. Experiments were conducted with the IN-NA shale ground to a particle size of 5 μm, with a velocity of 5 m/s and an applied voltage of 25,000 volts. Particles were collected from the 20 cm long segments of the layer deposited at both the electrodes and each sample was weighed and analyzed for its pyritic sulfur and kerogen contents.

Figure 3-61 shows the variation in kerogen concentration, at both the positive and the negative electrode with length. Maximum separation is achieved at the entrance of the separtor. This maximum in kerogen concentration, however, is a function of hydrodynamic conditions such as gas velocity and inlet configuration. Figures 3-62 and 3-63 show the weight of the particles deposited as a function of position at the negative and the positive electrodes, respectively. From these figures, it is evident that, in addition to a maximum in the concentration, the weight collected is also maximum at the entrance, indicating that good kerogen recoveries could be achieved.

Figure 3-64 shows the variation in pyritic sulfur concentrations at the positive and the negative electrode as a function of position. The feed has a pyritic sulfur content of 3.43% and at the negative electrode, where kerogen enrichment takes place, pyritic sulfur concentration is almost constant at a value around 2%. However, at the positive electrode, the pyritic sulfur composition varies from 4.3% to 0.83%. Furthermore, the pyritic sulfur content of the particles collected in the conical section was found to be 7%. This stream accounted for about 55% of the pyrites present in the shale. Tables 3-28 and 3-29 show the material balance for kerogen and pyritic sulfur, respectively, with the locations corresponding to the sample numbers shown in Figure 3-65. The material balance for both pyrites and kerogen matched within ±10%.

Effect of Inlet Geometry

The geometry of the inlet to the separator plays a vital role in the separation of kerogen from the shale. Accordingly, this effect was studied with 3 different inlet configurations. In addition, the separator was further modified. The copper screen used in the previous tests was replaced with a flat copper sheet (the same as the top electrode) and the conical section beneath the bottom electrode was removed. A sketch of this system is shown in Figure 3-66. The particles exited from the separator to a cyclone where they were collected. Figure 3-67 shows the three inlet geometries used:
1) Channel: A conical section to introduce the particles in a streamline fashion, 2) Rectangular slit jet: A rectangular slit of 10 cm X 1 cm was made for introduction of particles in the separator. The concept of this slit jet came from the fluidized beds used extensively at the IIT laboratory,
3) Circular jet: A 1/2-inch NPT pipe was used for introduction of particles to the separator.

Keeping all other conditions (velocity, electric field intensity and particle size) constant, beneficiation tests were made with each of these inlet configurations and a motionless-mixer type copper tribocharger was used for charging the particles. Particle layers were found to deposit on both the electrodes. Figures 3-68, 3-69 and 3-70 show the kerogen concentration profiles at positive and negative electrodes. The results show that there is a maximum in the kerogen concentration at the negative electrode and a minimum at the positive electrode in all the cases. However, the position of this maximum varies with the inlet configuration. This phenomena is related to the flow hydrodynamics. For the channel inlet, the maximum exists at the entrance, because the flow has already streamlined itself and there is maximum driving force for the separation at the entrance.

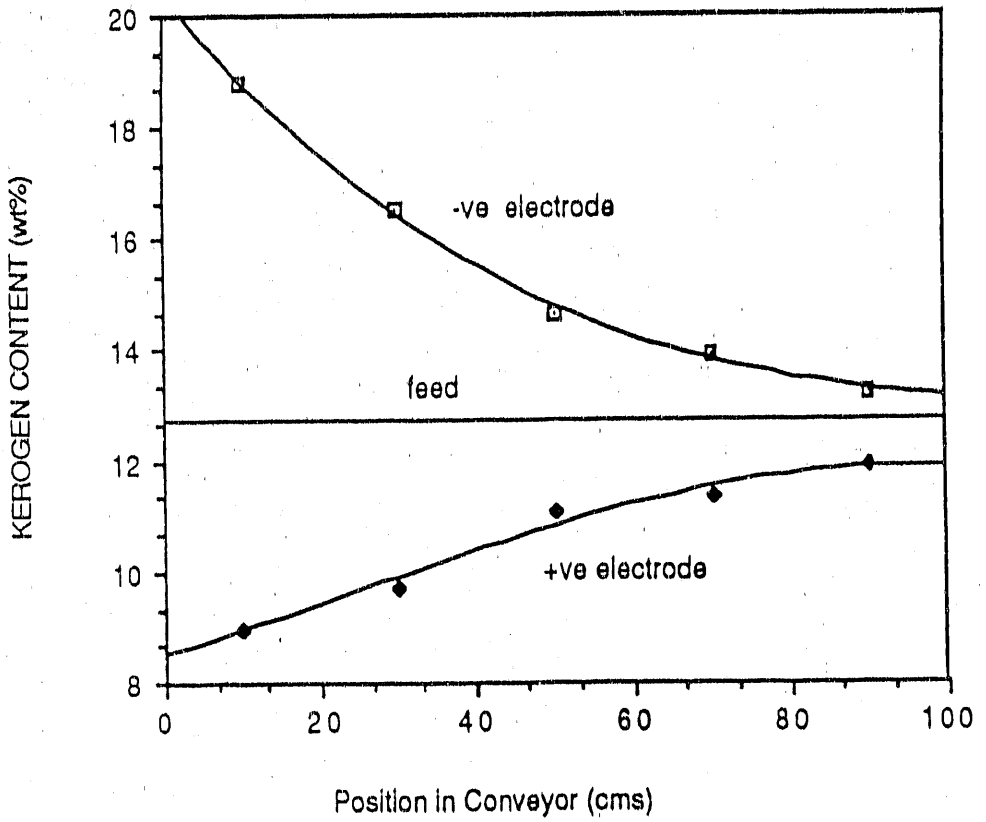

Figure 3-61. KEROGEN CONCENTRATION PROFILE OF THE LAYERS DEPOSITED AT NEGATIVE AND POSITIVE ELECTRODES

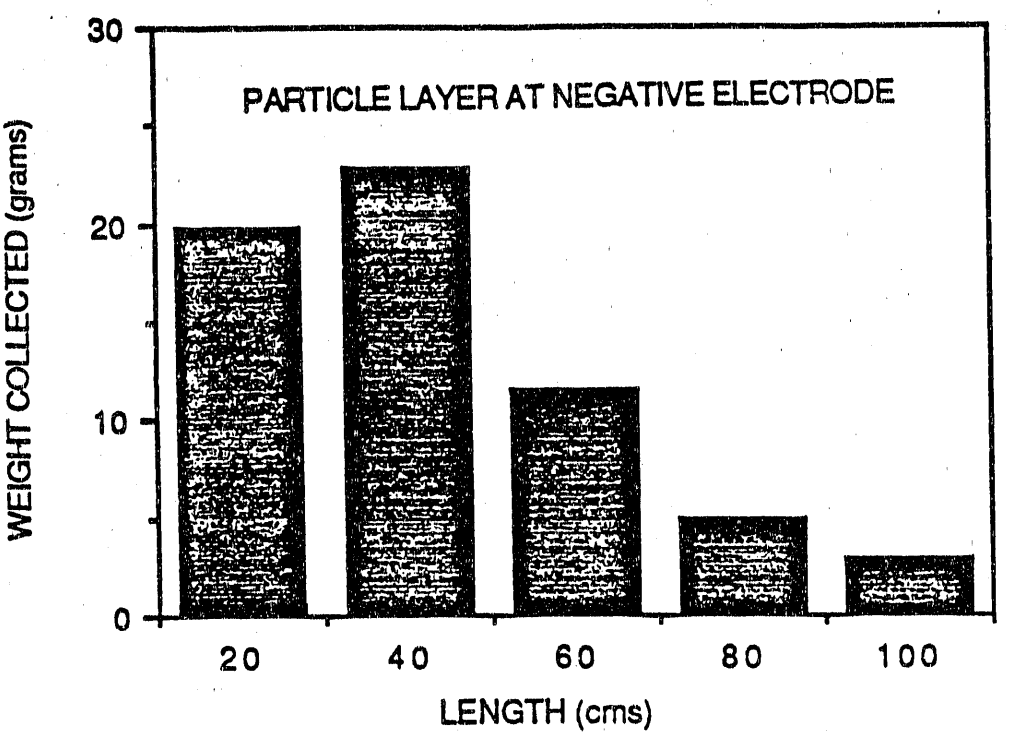

Fgireu 3-62. WEIGHT DISTRIBUTION PROFILE OF THE LAYER DEPOSITED AT NEGATIVF ELECTRODE

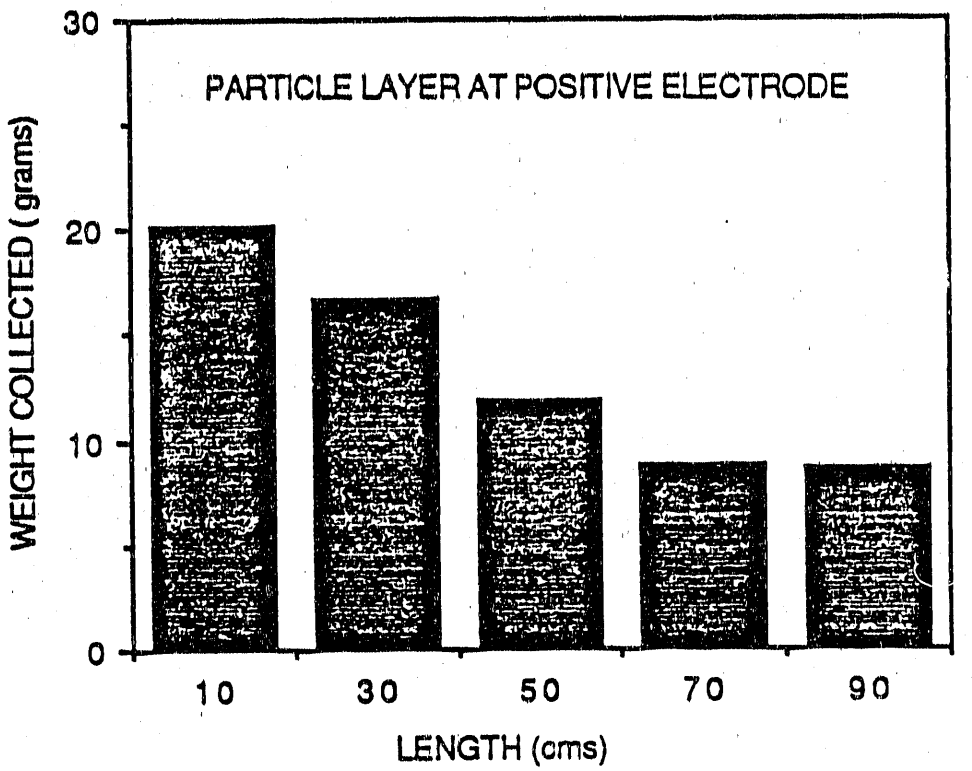

Figure 3-63. WEIGHT DISTRIBUTION PROFILE OF THE LAYER DEPOSITED AT POSITIVE ELECTRODE

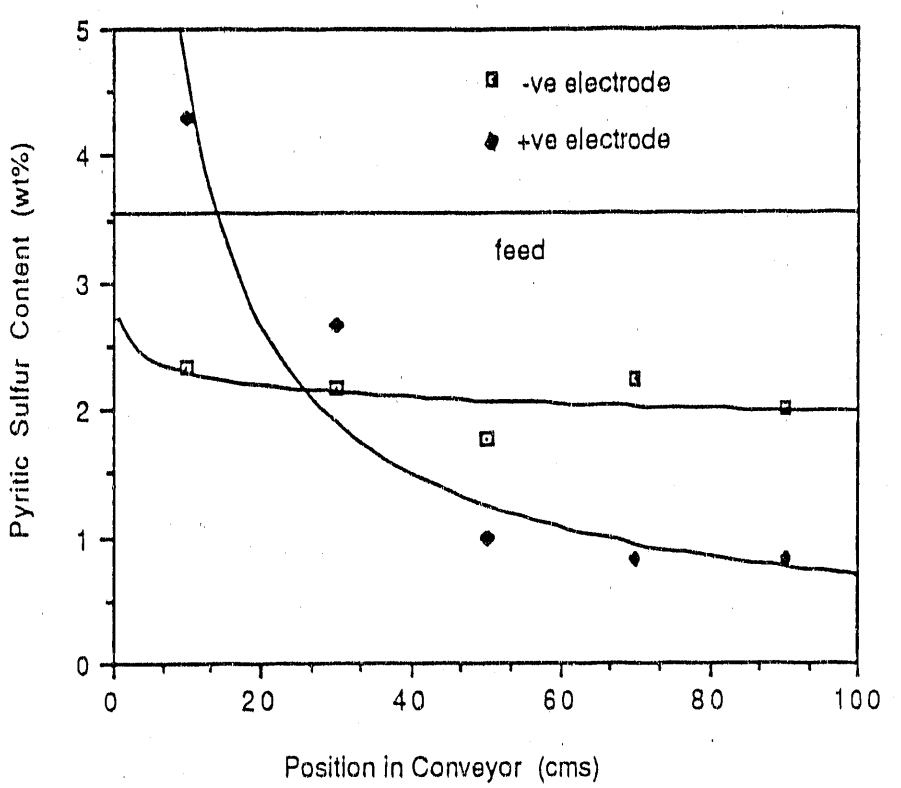

Figure 3-64. PYRITE CONCENTRATION PROFILE OF THE LAYERS DEPOSITED AT NEGATIVE AND POSITIVE ELECTRODES

Table 3-28. KEROGEN MATERIAL BALANCE

Stream #[a]	Wt. of Layer (gms.)	Kerogen Comp. (wt. %)	Wt. of Kerogen (gms.)
1.	19.6	18.8	3.6848
2.	22.9	16.52	3.7830
3.	11.6	14.68	1.7029
4.	4.9	13.90	0.6811
5.	2.9	13.26	0.3845
Sub-total	61.9	15.92	9.8518
6.	20.2	8.98	1.8140
7.	16.7	9.72	1.6232
8.	11.9	11.06	1.31614
9.	8.9	11.34	1.00926
10.	8.6	11.90	1.0234
Sub-total	66.3	10.23	6.786
11.	12.6	12.81	1.61406
12.	13.5	12.26	1.6551
13.[b]	55.7	11.93	6.645
TOTAL	210.0		26.552
FEED	210.0	12.55	26.355

Percent Error in Material Balance = 1%

a. Stream numbers are shown in Figure 3-65 (page II-141).

b. This stream accounts for 25% of the kerogen loss.

Table 3-29. PYRITE MATERIAL BALANCE

Stream #	Wt. of Layer (gms.)	Pyrite Comp. (wt. %)	Wt. of Pyrites (gms.)
1.	19.6	2.33	0.45668
2.	22.9	2.17	0.49693
3.	11.6	1.77	0.20532
4.	4.9	2.24	0.10976
5.	2.9	2.00	0.05800
Sub-total	61.9	2.14	1.32669
6.	20.2	4.3	0.86860
7.	16.7	2.66	0.44422
8.	11.9	1.00	0.11900
9.	8.9	0.83	0.07387
10.	8.6	0.83	0.07138
Sub-total	66.3	2.38	1.57707
11.	12.6	0.58	0.07308
12.	13.5	1.83	0.24705
13.[a]	55.7	7.00	3.89900
TOTAL	210.0		7.12289
FEED	210.0	3.43	7.20300

Percent Error in Material Balance = 1%

a. Stream 13 accounts for 54% of the total pyritic sulfur

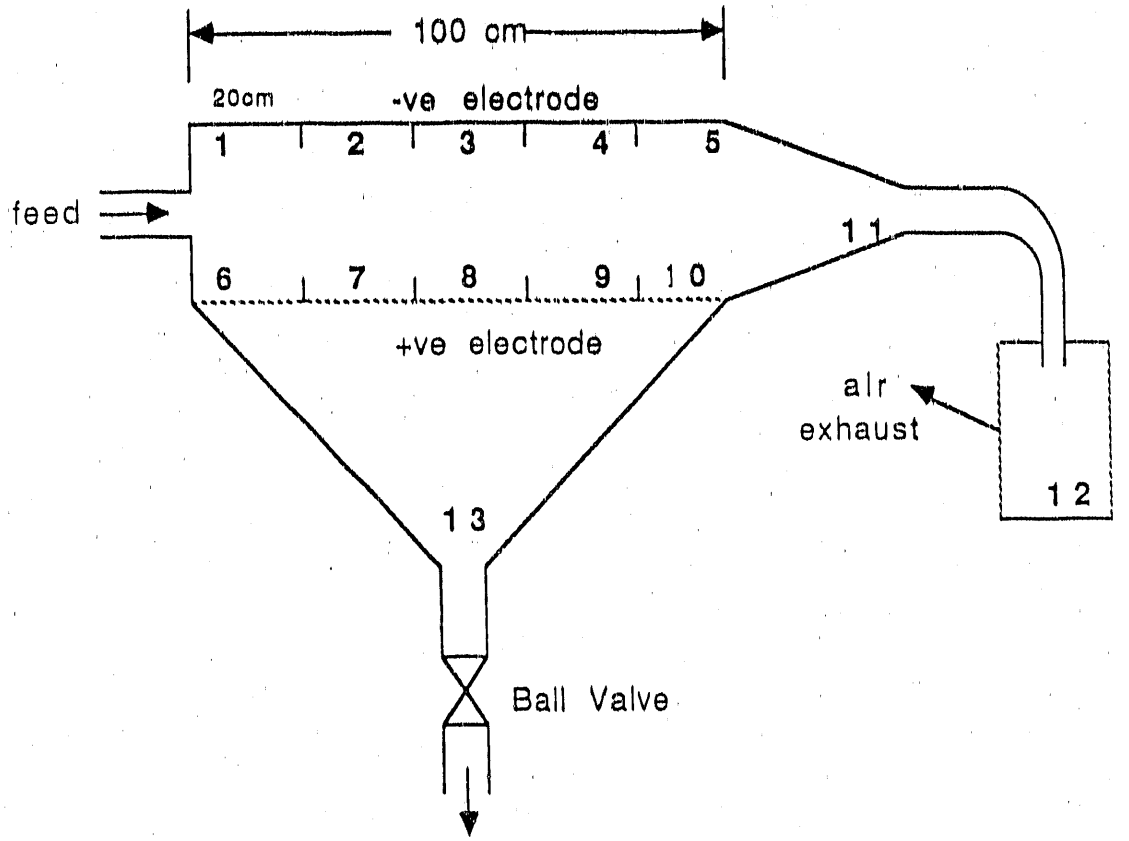

Figure 3-65. SAMPLE LOCATIONS CORRESPONDING TO THE SAMPLE NUMBERS IN TABLES 3-28 AND 3-29

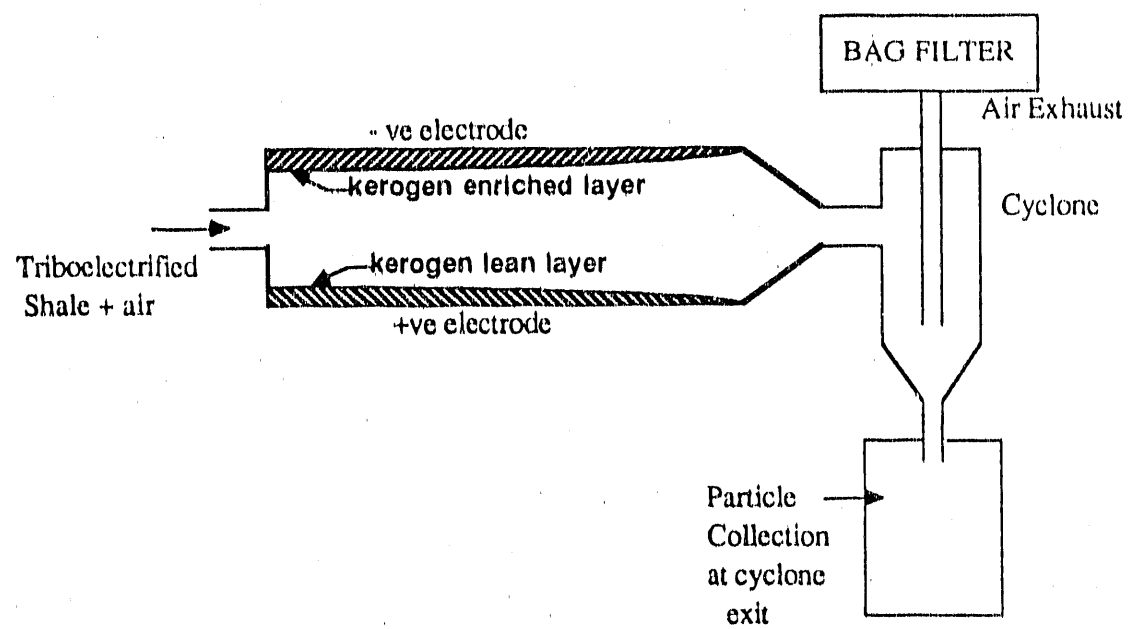

Figure 3-66. SCHEMATIC DIAGRAM OF THE BATCH ELECTROSTATIC SEPARATOR

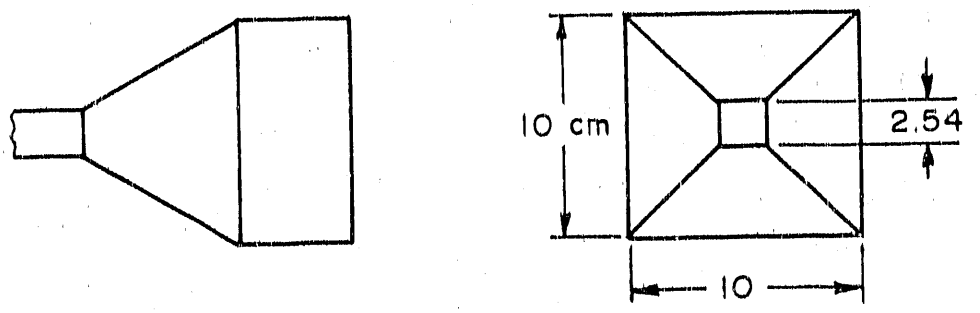

(a) CHANNEL TYPE INLET

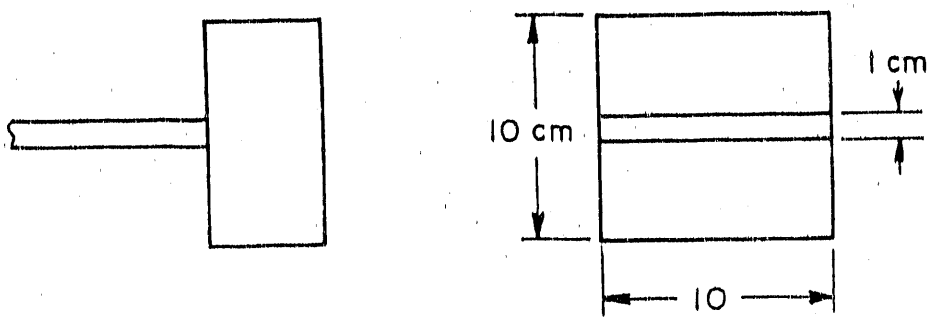

(b) RECTANGULAR SLIT JET

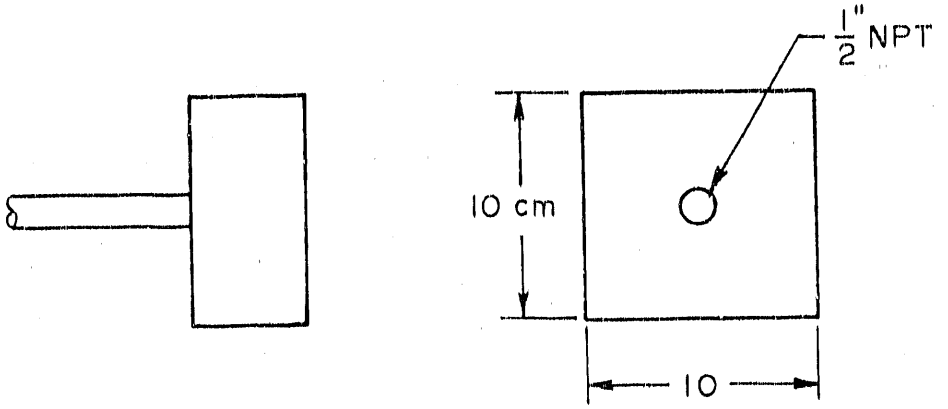

(c) CIRCULAR JET

Figure 3-67. VARIOUS INLET GEOMETRIES TESTED

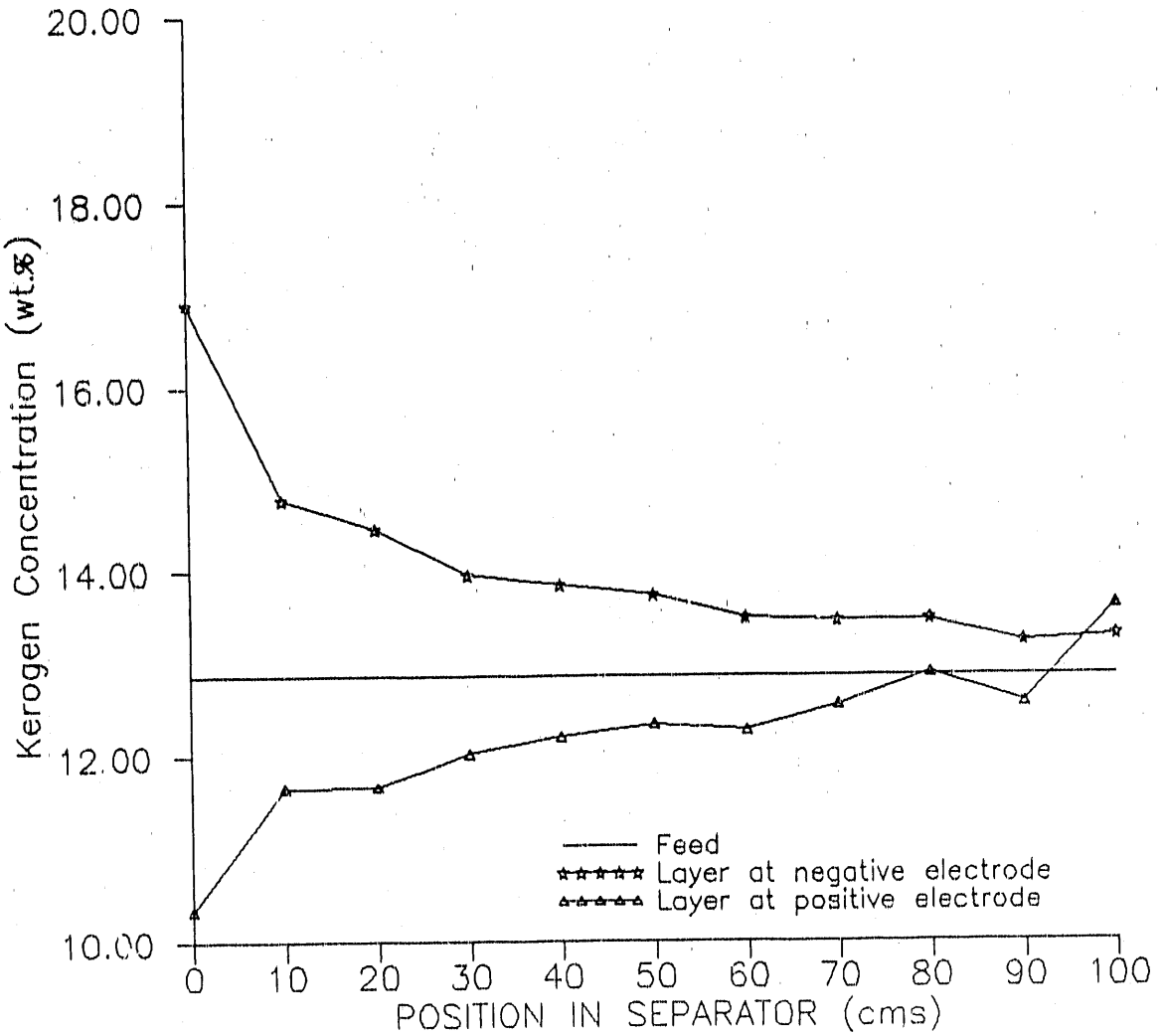

Figure 3-68. KEROGEN CONCENTRATION PROFILE OF LAYERS DEPOSITED ON NEGATIVE AND POSITIVE ELECTRODE IN BATCH SEPARATOR (Rectangular Channel Inlet and Air Flow of 20 cfm)

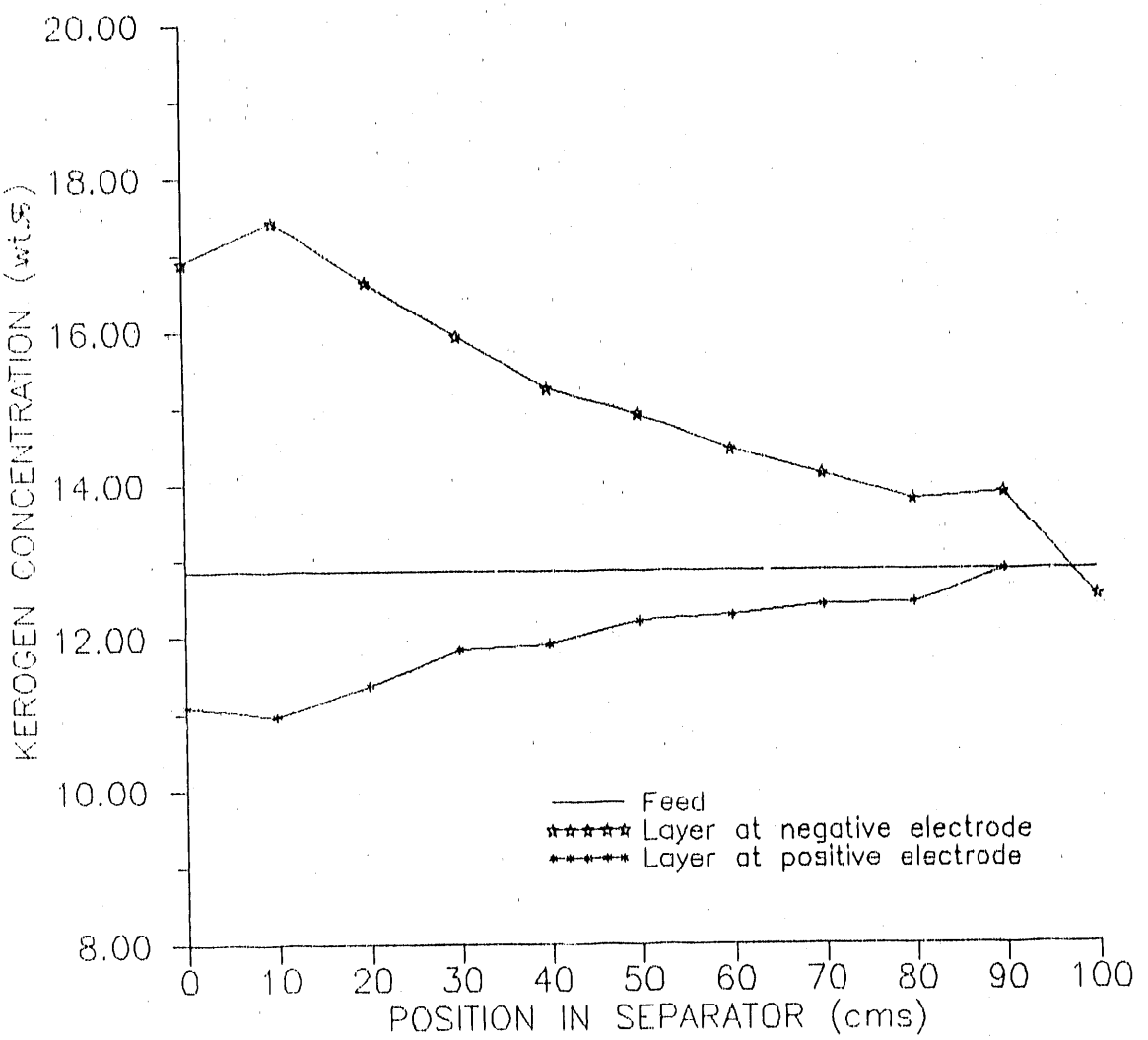

Figure 3-69. KEROGEN CONCENTRATION PROFILE OF LAYERS DEPOSITED ON NEGATIVE AND POSITIVE ELECTRODE IN BATCH SEPARATOR (Rectangular Slit Jet and Air Flow of 20 cfm)

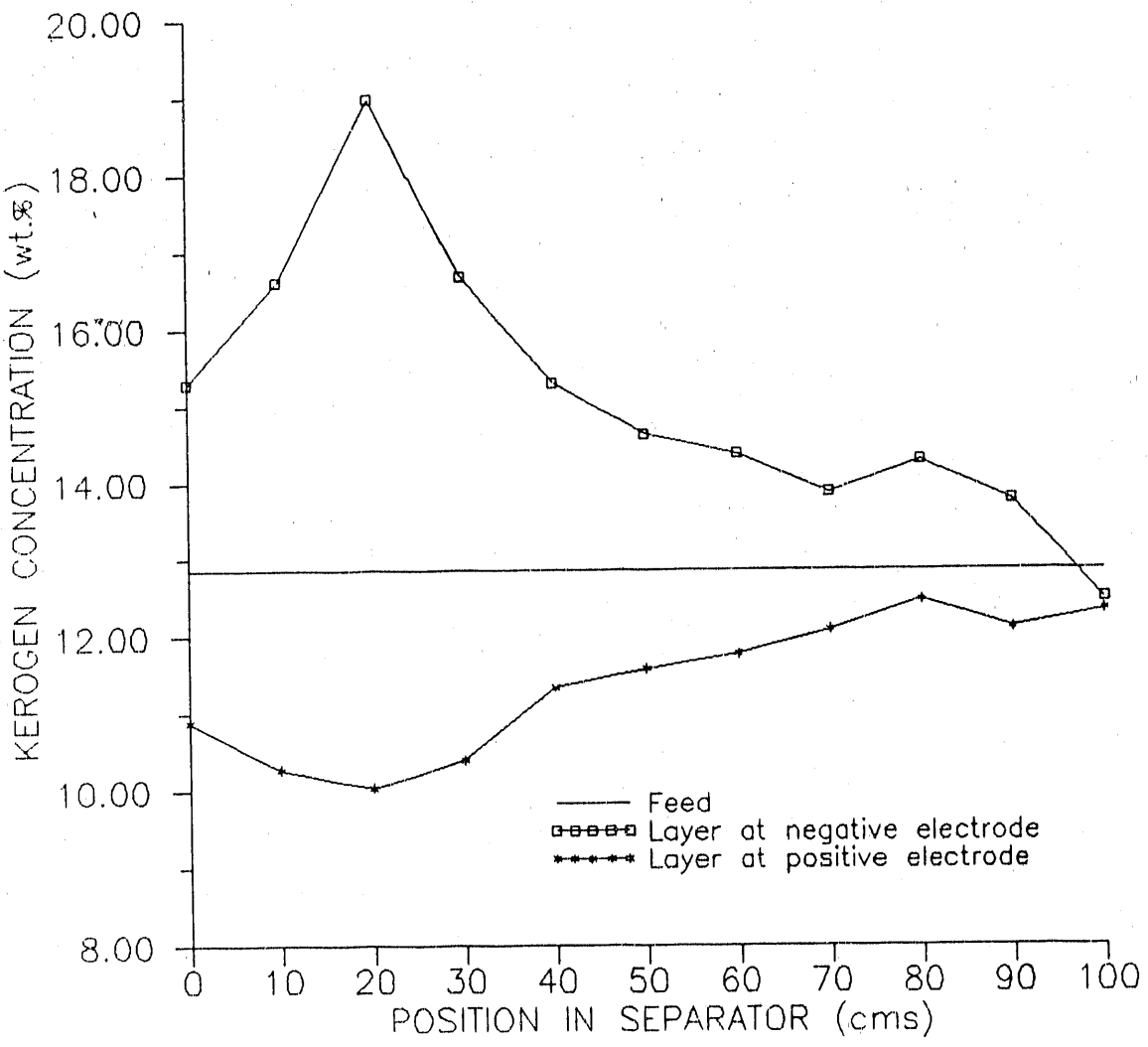

Figure 3-70. KEROGEN CONCENTRATION PROFILE OF LAYERS DEPOSITED ON NEGATIVE AND POSITIVE ELECTRODE IN BATCH SEPARATOR (Circular Jet and Air Flow of 20 cfm)

For the rectangular slit, there is an abrupt change in velocity as soon as particles enter into the separator. However, this change is not as abrupt as in the case of a circular jet (where the flow area is about one-fifth that of the rectangular jet). Also, the downstream velocity profiles for a circular jet inlet and for a rectangular slit jet are very different. The maximum kerogen concentration was also obtained for the case of the pipe jet inlet (Figure 3-69).

Effect of Gas Velocity

Having determined the best inlet geometry for the separator, the effect of gas velocity on separation was studied. Figures 3-70 and 3-71 show the kerogen concentration profiles at both electrodes at airflow rates of 20 and 24 cfm (566 and 679 L/min). The results show that separation at 24 cfm (679 L/min) airflow rate is significantly higher than at 20 cfm (566 L/min). The maximum in the kerogen concentration occurs almost at the same position for both cases, indicating that this maximum is primarily dependent on the inlet geometry. A kerogen enrichment of about 28% was observed.

Factors Limiting Separation

As shown in Figure 3-71, the best kerogen enrichment achieved was about 28%. The principal reason for not achieving higher kerogen enrichments was the agglomeration of fine shale particles. The inter-particle forces responsible for agglomeration are primarily of Coulombic nature, acting between the positively charged kerogen and the negatively charged mineral matter particles. As a result, the charge on the particles is neutralized and formation of particle clusters occurs. These particle clusters or agglomerates have either a "+" or "-" charge depending on how the attraction takes place. An agglomerate rich in kerogen will have a slight positive charge and vice-versa. These agglomerates then move toward the electrodes as independent species, resulting in a poor separation.

In order to determine the strength of the agglomerates formed during the transport and triboelectrification of the particles, the cohesive force between the finely ground oil shale particles was measured using a cohetester. The details of these measurements with pertinent experimental data are described in Appendix B. The cohesive force on the raw oil shale particles is 4 to 5 times larger than that of the same size wheat flour particles. The measurements of cohesive force for beneficiated oil shale particles, however, show that the cohesive force increases with an increase in kerogen content or, in other words, with the extent of beneficiation. These results indicate that a shale rich in kerogen exhibits a greater tendency for agglomeration.

To quantify the strength of these agglomerates, the Weber number was estimated. This number is typically used in gas-liquid systems to determine the coalescence and the breakage of drops and bubbles. It is essentially the ratio of the drag force to the surface force. Surface tension or interfacial tension is a typical measure of the surface force for a gas-liquid system. This analysis was extended for determination of Weber number for the gas-solid system to understand the nature of agglomerate formation. The Weber number (N_w) can be defined as --

$$\text{Weber Number} = \frac{\rho_p (v_g - v_s)^2}{\text{tensile strength}}$$

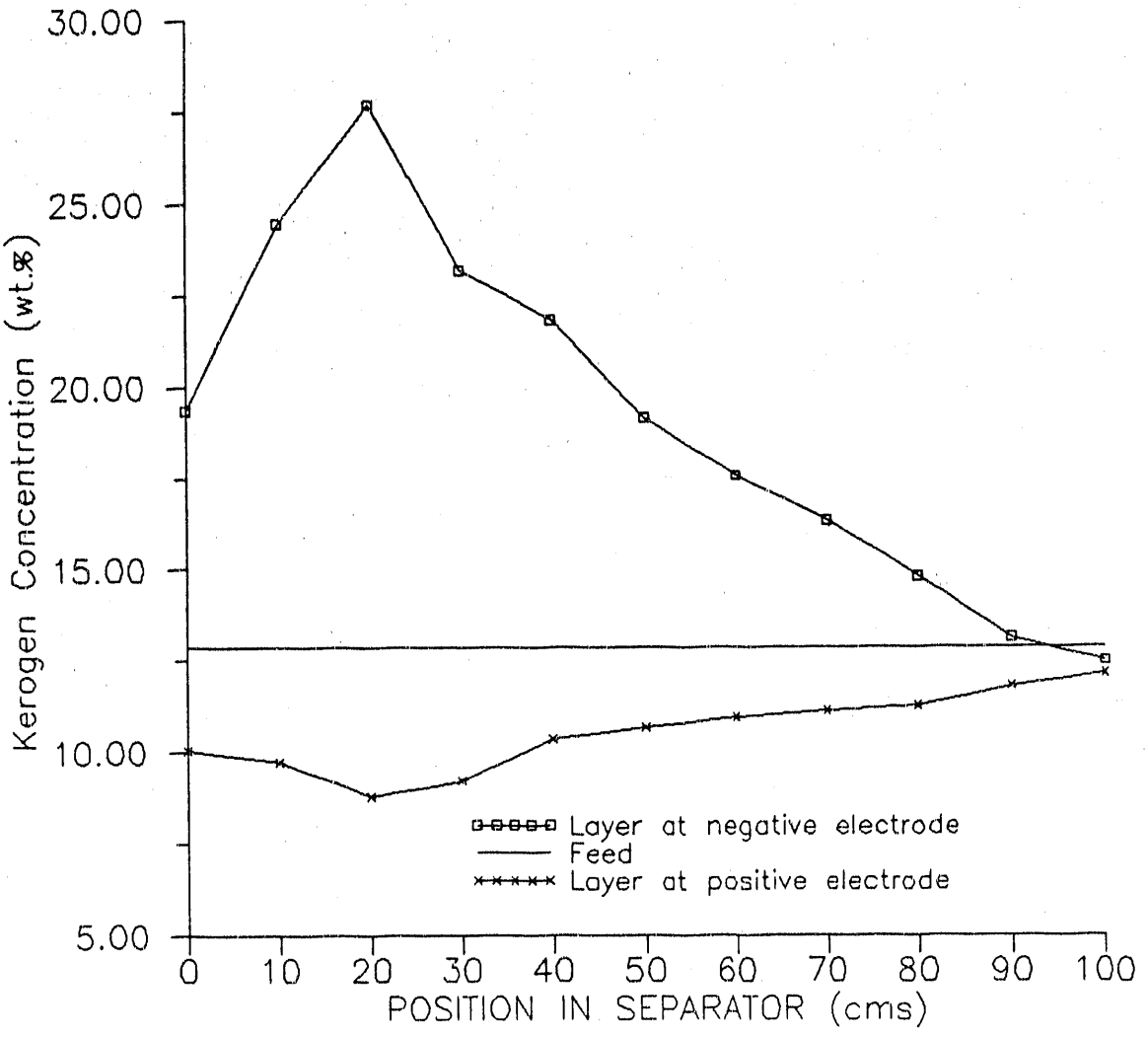

Figure 3-71. KEROGEN CONCENTRATION PROFILE OF LAYERS DEPOSITED ON NEGATIVE AND POSITIVE ELECTRODE IN BATCH SEPARATOR (Circular Jet and Air Flow of 24 cfm)

The value of tensile strength or cohesive force was measured experimentally as described above. The typical value of the Weber number was determined to be about 4. At a critical value of 1.2 for a gas-liquid system, drops become stable and normally would not break. Thus, with a Weber number of 4, the agglomerates would not break and, irrespective of operating the separator under the hydrodynamic conditions best suited for separation, better kerogen enrichments will not be achieved. This should also be true for the wet separation techniques, such as froth flotation, by which the best kerogen enrichments achieved so far are about 50%.

Discussion

It has been shown that an electrostatic process can be used to beneficiate shale. The carbonaceous material in the shale can be made to acquire a positive charge while mineral matter, including pyrites, could be charged negatively. This charge differential can then be used to make a separation. However, the efficacy of the separation was found to be restricted due to the formation of agglomerates. Nevertheless, this dry electrostatic separation is a feasible means of enriching kerogen.

Separation Tests With Model Mixtures

Introduction

Because coal and shale are heterogeneous compounds, it is not possible to determine directly the surface charge characteristics of their various petrographic constituents. IIT made efforts to design a separator for beneficiating shale by extrapolating the surface charge of kerogen and mineral matter. Similar attempts were made to design an electrostatic separator to beneficiate and/or desulfurize coal. Partial successes were achieved in both the cases with the reason for the poor performance being a lack of understanding of the surface charge characteristics and flow behavior of various constituents of coal and shale.

In view of these problems, a model system, using a mixture of charcoal and silica, was chosen to study the separation. The charcoal simulated the carbonaceous component of either coal or shale while silica represented the mineral matter. A mixture of 50% silica and 50% charcoal was prepared by mixing them thoroughly and this mixture was then used as a feed to the separator.

Experimental

Tests were made using the same procedure described previously in the electrostatic separator. As expected, the charcoal acquired a positive charge, the silica charged negatively. A layer rich in charcoal deposited at the negative plate, while a silica-rich layer formed at the positive electrode with the separation being visually evident. The color of feed particles was black, while the silica-rich layer had a clear white color. The carbon content of both the layers was analyzed as a function of position in the separator.

Figure 3-72 shows the carbon content of both the layers deposited at the negative and positive electrodes, respectively. Feed having about 39% carbon

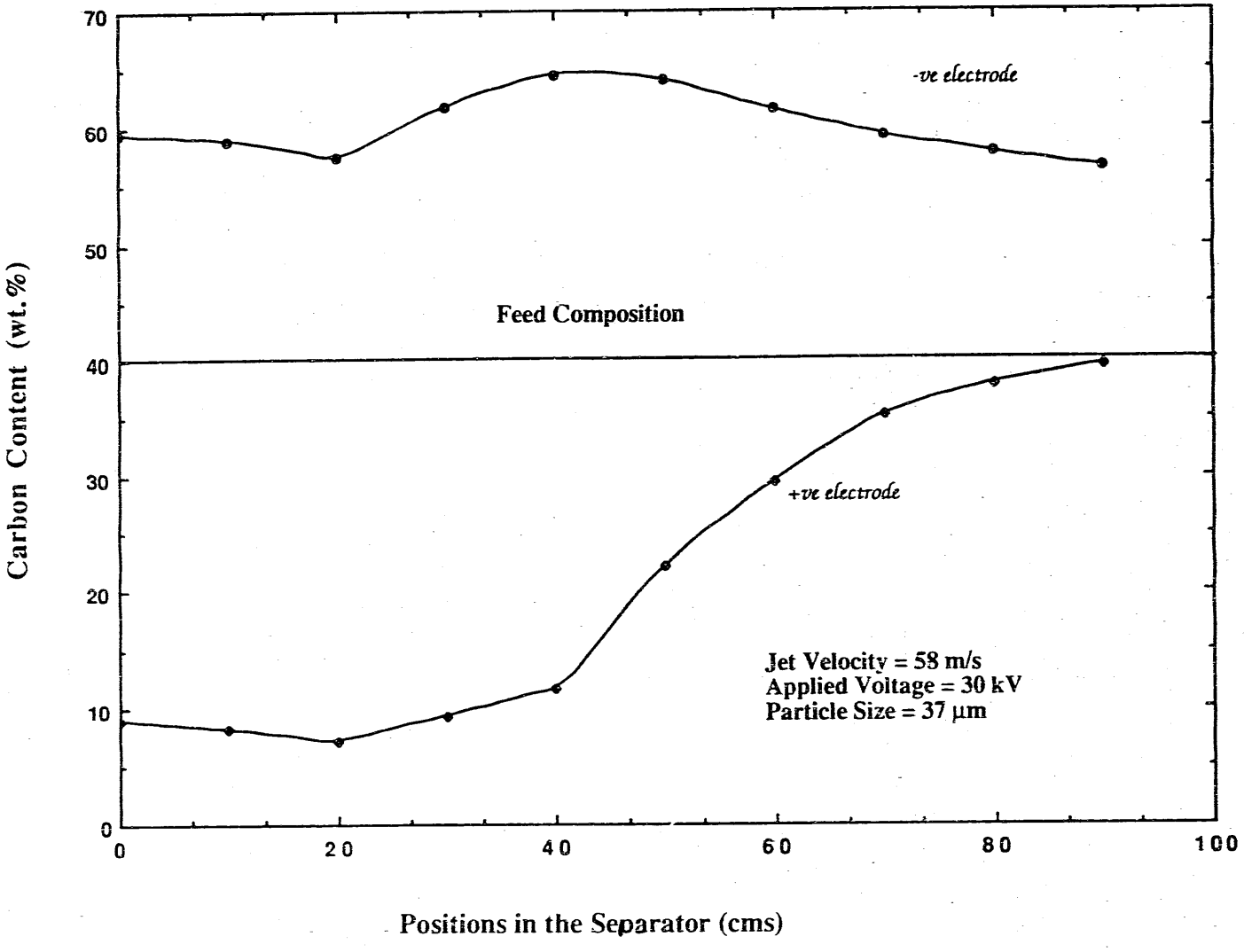

Figure 3-72. CARBON CONCENTRATION PROFILE OF LAYERS DEPOSITED AT POSITIVE AND NEGATIVE ELECTRODES

as enriched to a value of about 64% while a carbon-lean stream (containing about 8% to 10% carbon) was deposited at the positive electrode. The carbon content of both layers varied with position.

Parametric Studies

A systematic parametric study was conducted to determine the effects of various process variables on the separation, including: 1) gas velocity, 2) electric field strength, and 3) inlet configuration. Each of these is described below.

Effect of Gas Velocity

Experiments were conducted at gas velocities of 24, 36, 48 and 58 m/s through the 1/2-inch circular jet inlet. These velocities corresponded to air flow rates of 10, 15, 20, and 24 cfm (283, 425, 566, and 679 L/min), respectively. Carbon composition profiles were determined for the layers deposited at the negative (Figure 3-73) and positive (Figure 3-74) eletrodes. The curves show a maximum in carbon concentration, which is a function of velocity. With an increase in velocity, the maximum shifts to a position farther away from the inlet. As the particle trajectories strongly depend on the initial conditions, this is expected. Also, although the increase is not significant, the carbon concentration corresponding to these maxima increases with an increase in velocity. This indicates that, for efficient separation, higher jet velocities should be used.

Figure 3-74 shows that at the positive electrode, minima in carbon concentrations are observed similar to the maxima shown in Figure 3-73. The position and carbon concentration corresponding to these minima are functions of velocity.

Effect of Applied Voltage

Experiments were conducted with applied electric field strengths of 30,000, 10,000 and 0 volts. The inter-electrode distance was 10 cm. The formation of layers was observed at both electrodes for the applied electric field of 10,000 and 30,000 volts. But, when the applied electric field was zero, no layer was observed.

Figures 3-75 and 3-76 show the effect of the applied electric field strength on the carbon concentration profiles for the layers deposited at the negative and positive electrodes, respectively. With no applied voltage, there was no separation, indicating that the electric force is responsible for the separation. No significant difference in carbon concentration values were observed for the 30 and 10 kV fields. The primary reason for this behavior is that the electrostatic force dominates over gravitational and inertial forces. Maxima and minima in carbon concentration were observed, with their position being a function of applied electric field strength. The change was not significant.

Effect of Inlet Geometry

Because the inlet geometry plays a role in separation, experiments were conducted to study the effect of this variable. Two inlet configurations were

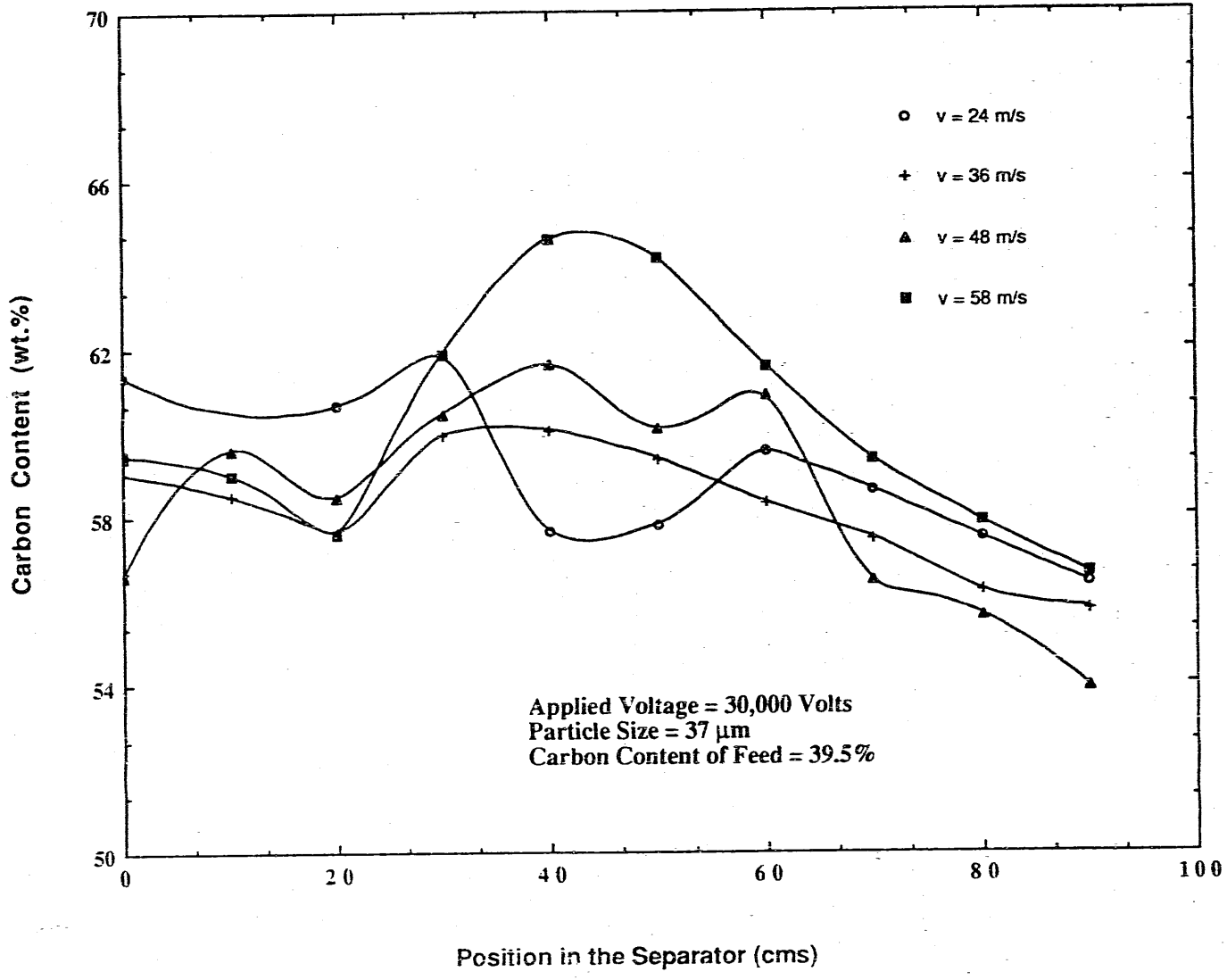

Figure 3-73. CARBON CONCENTRATION PROFILE OF LAYERS DEPOSITED AT NEGATIVE ELECTRODE AS A FUNCTION OF GAS VELOCITY

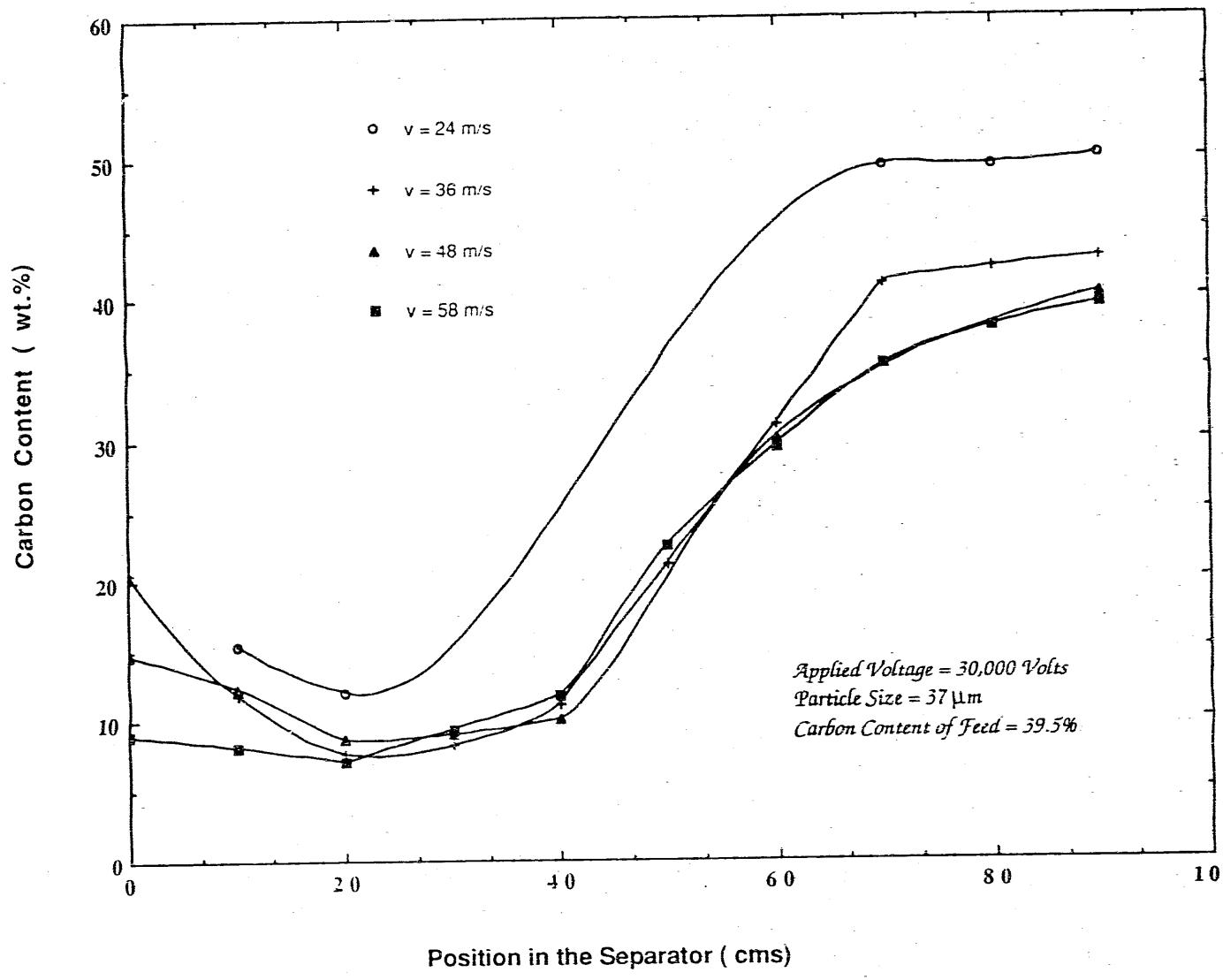

Figure 3-74. CARBON CONCENTRATION PROFILE OF LAYERS DEPOSITED AT POSITIVE ELECTRODE AS A FUNCTION OF GAS VELOCITY

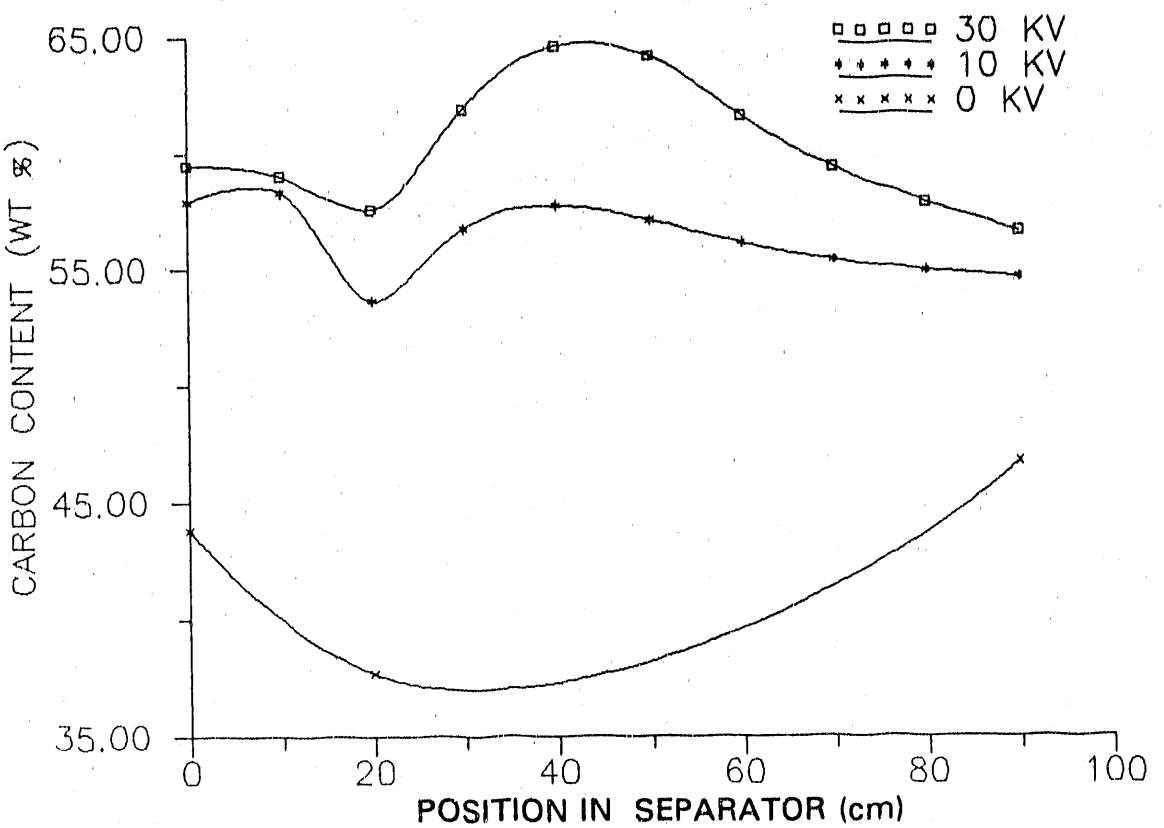

Figure 3-75. CARBON CONCENTRATION PROFILE OF LAYERS DEPOSITED AT NEGATIVE ELECTRODE AS A FUNCTION OF APPLIED VOLTAGE

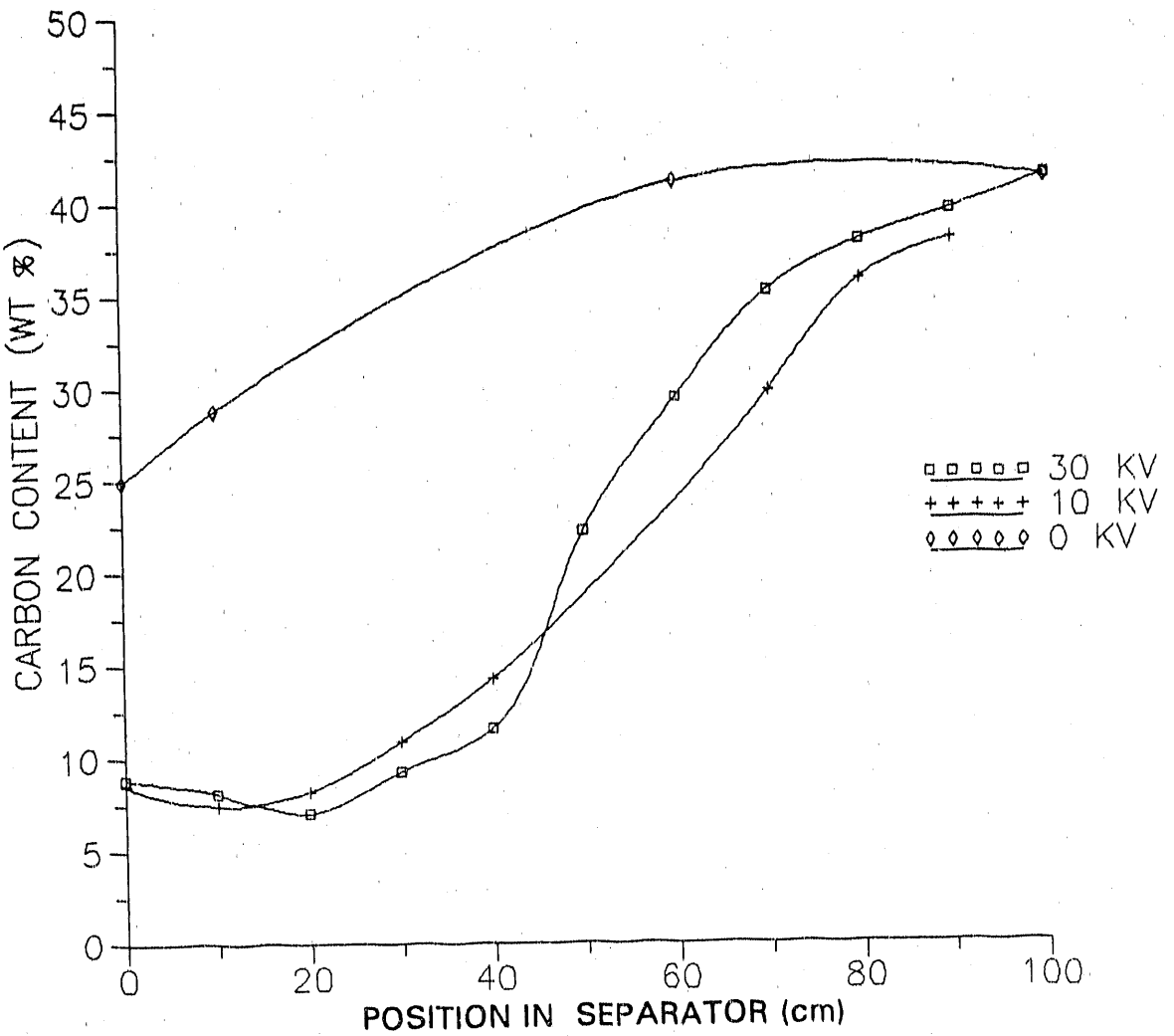

Figure 3-76. CARBON CONCENTRATION PROFILE OF LAYERS DEPOSITED AT POSITIVE ELECTRODE AS A FUNCTION OF APPLIED VOLTAGE

tried: 1) a circular jet and 2) a rectangular channel (see Figure 3-67). Since the flow area at the entrance was different in both the cases, it was not possible to keep the inlet velocity constant. However, the air flow rate was kept at constant, so the velocity away from the inlet is the same.

Figure 3-77 shows the carbon concentration profiles at the negative electrode for both geometrical inlet configurations. As one would expect, the maximum in carbon concentration occurs at the entrance for the channel type inlet. For the circular jet inlet, it occurs a little farther downstream because it takes a while for the particles to come into a streamline.

Discussion

The parametric study conducted for the model mixture of silica and charcoal could be useful in verifying a hydrodynamic model, which can then be used as a tool for designing and optimizing more efficient separators for beneficiation of coal and shale.

Modeling of a Batch Separator

Introduction

The operation of IIT's batch electrostatic separator is similar to that of a two-stage electrostatic precipitator. The only difference is that the latter separates particles from a gas stream, while a gas stream is used to separate one kind of particles from a solid mixture in the former. The difference in surface charge is employed for the separation. The IIT system works in dilute mode (solid loadings of about 0.1 lb solid/lb air). The forces on the particles in the system are such that --

Electrostatic force > Fluid (drag) force > Inertia force

For the dilute suspension of fine particles, it is assumed that the state of fluid motion is unaffected by the presence of the particles.

Governing Equation

For a dilute suspension, the diffusion equation of the species can be written as (Soo, 1973) --

$$\frac{\partial C_p}{\partial t} + \mathbf{u} \cdot \frac{\partial C_p}{\partial r} = -\nabla \cdot [-D_p \nabla C_p + C_p (\mathbf{u}_p - \mathbf{u})] \qquad (3\text{-}21)$$

Where C_p is the particle concentration, D_p is the particle diffusivity and r is the spatial coordinate. $\mathbf{u}$ and $\mathbf{u}_p$ are the fluid and particle velocity vectors, respectively.

Assumptions

1. Motion of the fluid phase is unaffected by the motion of the particles.

2. The field created by the charged particles is negligible compared to the applied electric field, since the suspension is very dilute.

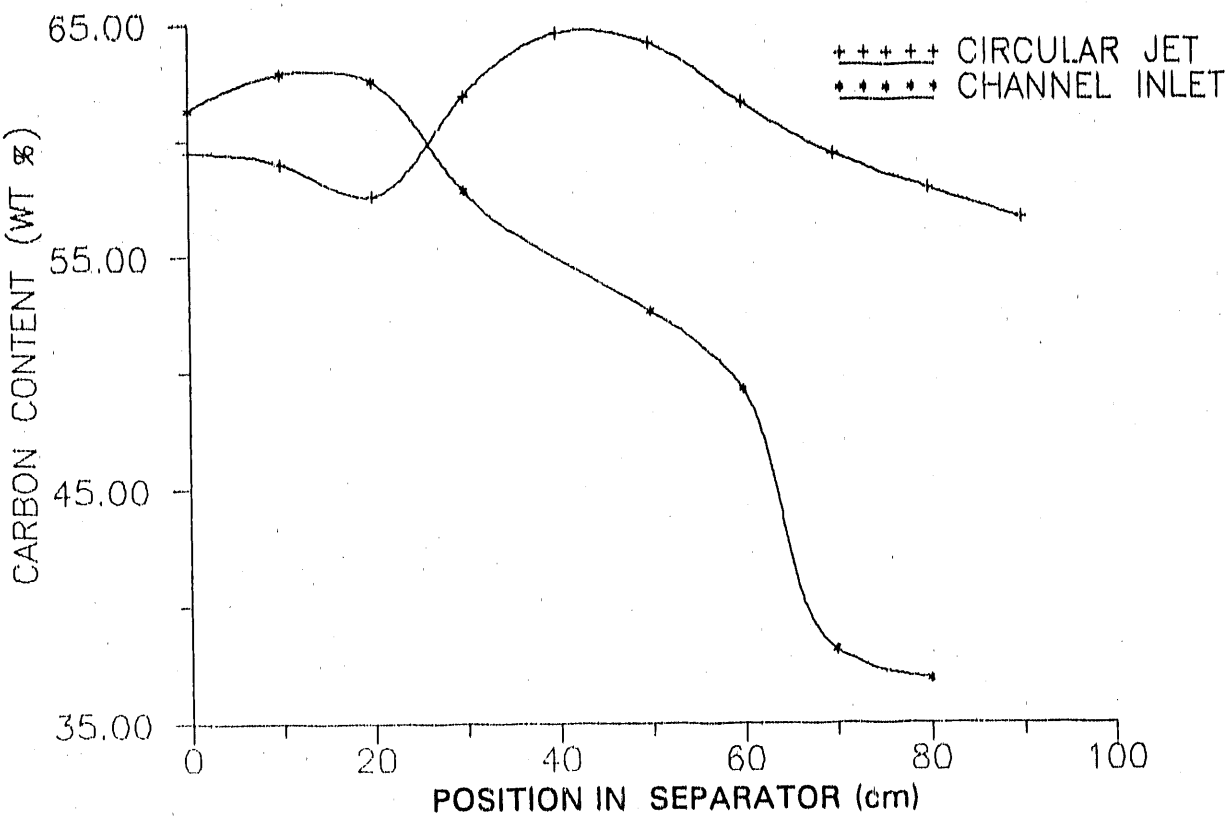

Figure 3-77. CARBON CONCENTRATION PROFILE OF LAYERS DEPOSITED AT NEGATIVE ELECTRODE FOR THE VARIOUS INLET GEOMETRICAL CONFIGURATIONS

3. The adhesion of the particulate matter to the walls or electrodes is due to the presence of field forces.

4. Steady state prevails, that is, as soon as particles deposit, they are removed.

5. Slug flow conditions exist in the channel.

Figure 3-78 shows the geometrical configuration used in the modelling. With these assumptions, the diffusion equation reduces in the form:

$$u \cdot \frac{\partial C_p}{\partial r} = -\nabla \cdot (-D_p \nabla C_p) \qquad (3\text{-}22)$$

For a two-dimensional system as shown in Figure 3-78, we get --

$$U \frac{\partial C_p}{\partial x} + V \frac{\partial C_p}{\partial y} = D_p \left[\frac{\partial^2 C_p}{\partial x^2} + \frac{\partial^2 C_p}{\partial y^2} \right] \qquad (3\text{-}23)$$

Since field forces dominate

$$\frac{\partial^2 C_p}{\partial x^2} = 0 \left(\frac{1}{x^2}\right) \qquad (3\text{-}24)$$

and $x \gg y$, this term can be neglected.

Now, $V = KE$, where K is the electrophoretic mobility and $K = \left(\frac{q}{m}\right) \frac{1}{F}$, where F is the inverse relaxation time, given by --

$$F = \frac{18\mu}{d_p^2 \cdot \rho_p} \qquad (3\text{-}25)$$

where μ is the gas velocity, d_p is the particle diameter and ρ_p is the average particle density. $\left(\frac{q}{m}\right)$ is the charge-to-mass ratio for the particle and E is the applied electric field. Therefore, Equation 3-23 takes the form --

$$U \frac{\partial C_p}{\partial x} + KE \frac{\partial C_p}{\partial y} = D_p \frac{\partial^2 C_p}{\partial y^2} \qquad (3\text{-}26)$$

Solution of the Equation

To non-dimensionalize Equation 3-26, let $x^* = \frac{x}{b}$ and $y^* = \frac{y}{b}$, where b is the electrode spacing, then Equation 3-26 reduces to --

$$\frac{Ub}{D_p} \frac{\partial C_p}{\partial x^*} + \frac{KEb}{D_p} \frac{\partial C_p}{\partial y^*} = \frac{\partial^2 C_p}{\partial y^{*2}} \qquad (3\text{-}27)$$

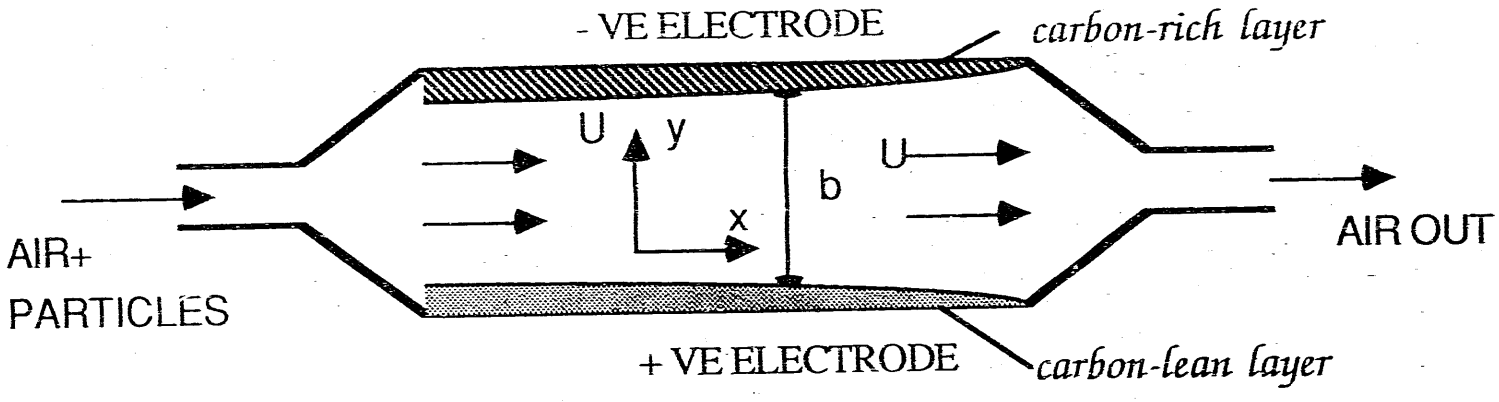

Figure 3-78. GEOMETRICAL CONFIGURATION OF AN ELECTROSTATIC SEPARATOR USED IN MODELING

Let the Electrodifussion Number $\alpha = \frac{KEb}{D_p}$ (3-28)

and the Peclet Number $Pe = \frac{Ub}{D_p}$ (3-29)

Therefore, Equation 3-27 can be written as follows:

$$Pe \frac{\partial C_p}{\partial x^*} + \alpha \frac{\partial C_p}{\partial y^*} = \frac{\partial^2 C_p}{\partial y^{*2}} \quad (3-30)$$

The particle concentration, C_p, can be expressed as a product of particle volume fraction, ε_p, and the particle density, ρ_p

$$C_p = \varepsilon_p \rho_p \quad (3-31)$$

Assuming the particle density, ρ_p, to be constant, then the Equation 3-30 becomes --

$$Pe \frac{\partial \varepsilon_p}{\partial x^*} + \alpha \frac{\partial \varepsilon_p}{\partial y^*} = \frac{\partial^2 \varepsilon_p}{\partial y^{*2}} \quad (3-32)$$

Here subscript p denotes the particle phase. Changing the subscript from p to c, where c denotes the carbon phase, Equation 3-32 can be written as follows:

$$Pe \frac{\partial \varepsilon_c}{\partial x^*} + \alpha \frac{\partial \varepsilon_c}{\partial y^*} = \frac{\partial^2 \varepsilon_c}{\partial y^{*2}} \quad (3-33)$$

This is a second order partial differential equation (pde). To solve this equation, one initial condition, that is, at $x^* = 0$ and two boundary conditions at $y^* = 0$ and at $y^* = 1$ are needed.

Initial Condition: at $x^* = 0$; $\forall y^*$ $\varepsilon_c = \varepsilon_{c0}$ (3-34)

Where ε_{c0} is the initial concentration of carbon in the feed.

Boundary Condition 1: at $y^* = 0$; $\forall x^*$ $\varepsilon_c = 0$ (3-35)

For $y^* = 0$, no carbon particles deposit at the positive electrode.

Boundary Condition 2: at $y^* = 1$; $\forall x^*$ $\varepsilon_c = 1$ (3-36)

For $y^* = 1$, only carbon particles deposit at the negative electrode.

Assuming Pe and α to be constant, Equation 3-33 can be solved to obtain a closed solution (Bateman, 1942). The final solution for ε_c would be as follows:

$$\varepsilon_c = \left[\frac{e^{\alpha y^*} - 1}{e^{\alpha} - 1} \right] + R_1 + R_2 \quad (3-37)$$

where --

$$R_1 = 2 \sum_{n=1}^{\infty} (-1)^n \gamma_n e^{\frac{\alpha}{2}(1-y^*)} \sin(n\pi y^*)\omega_n(x^*) \qquad (3\text{-}38)$$

$$R_2 = 2\varepsilon_{c0} \sum_{n=1}^{\infty} \gamma_n \left[1 - (-1)^n e^{-\frac{\alpha}{2}}\right] e^{\frac{\alpha}{2} y^*} \sin(n\pi y^*)\omega_n(x^*) \qquad (3\text{-}39)$$

$$\gamma_n = \frac{n\pi}{n^2\pi^2 + \frac{\alpha^2}{4}} \qquad (3\text{-}40)$$

$$\omega_n(x^*) = \exp\left[- \left(\frac{n^2\pi^2}{Pe} + \frac{\alpha^2}{4Pe} \right) x^* \right] \qquad (3\text{-}41)$$

Determination of Particle Diffusivity

The particle diffusivity plays an important role in the separation. Since the gas flow in the channel is turbulent, the Reynolds Number, Re, calculated using the equation

$$Re = \frac{U_o b \rho}{\mu} \qquad (3\text{-}42)$$

is about 7100 for the experimental conditions. The particle diffusivity can be related to the fluid diffusivity using the relation given by Soo (1989).

$$\frac{D_p}{D} \approx 1 - \frac{k^3}{2\sqrt{\pi}} \qquad (3\text{-}43)$$

where --

$$k = \frac{2 \langle u^2 \rangle^{1/2}}{\lambda F} \qquad (3\text{-}44)$$

Here λ is the mean free path of eddies and F is the inverse relaxation time for the momentun transfer as defined in Equation 3-25.

For very fine particles, $k \to 0$; then $D_p \approx D$. Now fluid diffusivity can be estimated using van Driest's correlation (1956).

$$D = 0.01231\ (Re)^{-1/8}(U_0)(2R) \qquad (3\text{-}45)$$

where 2R is the pipe diameter. In this case, U_0 = 1.1 m/s and 2R = 0.10 m and

$$D \approx D_p = 4.4 \times 10^{-4}\ m^2/s \qquad (3\text{-}46)$$

This value of the diffusivity was checked with the equation derived by Gidaspow and Liu (1981) using the relative velocity model, according to which

$$D_p = \frac{|v_g - v_p|\hat{v}}{\beta} \tag{3-47}$$

where v_g is the gas velocity, v_p is the particle velocity and β is drag or inverse relaxation time which is the same as F in the Stoke's law regime. $\hat{v}$ is an average velocity given by --

$$\hat{v} = \varepsilon_g v_g + (1 - \varepsilon_g) v_p \tag{3-48}$$

where ε_g is the gas volume fraction. For a very dilute suspension $\varepsilon_g \approx 1$, implying that $v \approx v_g$, then D_p becomes --

$$D_p \approx \frac{|v_g - v_p| v_g}{F} \tag{3-49}$$

Now $v_g = 0(1\ m/s)$ and $F = 10^4\ s^{-1}$, therefore --

$$D_p = 0\left[|v_g - v_p| \cdot 10^{-4}\right] \frac{m^2}{s} \tag{3-50}$$

Comparison With Experimental Data

The following values were estimated for α and Pe number for carbon phase.

$$\alpha = \left(\frac{q}{m}\right) \frac{Eb}{FD_p} \tag{3-51}$$

$\left(\frac{q}{m}\right) = +1.9 \times 10^{-3}$ C/kg; $E = 3 \times 10^5$ volts/m; $b = 0.10$ m; $D_p = 4.4 \times 10^{-4}$ m^2/s and

$$F = \frac{18\mu}{d_p^2 \cdot \rho_p} = 10^4 s^{-1} \tag{3-52}$$

Substituting these values in Equations 3-28 and 3-29, $\alpha = 13$ and Pe = 250.

Taking the only first term of Equations 3-37 and 3-38 and substituting the values of α and Pe, yields the following:

$$\varepsilon_c = \left[\frac{e^{13y^*} - 1}{e^{13} - 1}\right] + 0.1255\left[\varepsilon_{c0} e^{6.5y^*} - e^{-6.5(1-y^*)}\right] \sin \pi y^* \cdot e^{-0.2084x^*} \tag{3-53}$$

For a particle loading of 0.1 lb solids/lb air, $\varepsilon_{c0} = 5 \times 10^{-3}$. Furthermore, the layer thickness (δ) observed was of the order of 2 mm. Therefore, $\varepsilon_{c,avg}$ can be calculated as --

$$\varepsilon_{c,avg} = \frac{\int_0^{\delta} \varepsilon_c dy}{\delta} \qquad (3\text{-}54)$$

which can be calculated by numerical integration.

Figure 3-79 shows the comparison of experimental data with the values calculated using the above equations. Initially, the match between the data and the model is very good. The model, however, does not show the significant rate of drop with the length as observed by the experiment. This is because the assumptions of plug flow and steady-state condition do not hold good, and only the first term of the series is used in the computations.

Effect of Electrodiffusion Number (α)

This simplified model can now be used to qualitatively study the effect of various system variables. This analysis provides two dimensionless numbers, Electrodiffusion and Peclet numbers, which are characteristics of this system. Due to the simplifying assumptions, such as plug-flow motion, the utility of the Peclet number may not be significant. However, the Electrodiffusion number can be a very useful parameter for an engineering design of an electrostatic separator.

$$\alpha = \left(\frac{q}{m}\right) \frac{Eb}{FD_p} \qquad (3\text{-}51)$$

or

$$\alpha = \frac{qEb}{3\pi\mu d_p D_p} \qquad (3\text{-}55)$$

The following inferences can be drawn from this simple formula:

- Increase in the electrode spacing should result in a better separation.
- Increase in the applied electric field should also result in a better separation.
- Increase in the surface charge of the particle should lead to better separation efficiencies.
- Finer particles should separate better by an electrostatic process.
- The influence of particle diffusivity can be readily seen from this equation.

Figure 3-80 shows the volume fraction of carbon as a function of y^* for various values of α. As the value of α increases, the carbon concentration profiles become steeper. This indicates that for an efficient separation, one would like to have as high value of α as possible.

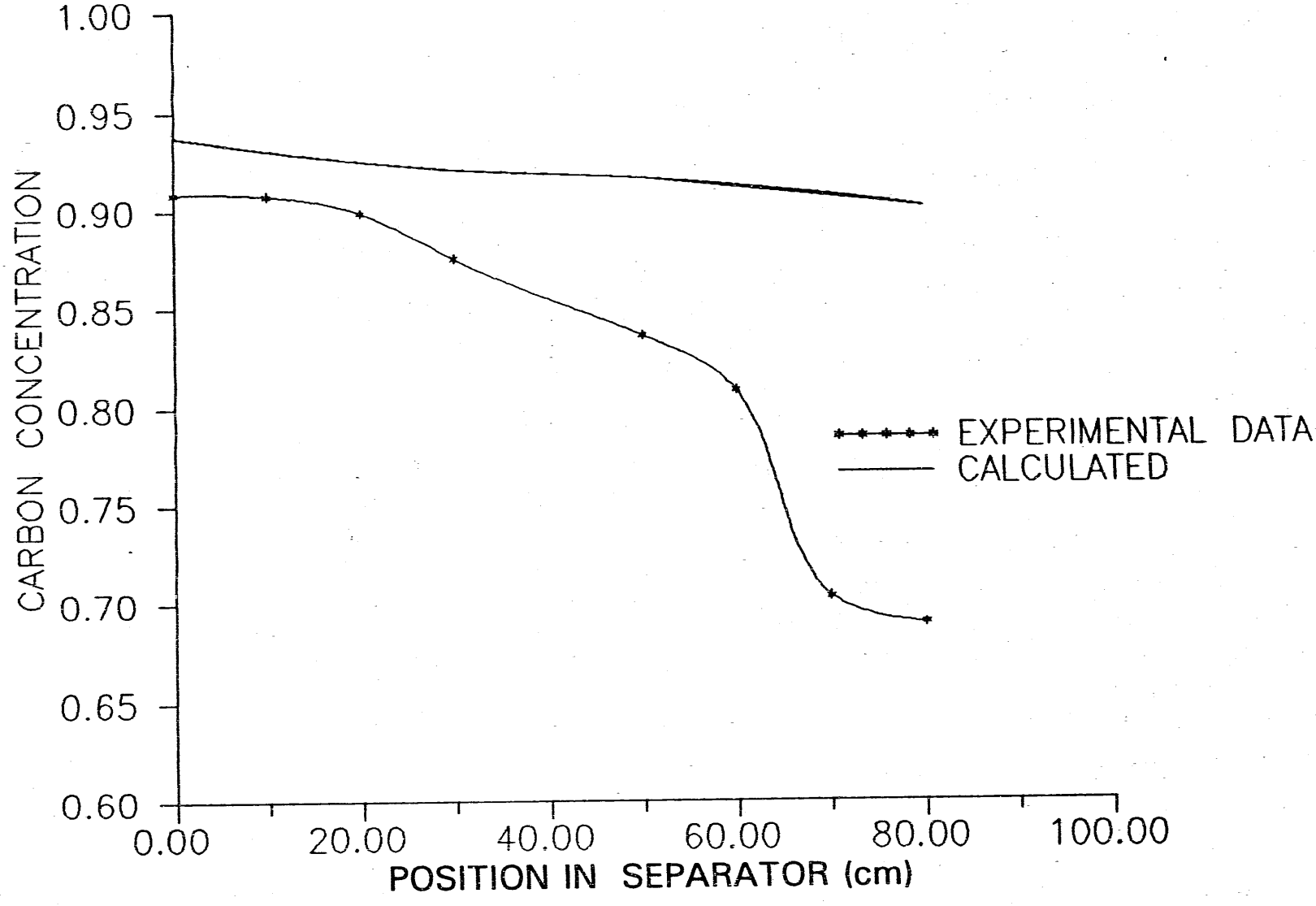

Figure 3-79. COMPARISON OF EXPERIMENTAL DATA WITH THE CALCULATED VALUES FOR THE SEPARATION OF CARBON FROM A MODEL MIXTURE OF CHARCOAL AND SILICA

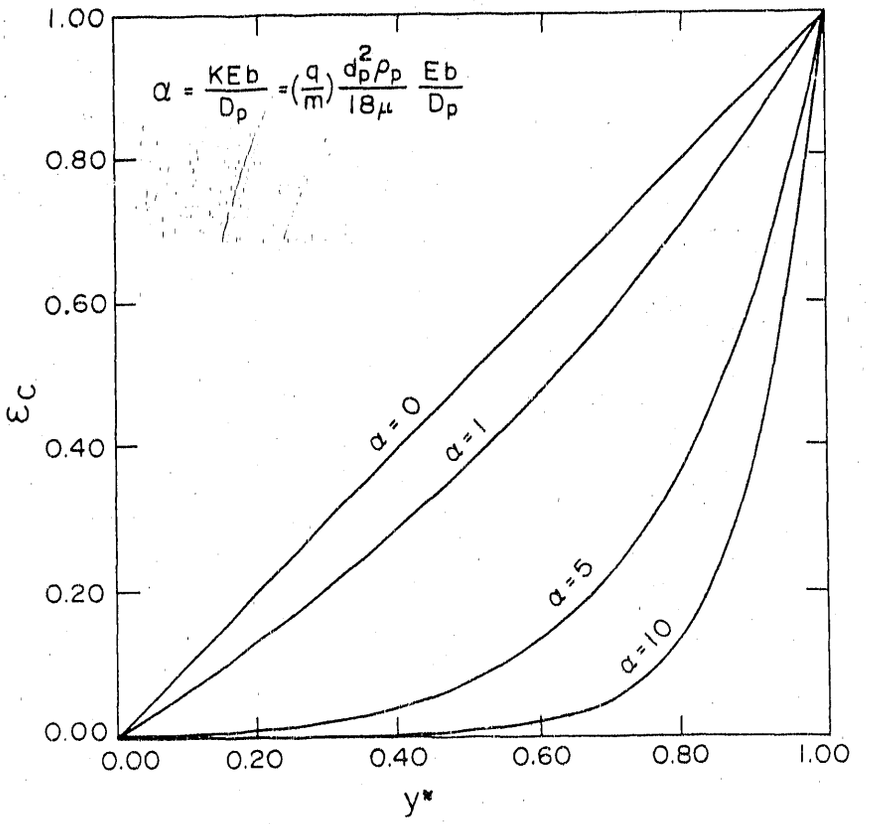

Figure 3-80. EFFECT OF ELECTRODIFFUSION NUMBER

Discussion

The model presented in this section is a simplified approach borrowed from electrostatic precipitator design. To model complex geometrical configurations, a more rigorous model is needed. Nevertheless, this simple analysis can be a valuable design tool.

Conclusions and Recommendations

IIT has invented a process for dry electrostatic beneficiation of shale. The process is based on the experimental findings that carbonaceous matter in shale can be made to acquire a positive charge, while minerals and pyrites assume a negative charge. Hence, an application of a direct electric field can, in principle, lead to a complete separation of shale into its constituents. To achieve an ideal separation, proper focussing of charged particles is required. Unfortunately, the design of such an ideal separator requires proper characterization of flow of cohesive fine particles. In view of these problems, a systematic approach is proposed, as outlined in Figure 3-81, to design the ideal separator shown in Figure 3-82.

Because the surface charge differential is the driving force for the separation, it is necessary to study the surface charge characteristics of various constituents of shale in a systematic fashion. Once these data are

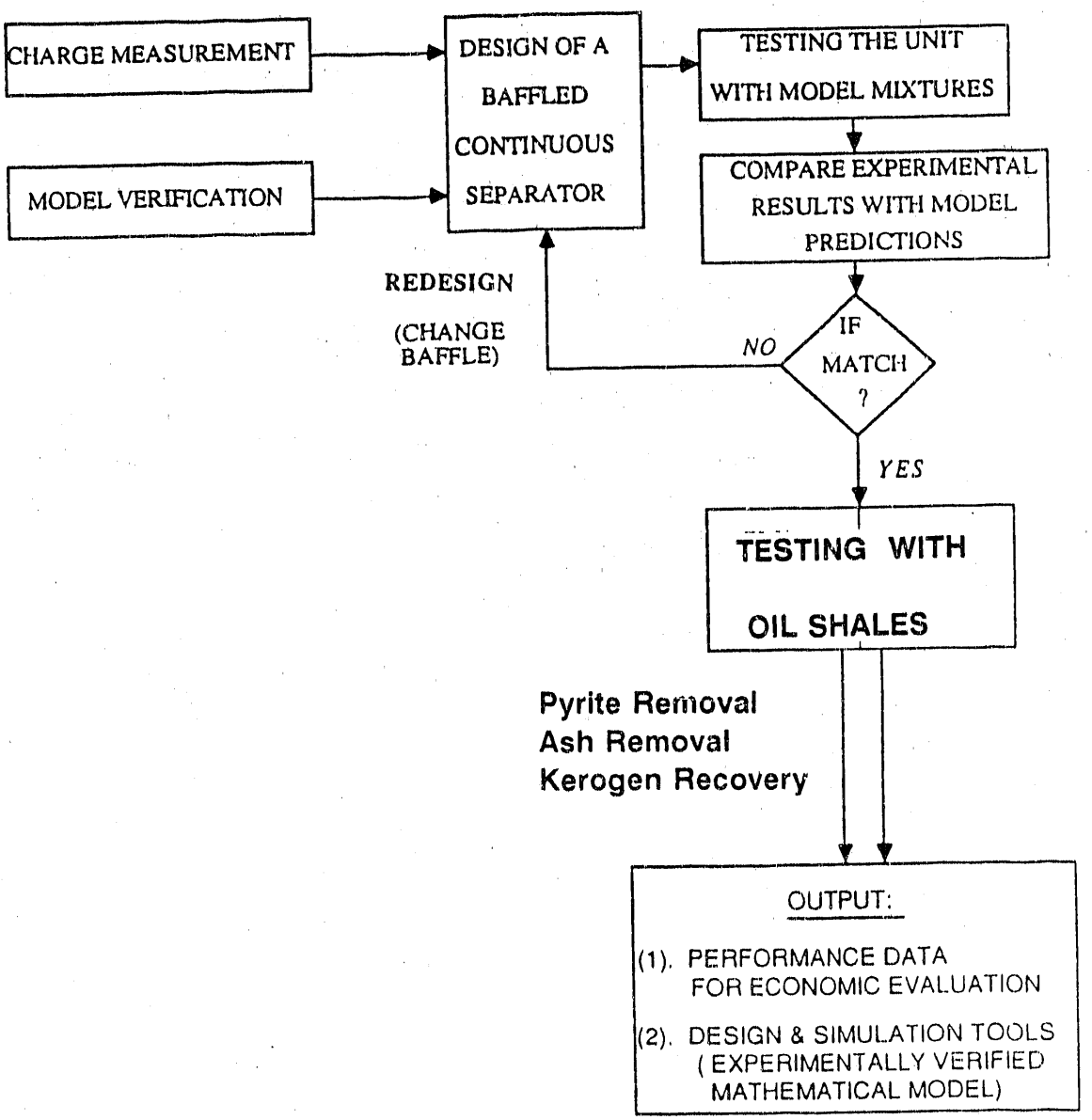

Figure 3-81. SYSTEMATIC APPROACH TO AN ELECTROSTATIC SEPARATOR DEVELOPMENT

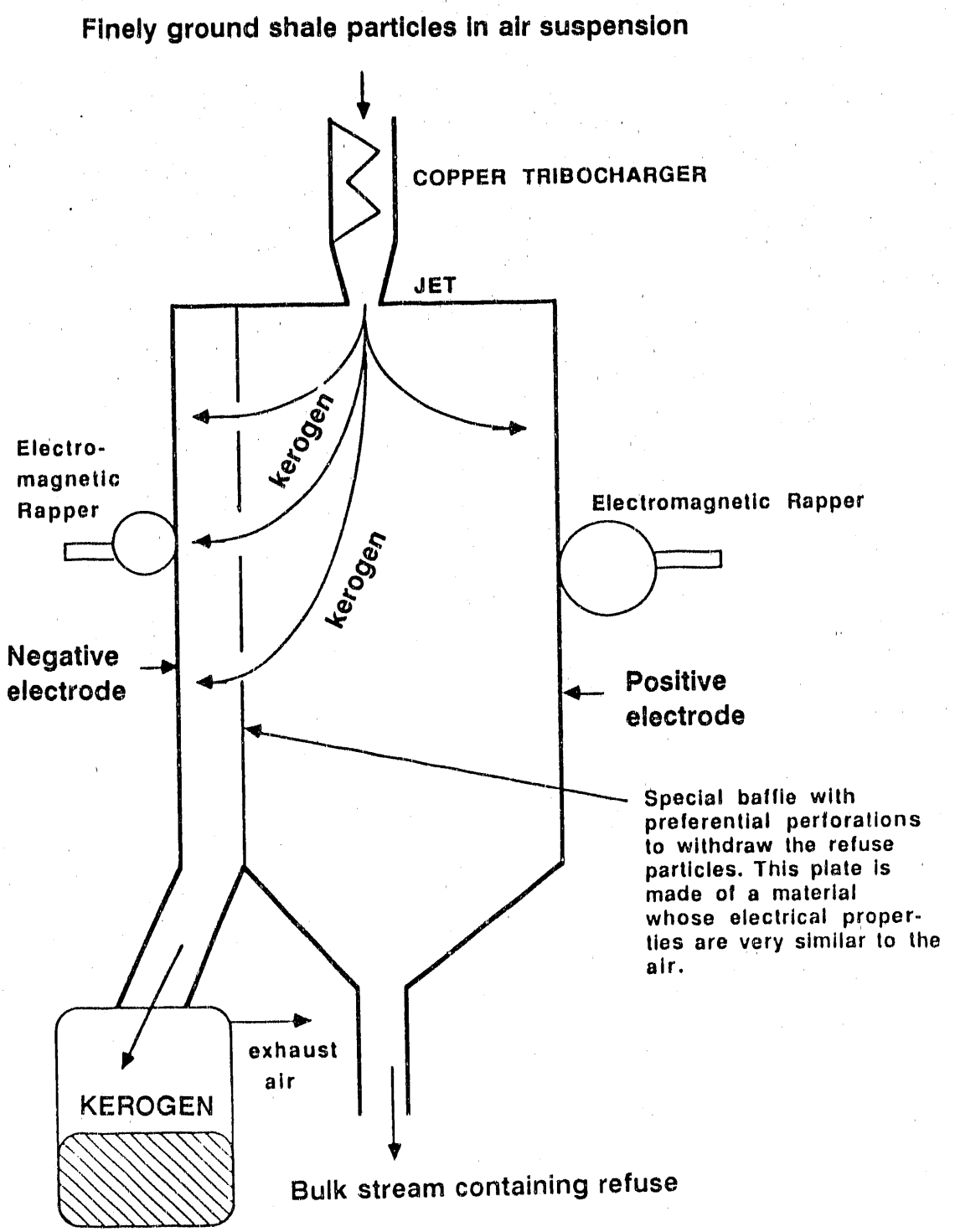

Figure 3-82. CONCEPTUAL DESIGN OF A CONTINUOUS ELECTROSTATIC SEPARATOR

collected, a semi-theoretical model could be used to correlate the experimentally measured charge values. This type of correlation will be very useful in designing electrostatic separators.

After development of a correlation for the surface charge, the next important step is to determine the low conditions most conducive to separation. To do this, a hydrodynamic model describing the flow behavior of particles inside the separator should be developed. The simplified model described in the previous section is not adequate for this purpose. Therefore, more rigorous models should be developed. One such model is that developed by Gidaspow et al. (1989). This model has been used for simulating the sieve separator, but the predictions were qualitative in nature.

In order to model an electrostatic separator correctly, the present model must be modified to incorporate the various phenomenon observed experimentally, such as sticking of particles to the electrode surface, accountability of the distortion created on the electric field due to the presence of perforations, etc. Then this model must be verified for separation of synthetic mixtures such as silica and charcoal, for which experimental data are reported. If there are major discrepancies between the data and predicted results, the model should be corrected.

As shown in Figure 3-81, the verified hydrodynamic model, in conjunction with experimentally measured values of surface charge, should be used to design the continuous separator as shown in Figure 3-82. Since both routes tested (perforated electrodes and solid copper plates) did not lead to efficient separator design, a combination of both these methods should result in design of an efficient separator. In this design, solid copper plates without any perforations should be used along with a specially designed baffle, to withdraw the refuse particles. This baffle should meet the following requirements.

1. The material of construction of the baffle should have very similar electrical properties to that of air, so the electric field is not distorted and the electrical resistivity and dielectric constant of the baffle material should be comparable to air.

2. The perforations in the baffle should be made only at the points where trajectories of kerogen particles meet the baffle surface. Particle trajectories depend on the following process variables: electric field strength, surface charge of mineral and pyrites, particle size distribution, and jet velocity, etc.

With these modifications, the experimentally verified hydrodynamic model of Gidaspow et al. (1989), may be used to simulate the effect of these variables and to properly design the perforations in the baffle. The charge conservation equation (Laplace or Poisson's Equation) should be incorporated into the model to account for the disturbance in the electric field due to the presence of the baffle.

Electromagnetic rappers, similar to those used in electrostatic precipitators (White, 1963), can be employed to prevent any sticking of particles to the solid electrodes. Refuse (mineral matter and pyrites) and kerogen can then be continuously collected in a bin.

The expected outcome of this approach will be 1) performance data on the baffled electrostatic separator for economic evaluation and 2) an experimentally verified hydrodynamic model which can be used as a design and simulation tool.

Nomenclature

b	Electrode Spacing
C	Concentration
C_0	Capacitance
d_A	Single Covalent Bond Length of Element A
d_p	Particle Diameter
D	Fluid Diffusivity
D_p	Particle Diffusivity
e	Charge on an Electron
E	Electric Field Strength
E_1	Modulus of Elasticity for Particle
E_2	Modulus of Elasticity for Charger Surface
E_{bk}	Breakdown Voltage for Air
F	Inverse Relaxation Time Defined by Equation 3-25
F_e	Electrical Force
F_g	Gravitational Force
g	Acceleration Due to Gravity
$\vec{H}$	Magnetic Field Intensity
I	Current
J	Current Density
k	Boltzmann's Constant
K	Electrophoretic Mobility
m	Mass of Particle
$\hat{m}$	Mass Flow Rate
$\vec{M}$	Magnetic Moment
P	Power Consumed in Grinding
Pe	Peclet Number Defined by Equation 3-29
q	Charge on Particles
Q	Surface Charge Generated by Triboelectrification
r	Spatial Coordinate
r_e	Zero Field Reflection Coefficient
r^*	Ratio of Rebound Speed to Incoming Speed

R	Particle Radius
S	Surface Area
T	Temperature
$\mathbf{u}$	Fluid Velocity Vector
$\mathbf{u_p}$	Particle Velocity Vector
U_{mf}	Minimum Fluidization Velocity
U_x	X-component of Velocity
U_y	Y-component of Velocity
v	Velocity
$\hat{v}$	Average Velocity Defined by Equation 3-48
V_c	Contact Potential Difference
W_i	Work Index Used in Grinding Calculations
x	Spatial Coordinate Parallel to Flow Direction
x^*	Dimensionless Spatial Coordinate Parallel to Flow Direction
y	Spatial Coordinate Perpendicular to Flow Direction
y^*	Dimensionless y

Greek Letters:

α	Electrodiffusion Number Defined by Equation 3-28
β	Drag
δ	Thickness of Layer Deposited at the Electrode
λ	Mean Free Path for Eddies
ε	Volume Fraction
σ	Electrical Conductivity
ρ	Density
ν	Poisson's Ratio
μ	Viscosity
χ	Electronegativity
χ_m	Magnetic Susceptibility
ϕ	Work Function

Subscripts:

g	Gas Phase
s	Solid Phase
b	Bulk
p	Particle
c	Carbon

Bibliography

Abel, W. T., M. Zulkoski, G. A. Brady and J. W. Eckerd, "Removing Pyrite from Coal by Dry Separation Methods," U.S. Bureau of Mines Report, 7732 (1973).

Advanced Energy Dynamics, Inc., "Advanced Physical Fine Coal Cleaning," Final report prepared for the U.S. Department of Energy, under Contract No. DE-AC22-85PC81211, December (1987).

Alberta Research Council, Monthly Progress Reports for the period of January 4 to February 4, 1988, February 5 to March 5, 1988, and March 5 to April 5, 1988. Program Manager: Ignasiak, B., Project No. RP 2655-12, Reference No. 2901-01-6 (1988).

Alfano, G., P. Carbini, M. Carta, R. Ciccu, C. Del Fa', R. Peretti, and A. Zucca, "Applications of Static Electricity in Coal and Ore Beneficiations," J. of Electrostatics, vol. 6, 315-328 (1985).

Allen, T., Particle Size Measurement, Chapman and Hall Ltd., London (1968).

Akande, A. R., and J. Lowell, "Contact Electrification of Polymers by Metals," J. of Electrostatics, vol. 16, 147-156 (1985).

Annual Book of ASTM Standards, Vol. 05.05, Gaseous Fuels; Coal and Coke, ASTM, Philadelphia, PA (1986).

Bateman, H., Partial Diffential Equations of Mathematical Physics, Dover Publications, New York (1944).

Bauma, J., "Electrostatic Separation of Coal and Flyash Components," IEEE IAS, vol. 34C, 966-971 (1984).

Bechtel National, Inc., "Advanced Physical Fine Coal Cleaning: Micro-bubble Floatation," Draft Final Report Prepared for the U.S. Department of Energy, under Contract No. DE-AC22-85PC81205, March (1988). Bechtel National, Inc., "Advanced Physical Fine Coal Cleaning: Spherical Agglomeration," Draft Phase I Report prepared for the U.S. Department of Energy/Pittsburgh Energy Technology Center, under Contract No. DE-AC22-87PC79867 (1988).

Boron, K., and A. Grodzicki, "The Application of an Electrostatic Method to the Concentration of Heavy Minerals in Some Polish Sands," J. of Electrostatics, vol. 2, 331-339 (1976).

Butcher, S. G., and D. F. Symonds, "A Review of Dry Cleaning Processes," Alberta Coal Mining Research Center Report, CMRC 81/21-T, March (1981).

Carta, M., C. Del Fa', and G. F. Ferrara, "A New Apparatus for Pneumatic Separation," 6th International Mineral Processing Congress, 245 (1963).

Carter, L., "Economic Evaluation of Dry Physical Coal Cleaning Processes," Final Report to Center for Research on Sulfur in Coal, Carterville, IL. Grant No. 88-137, September (1989).

Cheng, L., and S. L. Soo, "Charging of Dust Particles by Impact," J. of Chem. Physics, vol. 41, 2, February (1970).

Chiang, S.-H., "LICADO Process for Oil Shale Beneficiation," Paper presented at the Pressurized Fluidized-Bed Hydroretorting of Eastern Oil Shales Review Meeting held at the Institute of Gas Technology, Chicago, IL, June 20, 1989.

Ciocu, R., R. Peretti, A. Serci, M. Tamanini, and A. Zucca, "Experimental Study on Triboelectric Charging of Mineral Particles," J. of Electrostatics, Vol. 23, pp. 157-168 (1989).

Ciesla, A., and K. Chudyba, "Contributions to the Investigations of Electrification of Coal Grains by the Triboelectric Method," Archiwum Elektrotechniki, Zeszyt 1, SS, 1-80 (1978).

Clark, C. S., J. of San. Div. Am. Civil Engineers, vol. 92, 127 (1966).

Coal Age, page 23, July (1977).

Cross, J., Electrostatics: Principles, Problems and Applications, Adam Hilger, Bristol (1987).

Dahlstrom, D. A., and R. P. Klepper, "Practical Aspects of Filtration and Dewatering in Physical Cleaning of Fine Coal," in Physical Cleaning of Coal, Y. A. Liu, Ed., Marcel Dekker, New York (1982).

Davies, D. K., "Static Electrification," Inst. of Phy. Conf. Series, vol. 4, 29 (1967).

Davies, D. K. "Charge Generation on Dielectric Surfaces," J. Phy. D: App. Phy., vol. 2, pp. 1533-37 (1969).

Doctor, R. D., C. D. Livengood, L. E. Genens, C. E. Swietlik, and K. Foote, "Investigation of Open-Gradient Magnetic Separations for Illinois Coal," in Processing and Utilization of High Sulfur Coals, Y. P. Chugh and R. D. Caudle, Ed., Elsevier, New York, 149-162 (1987).

Dutta, A., and L. V. Dullea, "A Comparative Evaluation of Negatively and Positively Charged Submicron Particles As Flow Conditioners for a Cohesive Powder," Paper presented at the AIChE Annual Meeting in San Francisco, November, CA (1989).

Energy Statistics, vol. 11, 4, Institute of Gas Technology, Chicago (1989).

Fasso, L., B. T. Chao, and S. L. Soo, "Measurement of Electrostatic Charges and Concentrations of Particles in the Freeboard of a Fluidized Bed," Powder Technology, vol. 33, pp. 211-221 (1982).

Fomenko, V. S., Handbook of Thermionic Properties. V. Samsonov, Ed., Plenum Press Data Division, New York (1966).

Fomenko, V. S., "Emission Properties of Materials," NTIS, U.S. Department of Commerce Report, No. JPRS-56579 (1972).

Gajewski, A. "Measuring the Charging Tendency of Polystyrene Particles in Pneumatic Conveyance," J. of Electrostatics, vol. 23, pp. 55-66 (1989).

Geer, R., "Coal Microstructure and Pyrite Distribution," in ACS Symposium Series, Division of Fuel Chemistry, T. D. Wheelock, Ed., 3-15, March 23, 1977.

Geldart, D., "Types of Gas Fluidization," Powder Technology, vol. 7, pp. 285-292 (1973).

Gidaspow, D., and Y. Liu, "Solids Mixing in Fluidized Beds - A Hydrodynamic Approach," Chem. Eng. Sci., vol. 36, 3, pp. 539-547 (1981).

Gidaspow, D., R. Gupta, A. Mukherjee, and D. T. Wasan, "Separation of Pyrites from Illinois Coals Using Electrofluidized Beds and Electrostatic Sieve Conveyors," in Processing and Utilization of High Sulfur Coals II, Y. P. Chugh and R. D. Caudle, Ed., Elsevier, New York, pp. 271-281 (1987).

Gidaspow, D., U. K. Jayaswal, Y. Tsuo, and D. T. Wasan, "Design of an Electrostatic Separator for Coal Desulfurization," paper presented in AIChE Annual meeting in San Francisco, CA, November 1989.

Gidaspow, D., Multiphase Flow and Fluidization, American Society of Mechanical Engineers, New York (1990, in press).

Gonsalves, V. E., "Some Fundamental Questions Concerning the Static Electrification of Textile Yarns: Part I," Textile Research Journal, pp. 711-718, October 1953.

Gordy, W., and W. Thomas, J. Chem. Physics, vol. 24, 439 (1956).

Gray, V. R., and P. F. Whelan, "Electrostatic Cleaning of Low Rank Coal by the Drum Separator," Fuel, vol. 35, p. 184 (1956).

Hanna, H. S., and Lamont, W. E., "Physical Beneficiation Studies of Eastern Oil Shale," Third IGT Synfuels Symposium, IGT Publication, 295-321 (1983).

Harper, W. R., Contact and Frictional Electrification, Oxford University Press, London (1967).

He, D. X., G. Aranjo, B. I. Morsi, G. E. Klinzing, R. Venkatadri, and S.-H. Chiang, "Application of LICADO Process to High Sulfur Bituminous Coals," paper presented in the International Conference on Processing and Utilization of High Sulfur Coals III, Ames, Iowa (1989).

Hise, E. C., A. S. Holman, and J. E. Jones, "Initial Investigations of OGMS," ORNL Report, 5764, April (1982).

Holt, E. C., Jr., "An Engineering/Economic Analysis of the Coal-Pyrite Flotation Process," Final Report prepared for the U.S. Department of Energy, under Contract No. AC22-80PC30149, July (1981).

Hucko, E., H. B. Gala, and P. S. Jacobsen, "Status of DOE-sponsored Advanced Coal Cleaning Processes," DOE Report No. DE 89008772, March (1989).

Huggins, F. E., G. P. Huffman, and R. J. Lee, "Scanning Electron Microscopy - Based Automated Image Analysis (SEM - AIA) and Mossabauer Spectroscopy," in Coal and Coal Products: Analytical Characterization Techniques, E. L. Fuller, Ed., American Chemical Society, Washington, D.C., pp. 239-258 (1982).

Inculet, I. I., M. A., Bergougnou, R. M. Quigley, and J. D. Brown, "Fluidized Electrostatic Removal of Mineral Matter from Coals Mined at Hat Creek, British Columbia, Canada," Proceedings of 14th Annual Meeting of IEEE Industry Applications Society, Cleveland, pp. 112-116 (1979).

Inculet, I. I., Electrostatic Mineral Separation, John Wiley & Sons, New York (1984).

Institute of Gas Technology, "Coal Conversion Systems Technical Data Book," prepared for the U.S. Department of Energy by IGT under Contract No. AC-0181FE05157; available from NTIS (1982).

Iohn, P., "Fluidized Bed Heavy Medium Separation - A Modern Dry Separations Procedure," Aufbereitungs - Technik, vol. 3, p. 140 (1971).

Johnson, C. M., and H. Nishita, "Estimation of Sulfur in Plant Materials, Soils and Irrigation Water," Analytical Chemistry, vol. 24, 4, pp. 736-742 (1952).

Kindig, J. K., and R. L. Turner, "Dry Chemical Process to Magnetize Pyrite and Ash for Removal from Coal," SME-AIME Preprint No. 76-F-306 SME/AIME Meeting, Denver, (1976).

Kneller, W. A., and G. P. Maxwell, "Size, Shape and Distribution of Microscopic Pyrite in Selected Ohio Coals," in Processing and Utilization of High Sulfur Coals I, Y. Attia, Ed., Elsevier, New York, pp. 41-66 (1985).

Knoll, F. S., and D. W. Mitchell, "Electrostatic Separation," in Perry's Chemical Engineering Handbook, 6th edition, McGraw Hill, New York (1984).

Lawver, J. E., and W. P. Dyrenforth, "Electrostatic Separation" in Electrostatics and its Applications, A. D. Moore, Ed., John Wiley & Sons, New York, Chap. 10 (1973).

Levy, E. K., B. Kozanoghi, and M. D'Agostini, "Mechanical Cleaning of Coal in an Air Fluidized Bed," Proceedings of Fourth Annual Pittsburgh Coal Conference, pp. 371-386 (1987).

Lin, C. J., and Y. A. Liu, "Desulfurization of Coals by High Intensity High Gradient Magnetic Separation: Conceptual Process Design and Cost Estimation," in Coal Desulfurization - Chemical and Physical Methods, T. D. Wheelock, Ed., ACS Symposium Series, Division Of Fuel Chemistry, 121-142 (1977). Link, T. A., "TriboElectrostatic Beneficiation," Quarterly Report, Coal Preparation Division, PETC In-House Research and Development, October 1-December 31, 1987.

Link, T. A., "TriboElectrostatic Beneficiation," Quarterly Report, Coal Preparation Division, PETC In-House Research and Development, January 1-March 31, 1988.

Liu, Y. A., "High Gradient Magnetic Separation for Coal Desulfurization," in Physical Cleaning of Coal, Y. A. Liu, Ed., Marcel Dekker, Inc., New York, pp. 133-246 (1982).

Lockhart, N. C., "Dry Beneficiation of Coal," Powder Technology, vol. 40, pp. 17-42 (1984).

Lowell, J., and A. C. Rose-Innes, "Contact Electrification," Advances in Physics, vol. 29, 6, pp. 947-1023 (1980).

Luborsky, F. E., General Electric Company Report to U.S. Bureau of Mines, SRD 77-047 and 77-147 (1977).

Lytle, J. M., "Advanced Physical Fine Coal Cleaning by ISGS Aggregate Flotation," Final Technical Report Submitted to the Center for Research on Sulfur in Coal, Carterville, IL, November (1989).

Maronde, C. P., "Fine Coal Beneficiation via Heavy-Liquid Cycloning," Proceedings of International Coal Preparation Exhibition and Conference - COALPREP 88, March 22-24, Lexington, Kentucky (1988).

Masuda, H., T. Komatsu, and K. Iinoya, "The Static Electrification of particles in Gas-Solids Pipe Flow," AIChE Journal, vol. 22, 3, pp. 558-564 (1976).

Masuda, S., M. Torguchi, T. Takahasi, K. Haga, and Y. Tani, "Electrostatic Beneficiation of Coal," in Proceedings of International Symposium of Powder Technology, J. K. Beddow, Ed., pp. 789-796 (1981).

Matovich, E., "Onsite Disposal of Electrical Arc Furnace Dust Through Flash Direct Reduction," paper presented at the AIME/ISS 44th Electric Furnace Conference, Dallas, Texas, December 11, 1986.

McCabe, W. L., and J. C. Smith, Unit Operations of Chemical Engineering, McGraw Hill, New York (1976).

McCulloch, W. C., R. L. Leewellyn, K. K. Humphreys, and J. W. Leonard, in Dry Coal Preparation, J. W. Leonard and K. K. Humphreys, Ed., AIMS, New York, 3rd Edition, (1979).

Michaelson, H. B., "Electron Work Function of the Elements," in CRC Handbook of Chemistry and Physics, CRC Press, Boca Raton, FL, p. E-91 (1989).

Miller, K. J., "Laboratory Study to Determine the Effectiveness of Reverse Coal-Pyrite Flotation with High-Sulfur Ohio Coals," U.S. Department of Energy, PETC Quarterly Report, Research and Development, Coal Preparation Division, December (1987).

Miller, J. D., "The Air-Sparged Hydrocyclone for Fine Coal Flotation," prepared for presentation at the EPRI State-of-the-Art-Review: Microbubble Froth Flotation, December (1987).

Moore, A. D., Electrostatics and its Applications, John Wiley & Sons, New York (1973).

Morsi, B. I. et al., "Liquid CO_2 Coalescence of Fine Coal," Draft Final Report (October 1983-January 1988), prepared for the U.S. Department of Energy/Pittsburgh Energy Technology Center, under University of Pittsburgh Contract No. DE-AC22- 83PC6308, February (1988).

Moudgil, B. M., "Development of Reagent Coatings for Electrostatic Separation," paper presented at the PECT-DOE Workshop on Dry Coal Cleaning, March 15, 1989.

Mugeraya, S., and B. R. Prabhakar, "Charging Characteristics of Particles in Electrostatic Separators," IEEE-IAS, pp. 1315-1321, September (1985).

Mukherjee, A., Characterization and Separation of Charged Particles," Ph.D. Dissertation, Illinois Institute of Technology, Chicago, IL (1987).

Mukherjee, A., D. Gidaspow, and D. T. Wasan, "Surface Charge of Illinois Coal and Pyrites for Dry Electrostatic Cleaning," Preprints for ACS Fuel Chemistry, 1, vol. 32, pp. 395-407 (1987).

Nieh, S., and T. Nguyen, "Measurement and Control of Electrostatic Charges on Pulverized Coal in a Pneumatic Pipeline," Particulate Sci. and Technology, vol. 5, pp. 115-130 (1987).

Nieh, S., and T. Nugyen, "Effects of Humidity, Conveying Velocity and Particle Size on Electrostatic Charges on Glass Beads in a Gaseous Suspension Flow," J. of Electrostatics, vol. 21, pp. 99-114 (1988).

Olofinskii, N. F., Electric Corona Separation of Coal Fines and Certain Minerals, Moscow, 1957, Translated by Israel Program for Scientific Translations (1969).

Parekh, B. K., "A Review of Dewatering of Coal: State of the Art," in Processing and Utilization of High Sulfur Coals, Y. P. Chugh and R. D. Caudle, Ed., Elsevier, New York, 413-421 (1987).

Parkinson, G., "New Ways to Process Oil Shale," Chemical Engineering, February 22, 1982.

Perry, R. H., and D. Green, Perry's Chemical Engineering Handbook, 6th Edition, McGraw-Hill, New York (1984).

Ralston, O. C., Electrostatic Separation of Mixed Granular Solids, Elsevier Publishing Company, New York (1961).

Rapp, D. M., "Maceral Analysis of Illinois Basin Coal Samples," Private Communications, February (1987).

Rich, S. R., "Cleaning Pulverized Coal - Dust Free," Chemical Week, pp. 32-33, December 23, 1981.

Rich, S. R., "Coal Cleaning Route Gets Commercial Tryout," Chemical Engineering, February 20, 1984.

Ring, T. A., "Mineral Beneficiation of Oil Shale," University of Kentucky IMMR Report 82/066, pp. 305-309 (1982).

Riviere, J. C., "Work Function: Measurements and Results" in Solid State Surface Science, Mino Green, Ed., vol. 1, Marcel Dekker, New York, pp. 179-289 (1969).

Robinson, V.N.E., N. G. Cutmore, and R. G. Burdon, "Quantitative Composition Analysis Using the Backscattered Electron Signal in a Scanning Electron Microscope," Scanning Electron Microscopy, 1984/II, O. Johari, Ed., SEM Inc., Chicago, pp. 483-492 (1984).

Saxena, S., Desulfurization of Coal in an Electrofluidized Bed, M.S. Thesis, Illinois Institute of Technology (1985).

Secker, P. E., and J. N. Chubb, "Instrumentation for Electrostatic Measurements," J. of Electrostatics, vol. 11, pp. 1-19 (1984). Simmons, F. J., and Keller, D. V., Jr., "Sulfur and Mineral Matter Reduction in Coal Using Selective Agglomeration," Second Quarterly Technical Report (January 1-March 31, 1988), prepared for U.S. Department of Energy/Pittsburgh Energy Technology Center Under Otisca Industries, Ltd., Contract No. DE-AC22-87PC79880, March (1988).

Singewald, A, "Beneficiation of Potassium and Magnesium Mineral Salts in Electric Fields," Kaliand Steinsalt, vol. 8, p. 252 (1982).

Singh, S.P.N., and G. R. Peterson, "Survey and Evaluation of Current and Potential Coal Beneficiation Processes," Oak Ridge National Laboratory, ORNL/TM-S953 (1979).

Skoog, D. A., and D. M. West, Fundamentals of Analytical Chemistry, 3rd Edition, p. 750, Rinehart and Winston, New York (1976).

Smith, J. W., N. B. Young, and D. L. Lawlor, "Direct Determination of Sulfur Forms in Green River Oil Shale," Analytical Chemistry, vol. 36, p. 3, March (1964).

Soo, S. L., G. J. Trezek, R. C. Dimick and G. F. Hohnstreiter, "Concentration and Mass Flow Distributions in a Gas-Solid Suspension," Ind. & Eng. Chem. Fund., vol. 3, pp. 98-106 (1964).

Soo, S. L., Fluid Dynamics of Multiphase Systems, Blaisdell, Waltham (1967).

Soo, S. L., "Particle-Gas Surface Interactions in Collection Devices," Int. J. Multiphase Flow, vol. 1, pp. 89-101 (1973).

Soo, S. L., Multiphase Fluid Dynamics, S. L. Soo Associates, Urbana (1983).

Soo, S. L., Particulates and Continuum, Hemisphere, New York (1989).

Stanfield, K. E., I. C. Frost, W. S. McAuley, and H. N. Smith, U.S. Bureau of Mines Report Inv., No. 4825, 27 (1951).

Straszheim, E. E., K. A. Younkin, and R. Markuszewski, "Determination of Pyrite Association with Coal Particles by Automated Image Analysis," in Processing and Utilization of High Sulfur Coals, II, Y. P. Chugh and R. D. Caudle, Ed., Elsevier, New York, pp. 41-48 (1987).

Tsai, S. C., Fundamentals of Coal Beneficiation and Utilization, Elsevier Scientific Pub. Company, New York (1982).

Tuttle, M. L., M. B. Goldhaber, and D. L. Williamson, "An Analytical Scheme for Determining Forms of Sulfur in Oil Shales and Associated Rocks," Talanta, vol. 33, 12, pp. 953-961 (1986).

van Driest, E. R., J. of Aerosol Science, vol. 23, p. 1007 (1956).

Weschler, I., J. Doulin and R. Eddy, "Coal Preparation Using Magnetic Separation," Volume 3, Final Report prepared for EPRI by Sala Magnetics, CS-1517, July (1980).

White, H. J., Industrial Electrostatic Precipitation, Addition-Wesley Publishing Company, Reading, MA (1963).

Wilson, D. C., "Dry Table - Pyrite Removal from Coal," Preprint of papers presented at the 173rd National ACS meeting, Div of Fuel Chemistry, vol. 22 (2) p. 132, 1977.

Yamamoto, S., K. Susa, and U. Kawabe, "Work Functions of Binary Compounds," J. of Chem. Physics, vol. 60, 10, 15 May 1974.

Yang, D. C., "Reduction of Ash and Pyritic Sulfur by Static Tube Flotation of Fine Coal," Report Prepared for the EPRI/DOE Workshop on State-of-the-Art Review of Microbubble Froth Flotation, December 1987.

Yang, D. C., "Development and Demonstration of a Static Tube Flotation System for Producing Superclean Coal," Prepared for the U.S. Department of Energy under Contract No. DE-AC22-85PC87210, 11th Quarterly Technical Report, July 1988.

Yergey, A. L., F. W. Lamps and M. L. Vental, "Non-isothermal Kinetics Studies of the Hydrodesulfurization of Coal," Ind. Engg. Chem., Process Develop., vol. 13, pp. 233-240 (1974).

Yoon, R. H. et al., "The Virginia Tech Microbubble Column Flotation Technology," prepared for presentation at the EPRI State-of-the-Art Review: Microbubble Froth Flotation, December (1987).

Zenz, F. A., and D. F. Othmer, Fluidization and Fluid-Particle Systems, Reinhold Publishing Corporation, New York (1960).

52WP/61090T3-2/RPP

Subtask 3.3. Microbial Desulfurization and Denitrification

Subtask 3.3.1. Culture Development

This subtask was conducted by the Ohio State University (OSU).

Objective

The objective of Subtasks 3.3.1.1 and 3.3.1.2 was to develop cultures derived from oil shale and soil/water enrichments, respectively. The objective of Subtask 3.3.1.3 was to evaluate the ability of these cultures to desulfurize and/or denitrify oil shales.

Background

The large deposits of Devonian oil shale in the Eastern United States represent a substantial source of potential energy. Surface-mine accessible deposits are present in Alabama, Indiana, Kentucky, Michigan, Ohio, and Tennessee.[15] It has been proposed that the most efficient method of converting the organic material, kerogen, to a final synthetic liquid fuel product is pressurized fluidized-bed hydroretorting (PFH). This technique differs from other conventional retorting methods in that it operates at an elevated pressure and hydrogen is consumed in the process. Therefore, the economic feasibility of utilizing Eastern oil shale as an energy source can be enhanced by minimizing the amount of hydrogen consumed and by reducing the amount of process steps that must be accomplished under high pressure.

By reducing the amount of sulfur and nitrogen present in the feed shale, the amount of hydrogen consumed in the production of hydrogen sulfide (H_2S) and ammonia is reduced. Removal of these elements prior to retorting also reduces the requirement for pressurized removal systems associated with the PFH process. These systems would be necessary to protect the environment from release of such gases. A significant amount of the pyritic sulfur can be removed by beneficiating the raw shale. The separation and recovery of the organic portion from the inorganic material in this process requires that very small particles be suspended in water as a slurry. This feedstock would be in a form amenable to microbial processing to reduce the residual organic sulfur and nitrogen content prior to PFH. Studies have shown that a variety of microorganisms are capable of degrading several different sulfur and nitrogen containing compounds, which have been chosen as representative of the organic sulfur and nitrogen compounds found in coal.[1,5-13,16-21] Also, it has been demonstrated that microbial communities exist inside hard substrate such as sandstone, quartz and limestone.[2-4] Therefore, this research has been directed at isolating organisms from an Indiana New Albany oil (INA) shale, developing techniques to gain physical and chemical information about that substrate before and after various experimental treatments, and developing cultures capable of degrading sulfur- and nitrogen-containing compounds.

Project Description

The enrichment medium used to isolate microorganisms from handground INA shale consisted of (g/L): glucose, 5.0; $NaC_2H_3O_2$, 5.0; $NaNO_3$, 2.0; $NaSO_4$, 2.0; tryptophan, 1.0; lysine, 1.0; CaCl, 0.25; $FeCl_3$, 0.25; MgCl, 0.25; $MnCl_2$, 0.25; $NaMoO_4 \cdot 2H_2O$, 0.025, and ZnCl, 0.25. The buffer system used to prepare

this medium at pH 5, 6, 7, or 8 was comprised of 0.125 M KH_2PO_4 and 0.187 M Na_2HPO_4 in appropriate ratios. Sulfur-free (S-free) and nitrogen-free (N-free) media were prepared by excluding the $NaSO_4$ or the $NaNO_3$, tryptophan and lysine. The plating medium was either a formulation of the above with 16.7 g agar added per liter or nutrient agar. Organisms were Gram-stained and examined using standard microbiological techniques.

The National Institute of Occupational Safety and Health (NIOSH) method of asbestos fiber analyses by transmission electron microscopy (TEM) was modified to observe and measure the size of shale particles and microorganisms associated with shale and coal.[14] The particles were prepared for observation by suspending 1.5 mg shale samples in double distilled (dd) water and filtering through a Millipore type DA membrane filter (0.65 µm pore size, 25 mm diameter) in a glass Millipore vacuum filtration apparatus. Circular portions of the filters were cut out using a No. 4 cork borer and were affixed to glass microscope slides with ringbinder adhesive rings. The slides were placed on acetone-soaked Jaffee wicks in glass petri dishes for about 10 minutes or until the filters became clear. The samples were then coated with pure carbon in an Edwards E306A high vacuum evaporator. A portion (1/4) of the carbon coated filter was placed upside down onto 200 mesh copper EM grids that had previously been overlayered with collodion support film and coated with carbon. The grids were placed into an acetone distillation column bath for 2 hours to dissolve and wash away the cellulose filter. The grids were observed by TEM in a Zeiss 10 equipped with an ORTEC energy dispersive X-ray fluorescence spectrometer (EDXS).

The modified NIOSH method allows for microorganisms associated with the particles to be quantitated by direct count in the TEM, which is the accepted method for enumerating asbestos fibers in a sample. The number of cells per 10 openings in each grid were counted. The dimensions of about 100 randomly selected particles visible on the EM grid were measured using a Zeiss videoplan computer attached directly to the Zeiss EM 10, which calculated the average length, width, and area of each particle.

Particle surfaces and associated microorganisms were observed by scanning electron microscopy (Hitachi S500 SEM). Sections of microscope slides were affixed to SEM stubs with colloidal silver paint. The shale particles were suspended in dd water, a drop of which was placed onto the glass slide and allowed to air dry. These were then sputter coated with gold in a Technics Hummer III coating device.

The INA shale in all experiments was either handground with a mortar and pestle or crushed in a Spex stainless steel ball mill for about 2 minutes. The beneficiated INA oil shale was obtained from MRI through IGT. The particles were separated with respect to size by passing them through a stack of standard sieves either dry with physical agitation or rinsed with dd water. The sieves were 100, 200 and 325 mesh with pore openings of 149, 75, and 45 µm, respectively. The fractions collected were designated as +200 (-100+200), -200 (-200+325) and -325 mesh.

The elemental composition of bulk shale samples was determined using a Tracor Spectrace 4050 EDXS. The dry shale samples for these analyses were about 1.0 g and ground to uniform texture. The spectra were collected with the following low or high energy parameters (low/high): 12/45 kV tube

voltage, 0.15/0.20 mA tube current, none/No. 5 filter, 10/20 kEV maximum energy, and 100/100 seconds live time. The sulfur content of these bulk samples was also quantitated using the EDXS. This technique required sulfur standards composed of, or contained within, a matrix similar to shale. Therefore, since the sulfur content of the MH-6 shale sample obtained from MRI had already been determined by accepted analytical techniques, that quantity was used as the base value to which flowers of sulfur were added to develop standards containing 0.8 to 10.0 weight percent sulfur. The parameters for the standards and quantitative sulfur analyses were as follows: 12 kV tube voltage, 0.20 mA tube current, no filter, 10 kEV maximum energy and 50 seconds live time. Each sample was analyzed 3 times and the S contents represent an average of the 3 results.

Pretreatment experiments were conducted by collecting counts corresponding to the K(α) line energies of various elements with the EDXS at low and high energy levels for representative samples of the bulk shale before treatment. Samples of the ground shale (+200 and -200 mesh dry sieved) were placed into and shaken with 5.0, 1.0 and 0.5 M HNO_3 or NaOH; 100 mM on 100 μM EDTA; or dd water at a ratio of 1.0 g shale to 100 ml solvent for 1, 24, and 60 hours. The shale was recovered by centrifugation (10 minutes at 4500 rpm) after each time period, rinsed twice and dried overnight at 80°C. The samples were then stirred and/or gently crushed to restore the mixture to its original form, weighed and transferred to sample holders for EDXS analysis. The shale samples were all analyzed under conditions identical to those employed prior to incubation.

Various inocula were applied to pretreated ground shale samples. In all experiments, the shale was pretreated with 5.0 M HNO_3 for 4 hours and the harvested shale was rinsed until the final supernatant was at pH 3.5 to 4.0. The sulfur content was determined using the EDXS for each sample before and after pretreatment. In the first set of experiments the inoculum was prepared by placing colonies of the INA shale isolates into 20 ml sterile physiological saline, centrifuging the suspension and resuspending the resulting pellet in 15 ml sterile saline. The CFU*/ml were determined by standard dilution and spread plating techniques using plate count agar. Two flasks containing 100 ml S-free medium at each temperature and pH combination (pH 6 at 35°C; pH 7 and 8 at 25°C and 35°C) had the pretreated -100+200 or -200+325 mesh (dry-sieved) shale samples added. One each of these flasks had 1.0 ml of the inoculum added and the other was an uninoculated control. After 7 days incubation, the CFU/ml for each flask were determined, the shale was harvested by centrifugation, dried and analyzed with the EDXS. The inoculum for the next set of experiments was 1.0 ml of the supernatant from the previous experiment that contained a +200 mesh shale sample, had an inoculum added and was incubated at pH 7 and 25°C. Two test flasks and 2 control flasks for each size shale (+200 and -200 mesh dry-sieved) containing 100 ml S-free medium at pH 7 were prepared. The test and control flasks each contained a shale sample and 1.0 ml of the inoculum was added to the test flasks. All flasks were incubated for 18 days at 25°C on a rotary shaker.

The shale was recovered by filtration (Whatman No. 4), dried overnight at 80°C and analyzed with the EDXS. In the next experiments, the S-free medium

* CFU = colony-forming units.

without sodium acetate was amended with either glucose or glycerol (0.5 weight percent) or had no carbon source added. Two test flasks and 2 control flasks containing 1.5 g pretreated -325 mesh (wet-sieved) shale and 100 ml nutritionally amended S-free media (pH 7.0) were prepared. The inoculum added to the test flasks was from the same source and prepared in the same manner as that described for the previous experiment. The flasks were incubated at 25°C for 18 days on a rotary shaker. The shale was recovered by filtration (Whatman 0.45 µm pore opening, cellulose nitrate), dried overnight at 80°C and analyzed in the EDXS. For the next experiment, a second mixed starter culture was developed as previously described for the initial inoculum. A 1.0-ml aliquot of the inoculum was added to each of 5 flasks containing 100 ml sterile S-free medium (ph 7.0) amended with glycerol. Each of 2 of these flasks had a 1.0 g wet-sieved +200 or -325 mesh shale sample added to it. The fifth inoculated flask had a 1.0 g sample of -200 mesh pretreated wet-sieved shale. Three flasks, each containing the same medium as the test flasks and either a 1.0 g sample of +200, -200, or -325 mesh pretreated wet-sieved shale were not inoculated. After 20 days incubation at 25°C on a rotary shaker, plate counts were done and the shale was recovered by filtration as described above, dried overnight at 70°C and analyzed in the EDXS under the same parameters as run prior to pretreatment and incubation.

Sample preparation and spectrophotometric protocols for experiments pertaining to pyridine utilization were developed. One milliliter of culture medium was taken from each flask and microfuged for 1.5 minutes. Two 0.32-ml aliquots of the samples taken from flasks containing 0.0 to 0.1 weight percent pyridine were each diluted with 3.0 ml dd deionized water. Samples taken from flasks containing 0.4 weight percent pyridine had two 0.16-ml aliquots each diluted in 6.0 ml of dd deionized water. These diluted samples were transferred to a cuvette and analyzed in a Varion 2200 UV-visible spectrophotometer from 340 to 220 nm against a dd deionized water blank.

In the first set of experiments the medium contained $NaSO_4$ (1.0 g) and yeast extract (YE, 0.6 g) per 1200 ml of pH 7.0 buffer with 120 ml trace metal solution added. The inocula were 0.5 ml washed cell suspensions taken from a mixture of shale isolates and isolate No. 6, which had been incubated in a similar medium containing 0.1 weight percent pyridine for 25 days. A third inoculum was a 0.5 ml aliquot of raw sewage. Two test flasks per inoculum supplemented with 0.1 weight percent filter sterilized pyridine were prepared. Two uninoculated control flasks without added pyridine were included. These flasks were incubated at room temperature on a rotary shaker and sampled at various time intervals.

The second set of pyridine experiments was designed to investigate the mixed culture inoculum that arose from the flasks inoculated with raw sewage in the previous experiment. Ten 250-ml flasks containing 100 ml pH 7.0 buffer and 0.08 g $NaSO_4$ were prepared. Five flasks were amended with YE to a final concentration of 50 mg YE/100 ml and the second set of 5 flasks to a final concentration of 15 mg YE/100 ml. Three of the flasks containing 50 mg YE and 2 containing 15 mg YE had 0.4 ml filter-sterilized pyridine added. The remaining 5 flasks (2 containing 50 mg YE and 3 containing 15 mg YE) had 0.1 ml filter-sterilized pyridine added. A flask containing 0.1 weight percent pyridine (15 mg YE/100 ml) and another containing 0.4% pyridine (50 mg YE/100 ml) were not inoculated and served as the control flasks. The remaining 8 flasks had 1.0 ml of inoculum added to each. All flasks were incubated

at room temperature on a rotary shaker. The inoculum was prepared by aseptically removing 10 ml of culture medium from the Sewage A flask of the previous experiment. This was centrifuged and the supernatant decanted. The cell pellet was resuspended in 10 ml sterile water, spun and the supernatant decanted. The pellet was rinsed a second time and finally resuspended in 10 ml of N-free medium. The inoculum was determined to contain 1.4×10^7 CFU/ml. The amount of pyridine present in the control and test flasks was determined initially and was monitored throughout the experiment.

Results

A list of the Gram reactions and morphologies of microorganisms isolated from INA shale is given in Table 3-30. The most prevalent types of microorganisms were Gram-positive cocci. The weight distillation of the +200, -200 and -325 mesh fractions collected after dry- and wet-sieving handground or wet-sieving beneficiated INA shale is presented in Table 3-31. More than 70% of the handground shale was retained by the 200 and 325 mesh sieves when dry. However, more than 70% of the handground and about 90% of the beneficiated shale was washed through the -325 mesh sieve with water. Figure 3-83 contains SEM photographs of the 3 different sized fractions collected by wet-sieving. Figure 3-84 contains TEM photographs of shale particles with the microorganisms associated with those materials visible. The numbers of microorganisms in samples of wet-sieved shale determined by direct count in the TEM, are presented in Table 3-32. The INA shale samples were determined to contain 4.0×10^{10} cells per gram, calculated as follows:

$$\text{No. of Cells/g Particles} = \frac{\text{Ave. No. Cells}}{\text{1 Grid Opening}} \times \frac{\text{1 Grid Opening}}{\text{Area of Grid Opening}}$$

$$\times \frac{\text{Area of Filter}}{\text{1 Filter}} \times \frac{\text{3 Filters}}{\text{Total Grams Particles}}$$

where the area of 1 grid opening was 0.005 mm^2, the area of 1 filter was 201 mm^2 and the total grams of particles applied to the filters were 0.0015 g. Listed in Table 3-33 are the average length, width, and area of particles in wet-sieved fractions of ground INA shale determined using TEM. The average area of a particle in wet-sieved samples determined to be +200, -200, or -325 mesh was 1.38, 0.532, or 0.265 mm^2, respectively. The average sulfur content in dry- and wet-sieved handground or wet-sieved beneficiated INA shale is presented in Table 3-34. The fraction of handground shale that would not pass through the 200 mesh sieve when dry contained 3.64% sulfur, whereas the fraction that was retained by this sieve when washed through contained only 3.30% sulfur. The smallest sized particles collected by dry- and wet-sieving handground shale contained very similar amounts of sulfur, 3.82% and 3.87%, respectively. The +200 mesh wet-sieved beneficiated samples contained 2.99% sulfur and the -325 mesh beneficiated samples contained 3.36% sulfur.

Listed in Table 3-35 is the reduction of several elements in ground (dry-sieved) INA shale after various chemical pretreatments for 60 hours. The decrease in the sulfur content was calculated as follows.

$$\text{Decrease, \%} = \frac{(\text{Avg. S\% or Avg. No. of Counts})_{\text{initial}} - (\text{Avg. S\% or Avg. No. of Counts})_{\text{final}}}{(\text{Avg. S\% or Avg. No. of Counts})_{\text{initial}}} \times 100$$

Table 3-30. GRAM STAIN REACTION AND MORPHOLOGIES FOR 16 MICROORGANISMS ISOLATED FROM INDIANA NEW ALBANY SHALE

Isolate	Gram Reaction	Morphology
1	+	Cocci in clusters
2	+	Tiny cocci, pairs, short chains, clusters
3	-	Small coccobacilli, pairs, short chains, clusters
4	-	Rods, chains
5	-	Rods, long chains with sheaths
6	+	Tiny cocci, pairs, chains, clusters
7	+	Cocci, pairs, short chains
8	+	Cocci/oval, pairs, short chains
9	-	Coccobacilli, short chains
10	+	Cocci, short chains (flattened at junctions)
11	+	Rods with spores
12	+	Cocci, pairs, tetrads
13	+	Coccobacilli, pairs, tetrads, clusters
14	-	Rods (curved)
15	-	Short rods, pairs
16	+	Coccoid, "coryneform"-like

Table 3-31. AVERAGE PERCENTAGE OF +200, -200, AND -325 MESH FRACTIONS COLLECTED AFTER DRY- AND WET-SIEVING HANDGROUND OR WET-SIEVING BENEFICIATED INDIANA NEW ALBANY OIL SHALE

Oil Shale	+200	-200	-325
	----- wt % of total -----		
HANDGROUND			
Dry-sieved	40.0	31.4	26.1
Wet-sieved	19.3	7.7	73.0
BENEFICIATED			
Wet-sieved	9.9	2.5	87.2

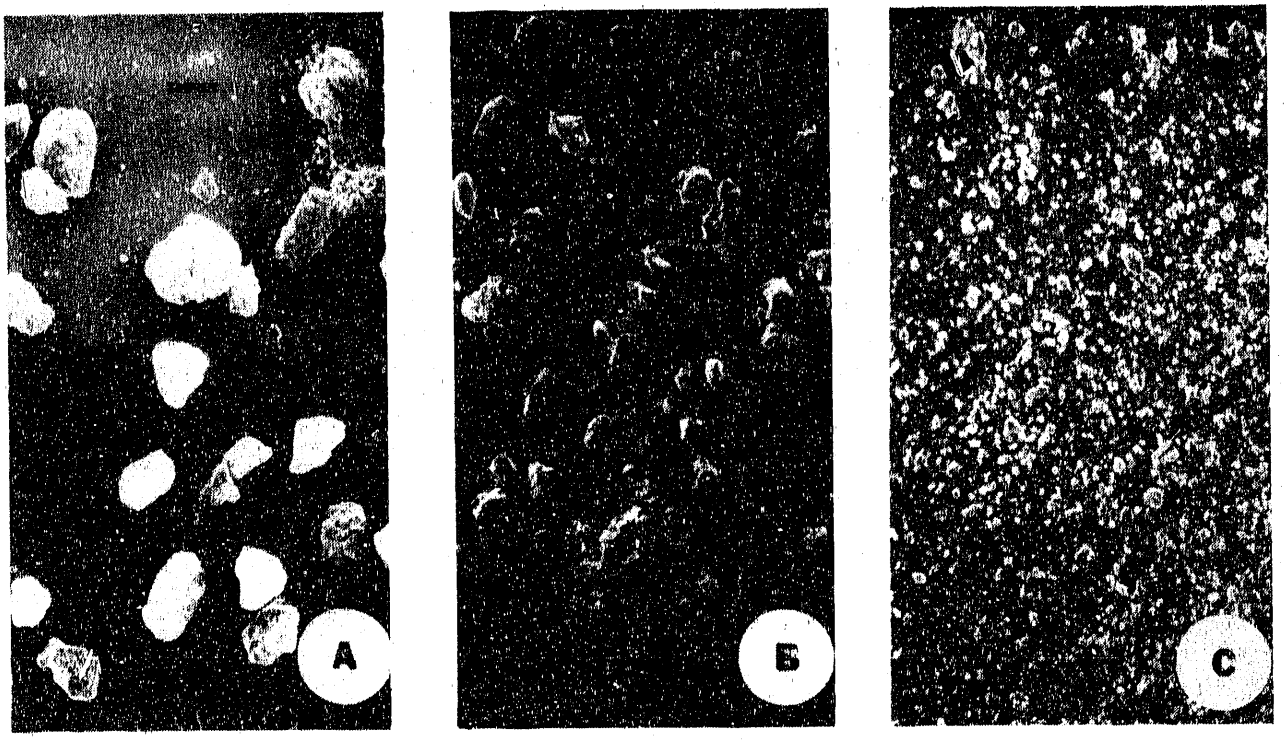

Figure 3-83. SCANNING ELECTRON MICROGRAPHS OF SHALE PARTICLES DETERMINED BY WET-SIEVING TO BE: (A) -100+200; (B) -200+325; AND (C) -325 MESH (x 65, Size Bar = 100 μm)

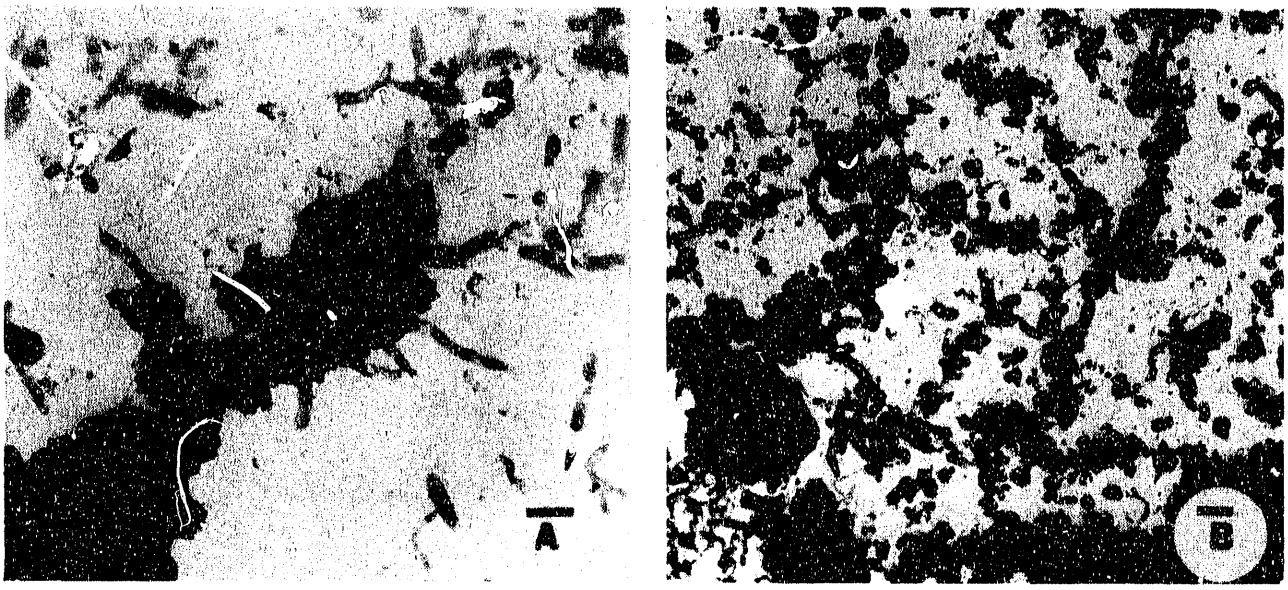

Figure 3-84. TRANSMISSION ELECTRON MICROGRAPHS SHOWING VARIOUS MICROORGANISMS ASSOCIATED WITH FRESHLY GROUND INDIANA NEW ALBANY OIL SHALE. (A) x 3150, Size Bar = 2 μm; and (B) x 2500, Size Bar = 2 μm

Table 3-32. ENUMERATION OF MICROORGANISMS FOUND IN WET-SIEVED INDIANA NEW ALBANY OIL SHALE BY DIRECT COUNTING IN A TRANSMISSION ELECTRON MICROSCOPE

Control	Average Cells/Grid Opening	Std. Dev.	No. Cells/g
1	0.9	0.99	
2	1.5	1.43	
	$Average_{20}$ = 1.2	1.24	
SHALE			
+200	513.9	61.0	
-200	519.3	103.1	
-325	469.1	90.9	
	$Average_{30}$ = 500.8	86.8	4.0×10^{10}

Table 3-33. THE AVERAGE LENGTH, WIDTH, AND AREA OF PARTICLES IN WET-SIEVED FRACTIONS OF GROUND INDIANA NEW ALBANY SHALE DETERMINED USING TRANSMISSION ELECTRON MICROSCOPY

Mesh Size	Average Length, μm	Average Width, μm	Average Area, mm^2
+200 (101)[a]	21.1 (15.2)[b]	22.5 (14.0)	1.38 (2.30)
-200 (115)	11.9 (10.4)	12.3 (10.2)	0.532 (1.64)
-325 (106)	9.0 (7.6)	9.0 (7.4)	0.265 (0.566)

[a] Number of particles sized.

[b] Standard deviation.

Table 3-34. AVERAGE SULFUR CONTENT IN THE +200, -200, AND -325 MESH FRACTIONS COLLECTED AFTER DRY- AND WET-SIEVING HANDGROUND OR WET-SIEVING BENEFICIATED INDIANA NEW ALBANY SHALE

	Average % S	Standard Deviation
	Sulfur Content, wt %	
HANDGROUND		
Dry-sieved		
+200	3.64	0.051
-200	3.82	0.147
Wet-sieved		
+200	3.30	0.065
-200	3.15	0.098
-325	0.87	0.070
BENEFICIATED		
Wet-sieved		
+200	2.99	0.025
-325	3.35	0.019

Table 3-35. EFFECT OF CHEMICAL PRETREATMENT ON SELECTED ELEMENTS IN DRY-SIEVED HANDGROUND INDIANA NEW ALBANY OIL SHALE

Treatment*	Mesh Size	% Decrease							
		Si	S	K	Ca	Mn	Fe	Zn	As
5.0 M HNO_3	+200	9.37	3.8	1.9	83.8	29.5	75.0	87.0	67.6
	-200	5.5	69.9	0.0	80.6	23.1	73.0	78.7	63.4
5.0 N NaOH	+200	16.6	66.0	5.8	9.0	0.0	0.0	35.8	65.4
	-200	26.9	58.1	9.0	0.0	0.0	0.0	**	**
dd H_2O	+200	18.6	18.9	8.2	25.5	0.0	0.0	14.9	0.0
	-200	10.0	13.9	6.5	27.7	0.0	0.0	10.8	0.0
100 mM EDTA	+200	13.0	8.3	8.8	82.6	18.9	8.4	21.3	29.8

* 60 hours.

** Data not available.

The 5.0 M HNO_3 treatment for 60 hours removed 70% to 75% sulfur and iron and 80% to 84% calcium. Whereas, the 5.0 N NaOH treatment for the same length of time removed 58% to 66% sulfur, but apparently no iron and only 16% to 27% calcium. The dd water and EDTA treatments remove much lower amounts of these elements. After 1 hour of treatment with 5.0 M HNO_3 (data not shown), 67% to 72% sulfur, 70% to 73% iron and 81% to 84% calcium were removed. However, after 1 hour of treatment with 5.0 N NaOH (data not shown), only 15% to 20% sulfur, negligible amounts of iron and 16% to 20% calcium were removed.

Figure 3-85 represents spectra collected with the EDXS from a sample of dry-sieved -200 mesh shale before and after the 60-hour treatment with 5.0 M HNO_3. In addition to the elements listed in Table 3-35 and labelled in Figure 3-85 (Si, S, K, Ca, Mn, Fe, Zn, As), the following elements have been determined by these analyses to be present: Ti, V, Ni, Cu, Sr, Y and Mo. The results from the experiments in which a mixed inoculum of shale isolates was incubated with 5.0 M HNO_3 pretreated shale (+200 and -200 dry-sieved) are presented in Table 3-36. The pretreatment resulted in a 56.4% and 57.3% decrease in the sulfur content of the +200 and -200 mesh shale samples, respectively. The largest further reduction in sulfur was 9.5%, which occurred in the +200 mesh sample in the pH 7.0 inoculated flask incubated at 25°C. Further sulfur reductions of 7.4% and 7.9% sulfur were observed in the -200 mesh samples incubated after inoculum was added at 25°C in pH 7 and 8, respectively.

The results from the experiment in which an inoculum derived from the initial mixed cultures experiment are presented in Table 3-37. The +200 and -200 mesh dry-sieved samples were pretreated in 5.0 M HNO_3 resulting in 55.2% and 56.7% reduction in sulfur content. The average percent decrease for the +200 mesh controls and test samples was 4.46% (± 1.55) and 7.06% (± 0.156), respectively. The -200 mesh controls showed a 5.44% (± 1.15) average decrease and the test samples a 12.6% (± 2.26) average decrease.

The results from the nutrient amendment experiments are presented in Table 3-38. The pretreatment of the -325 mesh wet-sieved shale with 5.0 M HNO_3 resulted in a 54.9% reduction in sulfur content. After 18 days of incubation, the sulfur content in the shale from the test flasks amended with glucose or glycerol decreased by 8.51% and 6.71% or 9.10% and 5.11%, respectively. However, the decrease in the sulfur content of the shale from the control flasks was only 3.33% and 1.21% or 1.99% and 1.92%, respectively. There appeared to be no significant decrease in the average sulfur content of the shale from the test flasks without an added carbon source as compared to the shale from those control flasks.

The results of the experiment in which mixed culture inoculum developed from the original INA shale isolates are listed in Table 3-39. The decrease in sulfur content of the +200, -200 and -325 mesh wet-sieved samples as a result of pretreatment was 50.4%, 50.5%, and 56.3%, respectively.

After 20 days of incubation the shale from the inoculated flasks showed the following decreases in sulfur content: +200, 5.96% and 2.80%; -200, 8.73%; -325, 6.50% and 6.00%. The uninoculated controls for the 3 size fractions showed less than 1% reduction in sulfur. Figure 3-86 (SEM photograph) shows shale particles coated with microorganisms following incubation with a mixed culture inoculum.

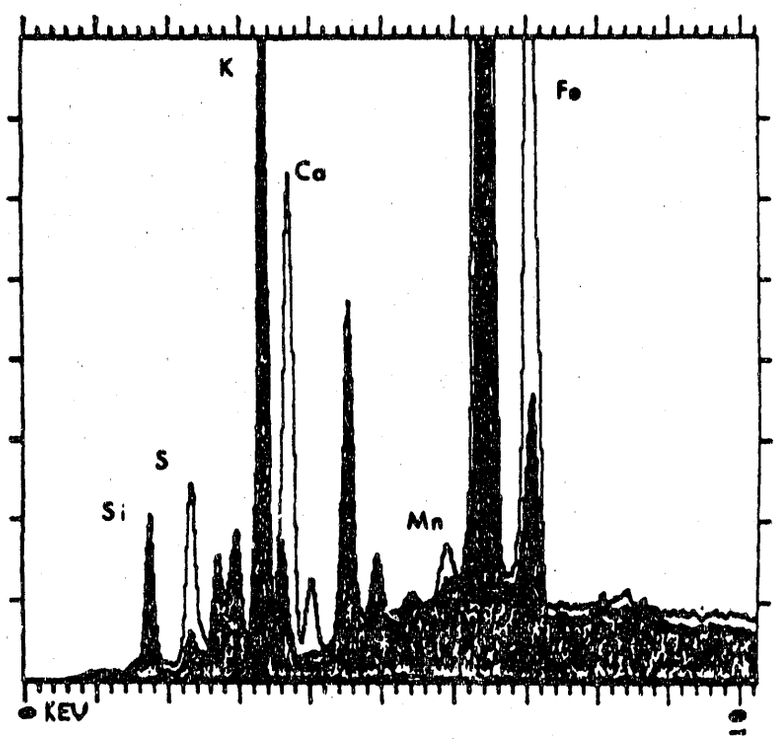

Figure 3-85. TWO SPECTPA OBTAINED USING AN ENERGY DISPERSIVE X-RAY FLUORESCENCE SPECTROMETER TO ANALYZE A SAMPLE OF -200 MESH, DRY-SIEVED INDIANA NEW ALBANY OIL SHALE BEFORE (Unshaded Spectrum) AND AFTER (Shaded Spectrum) PRETREATMENT FOR 60 HOURS WITH 5.0 M HNO_3

Table 3-36. THE PERCENT CHANGE IN THE SULFUR CONTENT OF +200 AND -200 MESH (Dry-Sieved) INDIANA NEW ALBANY SHALE BEFORE AND AFTER INCUBATIONS WITH A MIXED CULTURE INOCULUM

	Sample		% Change in Sulfur Content	
	pH	Temperature, °C	+200 Mesh	-200 Mesh
TEST	6	35	-3.71*	+3.84*
	7	25	-9.45	-7.35
	7	35	+1.41	-2.88
	8	25	-2.41	-7.94
	8	35	-5.90	-2.44
CONTROl	6	35	+0.57	-3.17
	7	25	-2.96	-6.07
	7	35	-0.56	+0.51
	8	25	+0.88	-5.42
	8	35	-0.19	-4.21

* "-" Indicates an apparent decrease in sulfur.
"+" indicates an apparent increase in sulfur.

Table 3-37. THE AVERAGE PERCENT SULFUR CONCENTRATION OF +200 AND -200 MESH (Dry-Sieved) INDIANA NEW ALBANY SHALE SAMPLES DETERMINED IN AN EDXS BEFORE AND AFTER INCUBATION WITH A MIXED CULTURE INOCULUM (S-Free Medium was pH 7 and the Incubation Temperature was 25°C)

	Initial		Final			
	Average % S	Std. Dev.	Average % S	Std. Dev.	CFU/ml	% Decrease
TEST						
+200	1.60	0.03	1.49	0.03	1.9×10^{11}	6.95
	1.63	0.01	1.51	0.06	2.1×10^{10}	7.17
-200	1.68	0.04	1.50	0.08	1.2×10^{11}	11.0
	1.71	0.01	1.47	0.04	3.5×10^{11}	14.2
CONTROL						
+200	1.62	0.02	1.53	0.06	$<10^5$	5.55
	1.64	0.03	1.58	0.04	7.7×10^9	3.36
-200	1.70	0.05	1.59	0.08	2.7×10^6	6.25
	1.69	0.04	1.61	0.07	4.2×10^7	4.62

Table 3-38. THE PERCENT SULFUR IN -325 MESH (Wet-Sieved) PRETREATED INDIANA NEW ALBANY SHALE SAMPLES BEFORE AND AFTER 18-DAY INCUBATION WITH A MIXED CULTURE INOCULUM IN S-FREE MEDIUM (pH 7) ALTERED WITH RESPECT TO CARBON SOURCE

	Before		After			
Amendment	Average % S	Std. Dev.	Average % S	Std. Dev.	CFU/ml	% Decrease
TEST						
Glucose	1.57	0.023	1.44	0.016	2.6×10^{11}	8.51
	1.58	0.024	1.47	0.016	2.1×10^{10}	6.71
Glycerol	1.57	0.028	1.43	0.034	1.2×10^{10}	9.10
	1.57	0.023	1.49	0.016	3.4×10^{11}	5.11
None	1.57	0.025	1.48	0.026	3.8×10^{8}	5.93
	1.56	0.016	1.49	0.028	3.6×10^{8}	4.12
CONTROL						
Glucose	1.59	0.027	1.54	0.027	2.0×10^{3}	3.33
	1.56	0.011	1.55	0.029	1.0×10^{3}	1.21
Glycerol	1.56	0.028	1.53	0.004	$<10^{3}$	1.99
	1.57	0.018	1.54	0.019	$<10^{3}$	1.92
None	1.56	0.017	1.52	0.016	1.1×10^{4}	2.31
	1.59	0.016	1.52	0.033	2.6×10^{5}	4.6

The sample preparation and spectrophotometric protocols developed resulted in detection of peaks at 244, 250, 256 (maximum) and 262 nm for samples containing pyridine. No peaks in this region were seen when samples of the identically inoculated medium without pyridine added were analyzed.

The results from the pyridine utilization experiment involving several inocula are presented in Table 3-40. It appears that between 4 and 15 days of incubation the pyridine was completely degraded by the mixed culture which arose from the raw sewage inoculum (Figure 3-87). The decrease from the initial absorbance at 256 nm after 16 days incubation for the rest of the flasks are as follows: Control A and B, 13% and 18% respectively; Mix A and B, 16% and 21% respectively; and isolate No. 6 A and B, 12% and 14% respectively. Plate counts performed at 17 days indicated that all test flasks contained between 10^7 and 10^8 CFU/ml and the control flasks were contaminated, containing greater than 10^4 CFU/ml.

The results from the experiments in which an inoculum derived from the Sewage A flask of the previous experiment was exposed to different concentrations of pyridine in media containing either 15 of 50 mg YE/100 ml are presented in Table 3-41. The inoculum completely degraded the 0.1 weight

Table 3-39. THE AVERAGE PERCENT SULFUR CONCENTRATION OF PRETREATED WET-SIEVED INDIANA NEW ALBANY SHALE SAMPLES DETERMINED IN AN EDXS BEFORE AND AFTER INCUBATION WITH A MIXED CULTURE INOCULUM (S-Free Medium Amended With Glycerol was at pH 7.0 and the Incubation Temperature was 25°C)

	Initial		Final			
	Average % S	Std. Dev.	Average % S	Std. Dev.	CFU/ml	% Decrease
TESTS						
+200	1.66	0.037	1.56	0.010	1.4×10^{11}	5.96
	1.64	0.035	1.60	0.017	3.6×10^{10}	2.80
-200	1.62	0.045	1.48	0.023	4.0×10^{9}	8.73
-325	1.69	0.046	1.58	0.005	5.0×10^{10}	6.50
	1.65	0.014	1.55	0.012	3.7×10^{10}	6.00
CONTROLS						
+200	1.64	0.026	1.62	0.0365	5.0×10^{5}	0.86
-200	1.63	0.024	1.61	0.008	$<10^{5}$	0.74
-325	1.67	0.024	1.69	0.030	6.7×10^{6}	0.96

percent pyridine present in both flasks containing 50 mg YE/100 ml between 3 and 5 days. In the same period of time, the 0.1 weight percent pyridine in 1 of the flasks containing 15 mg YE/100 ml was completely degraded. However, the pyridine in the other flask at this YE concentration appeared to have decreased by only 7.2% after 5 days. The inoculum did not appear to successfully degrade pyridine within this time period to levels much above controls.

Discussion

A large number and variety of microorganisms are present in the INA shale samples examined. Although a significant number have been isolated from the shale in the OSU enrichment protocols, it is likely that there are organisms present that may not be viable or are viable but not culturable by methods used by OSU. The TEM technique developed to enumerate microorganisms by direct count has provided data to support this observation. The shale samples were determined to have about 10^{10} cell/g present, however, when aliquots of the sterile water used to wet-sieve the samples were spread plated, only 10^{6} cell/g were observed.

About 40% of the shale particles that were unable to pass through the -325 mesh screen when dry were able to be washed through with water. This suggests that smaller particles remain associated with one another or with larger particles when handled dry, but become dissociated when suspended in water. The beneficiated material that was prepared by a process involving

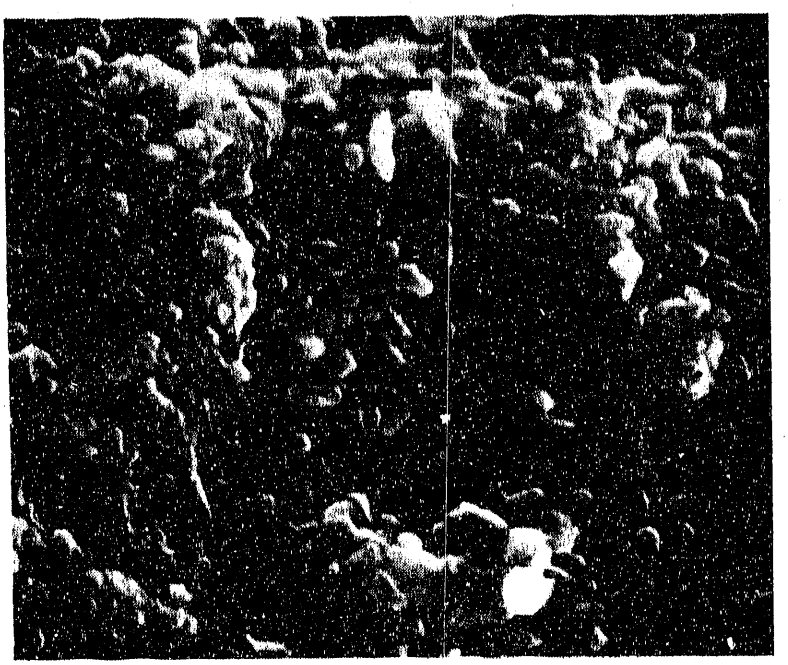

Figure 3-86. SCANNING ELECTRON MICROGRAPH OF PRETREATED SHALE PARTICLES COATED WITH MICROORGANISMS FOLLOWING INCUBATION WITH A MIXED CULTURE INOCULUM (x 6000, Size Bar = 2 μm)

Table 3-40. THE AVERAGE ABSORBANCE OF SAMPLES CONTAINING PYRIDINE COLLECTED FROM UNINOCULATED FLASKS (Control A and B) AND FLASKS INOCULATED WITH A MIXTURE OF OIL SHALE ISOLATES (Mix A and B), ISOLATE No. 6 (Micro A and B), AND AN ALIQUOT OF RAW SEWAGE (Sewage A and B) AFTER 0, 2, 3, 4, 15, AND 16 DAYS INCUBATION

		Average Absorbance (256 nm)					
		0[a]	2	3	4	15	16
Control	A	3.14 (0.04)[b]	3.01 (0.00)	3.02 (0.01)	2.99 (0.04)	2.67 (0.03)	2.72 (0.00)
	B	3.13 (0.02)	3.10 (0.02)	3.04 (0.04)	3.05 (0.03)	2.92 (0.02)	2.88 (0.04)
Mix	A	3.10 (0.00)	3.02 (0.03)	3.00 (0.04)	2.98 (0.04)	2.64 (0.02)	2.61 (0.03)
	B	3.12 (0.01)	2.88 (0.19)	2.98 (0.01)	2.96 (0.03)	2.54 (0.02)	2.46 (0.04)
Isolate #6	A	3.12 (0.00)	3.00 (0.03)	ND	2.95 (0.03)	2.86 (0.03)	2.75 (0.00)
	B	3.05 (0.02)	2.95 (0.03)	ND	2.89 (0.03)	2.62 (0.03)	2.61 (0.04)
Sewage	A	3.12 (0.01)	2.92 (0.00)	2.94 (0.04)	2.92 (0.04)	0.11 (0.00)	0.11 (0.00)
	B	ND	2.96 (0.01)	2.95 (0.01)	2.92 (0.02)	0.11 (0.00)	0.11 (0.00)

[a] Number of days after inoculation.

[b] Standard deviation.

ND = not determined.

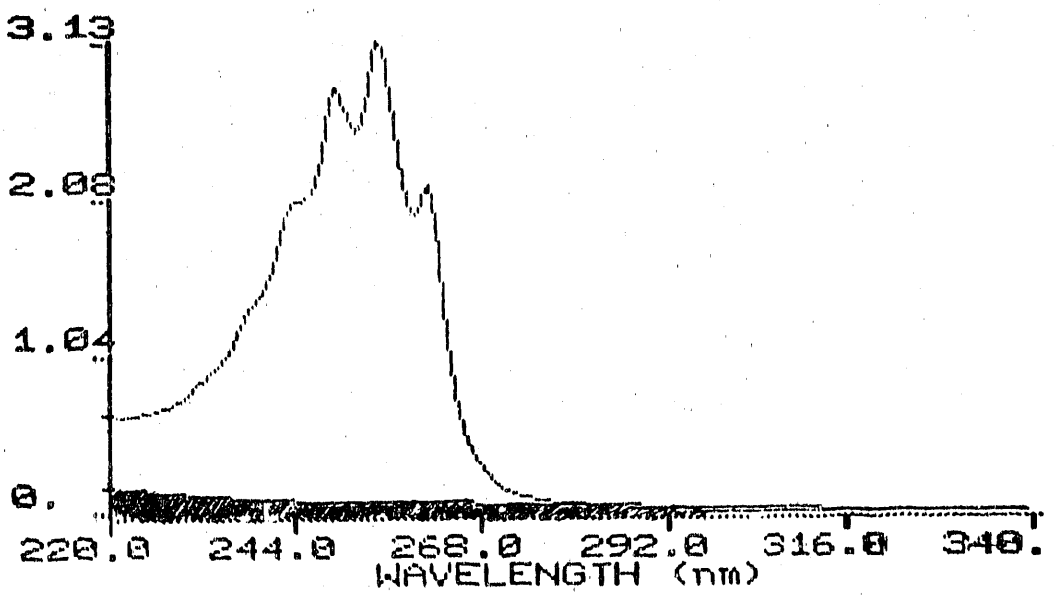

Figure 3-87. SPECTRA COLLECTED OF SAMPLES FROM THE SEWAGE A FLASK INITIALLY (Unshaded) AND AFTER 17 DAYS OF INCUBATION (Shaded)

Table 3-41. THE AVERAGE ABSORBANCE OF SAMPLES CONTAINING PYRIDINE COLLECTED FROM UNINOCULATED FLASKS (Control A and B) AND FLASKS INOCULATED WITH A MIXED CULTURE DEVELOPED FROM RAW SEWAGE AFTER 0, 3, 5, AND 7 DAYS INCUBATION (The Medium Contained Either 15 or 50 mg YE/100 ml and Either 0.1 or 0.4 wt % Pyridine)

Sample	YE (mg/100 ml)	Pyridine (% w/v)	Average Absorbance (256 mm)			
			0[a]	3	5	7
Control	15	0.1	3.18 (0.04)[b]	3.13 (0.00)	3.08 (0.01)	3.02 (0.01)
Control	50	0.4	3.44 (0.06)	3.48 (0.04)	3.36 (0.08)	3.36 (0.04)
A	50	0.1	3.26 (0.01)	3.12 (0.04)	0.08 (0.01)	0.08 (0.00)
B	50	0.1	3.34 (0.04)	3.11 (0.01)	0.11 (0.04)	0.11 (0.00)
C	50	0.4	3.50 (0.06)	3.31 (0.01)	3.15 (0.08)	3.28 (0.03)
D	50	0.4	3.39 (0.01)	3.38 (0.18)	3.24 (0.05)	3.08 (0.05)
A	15	0.1	3.28 (0.02)	3.11 (0.01)	3.05 (0.01)	2.94 (0.02)
B	15	0.1	3.24 (0.02)	3.01 (0.03)	0.05 (0.00)	0.05 (0.00)
C	15	0.4	3.27 (0.04)	3.26 (0.02)	3.39 (0.01)	3.08 (0.12)
D	15	0.4	3.40 (0.00)	3.16 (0.02)	3.04 (0.03)	3.02 (0.04)

[a] Number of days after inoculation.

[b] Standard deviation.

suspension in water appeared to be comprised mainly of particles smaller than -325 mesh. The TEM technique for particle analysis also provided information concerning the actual size of the particles in the wet-sieved samples. The areas of the +200, -200, and -325 mesh particles were calculated to be 1.38, 0.532, and 0.265 mm^2, respectively. The relatively large standard deviations associated with these areas are due to the random selection of more than 100 particles to measure, in which a few uncharacteristically small and/or large particles were included. If only the size ranges that included the majority (85%) of the particles, thereby excluding some of the infrequently measured sizes the area of the particles in each of the fractions were 0.012 to 3.05, 0.001 to 1.67, or 0.01 to 0.40 mm^2 (data not shown). In each case, a portion of the remaining 15% was an entire order of magnitude larger and their exclusion would greatly decrease the standard deviations associated with the size ranges reported.

The EDXS technique is an effective method to quantify the sulfur content of bulk shale samples as well as to identify and evaluate changes in a wide range of other elements that may also be of interest. It appears that the samples comprised of the smallest particles consistently contain the highest sulfur contents and that fraction of the beneficiated shale contains about 10 to 15% less sulfur than the handground shale.

Pretreatment of shale with 5.0 M HNO_3 resulted in greater than 50% reduction in sulfur content within the first hour. Treatment with 5.0 N NaOH required 60 hours of contact to remove about the same amount of sulfur. Since the iron content was also decreased by about the same amount as the sulfur when treated with 5.0 M HNO_3, this treatment is presumably removing the pyrite present and the sulfur that remains is likely to be of an organic nature.

The mixed culture experiments indicate that the consortium derived from INA shale can further reduce the amount of sulfur present in pretreated, handground shale. Under growth conditions tested at OSU, it appears that the highest reductions in sulfur occur at pH 7.0 and 25°C. The results also indicate that reduction in sulfur by this inoculum requires that the medium be supplemented with a carbon source and that no significant difference in sulfur removal is seen when either glucose or glycerol is added. As seen by SEM, microorganisms after inoculation and incubation coat the particle surfaces. SEM has also been used to demonstrate that cells are present on the surfaces of freshly ground particles (micrographs not shown). Also, since uninoculated pretreated controls in these experiments result in 10^5 to 10^7 CFU/ml and uninoculated pretreated controls with essentially no nutrients supplied supported 10^4 to 10^5 CFU/ml, it appears that native shale contains, protects, and supplies the necessary nutrients for a community of microorganisms.

A mixed culture inoculum derived from raw sewage has been developed that degrades 0.1 weight percent pyridine in less than 5 days. Twelve different microorganisms have been isolated from this mixture.

References Cited

1. Fedorak, P. M. and D.W.S. Westlake. "Microbial Degradation of Organic Sulfur Compounds in Prudhoe Bay Crude Oil." Can. J. Microbiol., 29, pp. 291-296, 1983.

2. Fliermans, C. B. and D. L. Balkwill. "Microbial Life in Deep Terrestrial Subsurfaces." Bioscience, 36, pp. 370-377, 1989.

3. Friedman, E. I. "Endolithic Microorganisms in the Antarctic Cold Desert." Science, 215, pp. 1045-1053, 1982.

4. Golubic, S., I. Friedman, and J. Schneider. "The Lithobiontic Ecological Niche, With Special Reference to Microorganisms." J. Sed. Petrol., 51, pp. 475-478, 1981.

5. Houghton, C. and R. B. Cain. Microbial Metabolism of the Pyridine Ring. J. Biochem., 130, pp. 879-893, 1972.

6. Kargi, F. "Biological Oxidation of Thianthrene, Thioxanthene and Dibenzothiophene by the Thermophilic Organism Sulfolobus acidocaldarius." Biotechnol. Lett., 9, pp. 478-482, 1987.

7. Kodama, K. "Induction of Dibenzothiophene Oxidation by Pseudomonas jianii." Agric. Biol. Chem., 41, pp. 1193-1196, 1977.

8. Kodama, K., K. Umehara, K. Shimizu, S. Nakatani, Y. Minoda and K. Yamada. "Identification of Microbial Products From Dibenzothiophene and its Proposed Oxidation Pathway." Agric. Biol. Chem., 37, pp. 45-50, 1973.

9. Kodama, K., S. Nakatani, K. Umehara, K. Shimizu, Y. Minoda and K. Yamada. "Microbial Conversion of Petro-Sulfur Compounds. Part III. Isolation and Identification of Products From Dibenzothiophene." Agric. Biol. Chem., 34, pp. 1320-1324, 1970.

10. Laborde, A. L. and D. T. Gibson. "Metabolism of Dibenzothiophene by a Beijerinckia Species." Appl. Environ. Microbiol., 34, pp. 783-790, 1977.

11. Monticello, D. J., D. Bakker and W. R. Finnerty. "Plasmid-mediated Degradation of Dibenzothiophene by Pseudomonas Species." Appl. Environ. Microbiol., 49, pp. 756-760, 1985.

12. Mormile, M. R. and R. M. Atlas. "Mineralization of the Dibenzothiophene Biodegradation Products 3-hydroxyl-2-formyl Benzothiophene and Dibenzo-Thiophene Sulfone." Appl. Environ. Microbiol., 54, pp. 3183-3184, 1988.

13. Nakatani, S., T. Akasaki, K. Kodama, Y. Minoda and K. Yamada. "Microbial Conversion of Petro-Sulfur Compounds. Part II. Culture Conditions of Dibenzothiophene-Utilizing bacteria." Agric. Biol. Chem., 32, pp. 1205-1211, 1968.

14. "Physical and Chemical Analysis Method 239," Natl. Inst. Occup. Safety and Health, USPH/NIOSH "Membrane Filter Method for Evaluating Airborne Asbestos Fibers," U.S. Dept. Health, Education, and Welfare, 1979.

15. Rajaram, V. "Commercialization of Eastern United States Oil Shales -- a Review." Mining Eng., 37, pp. 1381-1385, 1985.

16. Shukula, O. P. "Microbial Transformation of Pyridine Derivatives." J. Sci. Indust. Res., 43, pp. 98-116, 1984.

17. Shukla, O. P. and S. M. Kaul. "A Constitutive Pyridine Degrading System in Corynebacterium sp." Ind. J. Biochem. Biophys., 11, pp. 201-207, 1974.

18. Sims, G. K. and L. E. Sommers. "Biodegradation of Pyridine Derivatives in Soil Suspensions." Environ. Tox. Chem., 5, pp. 503-509, 1986.

19. Sims, G. K., L. E. Sommers and A. Konopka. "Degradation of Pyridine by Micrococcus lateus Isolated From Soil." Appl. Environ. Microbiol., 51, pp. 963-968, 1986.

20. Sims, G. K. and L. E. Sommers. "Degradation of Pyridine Derivatives in Soil." J. Environ. Qual., 14, pp. 580-584, 1985.

21. Yamada, K., Y. Minoda, K. Kodama, S. Nakatani and T. Akasaki. "Microbial Conversion of Petro-Sulfur Compounds. Part I. Isolation and Identification of Dibenzothiophene-Utilizing Bacteria." Agric. Biol. Chem., 32, pp. 840-845, 1968.

54WP/61090-331/RPP

Subtask 3.3.2. Microbial Process Development

This subtask was conducted by IGT.

Objective

The objective of this subtask was to determine the effects of process conditions and inocula from Subtask 3.3.1 (which involves development of cultures to desulfurize and/or denitrify oil shale) on the efficiencies and rates of organic nitrogen and sulfur removal from Eastern oil shale.

Summary

Mixed heterotrophic cultures isolated by OSU in Subtask 3.3.1 or by IGT from oil shale enrichments in which the oil shale served as the only available source of sulfur, and pure (IGTS8) and mixed (IGTS7) cultures isolated by IGT from coal bioreactors under a separate DOE-funded program were examined for their ability to remove the sulfur from oil shale. In addition, the chemolithotrophic microorganism Thiobacillus ferrooxidans was examined for its ability to remove the sulfur from oil shale. Shake flask experiments were performed. All cultures were pregrown and added at a final concentration of 10^8 cell/ml to slurries containing 4 weight percent oil shale.

The results show that the heterotrophic mixed cultures were transforming the sulfur in oil shale. The cultures removed the pyritic sulfur and utilized it for their organic sulfur needs. Chemical analyses indicated that these cultures transformed 78% of the pyritic sulfur from oil shale within 30 days. The results also showed that T. ferrooxidans transformed 44% of the pyritic sulfur from oil shale within 42 days. The chemolithotrophic organism oxidized the iron in the oil shale pyrite to obtain its energy for growth and released the sulfur as sulfate into the liquid medium. However, the cellular mass could not be separated from the particles of beneficiated shale, and therefore, the organic sulfur remaining in the shale could not be distinguished from that incorporated into the microbial cells.

Mixed cultures isolated by IGT and OSU from oil shale enrichments in which the oil shale served as the only available nitrogen source were examined for their ability to remove the nitrogen from oil shale. Shake flask experiments were performed. All cultures were pregrown and added at a final concentration of 10^6 cell/ml to slurries containing 4 weight percent oil shale in a nitrogen-free atmosphere.

The results show that the mixed cultures were transforming the nitrogen in oil shale. Chemical analyses indicated that these cultures removed about 50% of the nitrogen within 7 days.

For efficient removal of sulfur and nitrogen from oil shale, the shale particles and microbes should remain suspended in the bioreactor. The settling characteristics of oil shale in a bioreactor were examined with and without microbes. In the presence of microbes, there was minimal to no settling of the oil shale, whereas without microbes, the shale settled. Also, the mixing characteristics of the oil shale in the bioreactor were examined. Generally, a mixing rate of 300 rpm resulted in a uniform shale particle concentration at different levels in the bioreactor and an increased microbial growth.

Introduction

The Devonian oil shales of the Eastern United States constitute a significant energy resource for the production of synthetic liquid fuels. It is estimated that over 400 billion barrels of oil may be recovered from these oil resource deposits located in Alabama, Indiana, Kentucky, Michigan, Ohio, and Tennessee. These deposits are located in close proximity to oil refineries, distribution facilities and markets, and water supplies which allows them to be more easily processed.[1]

Oil shale contains organic material (primarily kerogen) and a small amount of bitumen. The kerogen is a polymer of high molecular weight containing on average several saturated rings with hydrocarbon chains having an occasional isolated carbon-carbon double bond and also containing oxygen and small amounts of nitrogen and sulfur. The sulfur in oil shale is in both organic and inorganic form. The inorganic sulfur is present primary as pyrite. The organic sulfur occurs in C-S-C bonding in which the carbon atoms may be either unsaturated or saturated. This three-atom grouping may be part of either acyclic or cyclic systems. Some of the sulfur groups in oil shale are thiols, disulfides, and thiophenes.[2-4]

Because of the promising results obtained in the microbial desulfurization of coal, that is, >90% removal of inorganic and organic sulfur, microbial desulfurization of oil shale may be feasible.[5-7]

Microbial denitrification of oil shale may also be feasible. Researchers have reported that microorganisms can remove heterocyclic nitrogen compounds from shale oils.[8]

This present research has been directed toward:

- Evaluating cultures developed at IGT that are able to remove sulfur from coal and model organic compounds for their ability to remove the sulfur from oil shale
- Evaluating the cultures developed at OSU for their ability to remove sulfur and/or nitrogen from oil shale
- Evaluating the chemolithotrophic organism, Thiobacillus ferrooxidans, which is able to remove the pyritic sulfur from coal for its ability to remove the sulfur from oil shale.
- Developing cultures at IGT that have the ability to remove nitrogen from oil shale
- Determining bioreactor process conditions, that is, examining the physical and chemical characteristics of oil shale slurries in the bioreactor on the efficiencies and rates of microbial removal of organic sulfur and nitrogen from oil shale.

Technical Discussion

Experimental Equipment and Test Procedures

Desulfurization Cultures

IGTS7 and IGTS8 were isolated from coal bioreactors in which coal served as the only available source of sulfur. IGTS7 was a mixed culture and IGTS8 was a pure culture of Rhodococcus rhodochrous isolated from IGTS7. These cultures were maintained in a nutrient broth (Difco) or on nutrient agar plates (Difco, Inc., Detroit, MI) at 30°C.

IGTS7M was isolated from an oil shale bioreactor at IGT in which oil shale (4 weight percent) served as the only available source of sulfur. The culture was maintained on nutrient agar plates at 30°C.

Sixteen pure cultures isolated from oil shale enrichments in which the oil shale served as the only available source of sulfur were obtained from Dr. R. Pfister, at OSU. These were maintained on nutrient agar slants at 30°C.

Thiobacillus ferrooxidans ATCC 23270 was obtained from the American Type Culture Collection and maintained in a Thiobacillus medium.[9]

Denitrification Cultures

A mixed culture (IGTD1) was isolated at IGT from oil shale enrichments in which the shale served as the only available nitrogen source in a nitrogen-free atmosphere. These cultures were maintained in a salts medium (composition 17 g KH_2PO_4; 26.5 g Na_2HPO_4; 0.8 g Na_2SO_4; 0.15 g yeast extract and 1 ml of a filter-sterilized solution of pyridine; per liter of distilled water), pH 7 at ambient temperature. To ensure the absence of nitrogen, the culture was purged with CO_2:O_2:He (2:20:78), closed with butyl rubber stoppers and crimped sealed.

Mixed cultures isolated from sewage sludge in which pyridine (0.1% v/v) served as a source of nitrogen were also obtained from Dr. Pfister. These cultures were maintained in the salts medium described above in an atmosphere free of nitrogen.

Oil Shale

Beneficiated oil shale (Indiana New Albany, particle size 40 μm) was used in this study. The oil shale was obtained from MRI. Ultimate analyses of the sample are given in Table 3-42.

Desulfurization Studies

Shake Flask Experiments. For examining the ability of IGTS7M, IGTS8, and the cultures from OSU to remove the sulfur from oil shale, the cultures were pregrown for several days to late logarithmic phase at 30°C on a rotary shaker (140 rpm). The cells were grown in a basal salts medium (composition 4 g K_2HPO_4; 4 g Na_2HPO_4; 1.4 g Na_2SO_4; 2 g NH_4Cl; 0.2 g $MgCl_2$, 0.001 g $CaCl_2$, and 0.001 g $FeCl_3$ per liter), pH 6.8, containing glucose (15 mM) as the carbon◇

Table 3-42. ULTIMATE ANALYSES OF RAW AND BENEFICIATED INDIANA NEW ALBANY OIL SHALE

Shale Type	Raw	Beneficiated
Ultimate, % dry		
Carbon	13.98	27.42
Hydrogen	1.60	2.79
Nitrogen	0.59	0.97
Sulfur	3.43	2.65
Silicon	--	19.3

source for IGTS7M and cultures from OSU and glycerol (1%) as the carbon source for IGTS8 (500 ml in 1 liter flasks). The cells were harvested and washed several times to remove residual sulfur. After harvesting and washing, the cells were concentrated and added to sterilized (salts medium 121°C, 15 minutes and oil shale 121°C, 90 minutes) 4 weight percent oil shale slurries (50 ml in 250 ml flasks) with glucose (15 mM) as the carbon source at a final concentration of 10^8 cell/ml. Cells were periodically added to maintain the concentration in the control and sample flasks at 10^8 cells/ml. The control condition was: autoclaved oil shale + glucose + autoclaved cells, and the sample condition was autoclaved oil shale + glucose + cells. In this study, the pH and microbial growth were monitored.

For sulfur chemical analysis from oil shale, 1-gram portions were removed from the sample and control flasks. To facilitate the separation by centrifugation of the cells from the oil shale, the cells were killed by heating. After separation, the oil shale samples were dried in an oven at 103°C. Sulfur-by-type analyses and silicon determinations were done on the samples and controls and the sulfur by type to Si ratios compared to determine sulfur removal. To determine if the organic sulfur was removed, sulfur-by-type chemical analyses were performed on oil shale/cell samples that had been treated with heat (90°C/10 min) and alkaline (1 N NaOH solution) to solubilize the protein. After treatment, the oil shale alkaline solution was centrifuged, the solid oil shale washed and dried in an oven at 103°C and submitted for sulfur-by-type analyses.

For examining the ability of T. ferrooxidans to remove the sulfur from oil shale, the culture was pregrown for 1 week to a cell concentration of 10^{11} cell/ml. They were grown in 6-liter flasks containing 4 liters of a salt medium (composition 1.22 g NH_4Cl; 0.1 g KCl; 0.5 g K_2HPO_4; 0.4 g $MgCl_2$; and 0.01 g $Ca(NO_3)_2$ per liter of deionized water) pH 2.6 (adjusted with a 10 N solution of HCl) at ambient temperature. The flasks were aerated and rotameters were used to control air flow rates. The air flow rate was maintained at about 860 ml/min. After 1 week, the cells were harvested as described by Silverman[10] and added to sterilized (salts medium 121°C, 15 minutes and oil shale 121°C, 90 minutes) 4 weight percent oil shale slurries (100 ml/250 ml flask). The cells were added at a final concentration of 10^8 cell/ml to controls and samples. The sample conditions were: oil shale + medium (pH 2.6) + cells, and oil shale and deionized water (pH 2.6) + cells. The control conditions were: oil shale + medium (pH 2.6), oil shale + deionized water (pH 2.6), medium (pH 2.6) alone, deionized water (pH 2.6)

alone, medium (pH 2.6) + cells and deionized water(pH 2.6) cells. Samples and controls were grown at ambient temperature on a rotary shaker (150 rpm). The pH of the samples and controls were monitored periodically.

Triplicate oil shale samples and controls were analyzed for sulfur removal. Sulfur by type analysis was performed on 1-gram portions of oil shale that had been washed and dried in an oven at 103°C.

Denitrification Studies

Shake Flask Experiments. For examining the ability of IGTD1 and OSU's cultures to remove nitrogen from oil shale, the cultures were pregrown in the salts medium described in the Denitrification Culture section in a N-free atmosphere. They were grown at ambient temperature on a rotary shaker (140 rpm). After growth, the cells were harvested, washed several times to remove residual nitrogen, concentrated and added to sterilized (salts medium 121°C, 15 minutes and oil shale 121°C, 90 minutes) 4 weight percent oil shale slurries (100 ml in 160 ml serum bottles) with glucose (15 mM) as the carbon source at a final concentration of 10^6 cell/ml in a N-free atmosphere. Samples and controls flasks were incubated at ambient temperature on a rotary shaker (150 rpm). The control condition was autoclaved oil shale + glucose + autoclaved cells and the sample condition was autoclaved oil shale + glucose + cells. In this study microbial growth and protein concentration were monitored.

Triplicate oil shale samples and controls were analyzed for nitrogen transformation. For nitrogen chemical analysis, 1-gram portions of oil shale were removed, washed and dried in an oven at 103°C. For determining nitrogen removal, the oil shale/cell samples were treated with heat (90°C/10 min) and alkaline (1 N NaOH solution) to solubilize the protein. After treatment, the oil shale alkaline solution was centrifuged, the solid oil shale washed and dried in an oven at 103°C, and submitted for nitrogen chemical analyses.

Stimulation/Inhibition Shake Flask Experiments

For examining the stimulation or inhibition of various oil shale concentrations on the growth of IGTS7, the culture was pregrown, and the cells harvested and washed as described in the Desulfurization Studies section. After washing, the cells were concentrated (final concentration in flasks 10^6 cells/ml) and added to 4, 8, 12, 20 and 50 weight percent oil shale slurries (50 ml in 250 ml flasks) with and without glucose as the carbon source. Glucose (15 mM) was added weekly to the samples. Control flasks contained the oil shale with glucose and no culture. Microbial growth and pH were monitored weekly.

Settling and Mixing Characteristics Experiments

For determining the settling characteristics of oil shale slurries, batch settling tests without agitation were performed and analyzed based on a method by Kynch as described by Badger and Banchero (1955).[11] The change in height of the interface which is the solid-liquid interface between the oil shale and clear liquid, with time was monitored. The settling characteristics of 4 weight percent oil shale slurries prepared in either deionized water or phosphate buffer, and 8 and 12 weight percent oil shale slurries prepared in deionized water and 4% oil shale slurries with cells were determined.

Agitation Studies

One-liter reactors with 8 cm magnetic spinners were used. These reactors were placed on magnetic stirrers and different rates of agitation were obtained by adjusting the speed control. The different speeds were determined with a tachometer. For an accurate speed, an average of ten readings with the tachometer was taken.

For examining the effect of different rates of agitation, the uniformity of shale particle concentration at different levels in the bioreactor was determined. The reactors were 12.5 cm high, and samples were taken at 0 cm, 6.25 cm, and 12.5 cm levels. Oil shale samples were removed at these different levels and the wet weight of the shale pellet was determined and compared to a standard curve to determine the slurry concentration at the different levels. A standard curve of slurry concentration versus the wet weight of the shale pellet was constructed (Figure 3-88). Wet pellet weights for different slurry concentrations ranging from 2 to 20 weight percent were obtained in triplicate by centrifuging 25 ml samples at 14,000 rpm for 10 min.

Sulfur Bioassay

The bioassay was performed as described by Kilbane et al. (1989).[7]

Protein Assay

For determining the protein concentration in the oil shale slurries, the slurries were centrifuged to separate the supernatant, which may contain cells and the solid oil shale/cell residue. The liquid and solid residue were separately heated at 90°C/10 minutes in a 1 N NaOH solution to solubilize the protein. After treatment, the liquid and solid residue were centrifuged again to remove either cellular debris or oil shale cellular debris, respectively. A protein assay, as described by Pierce, was performed on the two liquid samples to determine total protein concentration in the oil shale slurries.[12]

Discussion

Desulfurization Studies

Shake Flask Experiments with IGTS8, IGTS7, and OSU's Mixed Culture. IGTS8, IGTS7M, and the sixteen cultures mixed together from OSU were examined for their ability to remove sulfur from Eastern oil shale. The individual cultures were added to a 4 weight percent oil shale slurry (50 ml in 250 ml flasks) with glucose at a final concentration of 10^8 cell/ml. This cell concentration was maintained by periodically adding cultures to the shale. Chemical analyses of the sulfur content of the oil shale after 14 days incubation indicated a 24% sulfur reduction in the presence of IGTS8 and the mixed culture from OSU and 17% in the presence of IGTS7M. At 30 days, in the presence of all the cultures, sulfur was reduced by 31% (Table 3-43).

To determine which sulfur species was being removed, sulfur by type analyses were performed on the oil shale samples grown in the presence of IGTS7M and the mixed culture from OSU. Sulfur-by-type analyses indicated there was a loss in pyritic sulfur and an increase in organic sulfur (Table 3-44). At Day 14 and Day 30, in the presence of IGTS7M, there was a reduction in the

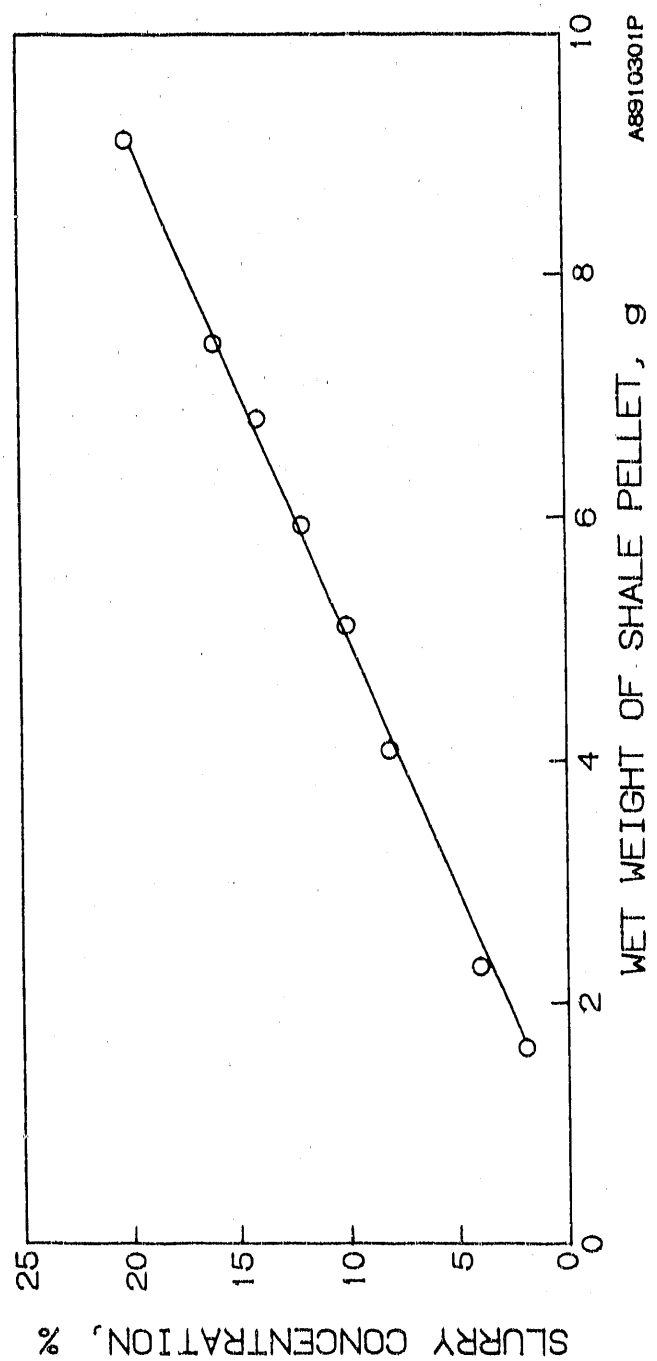

Figure 3-88. STANDARD CURVE: PLOT OF SLURRY CONCENTRATION VERSUS WET WEIGHT OF SHALE PELLET

Table 3-43. ULTIMATE CHEMICAL ANALYSIS ON OIL SHALE SAMPLES FOR SULFUR REMOVAL

Culture	Day 0 S:Si[b]	Day 0 SD[c]	Day 14 S:Si	Day 14 SD	% Sulfur Reduction	% Biological Sulfur Reduction[d]	Day 30 S:Si	Day 30 SD	% Sulfur Reduction	% Biological Sulfur Reduction
Control[a]	0.145	0.005	0.145	0.005	0	--	0.135	0.006	7	--
IGTS8	0.145	0.005	0.110	0.003	24	24	0.090	0.005	38	31
IGTS7M	0.145	0.005	0.120	0.007	17	17	0.090	0.007	38	31
Mixed Culture From Ohio State University	0.145	0.005	0.110	0.003	24	24	0.090	0.007	38	31

[a] Control consisted of autoclaved oil shale (4%) and autoclaved cells.

[b] S:Si is Sulfur:Silicon.

[c] Standard deviation of triplicate samples.

[d] Difference of % sulfur reduction in sample minus % sulfur reduction in control.

Table 3-44. SULFUR BY TYPE ANALYSIS ON OIL SHALE SAMPLES TREATED WITH IGTS7M OR OSU MIXED CULTURE

Sulfur Species	Day 0 (Control & Sample)	Day 14 Control	Day 14 IGTS7M Sample	Day 14 % Sulfur Change	Day 14 Mixed Culture From OSU Sample	Day 14 % Sulfur Change	Day 30 Control	Day 30 IGTS7M Sample	Day 30 % Sulfur Change	Day 30 Mixed Culture From OSU Sample	Day 30 % Sulfur Change
Total Sulfur:Silicon	0.145±0.005	0.145±0.006	0.120±0	- 17	0.110±0	-24	0.135±0.006	0.090±0	-33	0.090±0	-33
Organic Sulfur:Silicon	0.034±0.009	0.030±0	0.060±0	+100	0.040±0	+33	0.0375±0.005	0.060±0	+60	0.040±0	+ 7
Pyritic Sulfur:Silicon	0.099±0.01	0.102±0.01	0.055±0.007	- 46	0.065±0.007	-36	0.090±0	0.020±0	-78	0.045±0.007	-50
Sulfate:Silicon	0.010±0	0.010±0	0.010±0	0	0.010±0	0	0.010±0	0.010±0	0	0.010±0	0

pyritic content by 46% and 78%, respectively, and an increase in the organic of 100% and 60%, respectively. At Day 14 and 30, in the presence of the mixed culture from OSU, there was a reduction in the pyritic content of 36% and 50%, respectively and an increase in the organic of 33% and 7%, respectively (Table 3-44). The data suggest that the organisms were removing the pyritic sulfur for their growth and utilizing it for their organic sulfur needs. The data further suggest that pyritic sulfur removal was increasing with time. It may be that if the oil shale samples were incubated for a longer period of time in the presence of the microbial culture, the remaining pyritic sulfur could be transformed by the cells and then the cells may possibly utilize the organic sulfur present in the oil shale. To test this hypothesis, IGTS7M was incubated for an additional 30 days, so that the total incubation was 63 days. At Day 63, there was a reduction in pyritic sulfur of 83% and an increase in organic sulfur to 74%, confirming the transformation of the pyritic sulfur into cellular organic sulfur, however, the data does not indicate that there was further removal of the pyritic sulfur or removal of the organic sulfur (Table 3-45). Maximal pyritic sulfur removal may have been reached at Day 30 because the reduction in pyritic sulfur was similar at Days 30 and 63, 78% and 83%, respectively.

To determine if the organic sulfur from oil shale was removed, the solid oil shale/cell residues from Day 63 were treated with heat (90°C/10 min) and alkaline (1 N NaOH solution) to solubilize the protein. The oil shale alkaline solution was then centrifuged, the oil shale separated, washed to remove cellular debris and submitted for sulfur analysis. Chemical analysis of the oil shale indicated that pyritic sulfur from the oil shale was utilized by the cells and transformed into cellular sulfur compounds. There was a reduction in the pyritic sulfur by 83%. However, based upon these results it does not appear that the organisms were utilizing the organic sulfur because there was no significant change in the organic sulfur:silicon ratio with time (Table 3-46).

Shake Flask Experiments With Thiobacillus ferrooxidans. T. ferrooxidans ATCC 23270 was examined for its ability to remove the sulfur from Eastern oil shale. The culture was added to a 4 weight percent oil shale slurry (100 ml in 250 ml flask) at a final concentration of 10^8 cell/ml. Chemical analysis of the sulfur content of the oil shale at Day 42 (in the presence of the salts medium) indicated a 46% reduction, whereas in the absence of the organism, total sulfur reduction was 25% (Table 3-47). Analyses of sulfur-by-type indicated there was greater pyritic sulfur removal in the presence of T. ferrooxidans, that is, 85% than in the absence of the culture in which there was only a 43% reduction.

Other researchers have reported that microbial pyritic oxidation can be inhibited by the salts present in the nutrient medium.[6] Therefore, sulfur reduction by T. ferrooxidans was examined in the presence and absence of nutrients. The salts did not affect microbial pyrite oxidation. Microbial pyrite removal was similar in the presence and absence of the salts (Table 3-47). The microbial sulfur reduction, that is, 49% total sulfur observed in the presence of the acidic deionized water solution indicated that the T. ferrooxidans can obtain all the nutrients required for its growth from the oil shale. The cost of nutrients is thus eliminated.

Table 3-45. SULFUR BY TYPE ANALYSIS ON OIL SHALE SAMPLES TREATED WITH IGTS7M

	Day 0	Day 14			Day 30			Day 63		
Sulfur Species	Control & Sample	Control	IGTS7M Sample	% S Change	Control	IGTS7M Sample	% S Change	Control	IGTS7M Sample	% S Change
Total S: Silicon	0.145±0.005	0.145±0.006	0.120±0	-17	0.135±0.006	0.090±0	-33	0.131±0.002	0.092±0.006	-30
Organic S: Silicon	0.034±0.009	0.030±0	0.060±0	+100	0.0375±0.005	0.060±0	+60	0.038+0.001	0.066+0.003	+74
Pyritic S: Silicon	0.099±0.01	0.102±0.01	0.055±0.007	-46	0.090±0	0.020±0	-78	0.082±0.004	0.014±0.003	-83
Sulfate: Silicon	0.010±0	0.010±0	0.010±0	0	0.010±0	0.010±0	0	0.01±0	0.01±0	0

Table 3-46. SULFUR REMOVAL FROM OIL SHALE IN THE PRESENCE OF IGTS7M

	Day 0	Day 63		
Sulfur Species	Control and Sample	Control	IGTS7M Sample	%S Removal
Total S:Silicon	0.143±0.006	0.130±0.006	0.061±0.007	53
Organic S:Silicon	0.034±0.009	0.037±0.005	0.036±0.003	3
Pyritic S:Silicon	0.099±0.01	0.082±0.01	0.014±0.005	83
Sulfate:Silicon	0.010±0	0.010±0	0.010±0	0

Comparing the sulfur removal by heterotrophic and chemolithotrophic cultures, the heterotrophic cultures were able to remove more of the pyritic sulfur (78%) in a shorter incubation period (30 days) than the chemolithotrophic culture (44% in 42 days). However, for a process, the chemolithotrophic organism may be more feasible. This culture does not need any added nutrients besides the oil shale for growth, whereas, the heterotrophic cultures needed the added mineral nutrients and a carbon source for their growth.

Denitrification Studies

Shake Flask Experiments With IGT and OSU Denitrifying Cultures. IGTD1 and a mixed culture from OSU, which was isolated from sewage sludge were examined for their ability to remove the nitrogen from Eastern oil shale. The cells were added to 4 weight percent oil shale slurries (100 ml in 160 ml serum bottles) with glucose (15 mM) as the carbon source at a final concentration of 10^6 cell/ml in a N-free atmosphere.

The cells may be utilizing the nitrogen from the oil shale for their growth and transforming the nitrogen into cellular protein. To determine if the cells were transforming the nitrogen from the oil shale to cellular protein, protein analyses were performed on the oil shale slurries. In addition to protein analysis, plate counts on nutrient agar were performed to monitor bacterial growth. There was an increase in bacterial cell counts and protein concentration in the oil shale slurries with the denitrifing cultures indicating that the organisms were transforming the nitrogen from the oil shale into cellular protein (Figures 3-89 and 3-90). Cell counts of oil shale/culture samples on nutrient agar indicated that maximum growth was reached within 48 hours (Figure 3-89). Corresponding to the increase in bacterial growth was the increase in protein cell concentrations (Figure 3-90). Whereas, the increase in bacterial growth and protein concentration was observed for the oil shale/culture samples, there was no growth or no increase in protein concentration in the controls indicating they remained sterile (Figure 3-90).

Based upon nitrogen analyses of oil shale and cell samples and protein concentration determinations, 59% of the nitrogen from the oil shale was transformed to protein in the presence of the OSU microbial culture at Day 7 and 42% was transformed in the presence of the IGT microbial culture at Day 7 (Table 3-48).

Table 3-47. SULFUR ANALYSIS ON OIL SHALE SAMPLES TREATED WITH THIOBACILLUS ferrooxidans

	Medium* + Oil Shale (4%)						dH_2O** + Oil Shale (4%)					
	Sample With T. ferrooxidans			Control Without T. ferrooxidans			Sample With T. ferrooxidans			Control Without T. ferrooxidans		
Sulfur Type, %	Day 0	Day 42	% S Reduction	Day 0	Day 42	% S Reduction	Day 0	Day 42	% S Reduction	Day 0	Day 42	% S Reduction
Total Sulfur	2.25	1.22	46	2.44	1.84	25	2.39	1.23	49	2.31	1.76	24
Sulfide	<0.030	<0.030		<0.030	<0.030		<0.050	<0.030		<0.030	<0.030	
Sulfate	0.43	0.35		0.33	0.39		0.48	0.47		0.45	0.41	
Pyritic	1.06	0.16	85	1.15	0.66	43	1.10	0.15	86	0.99	0.58	42
Organic (Calc.)	0.76	0.71		0.96	0.79		0.81	0.61		0.87	0.77	

* Mineral salts medium containing NH_4Cl 1.22 g; KCl 0.1 g; K_2HPO_4 0.5 g; $MgCl_2$ 0.4 g; Ca $(NO_3)_2$ 0.01 g per liter, pH 2.6.

** Deionized water solution without any salts, pH 2.6.

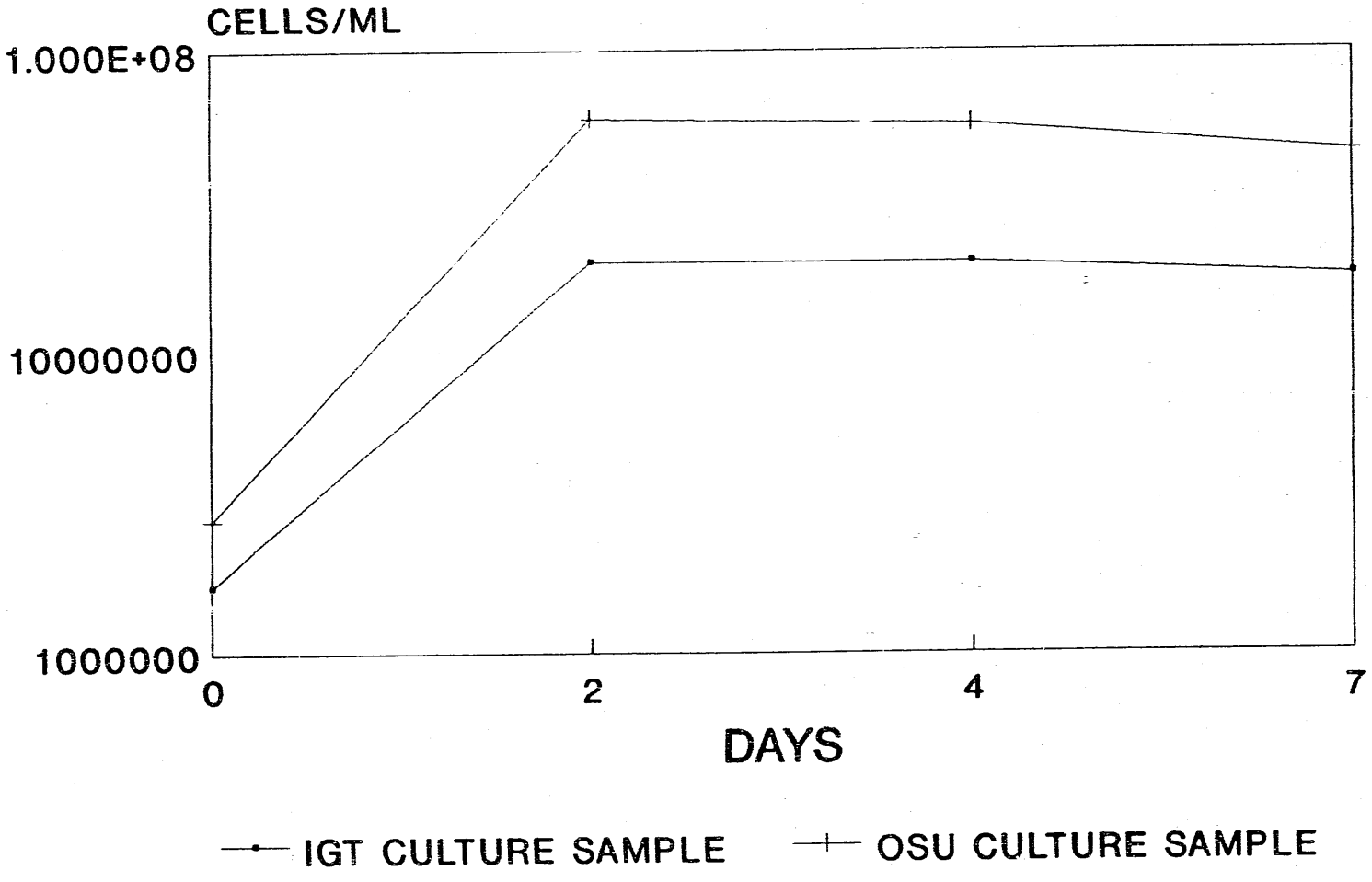

Figure 3-89. CELL COUNTS ON OIL SHALE SLURRIES AND DENITRIFYING BACTERIA

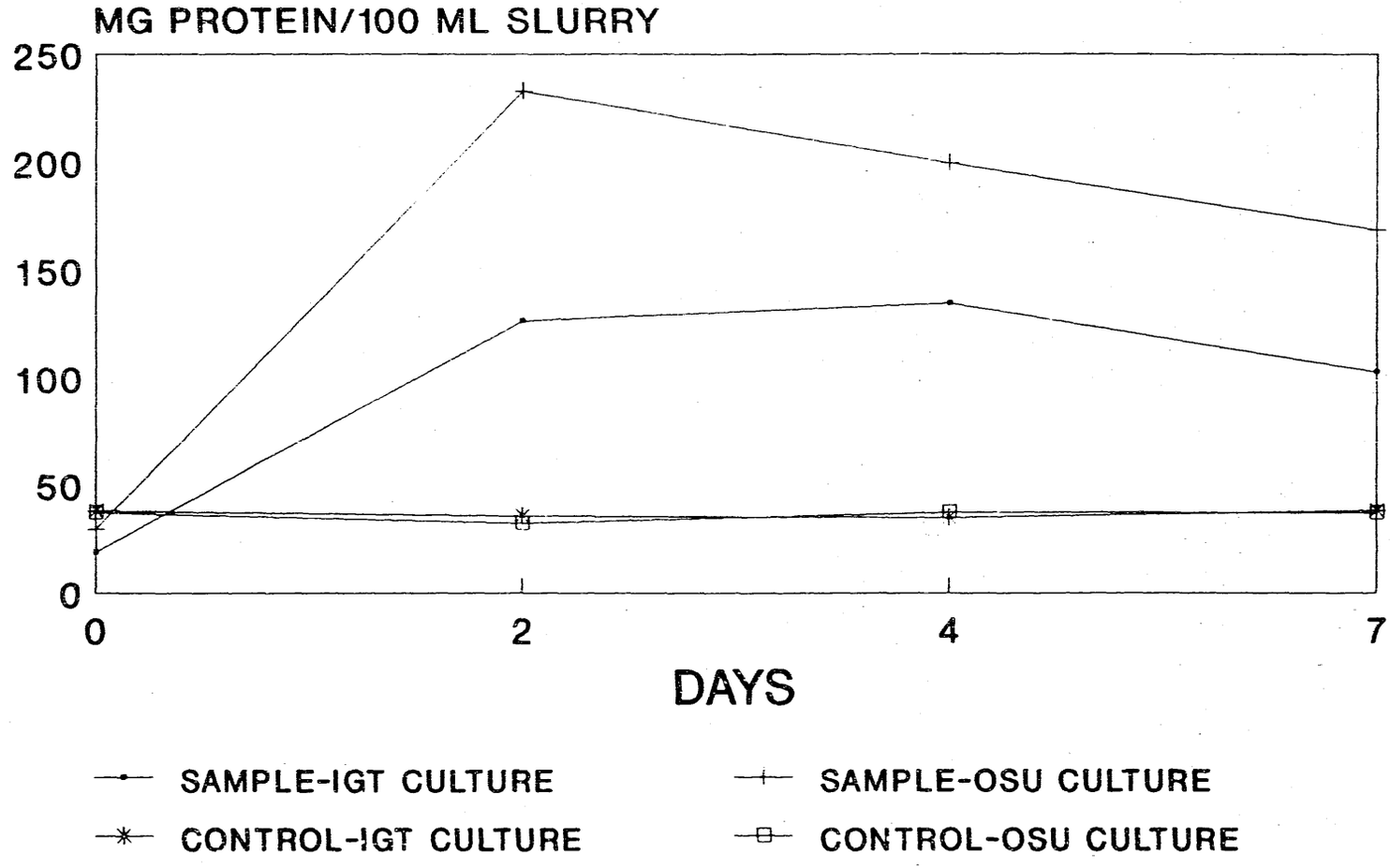

Figure 3-90. PROTEIN DETERMINATIONS ON OIL SHALE SLURRIES AND DENITRIFYING BACTERIA

Table 3-48. NITROGEN TRANSFORMATION IN THE PRESENCE OF IGTD1 AND OSU'S MIXED CULTURE

Day	Nitrogen Present[1] in Oil Shale and Cells mg/100 ml		Protein in Cells[2] mg/100 ml		Nitrogen Present[3] in Cells mg/100 ml		% Nitrogen Present[4] in Cells		% Nitrogen[5] Transformed	
	IGTD1	OSU's Mixed Culture	IGTD1	OSU's Mixed Culture	IGTD1	OSU's Mixed Culture	IGTD1	OSU's Mixed Culture	IGTD1	OSU's Mixed Culture
0	25.2±2.9	30.8±3.4	2.7	13	2.7	4.1	11	13		
7	31.8±4	36.4±3.7	17	72	17	26.2	53	72	42	59

[1] Average of three samples.

[2] Average of three samples.

[3] $\text{Nitrogen} = \frac{\text{protein}}{7.25}$

[4] $\text{\% nitrogen present in cells} = \frac{\text{Nitrogen present in cells}}{\text{Nitrogen present in cells and oil shale}} \times 100$

[5] $\text{\% nitrogen transformed} = \left(\frac{\text{Nitrogen present in cells}}{\text{Nitrogen present in cells and oil shale at Day 7}} \times 100\right) - \text{\% nitrogen present in cells at Day 0}$

To confirm that the nitrogen was transformed into cellular protein, that is, removed from the oil shale and utilized by the bacteria, the oil shale/cell samples were treated with heat/alkali to remove the cells. Chemical analyses of the treated 7-day oil shale samples indicated that 50% of the nitrogen was removed and utilized by the OSU mixed culture for cellular protein synthesis and 49% of the nitrogen was removed and utilized by IGTD1 for cellular protein synthesis (Table 3-49).

Stimulation/Inhibition Shake Flask Studies

The stimulation or inhibition of various oil shale concentrations on microbial growth was examined. The growth of IGTS7 in 4 to 50 weight percent oil shale concentrations with and without glucose was monitored by plate counts on nutrient agar. IGTS7 was capable of growing in oil shale concentrations of 4 to 50 weight percent and using oil shale as the sole source of sulfur (Figure 3-91). The cell growth increase in the 4 to 20 weight percent oil shale concentrations was 10-fold. By Day 18, in a 4 weight percent slurry, cell growth increased from an initial 2×10^6 to 4×10^7 cell/ml. By Day 18, in an 8 weight percent slurry, cell growth increased from an initial 2×10^6 to 6×10^7 cell/ml. By Day 18, in 12 and 20 weight percent slurry, cell growth increased from an initial 2×10^6 to 8×10^7 cell/ml. Faster growth was initially observed at the 50 weight percent oil shale concentration compared to the 4 to 20 weight percent, however, growth decreased more rapidly at the 50 weight percent than at the other concentrations. Growth began to decrease at about Day 20 in the 20 weight percent slurry whereas in the 4 to 20 weight percent slurries growth began to decrease after 24 days (Figure 3-91).

The addition of glucose to the oil shale slurry stimulated microbial growth. Without glucose, the organisms were not growing but just maintaining themselves. The cell growth increased from 2×10^6 cell/ml to 8×10^6 cell/ml by Day 24 without glucose whereas with glucose the cell growth increased from an initial 2×10^6 cell/ml to 8×10^7 cell/ml by 24 days (Figure 3-92).

Settling and Mixing Characteristic Studies

For the efficient operation of an oil shale bioreactor, the shale particles and microbes should remain suspended in the bioreactor. After the slurry leaves the bioreactor, however, it is desirable to have rapid settling of the shale particles to facilitate the separation of microbial cells. Settling characteristics can be influenced by several parameters that include the concentration and particle size distribution of the oil shale, modification of the particle surface by the adhesion of the microbial cells, and growth medium components.

Batch settling tests without agitation were performed on oil shale samples to determine the effect of oil shale concentration, microbial adhesion to the oil shale, and growth medium components on the settling characteristics. The test was performed by measuring the change in height of the interface which is the solid-liquid interface between the oil shale and clear liquid with time.

The settling of 4, 8 and 12 weight percent oil shale slurries prepared in deionized water was compared to determine the effect of concentration on

Table 3-49. NITROGEN REMOVAL IN THE PRESENCE OF IGTD1 AND OSU MIXED CULTURE

Day	Nitrogen Present[1] in Oil Shale and Cells mg/100 ml		Protein in Cells[2] mg/100 ml		Nitrogen Present[3] in Cells mg/100 ml		Nitrogen Present[4] in Oil Shale		% Nitrogen[5] Removal	
	IGTD1	OSU's Mixed Culture	IGTD1	OSU's Mixed Culture	IGTD1	OSU's Mixed Culture	IGTD1	OSU's Mixed Culture	IGTD1	OSU's Mixed Culture
0	25.2±2.9	30.8±3.4	20.3±4	20.3±5	2.8	2.8	22.4±2.8	28±2.1		
7	31.8±4	36.4±3.7	137.8±8.9	158.1±10	19	21.8	12.8±2	14.6±3.7	49[5]	51[5]

[1] Average of three samples.

[2] Average of three samples.

[3] $\text{Nitrogen} = \frac{\text{protein}}{7.25}$

[4] Average of three samples.

[5] $\text{\% nitrogen removed} = \left(\frac{\text{Nitrogen present in oil shale + cells at Day 7} - \text{Nitrogen present in oil shale at Day 7}}{\text{Nitrogen present in oil shale + cells at Day 7}}\right) - \left(\frac{\text{Nitrogen present in oil shale + cells at Day 0} - \text{Nitrogen present in oil shale at Day 0}}{\text{Nitrogen present in oil shale + cells at Day 0}}\right)$

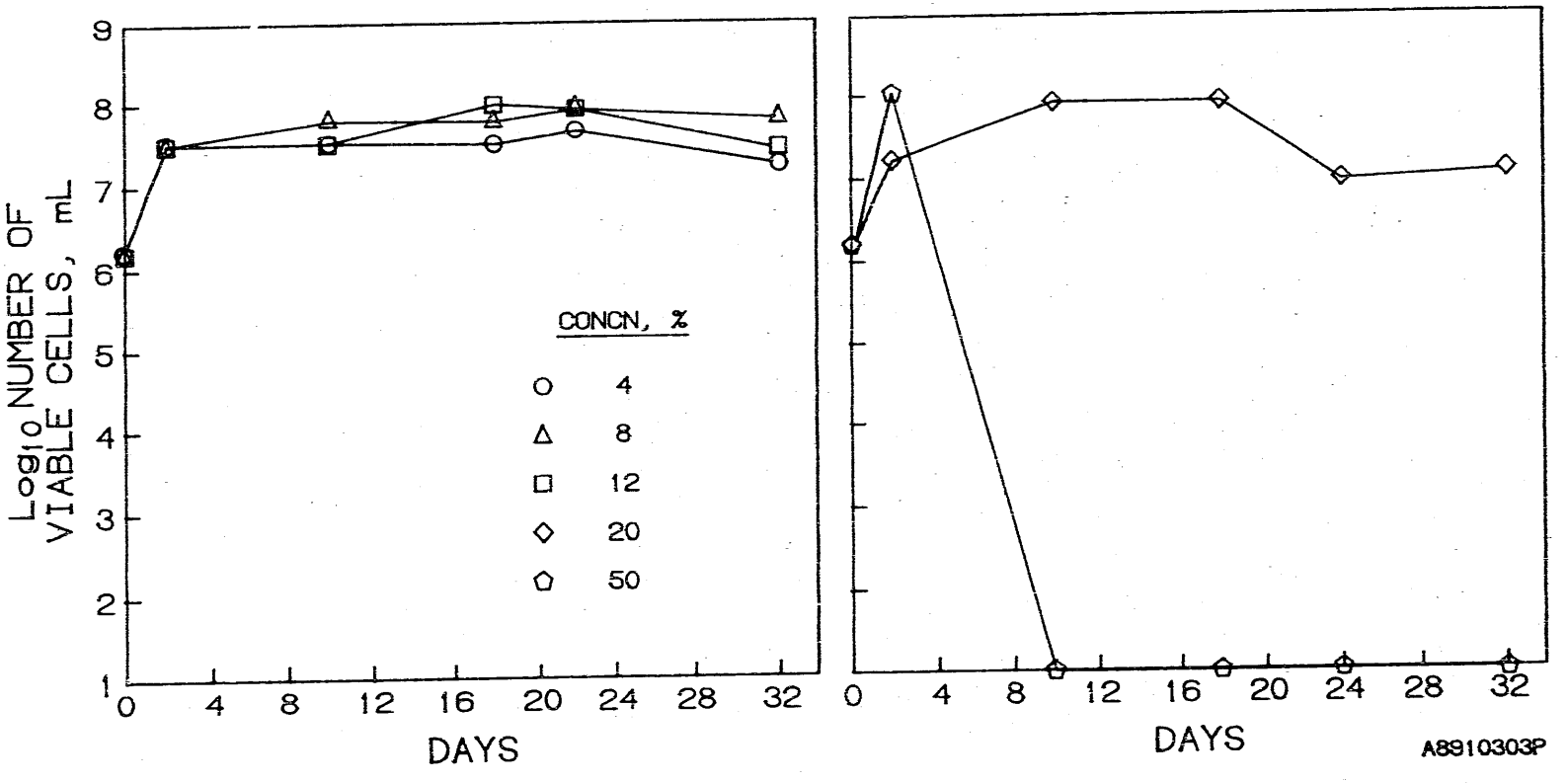

Figure 3-91. EFFECT OF VARIOUS OIL SHALE CONCENTRATIONS ON CELL GROWTH IN THE PRESENCE OF GLUCOSE

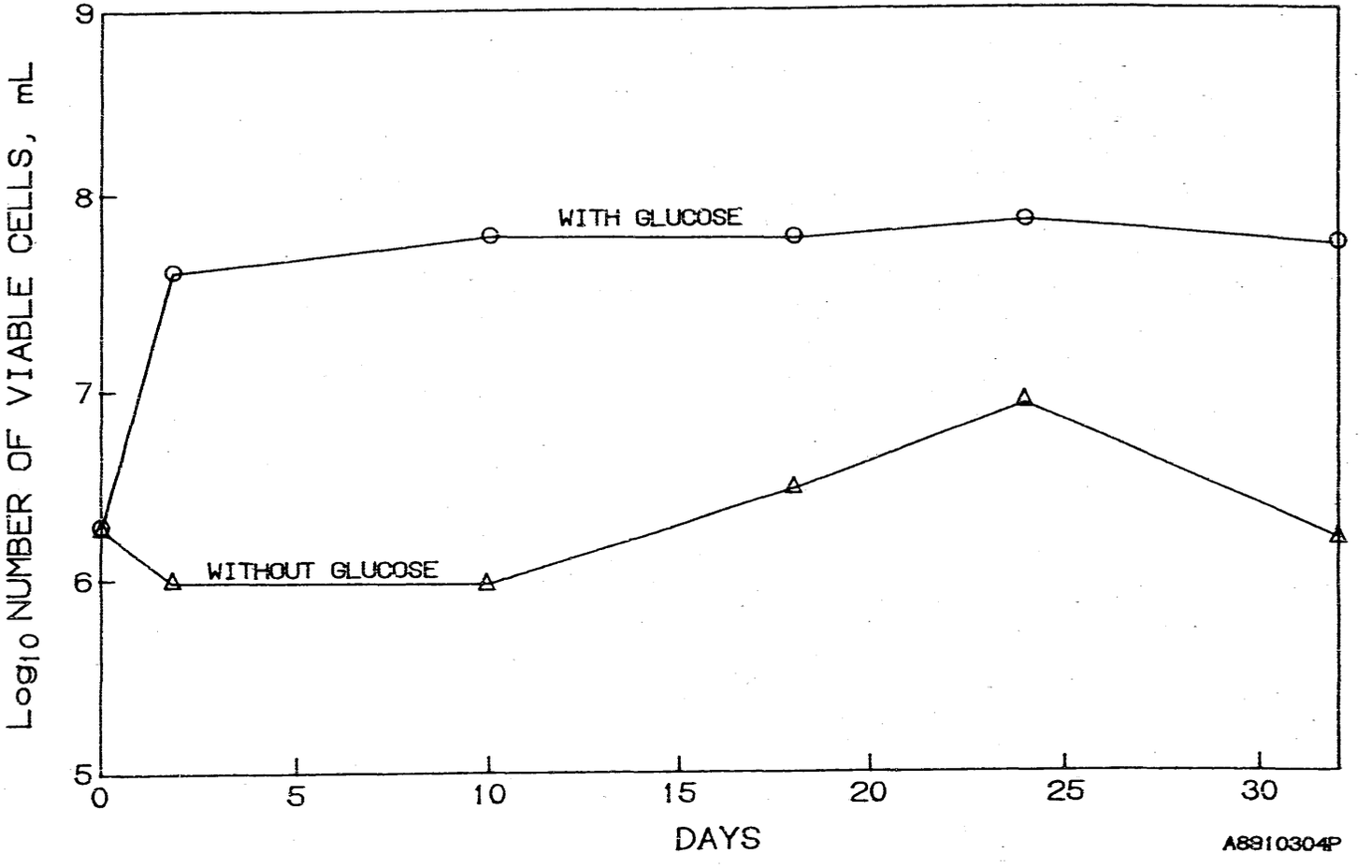

Figure 3-92. CELL GROWTH IN AN 8 WEIGHT PERCENT OIL SHALE SLURRY WITH AND WITHOUT GLUCOSE

settling. Concentration changes the settling characteristics of the oil shale. Increasing the oil shale concentration resulted in slower settling of the slurry (Figure 3-93).

To determine the effect of microbial adhesion to the oil shale on the settling, a 4 weight percent oil shale slurry from the bioreactor that was incubated with IGTS7 for 49 days and a 4 weight percent slurry from the bioreactor that had not been inoculated with IGTS7 were compared. There was no interface observed in the presence of the microbial culture, whereas in the absence of the culture, an interface was observed (Figure 3-94). The absence of an interface in the slurry from the bioreactor suggests there was minimal to no settling of the oil shale in the bioreactor. This is desirable for efficient microbial desulfurization of oil shale. A stable suspension, however, is undesirable for the post-bioreactor separation operation. A batch settling test without agitation was performed on an effluent from the bioreactor containing a 4 weight percent oil shale slurry inoculated with IGTS7 and on an effluent from the bioreactor containing no culture. A distinct interface was observed in the effluent from the bioreactor containing no culture whereas it was not observed in the effluent from the oil shale bioreactor containing the culture. The effluent from the bioreactor containing the culture was brownish in appearance. This color was attributed to the very fine particles of shale in suspension. The shale remained suspended probably because of microbial association. Microscopic observations revealed that the cells were adhering to the fine particles.

The settling of a 4 weight percent oil shale slurry prepared in deionized water and phosphate buffer were compared to determine the effect of growth medium components on settling. Settling did take place in the slurry prepared with deionized water and phosphate buffer. A distinct interface was observed in the slurry prepared in deionized water; however, for the slurry prepared in a phosphate buffer, no interface was observed. Coalescence took place which was attributed to settling. These observations suggest that growth medium components affect the settling. From these data, it can be suggested that in a microbial process, concentrated oil shale slurries can be prepared in an ionic medium where the microbes and oil shale remain suspended for efficient removal of sulfur and nitrogen.

Agitation Studies

The rate of agitation in a bioreactor has to be balanced to ensure that the microbes and the solid particles remain suspended, that adequate oxygen and nutrient transfer is achieved and that no excessive shear forces are generated to avoid abrasive destruction of the microbial cells or further reduction of the shale particle size. In this study, the effect of different rates of agitation (62, 170, 240, 300 and 350 rpm) on the uniformity of the shale particle concentration at different levels in the bioreactor and on cell growth was examined. To determine if settling was occurring in the bioreactor, wet pellet weights of oil shale samples from three different levels in the bioreactor were obtained and compared to a standard curve to determine slurry concentrations at the different levels (refer to Figure 3-88).

There was no settling of oil shale at the various agitation rates; however, the agitation rates affected cell growth. At lower rates of agitation (62 and 170 rpm) the increase in cell growth after 4 days was less

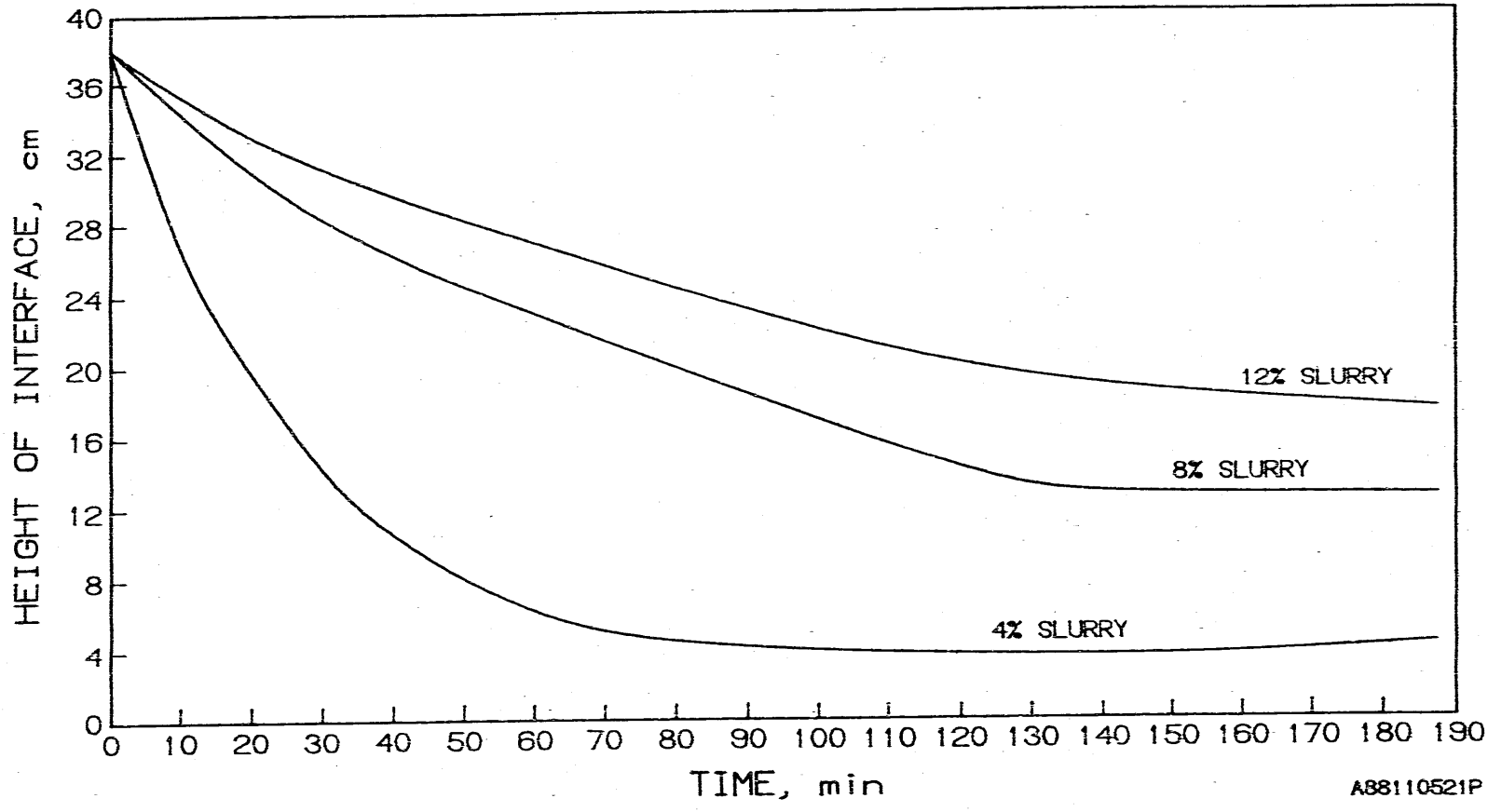

Figure 3-93. SETTLING CHARACTERISTICS OF SLURRIES WITH DIFFERENT OIL SHALE CONCENTRATIONS

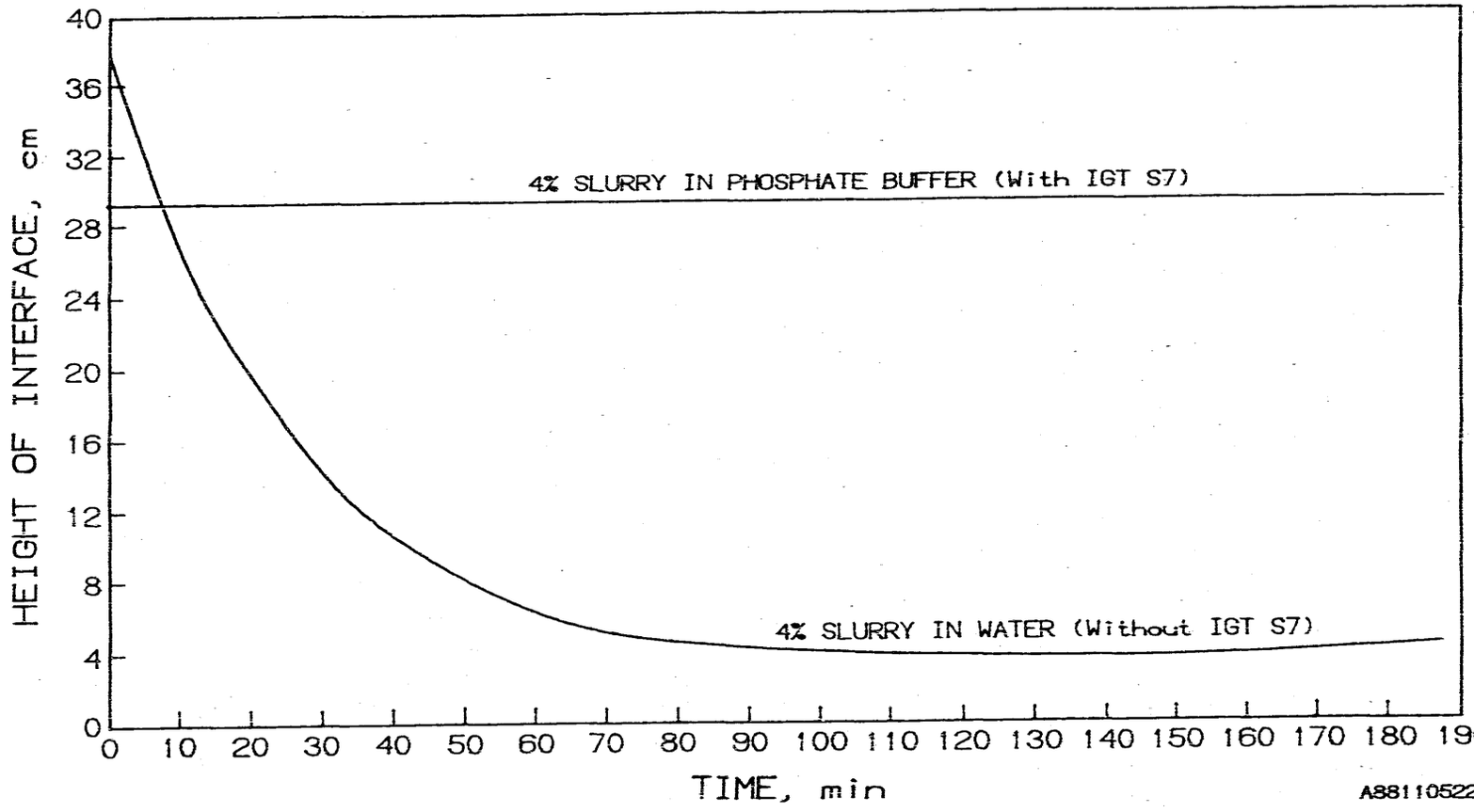

Figure 3-94. SETTLING CHARACTERISTICS OF OIL SHALE IN THE PRESENCE AND ABSENCE OF MICROBES (IGTS7)

than that obtained at higher rates of agitation (240, 300 and 350 rpm). The lower rates of agitation may not allow adequate oxygen and nutrient transfer and, therefore microbial growth did not increase at the lower compared to higher rates of agitation. At an agitation rate of 62 rpm, cell growth increased about 50-fold (from 1.36×10^5 to 7.0×10^6) and at an agitation rate of 170 rpm cell growth increased about 100-fold (from 1.36×10^5 to 1.0×10^7). At the higher rates of agitation, cell growth increased 1000-fold (from 10^5 to 10^8) (Table 3-50).

Conclusion

The results of the work conducted in this task suggest that a microbial system can be developed for the removal of sulfur and nitrogen from oil shale.

Future work is needed in the following areas before a microbial system can have commercial application.

- Improving the rates and amounts of desulfurization and denitrification. Identify bioreactor conditions that will improve microbial desulfurization and denitrification.
- Identify processes that will effectively separate the oil shale from the cells.
- Improve the settling characteristics of the oil shale after it leaves the reactor.

References Cited

1. Janka, J. C. and Dennison, J. M., "Devonian Oil Shale, A Major American Energy Resource." Paper presented at the 1979 Synthetic Fuels From Oil Shale Symposium; Atlanta, Georgia, December 3-6, 1979.

2. Orr, W. L., "Sulfur in Heavy Oils, Oil Sands and Oil Shales," In Oil Sand and Oil Shale Chemistry, ed. by Strausz, O. P. and Lown, E. L., p. 223-243, Verlag Chemie, New York, 1978.

3. Burnham, A. K., "Chemistry of Shale Oil Cracking," In Oil Shale, Tar Sands and Related Materials, ed. by Stauffer, H. C., p. 39-60, American Chemical Society, Washington, D.C., 1981.

4. Punwani, D. V., Lau, F. S. and Roberts, M., "Pressurized Fluidized-Bed Hydroretorting of Eastern Oil Shales," Paper presented at the 1988 Eastern Oil Shale Symposium," Lexington, Kentucky, pp. 359-363, 1988.

5. Kargi, F. and Robinson, J. M., "Removal of Sulfur Compounds from Coal by the Thermophilic Organism Sulfolobus acidocaldarius," Appl. Environ. Microbiol., 44:878-883, 1982.

6. Hoffmann, M. R., Faust, B. C., Panda, F. A., Koo, H. H. and Tsuchiya, H. M., "Kinetics of the Removal of Iron Pyrite From Coal by Microbial Catalysis," Appl. Environ. Microbiol., Vol. 42, No. 2, pp. 259-271, 1981.

Table 3-50. EFFECT OF DIFFERENT RATES OF AGITATION ON SETTLING AND GROWTH IN THE BIOREACTOR

Rates of Agitation, rpm	Settling[a]			Increase in Cell Growth, cells/ml
	Level in Bioreactor, cm	Sample[b] Slurry Concentration, %[d]	Control[c] Slurry Concentration, %[d]	After 4 Days in Sample Bioreactor
62	Top (0)	5.0	5.0	1.36×10^5 to 7×10^6
	Middle (6.25)	5.1	4.1	
	Bottom (12.5)	4.6	4.0	
170	Top (0)	4.1	4.0	1.36×10^5 to 1×10^7
	Middle (6.25)	4.0	3.9	
	Bottom (12.5)	4.6	4.0	
240	Top (0)	4.1	5.4	1×10^5 to 1×10^8
	Middle (6.25)	4.1	4.8	
	Bottom (12.5)	3.5	5.0	
300	Top (0)	4.1	5.4	1×10^5 to 3×10^8
	Middle (6.25)	3.8	5.4	
	Bottom (12.5)	4.0	5.4	
350	Top (0)	5.0	5.0	1×10^5 to 3×10^8
	Middle (6.25)	5.1	4.1	
	Bottom (12.5)	4.6	4.0	

[a] For determining if settling was occurring, wet pellet weights from three different levels in the bioreactor were determined and compared to a standard curve to determine slurry concentrations.

[b] Slurry and organisms.

[c] Slurry without organisms.

[d] The oil shale slurry in the reactors was a 4% concentration; 36 grams dry oil shale added to 900 ml.

7. Kilbane, J. and Maka, A., "Microbial Removal of Organic Sulfur From Coal," Final Report (Oct. 1985-1988) DOE Contract No. DE-AC22-85PC81201.

8. Aislabie, J. and Atlas, R., "Biodegradation of Nitriles in Shale Oil." Appl. Environ. Microbiol., Vol. 54, No. 9, pp. 2197-2202.

9. ATCC (American Type Culture Collection) Media Handbook.

10. Silverman, M. P. and Lundgren, D. G., "Studies on the Chemolithotrophic Iron Bacterium Ferrobacillus ferrooxidans, J. Bacteriol. 77:642-647, 1959.

11. Badger, W. L. and Banchero, J. T., In Introduction to Chemical Engineering, McGraw-Hill Book Co., New York, pp. 650-657, 1955.

12. Pierce BCA Protein Assay Reagent Instructions.

ACKNOWLEDGMENT

IGT acknowledges the significant work conducted on this project by IIT Professors D. T. Wasan and D. Gidaspow and OSU Professor R. M. Pfister, their principal investigators, and colleagues.

55WP/61090-332/RPP

APPENDIX A. An Analytical Method for Determination of Forms of Sulfur in Oil Shale

AN ANALYTICAL METHOD FOR DETERMINATION OF FORMS OF SULFUR IN OIL SHALE

A.1. Introduction

The determination of the various forms of sulfur in coal and shale is among the most important analytical parameters used to characterize a sample. The distribution of sulfate, pyritic, and organic forms of sulfur is a measure of its quality and, furthermore, an indication of the potential quality that is attainable after beneficiation. Many decisions must be made based on this information. Yet the methods that are available to obtain such information can often be difficult, tedious, expensive, subject to errors, and open to criticism.

The forms of sulfur in coal are determined by ASTM method D-2492 and total sulfur by ASTM method D-3177 (ASTM, 1986). These methods are the standards against which, ultimately, all other methods are compared. In D-2492, the initial step consists of extracting a sample of coal with boiling dilute HCl to dissolve the sulfates. The sulfate is then leached out as barium sulfate and determined gravimetrically. In the second step, the residue from the HCl extraction is leached with nitric acid to dissolve the pyrite. The extract is then analyzed for total iron by titration or by atomic absorption spectrophotometry and pyritic sulfur is calculated assuring the 1:2 stoichiometry of FeS_2. The organic sulfur is then determined by the difference between the total sulfur (determined using the D-3177 method with instrumental techniques, such as LECO analyzer) and the sulfate and pyritic sulfur. There may be some drawbacks in this method. This method, however, is used all over the world for determination of sulfur forms in coal.

A.2. Determination of Sulfur Forms in Oil Shale

The ASTM Method described for determination of sulfur forms in coal cannot be used for oil shales because: 1) In the initial step of extracting coal with boiling HCl to dissolve sulfates, there is no guarantee that all the non-pyritic iron forms are completely dissolved while none of the pyrite is solubilized, 2) The extent of sulfide sulfur in oil shale may be appreciable. Since D-2492 method does not involve the determination of sulfide sulfur, because it is present in coal in trace quantities, the sulfide sulfur may considerably affect the results, and 3) The basic assumption that the determination of iron can be used as a measure of the pyritic sulfur, is not valid. In addition to pyrites, iron in shale is present in other forms.

In view of these factors, it became necessary to develop a method to determine the forms of sulfur in oil shale.

A.3. Background

The sulfur in shale is known to occur as sulfate, monosulfide, disulfide and organical sulfur. The abundance of sulfate in oil shale is generally low (less than 4% of the total sulfur), although occurrences of monosulfides [pyrrhotite ($Fe_{(1-x)}S$) and wurtzite (ZnS)] and disulfides [pyrite (cubic FeS_2) and marcasite (orthorhombic FeS_2)] have been reported. Between 50% to 90% of the sulfur in most of the Eastern oil shales is believed to be in the form of pyrites, with the balance occurring as organically bound sulfur and sulfates

and sulfides. Sulfur containing organic compounds include thiophenes, benzothiophenes and polycyclic thiols.

Many analytical schemes have been reported in the literature for quantifying sulfur-by-type. In one scheme, (Stanfield et al. 1951) essentially the same as the ASTM procedure for determination of sulfur forms in coal, total sulfur is determined by Eschka fusion. Acid-soluble sulfates are dissolved with hydrochloric acid and pyritic sulfur is quantified by oxidation with nitric acid and subsequent determination of solubilized iron. Organic sulfur concentrations are determined by difference. Monosulfide sulfur is not separately determined. Furthermore, there is no collection of the sulfur associated with various forms which is believed to be a critical requirement for any geochemical study. The major drawbacks in this technique, are as follows:

1. There is some debate regarding the effectiveness of nitric acid in removing pyritic sulfur without removing some organically bound sulfur, and

2. Pyritic sulfur is generally overestimated if non-pyritic iron is released during the nitric acid oxidation.

The second procedure (Smith et al. 1964) uses perchloric acid to dissolve acid-soluble sulfates. Pyritic sulfur is determined by a lithium aluminum hydride (LAH) reduction technique. Organic sulfur is determined by difference or by an Eschka fusion of the residue from the LAH reduction. Monosulfide sulfur is not determined. The LAH technique, although commonly used in the analysis of other sedimentary materials, is not very useful because 1) the reagent can be explosive, 2) yields for LAH reduction for pure pyrites are low, 3) the concentrations of monosulfide sulfur can be significant, therefore, neglect of this sulfur form may not be justified, and 4) this method requires a particle size smaller than -400 mesh for quantitative recovery of pyritic sulfur.

A.4. IIT's Scheme

IIT's scheme is essentially an extension of the method developed by Tuttle et al. (1986) for determination of sulfur forms in Green River oil shale resids. IIT's scheme is designed to sequentially collect and volumetrically determine the sulfur species present in shale (Figure A-1). The sulfur associated with monosulfide and acid-soluble minerals is removed first by treatment of the sample with hydrochloric acid in an inert atmosphere. Monosulfide minerals evolve H_2S when treated with HCl and, hence, are referred to as acid-volatile sulfides. In the second step, disulfide sulfur bound in pyrites and marcasite is removed. These minerals do not decompose during HCl treatment, so disulfides can be easily separated from the monosulfide minerals. In this procedure, IIT used chromium (II) to reduce the disulfides to H_2S, which is then collected as CdS.

In the last step, the organically-bound sulfur is determined as the total sulfur remaining after removal of sulfatic, acid-volatile and disulfide sulfurs, either by fusion with an Eschka mixture or by a LECO analyzer.

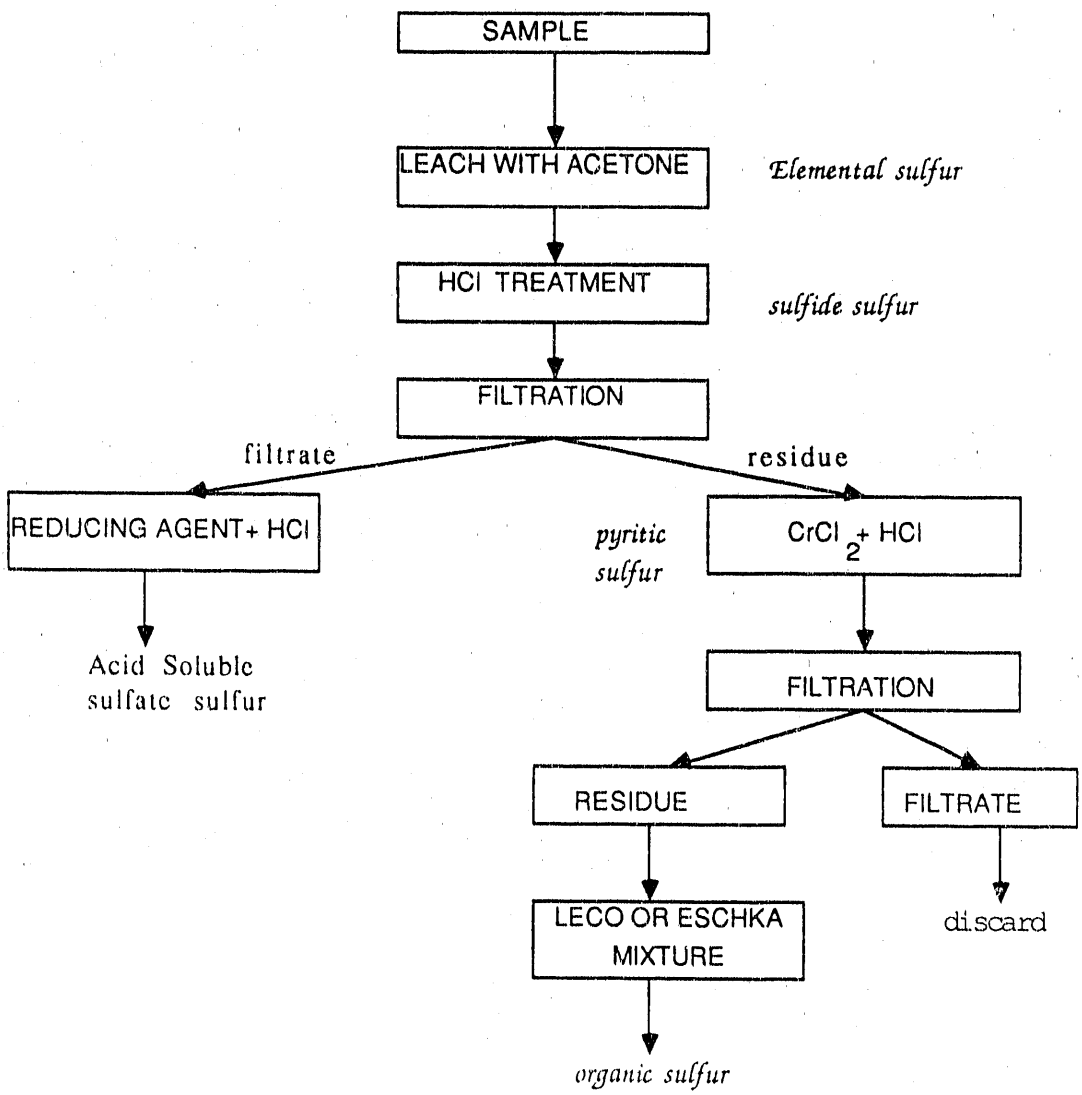

Figure A-1. FLOWCHART OF OUR METHOD OF DETERMINATION OF SULFUR FORMS IN OIL SHALES

Two Eastern oil shale samples, Indiana New Albany and Kentucky New Albany, were used for developing and testing the analytical scheme. Unlike Green River oil shale samples used by Tuttle et al. (1986), these samples have high pyritic sulfur concentration (3% to 5%). The samples were ground to particle size of less than 400 mesh, to ensure the liberation of pyrites from the organic matrix. A sample weight of 0.5 gm was used because of the high concentration of total sulfur.

Figure A-2 shows a schematic of the apparatus used for the analysis. It consists of a Jones Reductor (Skoog and West, 1976), which contains amalgamated zinc for reduction of chromium (III) to chromium (II), and a H_2S apparatus. The H_2S generated in the reaction flask passes through an aqueous wash solution buffered to a pH 4.0 via a condenser and is then as CdS by passage through a neutral solution of $CdSO_4$. The reaction flask is a 200-ml capacity three-neck round bottom flask (RB), SN 24/40 equipped with a magnetic bar, stirrer and a heating mantle.

1. Reagents: Concentrated HCl: 2 N or higher.

2. Amalgamated Zinc: Dissolve 3.25 g of $HgCl_2$ in 75 ml water and 2 to 3 ml of conc. HCl. Add glasswool to the bottom of the funnel. Add zinc dust to column C about half full. Pour $HgCl_2$ solution over the column and drain out the liquid. This is amalgamated zinc.

3. Chromic Chloride ($CrCl_3 \cdot 6H_2O$): Dissolve 133 g of $CrCl_3$ in 0.1 N HCl (500 ml solution). Pour about 75 ml over the amalgamated zinc and open the valve. Throw away first 10 ml. The solution color should change from bright green to deep blue. If color does not change to deep blue, throw away the solution and start again. Then attach the funnel to reaction vessel and start nitrogen supply. It is very important to maintain an inert atmosphere throughout the preparation of chromic chloride solution. Oxygen interferes with the reaction, therefore the system should be constantly purged with either high purity nitrogen, helium or argon gas. The chromium (II) solution is very unstable in air and should be prepared every few days.

4. $CdSO_4$ Solution: Dissolve 4.5 g of $3CdSO_4 \cdot 8H_2O$ in 125 ml of double distilled water. Mix 100 ml of HI (SG 1.7, methoxyl grade), 75 ml of hypophosphorous acid (150%), and 150 ml of formic acid (90%). Boil with a stream of nitrogen flowing through the solution for about 10 minutes gently after the temperature has reached 115°C. This a reducing mixture.

A.5. Sulfur Separation Procedure

Accurately weigh about 0.5 g of shale sample and introduce it into the reaction flask (Figure A-2). Since most of the Eastern oil shales contain iron (III), it is suggested that about 2 g of $SnCl_2$ be added with the sample. $SnCl_2$ reduces iron (III) to iron (II) and in no way affects the sulfur determination.

Wet the shale with either high-purity ethyl alcohol or acetone. Connect the apparatus and flush it for 5 minutes with high-purity grade nitrogen. Slowly introduce about 20 to 30 ml of concentrated HCl from column C into the reaction flask. Deareate the acid beforehand by passage of pure nitrogen through it. Establish a low flow of nitrogen through the whole system and

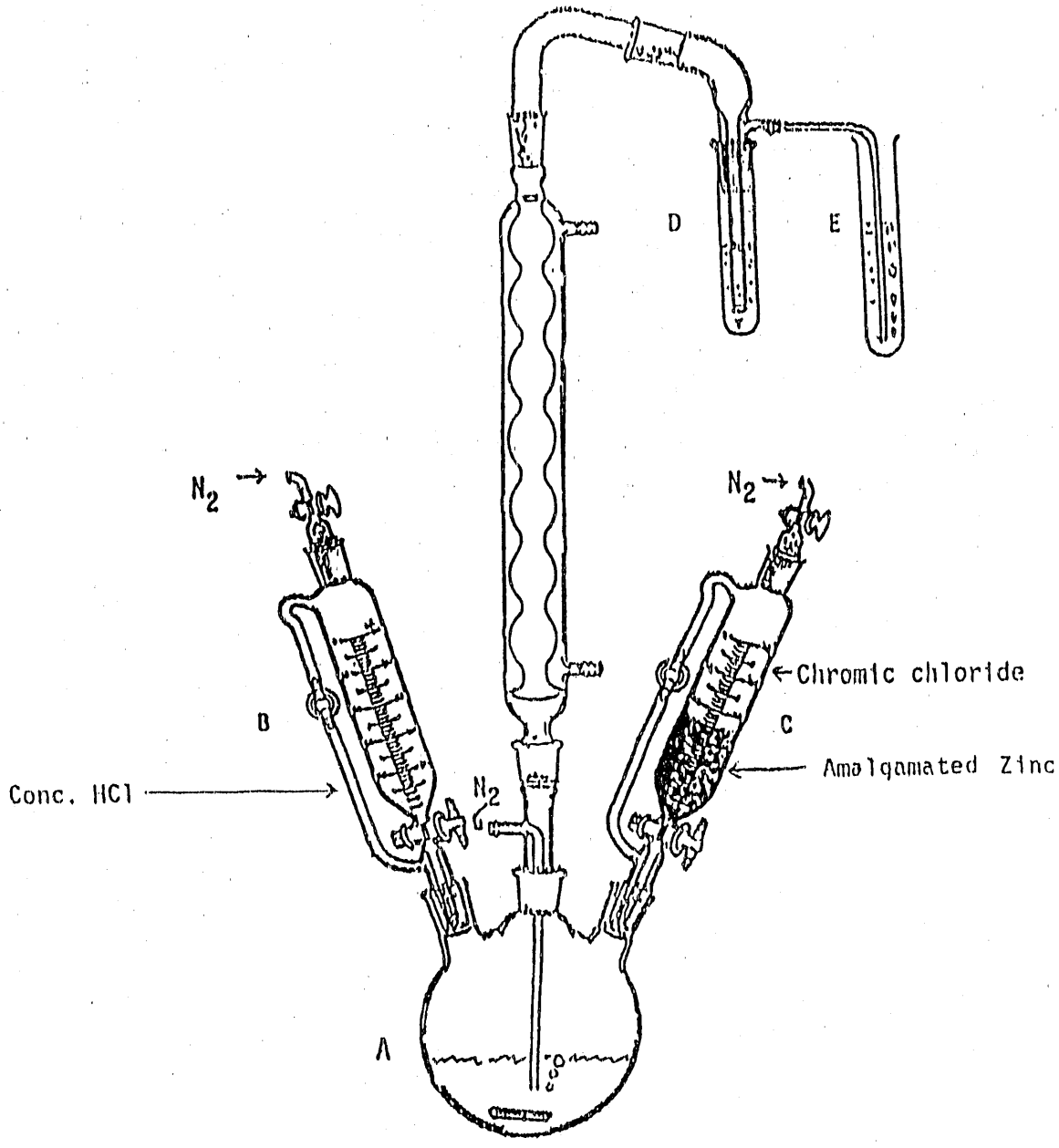

Figure A-2. SCHEMATIC DIAGRAM OF THE APPARATUS USED FOR THE ANALYSIS

allow the reaction to proceed at room temperature for 15 minutes. Heat slowly until the solution just begins to boil, reduce the heat and continue the reaction until the CdS is coagulated and no H_2S is detected when a paper wetted with silver nitrate solution is held in the gas stream issuing from the buffer. Disconnect the apparatus, filter off the residual solids, wash it with water, dry it, and save the filtrate for the sulfate sulfur determination.

A.6. Determination of Sulfide Sulfur

The H_2S evolved by the reaction of shale with concentrated HCl is absorbed in the neutral solution of $CdSO_4$ according to the reaction

$$CdSO_4 + H_2S \Longleftrightarrow CdS + H_2SO_4$$

The CdS forms a deep yellow precipitate. Both gravimetric as well as volumetric methods can be used to determine the sulfide sulfur. However, IIT found the volumetric method to be easier with better reproducibility. The H_2SO_4 formed in the above reaction was titrated against 0.1 N NaOH solution using methyl red indicator at a pH of 5.25.

$$H_2SO_4 + 2\ NaOH \Longleftrightarrow Na_2SO_4 + 2H_2O$$

The sulfide sulfur can then be determined using the following formula:

$S_{sulfide}$ = (ml of NaOH X Normality of NaOH X 1.6033)/sample weight (A-1)

The factor 1.6033 in Equation A-1 is from stoichiometry. If the sample contains elemental sulfur, it is detected along with the sulfide sulfur. Therefore, in order to determine the elemental sulfur, the shale sample should be leached with acetone prior to analysis of any sulfur forms.

A.7. Determination of Sulfate Sulfur

IIT followed the procedure of Johnson and Nishita (1952) to determine the sulfate sulfur in shale. In this method, take the filtrate from the sulfide separation that contains acid-soluble sulfur. Add 4 ml of reducing mixture. Boil and reflux with nitrogen. This reducing mixture converts sulfate ions into sulfide ions. Absorb the resulting H_2S gas in $CdSO_4$ as before and titrate the H_2SO_4 with 0.1 N NaOH to determine sulfatic sulfur using Equation A-1.

A.8. Determination of Pyritic Sulfur

Take the residue from sulfide filtration and wet it with about 5 ml of ethanol. Connect the apparatus and flush with nitrogen. Add about 1 g of $SnCl_2$ to prevent interference from Fe^{3+} ions present in the shale. Pour about 40 to 50 ml of concentrated HCl and add $CrCl_2$ drop by drop till the entire solution in the flask turns deep blue. Stir the contents of the reaction flask with the help of a magnetic bar. First, allow the reaction to proceed at room temperature for about 10 minutes and then slowly heat until the solution starts boiling; let the solution boil for 20 to 30 minutes. Allow the contents of the reaction flask to cool, filter the adsorbent, titrate the H_2SO_4 formed with 0.1 N NaOH and calculate the pyritic sulfur content using Equation A-1.

A.9. Determination of Organic Sulfur

Filter the contents of the reaction flask after determination of pyritic sulfur. Throw out the filtrate, wash the residue with water and dry it to be used for organic sulfur analysis. The organic sulfur can now be determined by two techniques, either Eschka fusion or LECO Analyzer. (IIT used a LECO analyzer.)

A.10. Determination of Total Sulfur

Total sulfur in shale can be determined by either fusing the sample with an Eschka mixture or by a LECO analyzer in the same way described for organic sulfur analysis.

$$S_{total} = S_{pyritic} + S_{sulfide} + S_{elemental} + S_{sulfate} + S_{organic}$$

A.11. Results

After establishing the applicability of this method for calibrated samples, such as a standard sulfur solution in pyridine, a sodium sulfide solution and pyrites, spiked in diatomaceous earth, IIT analyzed two shale samples. The calibration results with all these samples were found quite reproducible (after considerable trial and error).

A well-characterized Kentucky New Albany oil shale sample was then used to establish the applicability of this method. This sample was analyzed for sulfur forms at IGT's Analytical Laboratory by a Mössbauer spectroscopy technique. A comparison of results obtained by this method and by using a Mössbauer spectroscopy is given in Table A-1.

Table A-1. COMPARISON OF ANALYSIS RESULTS FOR KY-NA SHALE

Sulfur Form	Mössbauer Spectroscopy	Present Method
Sulfide + Elemental	0.09	0.07
Sulfate	0.45	0.78
Pyritic	4.31	4.10±0.21
Organic	0.77	0.75
Total	5.47	5.47

[a] The organic sulfur was not determined by difference, therefore, the total of all the sulfur forms does not add up to the value determined for the total sulfur.

[b] The sulfate sulfur shown by the IIT method is higher, because the pyrites in the shale were oxidized during storage, since both tests were not conducted at the same time.

IIT used this method extensively for determining pyritic sulfur, because this sulfur form was of primary interest. Tests with Indiana New Albany shale showed a pyrite content of 3.27%, while IGT reported a value for this sample of 3.3%.

A.12. Discussion

This procedure for determination of sulfur forms in shale is simple, easy to operate and rapid when compared with the conventional method. The main idea behind this technique came from the Dr. Chausak Chaven of the Illinois State Geological Survey.

APPENDIX B. Measurement of Cohesive Force Between Fine Particles Using a Cohetester

MEASUREMENT OF COHESIVE FORCE BETWEEN
FINE PARTICLES USING A COHETESTER

B.1. Introduction

Fine particles belonging to Geldart Group "C" are very difficult to fluidize. These particles are characterized by their cohesive behavior. Both coal and shale need to be ground fine to an average particle size of 5 μm for liberation of mineral inclusions from the organic matrix. At this particle size, IIT's electrofluidized bed could not be used because of the cohesive nature of the particles.

The principal factor behind the cohesive behavior of fine particle is the inter particle force. This force may be either van der Waals force or electrostatic force, or may be a combination of both. In the case of oil shale, where particles are very cohesive, these interparticle forces are probably electrostatic in nature. Since kerogen in the shale acquires a positive charge and mineral matter charges negatively, the attraction between oppositely charged particles probably results in agglomeration.

B.2. Instrument Description

A cohetester was used for the measurement of cohesive force or agglomeration tendency of powders. This instrument was manufactured by the Hosokawa Micron Corporation of Japan. This instrument mainly consists of 3 units as shown in Figure B-1: Main unit, Operational Amplifier, and X-Y Recorder.

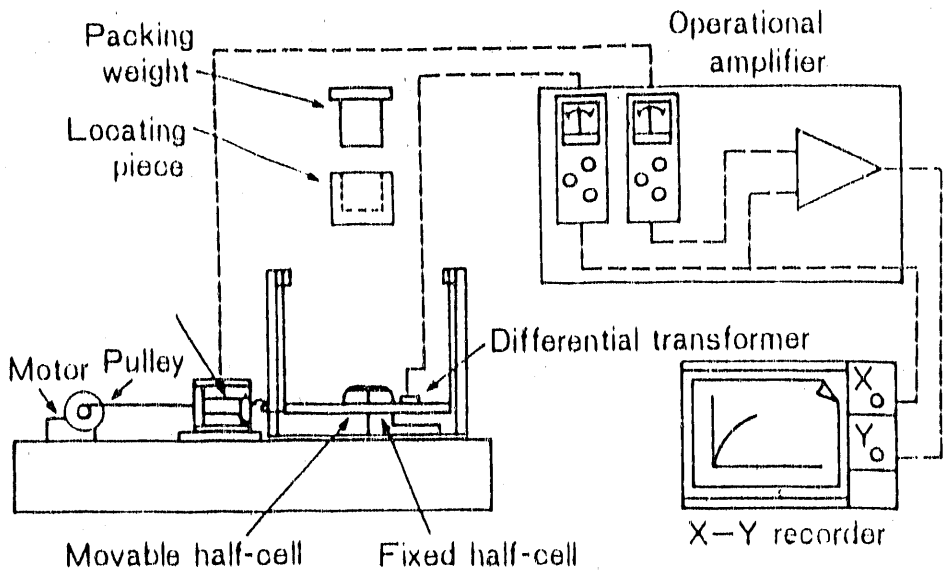

Figure B-1. SCHEMATIC DIAGRAM OF COHETESTER

The main unit consists of a motor section for pulling the cell, a suspended cell section, and the housing. Also housed in the main unit are a strain gauge for measurement of stress and a linear voltage differential transformer (LVDT) for measuring powder displacement.

The operational amplifier consists of a strain amplifier, displacement meter and a signal processor. The function of the signal processor is to indicate the actual load to the powder layer by subtraction of blank load. Blank load is determined by pulling the movable cell without any powder into it. The output of the operational amplifier is connected to a X-Y recorder where the x coordinate is the displacement and the y coordinate denotes the tensile strength. The measuring cell consists of 2 sections, one is fixed while the other one is movable. The inside diameter of the cell is 50 mm and it has a depth of 20 mm.

B.3. Test Procedure

A blank test is conducted to tune the amplifier and other instrument settings to check warping of plates, level of the machine, etc. The cell is filled with the known weight of a specimen powder. Normally, between 15 to 30 g of powder, depending upon particle density, is enough. The specimen is then placed under pressure (with compaction weights), and the powder layer is allowed to stabilize in order to adjust to a constant porosity of the powder bed. The porosity of the powder layer is calculated from the equation

$$\epsilon_s = W_p/\rho_p V \qquad \text{(B-1)}$$

Where W_p is the weight of the powder filled, ρ_p is the particle density and V is the powder volume, which is fixed. This volume has been measured at the factory before shipment of the instrument.

Once the powder bed is stabilized, compaction weight and cell extension tubes are removed. The motor is then turned on and the movable cell is released by slowly turning the securing knob. The motor starts pulling the movable cell. At some displacement, the powder layer is broken, and a peak is observed in the X-Y recorder. The height of this peak is proportional to the tensile strength.

B.4. Results

Figure B-2 shows the tensile strength as a function of solids volume fraction for flour and oil shale particles. The cohesive force or tensile strength increases with increase in solid volume fraction. The oil shale particles show a higher cohesive force than the flour.

Figure B-3 shows the tensile strength as a function of solids volume fraction for raw and beneficiated oil shales. The results show that the cohesive force is higher for the beneficiated shale than for the raw shale under identical conditions. Recent measurements made by Miss R. Bezbarauh on other beneficiated shales indicate that cohesive force between finely ground shale particle increases with an increase in kerogen content.

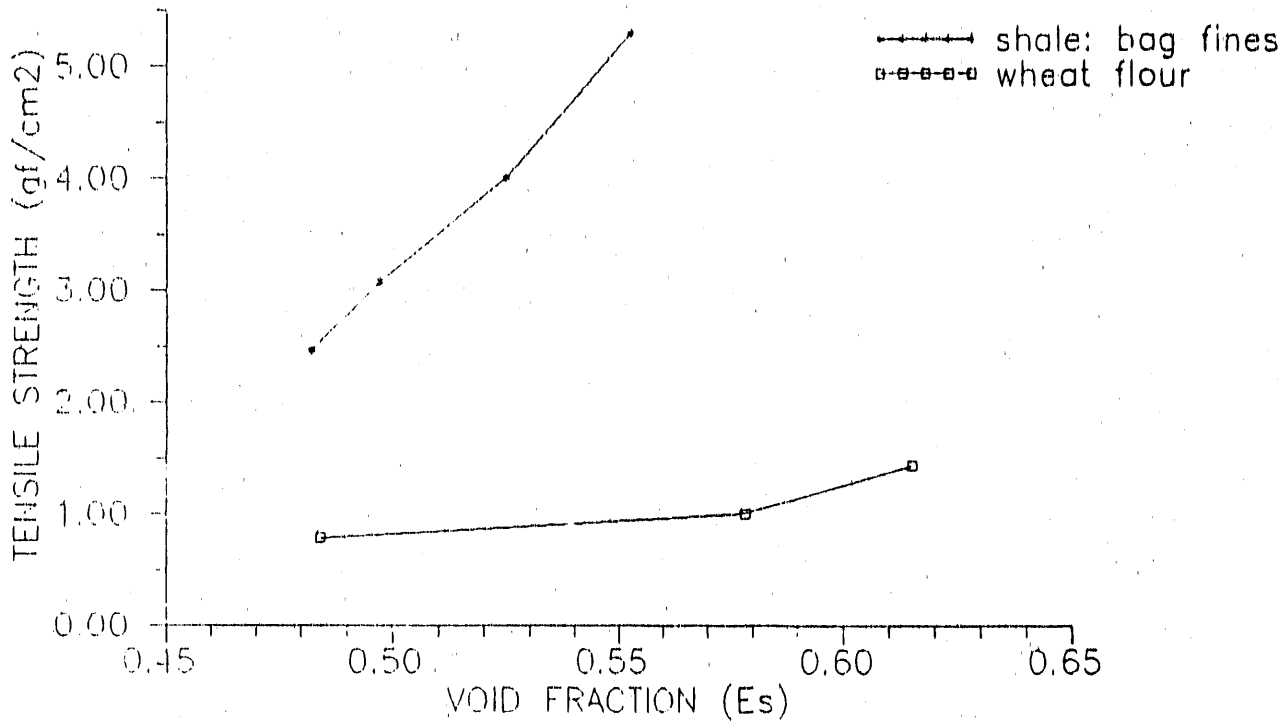

Figure B-2. COHESIVE FORCE FOR OIL SHALE AND WHEAT FLOUR

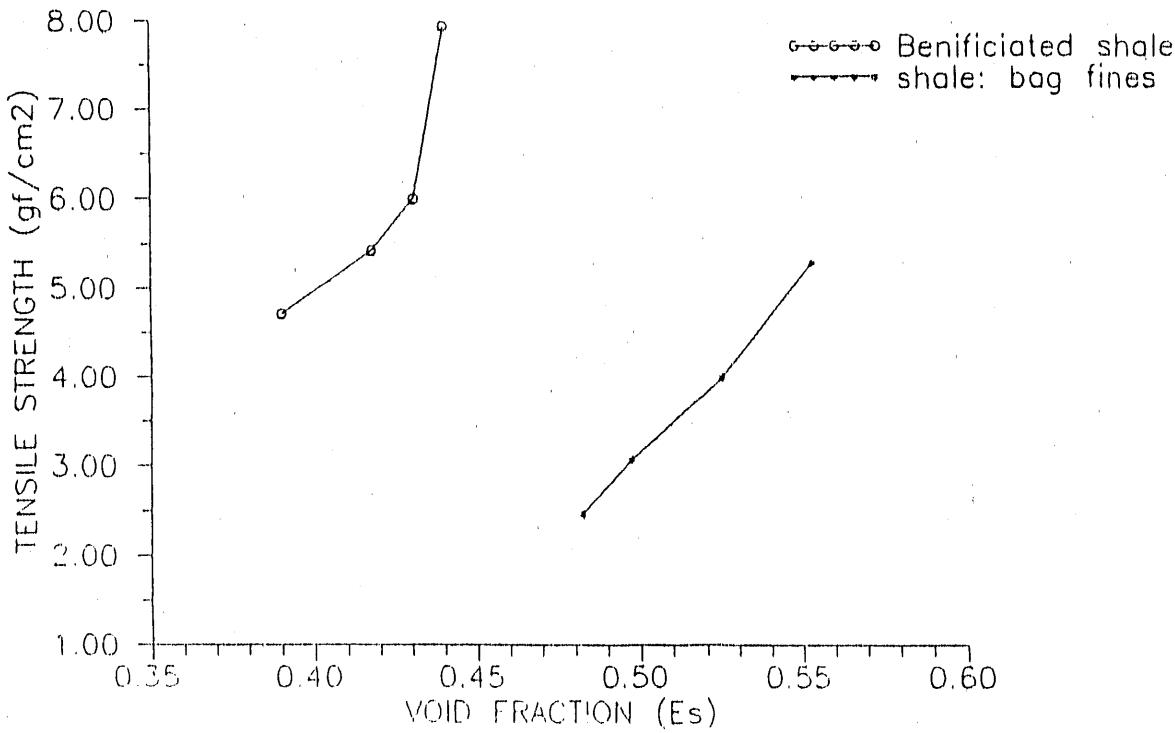

Figure B-3. COHESIVE FORCE FOR OIL SHALE PARTICLES AS A FUNCTION OF KEROGEN CONTENT

B.5. Discussion

The cohesive force measured by this instrument strongly depends upon the room temperature, humidity and the surface moisture of the powder. In order to obtain reproducible results, vibrations in surrounding area must be minimized.

52WP/T3App/RPP

END

DATE FILMED

11/20/92